APOCALYPTIC QUANTUM GRAVITY

by

DAVID WAKEHAM

A thesis submitted in partial fulfilment of the requirements for
the degree of

DOCTOR OF PHILOSOPHY

in

THE FACULTY OF GRADUATE AND POSTDOCTORAL STUDIES

(Physics)

THE UNIVERSITY OF BRITISH COLUMBIA

(Vancouver)

August 2022

The following individuals certify that they have read, and recommend to the Faculty of Graduate and Postdoctoral Studies for acceptance, the dissertation entitled:

Apocalyptic Quantum Gravity

submitted by David Wakeham in partial fulfillment of the requirements for the degree of Doctor of Philosophy in Physics.

Examining Committee

Mark Van Raamsdonk, Professor, Physics, UBC
Supervisor

Moshe Rozali, Professor, Physics, UBC
Supervisory Committee Member

Gordon Semenoff, Professor, Physics, UBC
University Examiner

Stephen Gustafson, Professor, Mathematics, UBC
University Examiner

Thomas Hartman, Professor, Physics, Cornell University
External Examiner

Additional Supervisory Committee Members
Robert Raussendorf, Professor, Physics, UBC
Supervisory Committee Member

Mark Halpern, Professor, Physics, UBC
Supervisory Committee Member

Abstract

The AdS/CFT dictionary connects bulk gravitational physics in an asymptotically anti-de Sitter (AdS) background to the quantum dynamics of a conformally invariant field theory (CFT), defined on the asymptotic boundary. In this thesis, we explore, extend and apply this dictionary for a boundary CFT (BCFT), with a particular focus on the physics of black holes.

In a BCFT, a physical boundary is added to the CFT. The simplest dual geometry is an asymptotically AdS spacetime cut off by a physical surface called an end-of-the-world (ETW) brane, homologous to the BCFT boundary. For certain highly symmetric configurations of the BCFT called boundary states, symmetry constrains these ETW branes to a one-parameter family labelled by extrinsic curvature. By placing the CFT boundary in Euclidean time, we construct a one-parameter family of black hole microstates in arbitrary dimension.

In two dimensions, we analytically calculate minimal surfaces in the bulk geometry and show that, for some parameter regimes, they pierce the black hole horizon and become disconnected. According to the Hubeny-Rangamani-Ryu-Takayanagi (HRT) formula, these surfaces compute entanglement entropy in the field theory. We find a set of conditions which ensure that the microscopic entanglement entropy, arising from a correlator of twist operators, agrees with the bulk result. In particular, the BCFT reproduces the phase transition between connected and disconnected minimal surfaces.

This twist correlator can be immediately evaluated on any conformally related background, giving access to entanglement entropy in a number of other contexts of physical interest. By analytically continuing the thermofield state of a half-line, we arrive at a simple toy model of an evaporating black hole, where the phase transition in minimal surface

corresponds to information escaping from the interior. For the BCFT on an interval, this transition can be recast in terms of the performability of a certain set of quantum tasks. We use related techniques to constrain the operator content of BCFTs dual to spacetimes with a sharp brane in arbitrary dimension. We discover they are finely tuned, with a fragile causal structure which becomes "fuzzy" under small changes to the spectrum.

Lay Summary

Black holes are regions of spacetime from which nothing can escape. Over time, quantum mechanics causes them to leak energy and disappear. What happens to information about the objects that fell inside? Gravity suggests it is trapped forever, and quantum mechanics that it somehow gets out. To see which is correct, we must understand how quantum and gravitational effects interact. One approach to understanding this interaction is the AdS/CFT correspondence, where data at the boundary of spacetime is related to geometric structure in the bulk. This thesis extends the correspondence and uses it to track how information moves around a black hole. In particular, we show how objects called end-of-the-world branes can reach inside and rescue information from the interior. We discover that although they are consistent with other aspects of AdS/CFT, branes are also surprisingly fragile, with small microscopic changes rendering them macroscopically "fuzzy".

Preface

Chapter 1 is an original overview of background material and research presented in subsequent chapters.

A version of Chapter 2 was published in [1] with Sean Cooper, Moshe Rozali, Brian Swingle, Mark Van Raamsdonk and Christopher Waddell. I developed the approach to calculating the equation of motion for the branes in the black hole background in arbitrary dimensions. I performed analytics in two dimensions, and the analysis of the Rindler spacetime analogue, along with Mark Van Raamsdonk. Moshe Rozali, Chris Waddell, Sean Cooper and Brian Swingle participated in discussion of all material. The work was stimulated by discussions with Tarek Anous, Stefano Antonini, Eliot Hijano, Andreas Karch, Alex May, Shiraz Minwalla, Volker Schomerus, and Tadashi Takayanagi.

A version of Chapter 3 was published in [2] with James Sully and Mark Van Raamsdonk. The initial calculation was suggested by Mark Van Raamsdonk, which I conducted along with James Sully and Mark Van Raamsdonk. I gave the general proof of the Ryu-Takayanagi formula for arbitrary subregions, and was responsible for the overall organization of the manuscript. The work was enriched by discussions with Tarek Anous, Tom Hartman, Eliot Hijano, Alex May, Dominik Neuenfeld, and Chris Waddell.

A version of Chapter 4 was published in [3] with Moshe Rozali, James Sully, Mark Van Raamsdonk and Christopher Waddell. I performed the field theory analysis of the one-boundary setup, and contributed to the discussion and organization of the remainder of the paper. Mark Van Raamsdonk suggested the initial approach, and performed the bulk classical analysis. James Sully and Chris Waddell worked on the evaporating case, and Mark Van Raamsdonk on the single-sided $\mathbb{Z}_2$ setup. All authors were involved in conceptual discussions of the material. Discussions with Ahmed Almheiri, Jordan Cotler,

Table of Contents

xi

List of Figures

xiii

Acknowledgments

Let the beauty we love be what we do.

Rumi

I've been exceptionally lucky to work on beautiful problems under the guidance of my supervisor, Mark Van Raamsdonk. His insight, intuition, and spirit of play have deeply informed my development as a physicist. He was also generous enough to let me goof around with quantum computers for a few months, where I benefited from the collegial supervision of Olivia Di Matteo at Xanadu. My senior collaborators Jason Pollack, Ning Bao, Moshe Rozali, and Jamie Sully have taught me more than any textbook possibly could. I view Jamie especially as a mentor; his extraordinary contributions to physics will be missed, though no doubt, the world will be a safer place as he shifts his focus to AI alignment. I am grateful to my committee for advice and encouragement, and to UBC for financial support via an International Doctoral Fellowship.

The other occupants of Room 418—Jonah Berean-Dutcher, Shovon Biswas, Sean Cooper, Pompey Leung, Alex May, Dominik Neuenfeld, Wyatt Reeves, Abhisek Sahu, Petar Simidzija, Chris Waddell, and Rana Zibakhsh—are unwritten co-authors of this thesis, and I imagine each page covered in the invisible marginalia and chalkboard dust of our conversations. We shared much more than physics; from Thanksgiving dinner to Sufi jazz to getting lost in rural Japan, they form the warm and human core of my graduate school experience. I would like to single out my academic brothers, Alex, Chris, and Petar, who have shared the journey as physicists and friends.

Finally, I would like to thank my family, who were geographically distant but never far

from my heart: my mother, Martine, who gave me life in more than one way; my brother, Yoshua, who in fatherhood, confronts a more daunting challenge than quantum gravity, and with greater rewards; and my sister, Ruth, whose creativity and verve always inspire me. I look forward to making up for lost time with you all.

Dedication

To Vered, who pointed the way out and made leaving joyful.

Chapter 1

Introduction

The *AdS/CFT correspondence* [8, 9, 10, 11] is the statement that some quantum field theories secretly encode theories of quantum gravity. In this thesis, we will use this correspondence to peer inside black holes and see how they evaporate. To do this, we will need to introduce non-perturbative objects called branes in the gravitational theory, which correspond to special boundary conditions in the field theory. We will carefully consider the consistency of these objects from a quantum-mechanical perspective, and find that they are non-generic, i.e. most boundary conditions do not correspond to branes.

This introductory chapter provides a review of the basic concepts involved, and summarizes the narrative flow of the remainder of the thesis. We draw on various resources, particularly [12, 13, 14, 15, 16]. Here is a more detailed chapter outline:

- In §1.1, we review background material on the AdS/CFT correspondence, black holes, and entanglement.

- In §1.2, we introduce boundary states of a CFT, and describe how they can be used to construct microstates of a black hole. Chapter 2 treats this is more detail.

- In §1.3, we discuss the microscopic calculation of entanglement entropy in two dimensions, and how CFT techniques can be used to verify the gravitational results. This is taken up in more detail in Chapter 3.

- In §1.4, we use two-dimensional conformal symmetry to transform the microstate picture into a description of a dynamically evolving black hole which exhibits some aspects of information loss. This is the theme of Chapter 4.

- In §1.5, we give a somewhat different perspective on the same problem, relating our construction to a distributed quantum computation in spacetime, dual to a bulk scattering problem. Chapter 5 discusses this further.

- In §1.6, we consider this bulk scattering from the microscopic perspective, in arbitrary dimensions, and discover that our boundary states and CFTs must be extremely finely tuned to give a bulk brane. This is the topic of Chapter 6.

1.1 Background

AdS/CFT tells us that d-dimensional conformal field theories (CFT_d) are dual to quantum gravity in negatively curved spacetimes, also called anti-de Sitter space (AdS_{d+1}), as in Fig. 1.1. Let us expand both sides of this equation.
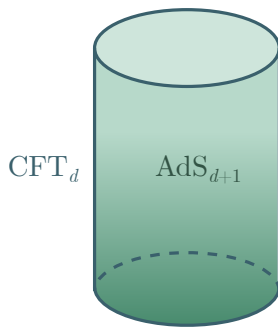
Figure 1.1: The AdS/CFT correspondence on a cylinder.

1.1.1 Anti-de Sitter space

Anti-de Sitter space AdS_{d+1} is a $(d+1)$-dimensional space with constant negative curvature. This means that nearby particles in initially parallel free-fall accelerate away from

each other at a constant rate proportional to their distance, $\ddot{\xi}^\mu = \xi^\mu/L_{\text{AdS}}^2$, where ξ is the initial separation vector and L_{AdS} is some scale we will call the *AdS radius*. Note that here and throughout the thesis, we will set $c = 1$. The simplest way to construct such a space is to embed it as a hyperboloid in the flat space $\mathbb{R}^{2,d,}$:

$$\eta_{MN} X^M X^N = -L_{\text{AdS}}^2. \tag{1.1}$$

Topologically, the hyperboloid takes the form $\mathbb{S}^1 \times \mathbb{R}_+ \times \mathbb{S}^{d-1}$, where $\mathbb{S}^k$ is the k-dimensional hypersphere. We can therefore parameterize it as

$$X^{-1} = L_{\text{AdS}} \cosh(\rho) \sin(\tau) \tag{1.2}$$

$$X^0 = L_{\text{AdS}} \cosh(\rho) \cos(\tau) \tag{1.3}$$

$$X^i = L_{\text{AdS}} \sinh(\rho) \Omega^i, \tag{1.4}$$

for $\tau \in \mathbb{S}^1, \rho \geq 0$, and $\Omega^i, i = 1, \ldots, d$, parameterizing $\mathbb{S}^{d-1}$.[1] Substituting this paramaterization into the flat metric gives the induced metric on the hyperboloid:

$$\begin{aligned} \mathrm{d}s^2 &= \eta_{MN} \, \mathrm{d}X^M \, \mathrm{d}X^N \\ &= L_{\text{AdS}}^2 \left[-\cosh(\rho)^2 \, \mathrm{d}\tau^2 + \mathrm{d}\rho^2 + \sinh^2(\rho) \, \mathrm{d}\Omega_{d-1}^2 \right]. \end{aligned} \tag{1.5}$$

These are called *global coordinates*. Equivalently, if we set $r = \sinh\rho$, we obtain a different expression

$$\mathrm{d}s^2 = -\left(1 + \frac{r^2}{L_{\text{AdS}}^2} \right) \mathrm{d}t^2 + \left(1 + \frac{r^2}{L_{\text{AdS}}}^2 \right)^{-1} \mathrm{d}r^2 + r^2 \, \mathrm{d}\Omega_{d-1}^2, \tag{1.6}$$

which will be useful below.

The *isometries* of AdS are the coordinate transformations which leave the metric invariant. From the embedding (1.1), these will be induced by coordinate changes of $\mathbb{R}^{2,d}$ which leaves the defining equation $X^2 = -L_{\text{AdS}}^2$ invariant. This is precisely the *Lorentz*

---

[1]For $d = 1$, the sphere $\mathbb{S}^0 = \{\pm 1\}$, and we can take $\rho \in \mathbb{R}$. This thesis only considers $d \geq 2$.

group $SO(2, d)$.[2] Geometrically, the group is generated by rotations in the timelike plane, rotations of the spacelike directions, and boosts between the two. Since there are $d + 2$ directions altogether, there are a total of $(d + 1)(d + 2)/2$ independent rotations, one for each pair of directions.

Although these act as rotations on the embedding space $\mathbb{R}^{2,d}$, this is the same as the number of basic symmetries of $\mathbb{R}^{1,d}$ including translations. Indeed, there are $d + 1$ translations and $d(d + 1)/2$ rotations and boosts, with

$$(d + 1) + \frac{d(d + 1)}{2} = \frac{(d + 1)(d + 2)}{2}. \tag{1.7}$$

This implies that AdS is a *maximally symmetric spacetime*. It looks the same at every point and in every direction, as we expect for a space of constant negative curvature. This curvature can be measured using the *Ricci tensor $\mathcal{R}_{\mu\nu}$*:

$$\mathcal{R}_{\mu\nu} = -\frac{d}{L_{\text{AdS}}^2} g_{\mu\nu}. \tag{1.8}$$

This implies that AdS is a vacuum spacetime, satisfying Einstein's equation

$$\mathcal{R}_{\mu\nu} - \frac{1}{2}\mathcal{R}^\lambda{}_\lambda g_{\mu\nu} + \Lambda g_{\mu\nu} = 0 \tag{1.9}$$

for vacuum energy $\Lambda = -d(d - 1)/2L_{\text{AdS}}^2$.[3]

Although AdS is maximally symmetric and everywhere looks the same, in the global coordinates (1.5) we can single out a region of interest, namely the *conformal boundary* at $\rho \to \infty$. The simplest way to exhibit this boundary is to make a change of coordinates $\tan(\theta) = \sinh(\rho)$, so that (1.5) becomes

$$ds^2 = \frac{L_{\text{AdS}}^2}{\cos^2(\theta)} \left[-d\tau^2 + d\theta^2 + \sin^2\theta \, d\Omega_{d-1}^2 \right].$$

---

[2]Rather than the Poincaré group $ISO(2, d)$, since translations change the defining equation. We also focus on orientation-preserving transformations continuously connected to the identity, taking $SO(2, d)$ rather than $O(2, d)$.

[3]This also implies our desired result for geodesic deviation, $\ddot{\xi} = \xi/L_{\text{AdS}}^2$.

In $d \geq 2$, $\rho \geq 0$ and hence $0 \leq \theta < \pi/2$. Up to an overall conformal factor, this has the geometry of $\mathbb{R} \times H\mathbb{S}^d$, where $H\mathbb{S}^d$ is half of the d-dimensional hypersphere $\mathbb{S}^d$.

We *conformally compactify* AdS by throwing away the conformal factor and adding the point $\theta = \pi/2$ at the boundary of the hemisphere. This corresponds precisely to the conformal boundary $\rho = \infty$. The metric at this point is conformally equivalent to

$$\mathrm{d}s^2|_{\theta = \pi/2} \sim -\mathrm{d}\tau^2 + \sin^2\theta\, \mathrm{d}\Omega_{d-1}^2.$$

The boundary of a hemisphere is a sphere, $\partial(H\mathbb{S}^d) = \mathbb{S}^{d-1}$, so the spatial geometry of the conformal boundary is $\mathbb{S}^{d-1}$. This gives rise to the solid cylinder of Fig. 1.1.

Note that the behaviour of null geodesics is unaffected by the conformal factor. In particular, since the geometry is conformally compact, a bulk AdS observer can send light rays to the conformal boundary and have them return in finite proper time. Thus, AdS behaves somewhat like a finite box whose boundary can be probed by light rays. Since information can be encoded into light rays, this already suggests a nontrivial relation between bulk and boundary physics.

To explore how energy and matter actually travel around AdS, let us introduce some matter fields. The simplest example is a scalar field which is perturbatively weak and not backreact on the metric. We follow the treatment of [14] and set $L_{\mathrm{AdS}} = 1$ for simplicity. A scalar field of mass m satisfies the Klein-Gordon equation

$$\Box\phi = \frac{1}{\sqrt{-g}}\partial_\mu\left(\sqrt{-g}g^{\mu\nu}\partial_\nu\phi\right) = m^2\phi. \tag{1.10}$$

Let us make an ansatz which separates the solution into a radial function and a spherical harmonic

$$f_{\omega\ell\vec{m}}(r, t, \Omega) = \psi_{\omega\ell}(r)e^{-i\omega t}Y_{\ell\vec{m}}(\Omega),$$

where $Y_{\ell\vec{m}}(\Omega)$ is the spherical harmonic with degree (angular momentum) ℓ and orders (magnetic quantum numbers) $\vec{m}$, on which the round Laplacian simply gives $-\ell(\ell + d - 2)$.

5

Then the Klein-Gordon equation (1.10) becomes an equation

$$(1+r^2)\psi'' + \left[\frac{d-1}{r}(1+r^2) + 2r\right]\psi' + \left[\frac{\omega^2}{1+r^2} - \frac{\ell(\ell+d-2)}{r^2} - m^2\right]\psi = 0 \quad (1.11)$$

for the radial function $\psi_{\omega\ell}$.

Rather than solve this explicitly, we can take limits. Near the centre of the cylinder, at small r, we have

$$\psi'' + \frac{d-1}{r}\psi' - \frac{\ell(\ell+d-2)}{r^2}\psi = 0. \quad (1.12)$$

This can be solved by a power law ansatz $\psi \propto r^{-p}$, with

$$0 = p(p+1) - (d-1)p - \ell(\ell+d-2)$$

$$\implies \quad p_\pm = \frac{d-2}{2} \pm \frac{1}{2}\sqrt{(d-2)^2 + 4\ell(\ell+d-2)}. \quad (1.13)$$

For a smooth solution, we must choose the positive sign p_+. On the other hand, as $r \to \infty$, (1.11) gives

$$r^2\psi'' + (d+1)r\psi' - m^2\psi = 0. \quad (1.14)$$

Once again, this is solved by a power law ansatz $\psi \propto r^{-\Delta}$, with

$$0 = \Delta(\Delta+1) - (d+1)\Delta - m^2$$

$$\implies \quad \Delta_\pm = \frac{d}{2} \pm \frac{1}{2}\sqrt{d^2 + 4m^2}. \quad (1.15)$$

Assuming that $m^2 \geq 0$ and $d \geq 2$, smoothness requires we choose the positive sign here also, $\Delta_+ = \Delta$. Since we now have boundary conditions at both $r = 0$ (in terms of ℓ) and $r = \infty$ (in terms of m), we expect that only certain values of ω will be allowed, so the spectrum is quantized. This is indeed what happens, with

$$\omega = \Delta + \ell + 2n \quad (1.16)$$

for $n = 0, 1, 2, \ldots$, as one can show by solving the full radial equation (1.11) explicitly in terms of Bessel functions and imposing the boundary conditions. For details, see [13].

6

These are the classical solutions. To quantize the field on this background, we introduce annihilation and creation operators $a_{n\ell\vec{m}}$ and $a_{n\ell\vec{m}}^\dagger$ for the corresponding modes, with commutation relations

$$[a_{n\ell\vec{m}}, a_{n\ell\vec{m}}^\dagger] = \delta_{nn'}\delta_{\ell\ell'}\delta_{\vec{m}\vec{m}'}. \tag{1.17}$$

The field expansion in the Heisenberg picture is then

$$\hat{\phi}(r, t, \Omega) = \sum_{n\ell\vec{m}} \left[f_{n\ell\vec{m}} a_{n\ell\vec{m}} + f_{n\ell\vec{m}}^* a_{n\ell\vec{m}}^\dagger \right], \tag{1.18}$$

where the f are mode functions

$$f_{n\ell\vec{m}}(r, t, \Omega) \propto \psi_{\omega_{n\ell}\ell}(r) e^{-i\omega_{n\ell}t} Y_{\ell\vec{m}}(\Omega).$$

In order to ensure unitarity, these are unit-normalized in the Klein-Gordon inner product:

$$\langle f, g \rangle = i \int_\Sigma \mathrm{d}^d y \, \sqrt{\gamma} n^\mu (g^* \partial_\mu f - f \partial_\mu g^*), \tag{1.19}$$

where Σ is any bulk Cauchy slice,[4] with induced metric γ and future-directed normal n^μ. Then the ground state of the corresponding Fock space is annihilated by all the $a_{n\ell\vec{m}}$, and we create excitations by acting with $a_{n\ell\vec{m}}^\dagger$. We can generalize to other (perturbatively weak) fields and interactions between them in the same fashion.

1.1.2 Conformal field theory

A *conformal field theory* CFT_d is a d-dimensional quantum field theory which is invariant under angle-preserving changes of coordinate. If the CFT is defined on a metric M with metric $g_{\mu\nu}[x]$ and coordinates x, the transformation $x \to x'(x)$ is conformal if

$$g'_{\mu\nu}[x'(x)] = g_{\alpha\beta}[x] \frac{\partial x^\alpha}{\partial x'^\mu} \frac{\partial x^\beta}{\partial x'^\nu} = \Omega(x)^{-2} g_{\mu\nu}[x], \tag{1.20}$$

---

[4]This is a surface such that every inextendible timelike curve in spacetime passes through it. Think of it as a horizontal slice of the cylinder, possibly with spacelike wobbles.

for some function $\Omega(x) = e^{-\omega(x)}$, where the first equation defines the metric $g'_{\mu\nu}[x']$ in the new coordinates, and the second gives a condition for the transformation to be conformal. We will typically consider Minkowski space $M = \mathbb{R}^{1,d-1}$ or the CFT on a cylinder $M = \mathbb{R} \times \mathbb{S}^{d-1}$, which are related by a conformal (stereographic) transformation. Let us consider Minkowski space explicitly, and set $g_{\mu\nu} = \eta_{\mu\nu}$.

To analyze conformal symmetry, we can consider infinitesimal transformations

$$x'(x) = x + \epsilon(x), \tag{1.21}$$

where we ignore quantities of order $O(\epsilon^2)$. Comparing the two expressions for $\eta'_{\mu\nu}$ in (1.20) and assuming $\Omega(x) = 1 - \omega(x) + O(\omega^2)$ is also infinitesimal, we obtain

$$\eta'_{\mu\nu} = \eta_{\alpha\beta}(\delta^\alpha_\mu - \partial^\alpha \epsilon_\mu)(\delta^\beta_\nu - \partial^\beta \epsilon_\nu) \approx \eta_{\mu\nu} - \partial_\mu \epsilon_\nu - \partial_\nu \epsilon_\nu$$

$$= (1 - 2\omega(x))\eta_{\mu\nu}$$

$$\implies \quad 2\omega(x)\eta_{\mu\nu} = \partial_\mu \epsilon_\nu + \partial_\nu \epsilon_\mu. \tag{1.22}$$

Contracting both sides of (1.22) gives $\partial_\mu \epsilon^\mu = \omega(x)d$, and substituting back in we find We can sneakily rewrite the second derivative $\partial_\mu \partial_\nu \epsilon_\rho$ using (1.22):

$$\partial_\mu \partial_\nu \epsilon_\rho = \frac{1}{2} \left[\partial_\mu(\partial_\nu \epsilon_\rho + \partial_\rho \epsilon_\nu) + \partial_\nu(\partial_\mu \epsilon_\rho + \partial_\rho \epsilon_\mu) - \partial_\rho(\partial_\mu \epsilon_\nu + \partial_\nu \epsilon_\mu) \right]$$

$$= \eta_{\nu\rho} \partial_\mu \omega + \eta_{\mu\rho} \partial_\rho \omega - \eta_{\mu\nu} \partial_\rho \omega. \tag{1.23}$$

Contracting with ∂^ρ and using $\partial_\mu \epsilon^\mu = \omega(x)d$ yields

$$[\eta_{\mu\nu} \partial^2 + (d-2)\partial_\mu \partial_\nu]\partial_\rho \epsilon^\rho = 0. \tag{1.24}$$

This is called the *conformal Killing equation*.

The conformal Killing equation is radically different for $d = 2$, so for the moment, we instead focus on $d > 2$. In this case, the LHS of (1.24) vanishes if $\epsilon(x)$ is at most

second-order in x, so we can write the general solution

$$\epsilon_\mu(x) = a_\mu - \sigma_{\mu\nu}x^\nu + \lambda x_\mu + b_\mu x^2 - 2x_\mu b_\beta x^\nu, \qquad (1.25)$$

for an antisymmetric matrix $\sigma_{\mu\nu} = -\sigma_{\nu\mu}$. We can interpret these matrices geometrically, and count the associated degrees of freedom. The vector a_μ represents the d-dimensional set of infinitesimal translations in $\mathbb{R}^{1,d-1}$. The antisymmetric matrix $\sigma_{\mu\nu}$ generates $d(d-1)/2$ independent infinitesimal Lorentz transformations (rotations and boosts), one for each pair of directions. The constant λ gives a *dilatation* or *scale transformation*, taking the infinitesimal form $x' = (1 + \lambda)x$. These exponentiate to give finite transformations of the form $x' = \lambda x$. Finally, the vector b_μ parameterizes a d-dimensional set of *special conformal transformations (SCT)*, with finite form[5]

$$x^\mu \to \frac{x^\mu + b^\mu x^2}{1 + 2b \cdot x + b^2 x^2}. \qquad (1.26)$$

The total number of generators is therefore

$$d + \frac{d(d-1)}{2} + 1 + d = \frac{(d+1)(d+2)}{2}.$$

We encountered this number earlier, in (1.7), where it counted the isometries of AdS, or equivalently, the Lorentz transformations of $\mathbb{R}^{2,d}$.

This is not a coincidence. In fact, the group of conformal transformation is precisely $\mathrm{SO}(2, d)$. To see this, we need to analyze the algebra of generators more carefully. To start with, consider the infinitesimal Lorentz transformations parameterized by $\sigma_{\alpha\beta}$, and all other coefficients set to zero. We can rewrite the infinitesimal shift in coordinates as a

---

[5]Exponentiating to obtain this is hard, but checking the infinitesimal expansion is consistent with (1.25) is straightforward.

sum over matrices $J_{(\beta\gamma)}$ called *generators*:[6]

$$
\begin{aligned}
x'^{\alpha} &= x^{\alpha} - \eta^{\alpha\beta}\sigma_{\beta\mu}x^{\mu} \\
&= (\delta^{\alpha}_{\mu} - \eta^{\alpha\beta}\sigma_{\beta\mu})x^{\mu} \\
&= \left(\delta^{\alpha}_{\mu} + \frac{i}{2}\sigma^{\beta\gamma}J_{(\beta\gamma)}{}^{\alpha}{}_{\mu}\right)x^{\mu},
\end{aligned}
\tag{1.27}
$$

where we have defined

$$
J_{(\beta\gamma)} = i(x_{\beta}\partial_{\gamma} - x_{\gamma}\partial_{\beta}).
\tag{1.28}
$$

Recall that a commutator of two matrices is the difference $[A, B] = AB - BA$. A little algebra confirms that the commutator of generators is

$$
[J_{(\mu\nu)}, J_{(\rho\sigma)}] = i(\eta_{\mu\rho}J_{(\nu\sigma)} + \eta_{\nu\sigma}J_{(\mu\rho)} - \eta_{\nu\rho}J_{(\mu\sigma)} - \eta_{\mu\sigma}J_{(\nu\rho)}).
\tag{1.29}
$$

These commutation relations define the Lie algebra $\mathfrak{so}(1, d-1)$.

More generally, we can define a generator G associated with some family of infinitesimal transformations κ^a by

$$
x'^{\alpha} = x^{\alpha} - i\kappa^a G_{(a)}x^{\alpha}.
$$

Thus, the generators $J_{(\beta\gamma)}$ are associated with $\sigma^{\beta\gamma}$, with a factor of $1/2$ coming from antisymmetry. For infinitesimal translations,

$$
x'^{\alpha} = x^{\alpha} + a^{\alpha} = x^{\alpha} - ia^{\beta}P_{(\beta)}x^{\alpha},
\tag{1.30}
$$

for the generator $P_{(\beta)} = -i\partial_{\beta}$. Similarly, dilatations (associated with λ) have generator

$$
D = -ix^{\alpha}\partial_{\alpha},
\tag{1.31}
$$

while SCTs are generated by

$$
K_{(\alpha)} = -i(2x_{\alpha}x^{\beta}\partial_{\beta} - x^2\partial_{\alpha}).
\tag{1.32}
$$

---

[6]Note that $(\beta\gamma)$ labels a generator, and not an entry in a matrix. These entries will be indicated without parentheses, e.g. $J_{(\beta\gamma)}{}^{\alpha}{}_{\mu}$. We will continue to use the Einstein summation convention with generator labels.

It is a standard exercise to show that, in addition to (1.29), these generators obey the commutation relations

$$[D, P_{(\alpha)}] = iP_{(\alpha)} \tag{1.33}$$

$$[D, K_{(\alpha)}] = -iK_{(\alpha)} \tag{1.34}$$

$$[K_{(\alpha)}, P_{(\beta)}] = 2i(\eta_{\alpha\beta}D - J_{(\alpha\beta)}) \tag{1.35}$$

$$[K_{(\alpha)}, J_{(\beta\gamma)}] = i(\eta_{\alpha\beta}K_{(\gamma)} - \eta_{\alpha\gamma}K_{(\beta)}) \tag{1.36}$$

$$[P_{(\alpha)}, J_{(\beta\gamma)}] = i(\eta_{\alpha\beta}P_{(\gamma)} - \eta_{\alpha\gamma}P_{(\beta)}). \tag{1.37}$$

This defines the Lie algebra of infinitesimal conformal transformations.

There is a beautiful way to reorganize this algebra, however, which makes its isomorphism to $\mathfrak{so}(2, d)$ manifest. Define $L_{(\alpha\beta)} = J_{(\alpha\beta)}$, and

$$L_{(-1,d+1)} = D \tag{1.38}$$

$$L_{(-1,\alpha)} = \frac{1}{2}(P_{(\alpha)} - K_{(\alpha)}) \tag{1.39}$$

$$L_{(d+1,\alpha)} = \frac{1}{2}(P_{(\alpha)} + K_{(\alpha)}). \tag{1.40}$$

Then the new set of generators, $L_{(MN)}$, can be shown to obey

$$[L_{(MN)}, L_{(RS)}] = i(\eta_{MR}L_{(NS)} + \eta_{NS}L_{(MR)} - \eta_{NR}L_{(MS)} - \eta_{MS}L_{(NS)}). \tag{1.41}$$

These are exactly the commutation relations for the Lorentz algebra $\mathfrak{so}(2, d)$. Exponentiating, we find that the group of conformal symmetries of $\mathbb{R}^{1,d-1}$ is $SO(2, d)$, as claimed. Since the cylinder $\mathbb{R} \times \mathbb{S}^{d-1}$ is stereographically equivalent to flat space, it also has conformal symmetry group $SO(2, d)$.

Let us now turn to field, assuming the reader is familiar with relativistic quantum field theory. A field ϕ is an irreducible representation (irrep) of the conformal symmetry group. As usual in field theory, we can use the method of induced representations, analyzing transformations which fix the position of the field ϕ at $x = 0$ and later acting with the translation generators $P_{(\alpha)}$. Since conformal symmetry includes the Lorentz group, we can

11

assume the field transforms under Lorentz generators via finite-dimensional representation $\mathcal{J}_{(\alpha\beta)}$, i.e.

$$[J_{(\alpha\beta)}, \phi(0)] = -\mathcal{J}_{(\alpha\beta)}\phi(0). \tag{1.42}$$

It remains to determine the behaviour under D and $K_{(\alpha)}$. We will assume ϕ is an eigenstate of D, with

$$[D, \phi(0)] = -i\Delta\phi(0) \tag{1.43}$$

for a constant Δ called the *scaling dimension*. This means that under dilatations $x' = \lambda x$, the field transforms as

$$\phi'(x') = \lambda^{-\Delta}\phi(x). \tag{1.44}$$

Finally, we define a *primary field* as one annihilated by $K_{(\alpha)}$, i.e.

$$[K_{(\alpha)}, \phi(0)] = 0. \tag{1.45}$$

From the commutation relations (1.33) and (1.34), we see that applying $P_{(\alpha)}$ increases Δ by one unit, while $K_{(\alpha)}$ decreases it. We will show in a moment that there is a lower bound on Δ, so that in any irrep, the lowest weight field is annihilated by $K_{(\mu)}$. These are precisely the primary fields, and the rest of the irrep is generated by acting with momentum operators. This gives the possible field content for our CFT.

To see where this bound on Δ comes from, we need an important property of CFTs called the *state-operator correspondence*. We first analytically continue to Euclidean time, $\tau = -it$. We then have a CFT defined on the Euclidean cylinder $M_E = \mathbb{R} \times \mathbb{S}^{d-1}$, with conformal symmetry group $\mathrm{SO}(1, d)$.[7] We can map the Euclidean cylinder to $\mathbb{R}^d$ minus a hole at the origin via $\varsigma = e^\tau$:

$$\mathrm{d}s^2 = \mathrm{d}\tau^2 + \mathrm{d}\Omega_{d-1}^2 = \frac{1}{\varsigma^2}(\mathrm{d}\varsigma^2 + \varsigma^2\mathrm{d}\Omega_{d-1}^2). \tag{1.46}$$

Up to an (irrelevant) overall conformal factor, ς acts as a polar radial variable, with the origin ς corresponding to $\tau = -\infty$. If the theory is quantized on the sphere, then Euclidean time evolution is given by dilatation, $\varsigma' = e^\lambda\varsigma = e^{\tau+\lambda}$, so we can interpret the dilatation

---

[7]In general, the conformal group for a manifold $\mathbb{R}^{p,q}$ is $\mathrm{SO}(p+1, p+q)$.

operator D as the operator implementing time evolution, i.e. the Hamiltonian. It follows that the energy of a field is simply related to the scaling dimension, $E = \Delta + E_0$ for ground state energy E_0. Thus, to obtain a stable theory with a Hamiltonian bounded below, we need a lower bound on Δ.

The state-operator correspondence itself is simple. If we add a point at the origin $\varsigma = 0$ ($\tau = -\infty$), we can insert an operator $\mathcal{O}(0)$ there, and evolve by dilatation to obtain a state $|\mathcal{O}(\varsigma)\rangle$ on the sphere at any later Euclidean time. We can view this as a Euclidean path integral over the solid ball which prepares the state. If our fields are collectively labelled by ϕ, and $|\Phi\rangle$ ranges over a basis of eigenstates for classical field configurations with $\hat{\Phi}(x)|\Phi\rangle = \Phi(x)|\Phi\rangle$, then

$$\langle\Phi|\mathcal{O}(\varsigma)\rangle = \int_{\varsigma=0}^{\phi(\varsigma)=\Phi} \mathcal{D}\phi\, e^{-S[\phi]}\mathcal{O}(0), \tag{1.47}$$

where we integrate over all classical configurations for ϕ on the ball of radius ς. This map is invertible, since we can contract a state on the boundary of the ball back to the origin by dilatation as well.

The Euclidean path integral can be used to define *correlation functions* (or *correlators* or *n-point functions*) more broadly:

$$\langle\mathcal{O}_1(x_1)\cdots\mathcal{O}_n(x_n)\rangle = \frac{1}{Z}\int \mathcal{D}\phi\, e^{-S[\phi]}\mathcal{O}_1(x_1)\cdots\mathcal{O}_n(x_n), \tag{1.48}$$

where we integrate over all field configurations and normalize by the partition function

$$Z = \int \mathcal{D}\phi\, e^{-S[\phi]}, \tag{1.49}$$

so that $\langle 1 \rangle = 1$. If the $\mathcal{O}_i$ are primary fields, then conformal symmetry forces the correlators to be constrained functions of the separations $x_{ij} = |x_i - x_j|$ only. For instance, one-point functions vanish, with

$$\langle\mathcal{O}(x)\rangle = 0, \tag{1.50}$$

since this is the only result consistent with scaling symmetry, $\mathcal{O} \to \lambda^{-\Delta}\mathcal{O}$ under $x \to \lambda x$.

Similarly, for the two-point function we have [12]

$$\langle \mathcal{O}(x)\mathcal{O}(y)\rangle = \frac{C_\mathcal{O}}{|x-y|^{2\Delta}} \tag{1.51}$$

for some constant $C_\mathcal{O}$, where Δ is the scaling dimension of $\mathcal{O}$. Typically, we normalize our fields so that $C_\mathcal{O} = 1$. If the fields have different scaling dimension, the two-point function $\langle \mathcal{O}_1 \mathcal{O}_2 \rangle$ vanishes.[8]

The three-point function is more interesting. Conformal symmetry now dictates [12]

$$\langle \mathcal{O}_1(x_1)\mathcal{O}_2(x_2)\mathcal{O}_3(x_3)\rangle = \frac{C_{123}}{x_{12}^{\Delta_1+\Delta_2-\Delta_3}x_{23}^{\Delta_2+\Delta_3-\Delta_1}x_{13}^{\Delta_3+\Delta_1-\Delta_2}} \tag{1.52}$$

for a constant C_{123}. This expression arises from a rather different perspective using the *operator product expansion* (OPE). In this case, we start by assuming an associative algebra of the operators of our theory, taking the form

$$\mathcal{O}_1(x_1)\mathcal{O}_2(x_2) = \sum_j \hat{C}_{12j}[x_{12}]\mathcal{O}_j(x_2), \tag{1.53}$$

where $\mathcal{O}_j$ ranges over all fields primary fields of the CFT, and $\hat{C}_{12j}[x_{12}]$ is a differential operator depending on the separation x_{12}. This will include for instance operators of the form

$$\mathcal{O}^{(n,\vec{\ell})} = \mathcal{O}_1 \partial^{2n}\partial_{\mu_1}\cdots\partial_{\mu_\ell}\mathcal{O}_2 \tag{1.54}$$

called *double-trace operators*. Substituting this into the three-point function and using the result for the two-point function, we obtain

$$\langle \mathcal{O}_1(x_1)\mathcal{O}_2(x_2)\mathcal{O}_3(x_3)\rangle = \sum_j \hat{C}_{12j}[x_{12}]\langle \mathcal{O}_j(x_2)\mathcal{O}_3(x_3)\rangle = \hat{C}_{123}[x_{12}](x_{23}^{-2\Delta_3}).$$

We can insert the OPE in higher-point correlator functions as well.

---

[8]This is easiest to see by applying the state-operator correspondence to the expectation value $\langle \mathcal{O}_1 D\mathcal{O}_2\rangle$.

Conformal field theory in two dimensions

In $d = 2$, the conformal Killing equation (1.24) simplifies considerably. Matters are clearer in Euclidean signature, so we use coordinates (x^0, x^1) and change $\eta_{\mu\nu} \to \delta_{\mu\nu}$, the identity matrix. The explicit components of (1.22) then give

$$\partial_0 \epsilon_1 = -\partial_1 \epsilon_0, \qquad \partial_0 \epsilon_0 = \partial_1 \epsilon_1. \tag{1.55}$$

These are precisely the *Cauchy-Riemann equations* of complex analysis. We are led to to recast out two coordinates as arguments of a single complex variable $z = x^0 + ix^1$, with $\epsilon = \epsilon^0 + i\epsilon^1$ giving rise to a conformal transformation just in case it is a holomorphic function of z. Similarly, $\bar{\epsilon} = \epsilon^0 - i\epsilon^1$ is anti-holomorphic.

We can thus perform a Laurent expansion[9] of $\epsilon(z)$ around $z = 0$:

$$\epsilon(z) = -\sum_{n \in \mathbb{Z}} c_n z^{n+1}, \tag{1.56}$$

and similarly for $\bar{\epsilon}(\bar{z})$. Since $z' = z + \epsilon$, we can consider the infinitesimal change in any field ϕ (taken to be spinless for simplicity) as

$$\delta\phi = \phi(z + \epsilon) - \phi(z) \approx \epsilon \partial_z \phi = -\sum_n c_n z^{n+1} \partial_z \phi. \tag{1.57}$$

Thus, each term c_n is associated with a differential operator

$$\ell_n = -z^{n+1} \partial_z =: -z^{n+1} \partial \tag{1.58}$$

which generates the corresponding infinitesimal deformation on fields, and similarly for $\bar{\ell}_n = -\bar{z}^{n+1} \partial_{\bar{z}} =: -\bar{z}^{n+1} \bar{\partial}$. A short calculation shows that these generators obey the *Witt algebra*

$$[\ell_n, \ell_m] = (m - n)\ell_{m+n}, \quad [\bar{\ell}_n, \bar{\ell}_m] = (m - n)\bar{\ell}_{m+n}, \quad [\ell_n, \bar{\ell}_m] = 0. \tag{1.59}$$

---

[9] You might argue that holomorphic implies analytic, so we should have a power series. We will in fact work on the Riemann sphere $\mathbb{C} \cup \{\infty\}$, and relax the condition of holomorphy to meromorphy.

15

The low-lying generators have a simple interpretation. First, ℓ_{-1} generates translations, while ℓ_0 generates rotations and scaling. Finally, ℓ_1 gives special conformal transformations, since $-cz^2$ is the infinitesimal version of $z/(cz+1)$, an instance of (1.26). Thus, along with their antiholomorphic counterparts, $\{\ell_{-1}, \ell_0, \ell_1\}$ give rise to the global conformal group we have already encountered,[10] but in $d = 2$. The remaining infinite set of generators have no parallel in higher dimensions, and are *local* in the sense that they do not map the complex plane (or Riemann sphere) to itself.

When we quantize the theory, we change the generators ℓ_n acting on classical fields to generators L_n acting on quantum fields. Quantum effects change their relations so that they instead satisfy the *Virasoro algebra*

$$[L_n, L_m] = (m - n)L_{m+n} + \frac{c}{12}m(m^2 - 1)\delta_{m+n,0}, \tag{1.60}$$

and similarly for $\bar{L}_n$. This is almost the Witt algebra (1.59), but there is a new term proportional to a constant c, called the *central charge*, associated with the theory.

We will briefly outline the physical meaning of c and how it is derived, but refer the curious reader to [12] for full details. Recall Noether's theorem, which states that every continuous symmetry gives rise to a conserved current. The current associated with translation is the stress-energy tensor,

$$T_{\mu\nu} = -\frac{2}{\sqrt{|g|}}\frac{\delta S_{\mathrm{CFT}}}{\delta g^{\mu\nu}}, \tag{1.61}$$

where S_{CFT} is the action and $g_{\mu\nu}$ a dynamical background metric. For a scale transformation, $\delta g^{\mu\nu} = -2\omega g^{\mu\nu}$ for fixed ω and hence

$$\delta S = -\int \frac{\delta S_{\mathrm{CFT}}}{\delta g^{\mu\nu}}\delta g^{\mu\nu} = -\omega \int \sqrt{|g|}T^\mu_\mu. \tag{1.62}$$

By definition, the action is invariant, $\delta S = 0$, and hence the stress-energy tensor is traceless: $T^\mu_\mu = 0$. This holds in any dimension, but on the Euclidean plane, this translates into

---

[10] Put differently, they generate Möbius transformations $\epsilon(z) = (az+b)/(cz+d)$, the rigid rotations of the Riemann sphere. Note also that the infinitesimal Möbius transformations $\mathfrak{sl}(2,\mathbb{C})$ technically give a double cover of the infinitesimal global symmetry group, $\mathfrak{so}(1,3)$.

the requirement that the non-vanishing components of the stress-energy are holomorphic, $T_{zz}(z) = T(z)$, and anti-holomorphic, $T_{\bar{z}\bar{z}}(\bar{z}) = \overline{T}(\bar{z})$.

We can show that these holomorphic and anti-holomorphic fields give rise to conserved currents. For a holomorphic deformation $\delta z = \epsilon(z)$, for instance, we have

$$J^{\bar{z}} = T(z)\epsilon(z), \quad J^z = 0. \tag{1.63}$$

It immediately follows that this is conserved, with $\partial_\mu J^\mu = \bar{\partial} J^{\bar{z}} = 0$. Similar statements hold for anti-holomorphic deformations. Consider the special case $\epsilon_n(z) = z^{n+1}$. The plane coordinates are related to coordinates on the cylinder by $z = e^{-iw}$, with $w = \theta + i\tau$ for $\theta \in \mathbb{S}^1$ and $\tau \in \mathbb{R}$. The Jacobian is $2\pi i$. Hence, the conserved charge associated with ϵ_n on the cylinder is given by the integral:

$$Q_n = \frac{1}{2\pi i} \oint dz\, T(z) z^{n+1}. \tag{1.64}$$

But this conserved charge is precisely the generator ℓ_n in the classical theory, or L_n in the quantum theory. We can therefore expand the stress-energy tensor as

$$T(z) = \sum_{n \in \mathbb{Z}} L_n z^{-(n+2)}, \tag{1.65}$$

using the residue theorem and (1.64) with $Q_n = L_n$.

In the quantum theory, the two components of the stress-energy tensor are promoted to operators. Some gymnastics [12] shows that the OPE is

$$T(z)T(w) = \frac{c/2}{(z-w)^4} + \frac{2T(w)}{(z-w)^2} + \frac{\partial T(w)}{z-w} + O((z-w)^0) \tag{1.66}$$

for some constant c depending on the theory, and consistent with the general expression (1.53). For instance, if we have some number of free bosonic fields, then c simply counts them, so it can be viewed as a measure of the local degrees of freedom. Finally, we can evaluate the commutator of Virasoro generators using (1.66) and (1.65) to find (after much

omitted algebra) that

$$[L_m, L_n] = \left(\oint \frac{\mathrm{d}w}{2\pi i} \oint \frac{\mathrm{d}z}{2\pi i} - \oint \frac{\mathrm{d}z}{2\pi i} \oint \frac{\mathrm{d}w}{2\pi i} \right) z^{m+1} w^{n+1} T(z) T(w)$$
$$= (m - n) L_{m+n} + \frac{c}{12} m(m^2 - 1) \delta_{m+n,0},$$

as claimed above.

1.1.3 The AdS/CFT correspondence

Having described both sides of the AdS/CFT equation, we can finally state what exactly the equals sign means. The correspondence was first conjectured as an equivalence between Type IIB superstring theory on $\mathrm{AdS}_5 \times \mathbb{S}^5$ and $\mathcal{N} = 4$ supersymmetric Yang-Mills theory on $\mathbb{R}^{1,3}$ with gauge group $\mathrm{SU}(N)$ [8, 9, 10]. We will focus on the simpler "bottom-up" version of the proposal, but for an expository overview of the stringy version, see [11, 13]. We have already seen that AdS_{d+1} has isometry group $\mathrm{SO}(d, 2)$. This is also the group of conformal symmetries of $\mathbb{R} \times \mathbb{S}^{d-1}$, which happens to lie at the conformal boundary of global AdS. In terms of matter content, we considered fields propagating on an AdS background, and conformal fields which transform in irreps of the conformal group. A shared ground state symmetry, and objects which transform according to this symmetry, furnish the natural ingredients for a duality.

Recall from (1.15) that, for a scalar field ϕ of mass m propagating on an AdS_{d+1} background, its near-boundary behaviour was

$$\phi(r, t, \Omega) \sim r^{-\Delta} \phi_{(0)}(t, \Omega), \quad \Delta = \frac{1}{2} \left(d + \sqrt{d^2 + 4m^2 L_{\mathrm{AdS}}^2} \right).$$

We did not choose the symbol Δ by accident, and indeed, according to the correspondence, this field is *dual* to a scalar CFT operator $\mathcal{O}$ with scaling dimension Δ. Moreover, we can think of the limit

$$\phi_{(0)}(t, \Omega) = \lim_{r \to \infty} r^{\Delta} \phi(r, t, \Omega) \tag{1.67}$$

as specifying the value of a source for the CFT operator $\mathcal{O}$. This relation between sources

and boundary values of bulk fields is called the *extrapolate dictionary*.

More generally, scattering problems in gravity are dual to correlators in the CFT. To make this precise, let us go to Euclidean signature and introduce a powerful object called the *generating functional* for computing correlators in the field theory:

$$Z_{\text{CFT}}[\phi_{(0)}] = \left\langle \exp\left(-\sum_i \int \mathrm{d}^d x\, \phi_{(0)}^i(x)\mathcal{O}_i(x)\right)\right\rangle, \tag{1.68}$$

where the $\mathcal{O}_i$ are and $\phi_{(0)}^i$ are the corresponding sources. We can compute CFT correlators by functionally differentiating Z_{CFT} with respect to sources and then setting them to 0:

$$\langle\mathcal{O}_1(t_1,\Omega_1)\cdots\mathcal{O}_n(t_n,\Omega_n)\rangle = \frac{(-1)^n}{Z_{\text{CFT}}[0]}\frac{\delta^n Z_{\text{CFT}}[\phi_{(0)}]}{\delta\phi_{(0)}^1(t_1,\Omega_1)\cdots\delta\phi_{(0)}^n(t_n,\Omega_n)}\bigg|_{\phi_{(0)}=0}. \tag{1.69}$$

We propose to compute this a second way, as a gravitational scattering problem in AdS:

$$\langle\mathcal{O}_1(t_1,\Omega_n)\cdots\mathcal{O}_n(t_n,\Omega_n)\rangle = \langle\mathcal{O}_1(t_1,\Omega_n)\cdots\mathcal{O}_n(t_n,\Omega_n)\rangle_{\text{AdS}}, \tag{1.70}$$

where the RHS is a gravitational path integral analogous to (1.48):

$$\langle\mathcal{O}_1(t_1,\Omega_n)\cdots\mathcal{O}_n(t_n,\Omega_n)\rangle_{\text{AdS}} = \int \mathcal{D}g\,\mathcal{D}\phi\, e^{-S_{\text{AdS}}[\phi,g]}\mathcal{O}_1(t_1,\Omega_n)\cdots\mathcal{O}_n(t_n,\Omega_n) \tag{1.71}$$

with $r^\Delta\phi(r,t,\Omega)\to\mathcal{O}(t,\Omega)$ as per the extrapolate dictionary, ϕ the matter configurations subject to the extrapolate constraint, and g Euclidean metrics with the appropriate conformal boundary. In fact, (1.71) can be extracted by functional differentiation just like the CFT correlator, but from the gravitational partition function subject to boundary conditions:

$$Z_{\text{AdS}}[\phi_{(0)}] = \int_{r^\Delta\phi\to\phi_{(0)}} \mathcal{D}g\,\mathcal{D}\phi\, e^{-S_{\text{AdS}}[\phi,g]}. \tag{1.72}$$

This immediately suggests a duality between the CFT generating functional and the gravitational path integral:

$$Z_{\text{CFT}}[\phi_{(0)}] = Z_{\text{AdS}}[\phi_{(0)}]. \tag{1.73}$$

19

This form of the AdS/CFT correspondence is called the *GPKW dictionary* [9, 10].

We have been deliberately vague about the regime under which we expect (1.73) to hold. In fact, we can regard it as a *non-perturbative definition* of the quantum gravity path integral Z_{AdS} in terms of the better-understood CFT generating functional Z_{CFT}. To see the virtue of this perspective, note that when the physics is highly stringy, there is currently no other known way to compute Z_{AdS} (Type IIB superstring theory on an AdS background at strong coupling) so this definition seems reasonable! But for this to be a reasonable definition of the UV, we should confirm it behaves reasonably in the IR. There, we can check against expectations from the relevant low-energy effective field theory, where quantum fields propagate over a curved background metric that they are not sufficiently strong to alter.

Since the gravitational action has a prefactor $\propto 1/G$, where G is Newton's constant, we will focus on the *semiclassical limit $G \to 0$*.[11] This means that the Euclidean gravitational path integral (1.72) can be evaluated using the saddlepoint approxiimation as a sum over on-shell configurations ϕ_ℓ^*, g_ℓ^*:

$$Z_{\mathrm{AdS}} = \int \mathcal{D}g \, \mathcal{D}\phi \, e^{-S_{\mathrm{AdS}}[\phi,g]} \sim \sum_\ell e^{-S_{\mathrm{AdS}}[\phi_\ell^*, g_\ell^*]}. \tag{1.74}$$

For small G, this will be dominated by the solution of lowest action, so we can simply solve the equations of motion and compare the action of different solutions to see which is semiclassically favoured.

CFTs with semiclassical duals

We will give a short qualitative summary of the class of CFTs which are believed to have semiclassical duals [17, 16, 14]. First, if our theory has free or perturbatively coupled fields, then any operator $\mathcal{O}$ will interact with a host of higher-spin conserved currents. For instance, a scalar ψ schematically couples to $\psi\partial\psi, \psi\partial^2\psi$, and so on, with each derivative increasing the spin. On the gravity side, these will manifest as a cascade of higher-spin

---

[11]The coupling constant for the graviton self-interaction is $\sqrt{G}$. The semiclassical limit means we are treating the gravitational background as classical. This does not mean semiclassical string theory.

particles, or equivalently, excited string modes. In a good semiclassical dual, we don't see this physics at low energies, so the naive perturbative expansion must break down, with tree-level diagrams comparable to loops. Thus, the CFT is *strongly coupled*. For similar reasons, we expect that the CFT operators dual to stringy physics only appear at high energies, so that the spectrum of particles has a "gap" between operators dual to low-energy fields and those dual to strings. This also requires strong coupling, since otherwise the light fields cascade into heavy ones. We will say such a CFT is *gapped*, with strong coupling left implicit.

As discussed above, a single semiclassical background metric requires $G \to 0$. It turns out that, in general, $G \sim 1/N$, where N measures the local degrees of freedom in the CFT.[12] Thus, a semiclassical dual requires large N, or rather, a family of CFTs labelled by N in which we take the limit $N \to \infty$. Since the spectrum has a gap, there will need to be many states crammed into higher energies, a statement we make more precise at the end of §1.1.4.

We conclude with a slightly more formal statement tying the two requirements together, following the clear treatment in [14]. A *gapped large-N* CFT_d is a family of d-dimensional CFTs, labelled by N, such that:

- There is a set of "single-trace" primaries $\{\mathcal{O}_i\}$ with scaling dimensions $\{\Delta_i\}$ in the CFT with the property that, if normalized so that $\langle \mathcal{O}\mathcal{O} \rangle \sim N^0$, then three-point functions are suppressed by N:

$$\langle \mathcal{O}_i \mathcal{O}_j \mathcal{O}_k \rangle \lesssim \frac{1}{N}. \tag{1.75}$$

  These single-trace primaries are dual to low-energy bulk fields ϕ_i, and acting with $\mathcal{O}_i$ creates a single-particle state in the bulk.

- The CFT energy momentum tensor $T_{\mu\nu}$ is the only single-trace primary with spin 2 and scaling dimension d, with a two-point function $\langle TT \rangle \sim N$.[13] This means

---

[12]One way to motivate this relation is to observe that, from the Bekenstein-Hawking formula (1.90) for black hole entropy to be proved below, we have $S \propto 1/G$. At the same time, we expect $S \propto N$, since each Planck area on the horizon presumably has N associated degrees of freedom.

[13]As an example, the TT OPE (1.66) in $d = 2$ leads to $\langle TT \rangle \propto c$, so $N \propto c$ here. The Brown-Henneaux

$T_{\mu\nu}$ is dual to the graviton and its two-point function is proportional to the expected gravitational coupling $1/G$.

- For any $n = O(N^0)$ set of single-trace primaries $\{\mathcal{O}_{i_1}, \ldots, \mathcal{O}_{i_n}\}$, there is an associated multi-trace primary $\mathcal{O}_{i_1, \cdots, i_n}$ with scaling dimension $\Delta_1 + \cdots + \Delta_n$. Acting with multi-trace primaries creates multi-particle states in the bulk.

- At leading order in $1/N$, correlators are "free" and can be computed by Wick contraction, with corrections of order $N^{-(n-2)}$ for n operators. This is the statement that bulk interactions are perturbatively weak, with interactions suppressed by G.

- Finally, all operators with $\Delta = O(N^0)$ are single- or multi-trace primaries and their descendants. This is simply the requirement of a gap.

When these conditions are satisfied, there is a low-energy semiclassical description in terms of weakly coupled fields ϕ_i propagating in the bulk [17]. The GKPW dictionary (1.73) relates single- and multi-trace primaries to these bulk duals. Quantizing the bulk fields ϕ_i gives a multi-particle Fock space, where acting with dual CFT operators creates particles in the bulk. The Fourier modes of these operators are precisely the creation and annihilation operators discussed at the end of §1.1.1.

1.1.4 Black holes and wormholes

The GKPW form the dictionary (1.73) was given for operators acting on the CFT vacuum state on the cylinder $M = \mathbb{R} \times \mathbb{S}^{d-1}$, and bulk fields propagating on a pure AdS background $\mathcal{M}$, with boundary $\partial\mathcal{M} = M$ (and the corresponding induced metric h). In general, our gravitational path integral requires boundary conditions not only for the matter fields ϕ, but the metric g. This suggests a generalization of GKPW, where we replace the cylinder by some other manifold M with metric h_M,[14] and the vacuum state on the cylinder with

---

relation [18] explicitly gives $c = 3L_{\text{AdS}}/2G$. We therefore have $N \sim 1/G$ as expected.

[14]There may be many metrics on M, so the conformal class of h_M is implicitly specified here.

the vacuum state $|\Omega_M\rangle$ of the CFT on M:

$$Z_{\text{AdS}}[\phi_{(0)}, M] = \int_{r^{\Delta}\phi \to \phi_{(0)}, g \to h_M} \mathcal{D}g\, \mathcal{D}\phi\, e^{-S_{\text{AdS}}[\phi, g]} \tag{1.76}$$

$$Z_{\text{CFT}}[\phi_{(0)}, M] = \left\langle \exp\left(-\sum_i \int \mathrm{d}^d x\, \phi^i_{(0)}(x) \mathcal{O}_i(x) \right) \right\rangle_{\Omega_M}, \tag{1.77}$$

with a correspondence

$$Z_{\text{AdS}}[\phi_{(0)}, \partial\mathcal{M} = M] = Z_{\text{CFT}}[\phi_{(0)}, M]. \tag{1.78}$$

Note that we are working in Euclidean signature. There are various subtleties in going to Lorentzian signature. Roughly speaking, however, we can think of Euclidean path integrals (including the sources) as defining states. To understand the corresponding Lorentzian correlators, we solve the bulk Euclidean equations of motion, slice them along a moment-of-time symmetry,[15] then analytically continue our expression for propagators to real time. This Lorentzian evolution is capped off by (conjugate) Euclidean bulk solutions at initial and final times, since these are providing the bra and ket in our correlator. See for instance [19, 20] for more details.

The most important application of this extended correspondence is to black holes. Consider the *AdS-Schwarzschild black hole*, with metric:

$$\mathrm{d}s^2 = -f(r)\,\mathrm{d}t^2 + \frac{\mathrm{d}r^2}{f(r)} + r^2\,\mathrm{d}\Omega_{d-1}^2, \tag{1.79}$$

where

$$f(r) = 1 + \frac{r^2}{L_{\text{AdS}}^2} - \frac{\mu_d}{r^{d-2}}. \tag{1.80}$$

For $d > 2$,

$$\mu_d = r_H^{d-2}\left(\frac{r_H^2}{L_{\text{AdS}}^2} + 1 \right) = \frac{16\pi GM}{(d-1)S^{d-1}},$$

---

[15]Also called a time-reflection symmetry, where derivatives with respect to the Killing time vanish. We can then analytically continue time derivatives without introducing unphysical factors of i.

where r_H is the *horizon* or *Schwarzschild radius*, satisfying $f(r_H) = 0$, M is the mass of the black hole, and S^{d-1} the volume of $\mathbb{S}^{d-1}$. Since $f(r) \approx r^2$ at large r, this clearly approaches the metric (1.6), so in Lorentzian signature it is asymptotically AdS.

If we Wick rotate to Euclidean signature $\tau = -it$, the metric becomes

$$ds_E^2 = f(r)\,d\tau^2 + \frac{dr^2}{f(r)} + r^2\,d\Omega_{d-1}^2. \tag{1.81}$$

The function $f(r) \to 0$ linearly at the horizon, so we can expand

$$f(r) \approx f'(r_H)(r - r_H) + O((r - r_H)^2). \tag{1.82}$$

Substituting into (1.81) and performing a near-horizon expansion, we obtain

$$ds_E^2 = f'(r_H)(r - r_H)\,d\tau^2 + \frac{dr^2}{f'(r_H)(r - r_H)} + \cdots.$$

We can go to polar coordinates by setting

$$\rho^2 = \frac{4(r - r_H)}{f'(r_H)}, \qquad \varphi = \frac{1}{2}f'(r_H)\tau, \tag{1.83}$$

so that the near-horizon Euclidean metric is

$$ds_E^2 = \rho^2\,d\varphi^2 + d\rho^2 + \cdots. \tag{1.84}$$

Thus, the Euclidean black hole has the near-horizon geometry of a disk. We picture this in Fig. 1.2 (left).

If φ subtends more or less than 2π, we will have a conical excess or deficit, which creates a sharp point in the fabric of spacetime and thus sources stress-energy.[16] Since there is no matter (away from the true singularity at $r = 0$), smoothness requires that φ have period 2π, and hence from (1.83), the Euclidean time $\tau \sim \tau + \Delta\tau$ is periodic with

---

[16]Think of slicing an angular wedge out of a piece of paper and gluing edges to obtain a cone. Similarly, a conical excess is a sort of inverse cone, bulging away from a dimple.

period

$$\Delta\tau = \beta = \frac{4\pi}{|f'(r_H)|} = \frac{4\pi r_H L_{\text{AdS}}^2}{(d-2)L_{\text{AdS}}^2 + dr_H^2}.$$ (1.85)

According to the lore of quantum statistical mechanics, a system with periodic imaginary time is in the canonical thermal state

$$\rho_\beta = \frac{1}{Z[\beta]} e^{-\beta\hat{H}}, \qquad Z[\beta] = \text{Tr}\left[e^{-\beta\hat{H}}\right] = \sum_E e^{-\beta E}.$$ (1.86)

with inverse temperature $\beta = 1/T$. This is a quick way to arrive at Hawking's startling insight that black holes are thermal systems [21, 22, 23].

This will turn out to be very natural in AdS/CFT. First, note that from the periodicity $\tau \in \mathbb{S}_\beta^1$, the boundary geometry of our Euclidean black hole is $M = \mathbb{S}_\beta^1 \times \mathbb{S}^{d-1}$. Thus, our extended GKPW prescription (1.78) suggests $Z_{\text{AdS}}[\partial\mathcal{M} = \mathbb{S}_\beta^1 \times \mathbb{S}^{d-1}] = Z_{\text{CFT}}[\mathbb{S}_\beta^1 \times \mathbb{S}^{d-1}]$, where we have set sources to zero. The vacuum state of a Euclidean CFT on $\mathbb{S}_\beta^1 \times \mathbb{S}^{d-1}$ is simply the canonical thermal state on $\mathbb{S}^{d-1}$. Thus, the black hole is dual to the thermal state, first suggested by Witten [24].
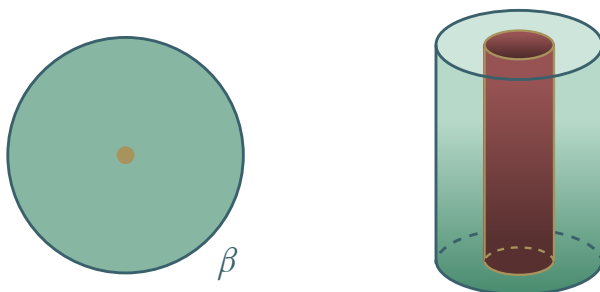
Figure 1.2: *Left.* The Euclidean disk with boundary $\mathbb{S}_\beta^1 \times \mathbb{S}^{d-1}$ preparing the black hole. *Right.* The AdS-Schwarzschild black hole in Lorentzian signature.

We should, however, be a little more careful. Our path integral will involve sums over arbitrary geometries g with boundary $\mathbb{S}_\beta^1 \times \mathbb{S}^{d-1}$. We not only need to take the semiclassical limit $G \to 0$ to obtain the Schwarzschild solution, we need to ensure that this has lowest action and therefore dominates the path integral (1.74). This will be non-trivial, since there is another vacuum solution to Einstein's equations with this boundary: *thermal AdS*,

which is simply the Euclidean version of (1.6) with imaginary time periodically identified, $\tau \sim \tau + \beta$, and (perturbatively weak) fields in a thermal state. As shown by Hawking and Page for $d + 1 = 4$ [25] and generalized by Witten to arbitrary dimension [24], the actions for both thermal AdS and the black hole are proportional to volumes of (Euclidean) spacetime. Both will therefore diverge, but we can compute the difference at some fixed radius R (with the periodicity of thermal AdS adjust to ensure the geometries match) and then take $R \to \infty$. The end result is finite:

$$\Delta S_{\text{AdS}} = \frac{d}{8\pi G} \lim_{R \to \infty} [V_{\text{BH}}(R) - V_{\text{thAdS}}(R)]$$

$$= \frac{\beta S^{d-1}}{16\pi r_H G L^2_{\text{AdS}}} (L^2_{\text{AdS}} r_H^{d-1} - r_H^{d+1}). \qquad (1.87)$$

It follows that the black hole spacetime dominates for $r_H > L_{\text{AdS}}$, which via (1.85) translates into a constraint on β. Note that we can also think of this as a *regularized* on-shell action for the black hole, subtracting off the appropriate "vacuum" action to get a finite answer.

We can use this result to compute the entropy of a black hole and learn about the density of states in our CFT. First, recall from statistical mechanics that the thermodynamic entropy can be computed from the partition function via

$$S = (1 - \beta \partial_\beta) Z[\beta]. \qquad (1.88)$$

Here, the partition function is the Euclidean gravity path integral

$$Z[\beta] = Z_{\text{AdS}}[\mathbb{S}^1_\beta \times \mathbb{S}^{d-1}] \approx e^{-S_{\text{AdS}}[g^*]}$$

for the saddlepoint geometry g^*. Below the Hawking-Page transition, thermal AdS g_{thAdS} dominates, and from its unbroken symmetry with respect to τ we learn $S_{\text{AdS}}[g_{\text{thAdS}}] \propto \beta$. Hence, the entropy vanishes, up to $O(G^0)$ corrections due to the matter fields outside the black hole. These will become very important below, but for the moment we ignore them.

Above the Hawking-Page transition, the black hole dominates. The entropy here is harder to calculate from (1.88), but we can use the fact that $-\partial_\beta \log Z = E(\beta)$, the energy

of the state, and $\log Z$ is the regularized on-shell action we gave above in (1.87). From Einstein's most famous equation, the energy of the black hole is simply its mass M, so from (1.80) we immediately have

$$E = M = \frac{(d-1)S^{d-1}}{16\pi G}(r_H^d L_{\text{AdS}}^{-2} + r_H^{d-2}). \tag{1.89}$$

Hence, inserting (1.87) and (1.89) into (1.88), we finally obtain the black hole entropy:

$$\begin{aligned}
S &= \beta M - \Delta S_{\text{AdS}} \\
&= \frac{\beta(d-1)S^{d-1}}{16\pi G}(r_H^d L_{\text{AdS}}^{-2} + r_H^{d-2}) - \frac{\beta S^{d-1}}{16\pi r_H G L_{\text{AdS}}^2}(L_{\text{AdS}}^2 r_H^{d-1} - r_H^{d+1}) \\
&= \frac{\beta S^{d-1}}{16\pi r_H L_{\text{AdS}}^2 G}[(d-1)(r_H^{d+1} + L_{\text{AdS}}^2 r_H^{d-1}) - (L_{\text{AdS}}^2 r_H^{d+1} - r_H^{d-1})] \\
&= \frac{r_H^{d-1} S^{d-1}}{4G},
\end{aligned} \tag{1.90}$$

where $\mathcal{A}_{\text{hor}} = r_H^{d-1} S^{d-1}$ is the "area" of the black hole horizon, appropriately generalized to higher dimensions. This is the celebrated *Bekenstein-Hawking entropy* [26, 27, 21, 28].

We see that the thermodynamic entropy S suddenly jumps from $O(G^0)$ to $O(1/G)$ at the Hawking-Page transition. In the microcanonical ensemble, the entropy is related to the density of black hole microstates $\delta(E)$ in a small window around energy E:

$$S(E) = \log \delta(E). \tag{1.91}$$

Since energy corresponds to scaling dimension Δ in the CFT, we see that the physics of this black hole transition is telling us directly about the gap in the spectrum. Below the Hawking-Page transition, we have a small number of primaries, and an $O(N)$ explosion above the transition. From the discussion at the end of §1.1.3, we morally expect these to correspond to stringy, higher-spin excitations. If they cause the semiclassical spacetime to break down, they must do so behind the horizon.

But what actually goes on behind the horizon is mysterious. An adventurous physicist can fall inside and see what happens, but they can never communicate their findings to

the less adventurous physicists who remained outside. From (1.79), $f(r)$ changes sign at $r = r_H$ and exchanges the roles of t and r. Information heads ineluctably towards the singularity at $r = 0$ simply by travelling forward in time. This horizon is picture in Fig. 1.2 (right). We have just argued that stringy, high-energy modes must be hidden inside, from which one might expect there is no good geometry at all. This is the flavour of the fuzzball program [29].

This point of view is in deep tension with the equivalence principle, according to which nothing special happens at the horizon. The Schwarschild metric (1.79) is singular at the horizon due to the factor of $1/f(r)$, but this singularity can be removed by choosing a different set of coordinates. A convenient choice is *Eddington-Finkelstein null coordinates*, defined by

$$v = t + r^*, \quad u = t - r^*, \quad r^*(r) = \int_{r_H}^{r} \frac{\mathrm{d}\hat{r}}{f(\hat{r})}. \tag{1.92}$$

Physically, curves of constant v (respectively u) are infalling (respectively outgoing) null rays. In these coordinates, the metric (1.79) becomes

$$\mathrm{d}s^2 = -f(r)\,\mathrm{d}u\,\mathrm{d}v + r^2\,\mathrm{d}\Omega_{d-1}^2, \tag{1.93}$$

which is no longer singular at the horizon, and can be extended into the interior. In fact, it is possible to extend the coordinate system even further by defining *Kruskal-Szekeres coordinates*

$$U(u) = -e^{-2\pi u/\beta}, \quad V(v) = e^{2\pi v/\beta}. \tag{1.94}$$

This yields the metric

$$\mathrm{d}s^2 = -\frac{\beta^2 f(r)}{4\pi^2 UV}\,\mathrm{d}U\,\mathrm{d}V + r^2\,\mathrm{d}\Omega_{d-1}^2. \tag{1.95}$$

Note that $U < 0$ and $V > 0$ in (1.94). However, by letting $U, V \in \mathbb{R}$, we obtain the *maximally extended AdS-Schwarzschild solution* or *eternal black hole*. Surprisingly, this contains a second asymptotic region with $U > 0$ and $V < 0$, as depicted in Fig. 1.3 (left). The Penrose diagram is obtained by compactifying the coordinates U, V and throwing away an overall conformal factor. These two regions are connected by a wormhole, with

the spatial geometry of a Cauchy slice drawn in Fig. 1.3 (right).

From the perspective of AdS/CFT, this looks very different from the original black hole/thermal state correspondence. In the maximally extended geometry, the asymptotic region consists of not one but two copies of $\mathbb{R} \times \mathbb{S}^{d-1}$. This suggests we need a new dictionary entry to describe this maximally extended solution. However, we can obtain the relevant entry by simply slicing the Euclidean path integral for the thermal state in half, as shown by Maldacena [30], inspired by an older proposal of Israel [31].
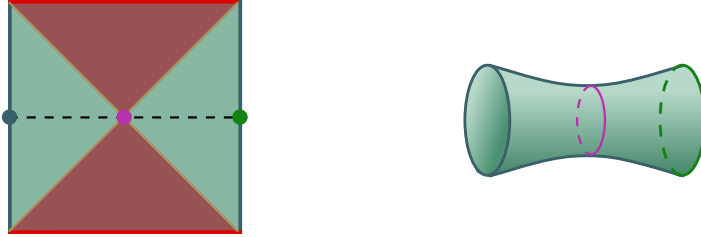
Figure 1.3: *Left.* The Penrose diagram for the maximally extended AdS-Schwarzschild geometry, with sphere $\mathbb{S}^{d-1}$ suppressed. *Right.* The embedding geometry of the dotted timeslice, with the sphere schematically shown as a circle.

The basic idea is to purify the canonically thermal state (1.86) on two copies of the CFT. More precisely, we define a pure state called the *thermofield double* (TFD) on the two CFTs with the property that, if we trace out one CFT, we obtain ρ_β on the other. Let CFT_1 denote our original CFT, and CFT_2 a second copy of the same system which is identical except that it is CPT conjugate.[17] The TFD is defined by

$$|\mathrm{TFD}(\beta)\rangle := \frac{1}{\sqrt{Z[\beta]}} \sum_E e^{-\beta E/2} |E\rangle_1 |\tilde{E}\rangle_2 \,, \tag{1.96}$$

where $|E\rangle_1$ denotes an energy eigenstate of CFT_1 and $|\tilde{E}\rangle_2$ the CPT conjugate. We can

---

[17]It is convenient to choose a Hamiltonian $\hat{H}_{12} = \hat{H}_1 - \hat{H}_2$ so that the TFD is an energy eigenstate. But with this choice, time runs "backwards" in CFT_2, and the energy eigenstates are therefore T conjugated. This is not always a symmetry of the theory, but CPT is, hence the upgrade.

check the partial trace recovers ρ_β:

$$
\begin{aligned}
\mathrm{Tr}_2\left[|\mathrm{TFD}(\beta)\rangle\langle\mathrm{TFD}(\beta)|\right] &= \frac{1}{Z[\beta]}\sum_{EE'}e^{-\beta(E+E')/2}{}_1|E\rangle\langle E'|_1\langle\tilde{E}|\tilde{E}'\rangle_2 \\
&= \frac{1}{Z[\beta]}\sum_{EE'}e^{-\beta(E+E')/2}{}_1|E\rangle\langle E|_1\delta_{EE'} \\
&= \rho_\beta.
\end{aligned}
\tag{1.97}
$$

To see how correlators in this state are computed by Euclidean path integral on the cylinder $C_\beta = [0,\beta/2]\times\mathbb{S}^{d-1}$, we need to view either end of the cylinder as kets in CFT_1 and CFT_2, with boundary conditions acting as bras for which we compute transition amplitudes, as in (1.47). If the bras at either end are $|\psi_i\rangle$, associated with CFT_i, then the transition amplitude for a Euclidean cylinder of length $\beta/2$ is

$$
\begin{aligned}
\langle\psi_1|e^{-\beta\hat{H}/2}|\psi_2\rangle &= \sum_E e^{-\beta E/2}\langle\psi_1|E\rangle\langle E|\psi_2\rangle \\
&= \sum_E e^{-\beta E/2}\langle\psi_1|E\rangle\langle\tilde{\psi}_2|\tilde{E}\rangle_2 \\
&= {}_1\langle\psi_1|_2\langle\psi_2|\mathrm{TFD}(\beta)\rangle,
\end{aligned}
\tag{1.98}
$$

where on the first line we inserted a resolution of identity in the energy basis, and in the second, we used the fact that CPT conjugates inner products. This is precisely what it means for the state to be prepared by the Euclidean path integral.
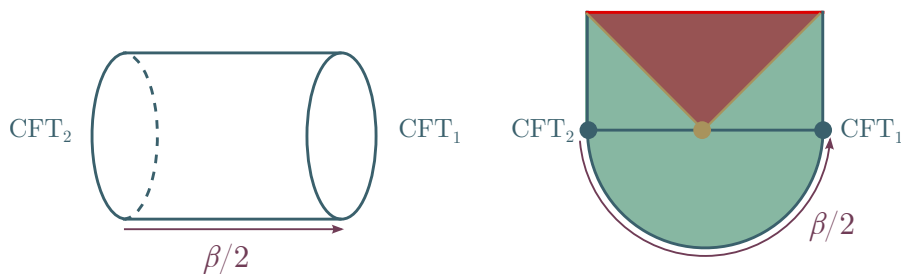
Figure 1.4: The Hartle-Hawking path integral on $[0,\beta/2]\times\mathbb{S}^{d-1}$ preparing the TFD. Below is the Euclidean part, above the Lorentzian continuation.

If we now apply the AdS/CFT dictionary in the form (1.78), we obtain

$$Z_{\text{AdS}}[\partial \mathcal{M} = C_\beta] = Z_{\text{CFT}}[C_\beta]. \tag{1.99}$$

Consulting Fig. 1.2 (left), we see that C_β is simply half the boundary of the disk. The bulk spacetime solving the equations of motion (which are local) is just half the disk, with the upper edge a moment-of-time symmetry. When we continue to Lorentzian signature, this gives the "upper-half" of the maximally extended solution. Thus, we can interpret the half-disk as preparing the maximally extended AdS-Schwarzschild solution, with a smooth future interior. In gravitational parlance, this is called the *Hartle-Hawking state* [22], and is often drawn by attaching (half) of the Lorentzian spacetime to the Euclidean half-disk, as in Fig. 1.4.

1.1.5 Entanglement

Above, we speculated that the microstates $|E\rangle$ in (1.91) accounting for black hole entropy involve non-classical physics hidden behind the horizon. These same high energy states appear in the thermodfield double (1.96), so why should there be a good interior geometry? Although we cannot send a message from the left to the right CFT (they are non-interacting), we can send messages which meet in the interior. One way to diagnose this is to look for nonzero correlators between operators on the right and left [30]. This is possible because the TFD state *entangles* the two CFTs, i.e. it cannot be factorized into a product of states on each CFT, $|\text{TFD}\rangle \neq |\psi_1\rangle_1 \otimes |\psi_2\rangle_2$. As in the EPR thought experiment [32], this type of correlation allows for action at a distance (between the CFTs) without violating causality. The crucial role of entanglement in creating this emergent spacetime was first emphasized by Van Raamsdonk [33, 34].[18]

In this setting, we are led to a profitable reinterpretation of the black hole entropy. From the perspective of either the left or right CFT, we have thermodynamic entropy

---

[18]Maldacena and Susskind [35] later made the even more radical proposal that *any* entanglement is dual to a non-traversable wormhole. This goes by the witty slogan ER = EPR, after Einstein et al.'s 1935 papers on entangelement and wormholes [32, 36].

$S = \mathcal{A}_{\text{hor}}/4G$. We can write S in terms of the density ρ_β as follows:

$$\begin{aligned}
S &= \beta E(\beta) + \log Z \\
&= \frac{1}{Z}\text{Tr}\left[e^{-\beta\hat{H}}\beta\hat{H}\right] + \frac{\log Z}{Z}\text{Tr}\left[e^{-\beta\hat{H}}\right] \\
&= \frac{1}{Z}\text{Tr}\left[e^{-\beta\hat{H}}(\beta\hat{H} + \log Z)\right] \\
&= -\text{Tr}\left[\rho_\beta \log \rho_\beta\right].
\end{aligned}$$
(1.100)

This is the von Neumman entropy of the matrix ρ_β. Since ρ_β is obtained by tracing out a CFT, this expression is also called the *entanglement entropy* between the two CFTs in the TFD state. It measures the uncertainty due to entanglement. In the wormhole geometry, the horizon is the minimal area surface separating the left and and right asymptotic region. It is the purple point in Fig. 1.3 (left), and the dotted "throat" in Fig. 1.3 (right).

Thus, the entanglement entropy is computed by the area of a bulk minimal surface separating the two CFTs. This observation is dramatically generalized by the *Ryu-Takayanagi* (RT) formula [37, 38]. This gives a precise relation between entanglement and geometry, and proposees that for any subregion A of a CFT in semiclassical state $|\Psi\rangle$, the entanglement entropy of the reduced density $\rho_A = \text{Tr}_{\bar{A}}[|\Psi\rangle\langle\Psi|]$ (where $\bar{A}$ is the spatial complement of A) is the area of the bulk minimal surface $\mathcal{X}_A$ anchored at A:

$$S[A] = \min_{\mathcal{X}_A \sim A} \frac{\mathcal{A}[\mathcal{X}_A]}{4G}.$$
(1.101)

Here, $\mathcal{X}_A \sim A$ indicates that the bulk surface $\mathcal{X}_A$ is *homologous* to A, with a co-dimension 2 spacelike region Ξ_A they together form the boundary of, $\mathcal{X}_A \cup A = \partial\Xi_A$. The bulk domain of dependence[19] $D[\Xi_A]$ is called the *entanglement wedge*, though we will often use the same name for Ξ_A. We depict the relevant surfaces in Fig. 1.5.

To return to black holes, Bekenstein-Hawking is the special case of Ryu-Takayanagi formula (1.101) where the "subregion" A is an entire CFT, since the minimal surface is the horizon. Remarkably, Casini, Huerta and Myers (CHM) [39] showed that for a ball-shaped

---

[19]This consists of all points such that an inextendible timelike curve through the point must also pass through Ξ_A. Alternatively, Ξ_A is a Cauchy slice of $D[\Xi_A]$.

region A in the vacuum state of a flat-space CFT, the (boundary) domain of dependence $\hat{D}[A]$ can be mapped to the thermal state on a hyperbolic cylinder $\mathbb{R} \times \mathbb{H}^{d-1}$. The bulk dual is a hyperbolic black hole whose horizon coincides with $\mathcal{X}_A$. Thus, the area law implies Ryu-Takayanagi for these ball-shaped regions in the vacuum.
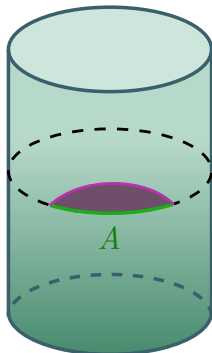
Figure 1.5: The RT formula for a green boundary region A. The minimal surface $\mathcal{X}_A$ is fuschia, and the entanglement wedge Ξ_A mauve.

A proof of (1.101) for general static geometries and regions A follows from a different set of ideas related to black hole physics. In [40], Lewkowycz and Maldacena started with the *replica trick*, which computes entanglement as a limit of partition functions on joined copies of the original theory. More precisely,

$$S[A] = \lim_{n \to 1} \frac{1}{n-1} \log \operatorname{Tr}[\rho_A^n], \tag{1.102}$$

where the trace $\operatorname{Tr}[\rho_A^n] \sim Z^{(n)}$ can be viewed as the partition function of the replica geometry $\mathcal{M}^{(n)}$ made by stitching n copies of the gravitational system (and its conformal boundary) cyclically together along the "cuts" A. For noninteger n, the Euclidean replica geometry $\mathcal{M}^{(n)}$ has a conical singularity that we must smooth out, just like the Euclidean disk. The resulting surface $\mathcal{X}_A^{(n)}$ is forced to obey a "cosmic string" action, and assuming Einstein's equations are satisfied to leading order in $n-1$, the string pulls taut, i.e. the surface $\mathcal{X}_A^{(n)}$ is minimal as $n \to 1$.

Hubeny, Rangamani and Takanagi (HRT) generalized (1.101) to time-dependent geometries, in which $\mathcal{X}_A$ is the minimal *extremal* surface instead of a minimal surface sim-

pliciter [41]. This can be proved using similar methods to the static case [42]. As shown by Wall [43], in spacetimes satisfying the *null energy condition* (NEC) $T_{\mu\nu}k^\mu k^\nu \geq 0$, the HRT formula can be expressed as a *maximin* condition:

$$S[A] = \max_{\Sigma} \min_{\mathcal{X}_A \subset \Sigma} \frac{\mathcal{A}[\mathcal{X}_A]}{4G}, \tag{1.103}$$

where we minimize over all homologous surfaces $\mathcal{X}_A$ in a bulk Cauchy slice Σ, and then maximize over the choice of Cauchy slice. RT and HRT formulas are also only correct to leading order in $1/G$, and (like the black hole entropy) receives $O(G^0)$ corrections from quantum fields. In particular, Faulkner, Lewkowycz and Maldacena (FLM) [44] argued that we must add the bulk entropy of fields in the region Ξ_A, so that

$$S[A] = \min_{\mathcal{X}_A \sim A} \frac{\mathcal{A}[\mathcal{X}_A]}{4G} + S_{\text{bulk}}[\Xi_A], \tag{1.104}$$

where we have suppressed additional $O(G^0)$ corrections from counterterms needed to regulate the entanglement entropy. Although this result is only correct to $O(G^0)$, it inspired Engelhardt and Wall [45] to conjecture that, to all orders in G, the entanglement entropy of a boundary region A is given by the minimal surface extremizing the sum of area and bulk entropy terms, also called the *generalized entropy*. In more detail, the *quantum extremal surface* (QES) prescription states that

$$S[A] = \min_{\mathcal{X}_A \sim A} \left[\frac{\mathcal{A}[\mathcal{X}_A]}{4G} + S_{\text{bulk}}[\Xi_A] \right], \tag{1.105}$$

where the term we are extremizing is the generalized entropy $S_{\text{gen}}[\Xi_A]$. This is a generalization of RT and FLM formulas to all orders in G, and like the HRT formula, is amenable to a maximin formulation [46]. It is also closely related to the generalized entropy of a black hole, where $O(G^0)$ corrections come from matter fields in the exterior:

$$S_{\text{gen}} = \frac{\mathcal{A}_{\text{hor}}}{4G} + S[\rho_{\text{ext}}] \tag{1.106}$$

for von Neumann entropy $S[\rho_{\text{ext}}]$. The generalized second law [27] arises from applying

34

the second law of thermodynamics to this generalized entropy for black holes. For further discussion, see e.g. [47] and references therein.

For the maximally extended AdS-Schwarzschild geometry, we know that the reduced density of a single CFT is thermal ρ_β and encodes the corresponding exterior. Prompted by this example, we can ask: in AdS/CFT, what is the bulk dual of a reduced density matrix ρ_A? In the black hole, the horizon terminates the bulk region described by ρ_β. Similarly, we might guess from the RT formula that the minimal surface $\mathcal{X}_A$ caps off the bulk region described by ρ_A, and hence the gravity dual is Ξ_A, or rather, the entanglement wedge $D[\Xi_A]$ [48]. As a plausibility argument, imagine varying the subsystem $a \subset A$, with A fixed, so the corresponding surfaces $\mathcal{X}_a$ sweep out all of Ξ_A.[20]

A formal argument was given in [49], though we follow the presentation in [50]. In field theory, the entanglement entropy is usually divergent, and depends on a choice of regulator. In contrast, the *relative entropy* between two states is finite and well-defined:

$$S(\rho|\sigma) = \text{Tr}[\rho(\log \rho - \log \sigma)] = -S[\rho] + \text{Tr}[\rho \hat{K}[\sigma]]. \tag{1.107}$$

For a density ρ, it is helpful to introduce an object called the *modular Hamiltonian* $\hat{K}$, defined by $\rho = e^{-\hat{K}[\rho]}$. Then the relative entropy can be written

$$S(\rho|\sigma) = \Delta \langle \hat{K}[\sigma] \rangle - \Delta S \tag{1.108}$$

where $\Delta(\cdot) = \text{Tr}[(\rho - \sigma)(\cdot)]$. The relative entropy is positive and vanishes at $\rho = \sigma$. Hence, for linearized perturbations $\rho = \sigma + \delta\sigma$ we obtain the *first law of entanglement* $\delta S = \delta \langle \hat{K}[\sigma] \rangle$. The FLM formula (1.104) or QES prescription (1.105) tell us that

$$S[\rho_A] = S[\rho_{\Xi_A}] + \frac{1}{4G}\text{Tr}[\rho_{\Xi_A} \hat{\mathcal{A}}], \tag{1.109}$$

where $\mathcal{X}_A$ extremizes some functional, and we view area as an operator $\hat{\mathcal{A}}$ acting on the bulk semiclassical Hilbert space. We will take this Hilbert space to consist of states with

---

[20]This argument has two issues. First, there may be holes in Ξ_A not probed by any minimal surface. Second, for some $a \subset A$, the minimal surface $\mathcal{X}_a$ may "poke out" of Ξ_A. The argument of [49] circumvents the first issue, and [43] shows no "poking out" occurs when the NEC is satisfied, at least for HRT.

extremal surfaces whose areas agree up to order G, so that the area contributions to entropy agree to order G^0.

If we linearize (1.109) and use the first law, we obtain

$$\delta\langle\hat{K}[\rho_A]\rangle = \delta\langle\hat{K}[\rho_{\Xi_A}]\rangle + \frac{1}{4G}\delta\langle\hat{\mathcal{A}}\rangle. \tag{1.110}$$

Both sides are linear in $\delta\rho$, and since this perturbation is independent of ρ, we can integrate to obtain

$$\mathrm{Tr}[\rho_A\hat{K}[\sigma_A]] = \mathrm{Tr}\left[\rho_{\Xi_A}\left(\hat{K}[\sigma_{\Xi_A}] + \frac{\hat{\mathcal{A}}^{(\sigma)}}{4G}\right)\right], \tag{1.111}$$

where $\hat{\mathcal{A}}^{(\sigma)}$ reminds us that it is extremizing a functional with respect to σ_A. Since this holds for any ρ, it follows that within the bulk semiclassical Hilbert space,

$$\hat{K}[\sigma_A] = \hat{K}[\sigma_{\Xi_A}] + \frac{\hat{\mathcal{A}}^{(\sigma)}}{4G}. \tag{1.112}$$

Combining (1.107), (1.109) and (1.112) gives

$$S(\rho_A|\sigma_A) - S(\rho_{\Xi_A}|\sigma_{\Xi_A}) = S[\rho_{\Xi_A}] - S[\rho_A] + \frac{1}{4G}\mathrm{Tr}[\rho_{\Xi_A}\hat{\mathcal{A}}^{(\sigma)}] \tag{1.113}$$

$$= \frac{1}{4G}\mathrm{Tr}[\rho_{\Xi_A}(\hat{\mathcal{A}}^{(\sigma)} - \hat{\mathcal{A}}^{(\rho)})] \tag{1.114}$$

using FLM or QES on the second line.

From our assumption about the bulk Hilbert space, this difference is $O(G)$. Thus, in this Hilbert space bulk and boundary relative entropy agree, up to $O(G)$ corrections, and in particular, the state ρ_{Ξ_A} on the entanglement wedge contains precisely the same information as the state on ρ_A. This motivates the program of *entanglement wedge reconstruction*, where bulk operators in the entanglement wedge are expressed in terms of boundary physics encoded in ρ_A. Approaches to performing this reconstruction include modular evolution (see [49, 51] for instance) and quantum error correction ([50, 52], see also [14] and references therein).

1.2 Boundary state black holes

Generically, the entanglement wedge is bigger than the *causal wedge* of bulk points that a boundary observer in A can send and receive messages from [53, 54, 43, 48]. In a one-sided black hole spacetime, we know that the causal wedge will not penetrate the horizon. But perhaps in some cases the entanglement wedge does, as in Fig. 1.6. We could then use entanglement wedge reconstruction to learn about the black hole interior. We might be suspicious of such an approach, however, given the intuition that in the mixed thermal state ρ_β, the horizon is hiding forbidden high-energy physics rather than a good semiclassical spacetime. And indeed, these efforts are doomed: the horizon is an impassable barrier to extremal surfaces anchored on the boundary [55], so the entanglement wedge cannot go inside. Another strategy is needed.
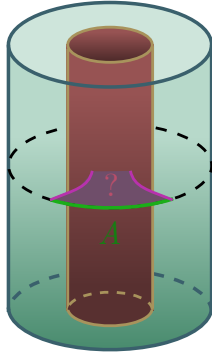
Figure 1.6: Attempting to look inside a black hole using entanglement wedge reconstruction.

If extremal surfaces cannot enter for the thermal state, we may nevertheless be able to find microstates $|E\rangle$ with an interior geometry that the entanglement wedge can probe. And we also know that the TFD (1.96) has a smooth interior, so we can exploit this to construct the desired state $|E\rangle$. In fact, a strategy for constructing one-sided black hole states was given by Maldacena when he proposed the TFD as dual to the eternal black hole [30], and developed by Hartman and Maldacena in [56]. The idea is simply to take a $\mathbb{Z}_2$ quotient of the left and right CFT, folding the Penrose diagram in Fig. 1.3 in half. This also folds the Hartle-Hawking path integral in Fig. 1.4 in half, with a Euclidean

preparation on $[0, \beta/4] \times \mathbb{S}^{d-1}$.
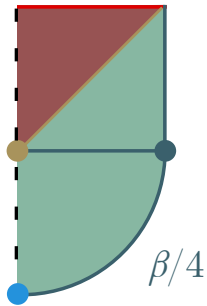
Figure 1.7: Folding the eternal black hole in half. The blue dot is a boundary state, enforcing symmetry-preserving boundary conditions.

There is an important subtlety, however. We need to ensure that the boundary conditions at the fold do not spoil the bulk spherical symmetry. On the boundary, the fold intersects the Euclidean CFT at the point $\tau = 0$ (the blue point at the bottom of Fig. 1.7). In the TFD, the ends of the Euclidean cylinder defined transition amplitudes, as per (1.98). Here, there is only CFT, and we replace the state on the left with a *boundary state* $|B\rangle$ enforcing symmetric boundary conditions. We are thus led to define

$$|B(\beta)\rangle = e^{-\beta \hat{H}/4}|B\rangle, \tag{1.115}$$

which corresponds to a one-sided black hole of inverse temperature $1/\beta$. The rule for computing transition amplitudes (1.98) is then

$$\langle \psi | e^{-\beta \hat{H}/4} | B \rangle, \tag{1.116}$$

where $|\psi\rangle$ is a state of the CFT (at the dull green dot on the right of Fig. 1.7).

We can generalize this story to other symmetry-preserved boundary states $|B\rangle$, and call this general class of one-sided black hole states *boundary microstates*. They are the subject of Chapter 2. Here outline a few salient results. In general, adding a boundary to a CFT breaks conformal invariance. However, a *boundary CFT* involves setting boundary conditions which are maximally conformally invariant. This is useful for studying surface critical behaviour [57]. In higher (Euclidean) dimensions, these boundary states break the

38

full $\mathrm{SO}(1, d+1)$ group to the subgroup $\mathrm{SO}(1, d)$, and may therefore plausibly be expected to maintain spherical symmetry in the bulk.

This by itself does not guarantee a classical interior geometry, but we can draw on another candidate entry to the AdS/CFT dictionary. The *AdS/BCFT dictionary* [58, 59] proposes that BCFTs are dual to AdS space cut off by a codimension-1 surface called a *brane*. The brane must respect the remaining $\mathrm{SO}(1, d)$ symmetry. The bulk metric takes the form

$$\mathrm{d}s_{d+1}^2 = \mathrm{d}\mu^2 + g(\mu)^2 \, \mathrm{d}s_d^2, \tag{1.117}$$

where $\mathrm{d}s_d^2$ denotes the metric of (Euclidean) AdS_d, with isometry group $\mathrm{SO}(1, d)$, and μ is called the *slicing parameter*. To maintain the appropriate symmetry, the brane must correspond to a surface of fixed μ. Thus, we are led to state AdS/BCFT in the style of GKPW (1.78):

$$Z_{\mathrm{AdS}}[\partial \mathcal{M} = M \cup \mathcal{B}(\mu_{|B\rangle})] = Z_{\mathrm{CFT}}[M_B], \tag{1.118}$$

where the CFT is defined on a manifold M with boundary and in boundary state $|B\rangle$, and the bulk spacetime on $\mathcal{M}$ has two boundary components: the asymptotic boundary M, and a brane $\mathcal{B}(\mu_{|B\rangle})$ at some fixed slicing parameter $\mu_{|B\rangle}$. These are called *constant tension branes*, pictured in Fig. 1.8 (left).

To determine $\mu_{|B\rangle}$, one approach is to use CFT entanglement data and the RT formula (1.101). For instance, in a $1 + 1$-dimensional BCFT on $\{(x, t) \in \mathbb{R}^2 : x \geq 0\}$, the entanglement entropy of the interval $A := [0, L]$ is given by

$$S[A] = \frac{c}{6} \log\left(\frac{2L}{\epsilon}\right) + g_B, \tag{1.119}$$

where c is the central charge, ϵ is a UV regulator, and $g_B := \log\langle B|0\rangle$ an L-independent constant called the *boundary entropy* [60]. Suggestively, this is half the ground state entropy of $[-L, L]$, plus the boundary entropy term [61, 62, 63]. Thus, to compute the entropy, it is as if we undid the $\mathbb{Z}_2$ quotient analogous to the method of images, did the calculation, then halved the result and added a boundary entropy term to account for entropy contributions from modes localized to the boundary itself. This is called the *doubling*

39

trick [57].[21]

To reproduce this universal result from the RT formula, we must compute the length of a minimal geodesic. The bulk equivalent of the doubling trick, however, is to shoot off a geodesic from the point $x = L$ and allow it to end normally on the brane, since that it will meet its mirror image with no "kink". It can be shown this reproduces the ground state BCFT entropy, and also determines $\mu_{|B\rangle}$ in terms of g_B [58, 59]. A similar story holds in higher dimensions. Using methods similar to CHM [39], Jensen and O'Bannon [64] showed that in arbitrary dimenion, universal results for the entanglement entropy of a boundary-centred half-sphere can are reproduced by minimal surfaces ending on a constant tension brane.

This suggests the following generalization of the RT formula in a BCFT:

$$S[A] = \min_{\mathcal{X}_A \sim_{\mathcal{B}} A} \frac{\mathcal{A}[\mathcal{X}_A]}{4G}, \tag{1.120}$$

where we have replaced the usual homology condition with a "brane-relative" condition $\mathcal{X}_A \sim_{\mathcal{B}} A$, meaning that there is a bulk co-dimension 2 region Ξ_A bounded by $\mathcal{X}_A$, A and part of the brane $\mathcal{B}_A \subset \mathcal{B}$:

$$\partial \Xi_A = \mathcal{X}_A \cup A \cup \mathcal{B}_A. \tag{1.121}$$

This homology constraint essentially just treats the brane as part of the bulk spacetime.[22] As usual, the entanglement wedge is $D[\Xi_A]$. The generalizations to HRT, FLM (1.104) and QES (1.105) formulas is immediate.

In Chapter 2, we use AdS/BCFT in the form (1.118) to explicitly construct the geometries corresponding to (1.115), in arbitrary dimension and with arbitrary $\mu_{|B\rangle}$. Here, we can use spherical symmetry and Birkhoff's theorem to fix the metric (1.117) to be a portion of either thermal AdS or the maximally extended Schwarzschild-AdS geometry. As usual, we compare actions for the two geometries (with $\mu > \mu_{|B\rangle}$) and give conditions for

---

[21]We might expect that Euclidean evolution of a boundary state by $\tau = \beta/4$ would be dual to a brane in a Schwarzschild background of inverse temperature β. Although this is always true for 3d black holes, and the $\mathbb{Z}_2$ quotient in arbitrary dimensions, we will see in Chapter 2 that changing the boundary entropy changes the effective temperature. Physically, more Euclidean time is needed to thermalize these boundary states.

[22]This can be motivated by considering top-down models with internal compact dimension that "pinch off", i.e. go to zero size, at the brane.
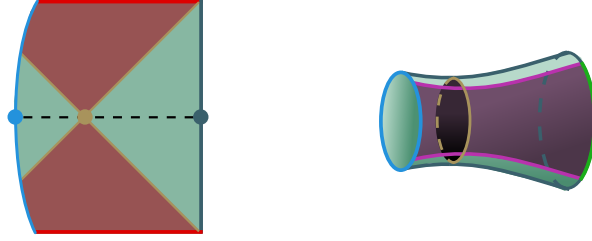
Figure 1.8: *Left.* A boundary state black hole with constant . *Right.* The embedding geometry at fixed time is a wormhole cut off by a brane. The RT surface for a large subregion on the right (green) passes through the horizon and ends on the brane.

the dominance of the black hole phase, generalizing the results of [58, 59]. From (1.120), we show that for sufficiently large CFT regions A and choices of $\mu_{|B\rangle}$, the extremal surface $\mathcal{X}_A$ falls in and hit a brane behind the horizon, as in Fig. 1.8 (right). This realizes the ambition of Fig. 1.6, and via entanglement wedge reconstruction, give us in principle access to physics behind the horizon.

1.3 Entanglement entropy in 2d BCFTs

We have assumed that the dual of a BCFT obeys (1.118) and (1.120), and from these assumptions, we seem to be able to peer inside black holes. But how do we know there is a classical bulk geometry whose entanglement structure is captured by the RT formula? These are questions about the microscopics of quantum gravity. In Chapter 3, we solve this problem in the tractable but nontrivial setting of a 2d BCFT. The basic idea is to use evaluate entanglement entropy replica using the replica trick (1.102), where we recall that

$$S[A] = \lim_{n \to 1} S_A^{(n)} = \lim_{n \to 1} \frac{1}{n-1} \log \text{Tr}[\rho_A^n]$$

for the *n-Rényi entropies* $S_A^{(n)}$, related to the partition functions $Z^{(n)} \sim \text{Tr}[\rho_A^n]$ on a n-replicated CFT manifold $M^{(n)}$.

Evaluating these replica partition functions explicitly is impossible in higher dimensions. But in a 2d CFT, the replica geometry can be "mocked up" by local operators called *twists* Φ_n, implementing the cyclic boundary conditions which define the replica [62, 63].

We give an example in Fig. 1.9 (left). The Rényi entropy is then just a correlator of twists. Hartman [65] performs the replica calculation in a 2d CFT without boundary, explicitly matching the predictions of the RT formula given the assumption of large central charge and a sparse spectrum of primary operators. Chapter 3 repeats these steps for a 2d BCFT.
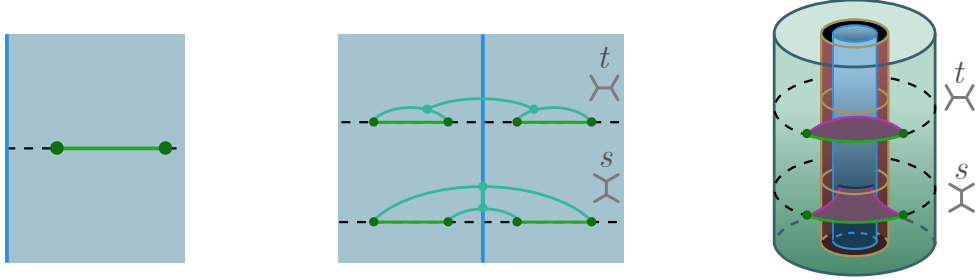
Figure 1.9: *Left.* The entanglement entropy of an interval computed by a correlator of dark green twists. *Middle.* Doubling the twists in an auxiliary CFT, with two OPE channels. *Right.* The corresponding RT surfaces in the bulk.

In more detail, we first note that the Euclidean correlator

$$\langle B(\beta)|\mathcal{O}_1(x_1)\cdots\mathcal{O}_n(x_n)|B(\beta)\rangle = \langle B|e^{-\beta\hat{H}/4}\mathcal{O}_1(x_1)\cdots\mathcal{O}_n(x_n)e^{-\beta\hat{H}/4}|B\rangle \quad (1.122)$$

can be evaluated in imaginary time on a strip of height $\beta/2$ and infinite width, with boundary conditions $|B\rangle$ on both edges [63].[23] This is the image of the upper half-plane (UHP) under a conformal transformation, with a boundary at $x = 0$ mapping to the edges of the strip; by conformal symmetry, we can work in this simpler geometry.

Consider a collection of k intervals $A = \bigcup_i [x_{2i}, x_{2i+1}]$ on the half-plane. The n-Rényi entropy can be computed using the doubling trick, pictured in Fig. 1.9 (middle). This is based on the observation that the representation theory of the BCFT is equivalent to doubling the insertions and placing them in a regular CFT. In this auxiliary CFT, we define the "doubled" interval

$$-A \cup A = \bigcup_i [x_{2i}, x_{2i+1}] \cup [-x_{2i+1}, -x_{2i}].$$

---

[23]Technically, the CFT is on a spatial circle, but we decompactify it and invoke large-N volume independence [66]. In Fig. 1.9 (right), we have compactified again.

The usual CFT replica calculation gives

$$e^{(1-n)S_A^{(n)}} = \left\langle \prod_i \Phi_n(x_{2i})\bar{\Phi}_n(x_{2i+1})\Phi_n(-x_{2i+1})\bar{\Phi}_n(-x_{2i}) \right\rangle_{\text{UHP}}, \qquad (1.123)$$

with the boundary entropy encoded into the normalization of the twists [67]. For large central charge, $c \to \infty$, and a gapped spectrum, this correlator is dominated by the exchange of the identity operator, which we can view as a virtual particle running in a cubic graph which joins insertions, i.e. a Feynman diagram for the operator product expansion like Fig. 1.9 (middle). There are different diagrams, but from a large-c saddlepoint expansion, one graph will dominate. In the bulk, pictured in Fig. 1.9 (right), this corresponds to the minimal length geodesic pairing of endpoints with each other or the brane, which is precisely our modified RT formula in the limit $n \to 1$.

This is a strong consistency check in the following sense. We start by identifying the bulk dual which correctly reproduces the *universal* result for the entanglement entropy of a half-interval via the RT formula. The RT formula then makes some non-universal predictions about entanglement entropy. We find that, for some set of spectral conditions, we can reproduce these non-universal predictions. Our procedure thus determines the holographic BCFTs self-consistently encoded by our choice of bulk geometry and "brane-relative" RT formula.

1.4 Information radiation

The consistency of the AdS/BCFT prescription for $d = 2$ gives us confidence in the microstate construction of Chapter 2. But in two dimensions, we also have an infinite-dimensional symmetry group, the Virasoro algebra (1.60), which allows us to compute the twist correlator on infinite number of conformally related backgrounds. We used this symmetry in Chapter 3 to map entanglement entropy on a strip to the upper half-plane, where the doubling trick is simplest. It will turn out that, by a different conformal transformation, we can learn about a dynamically evolving black hole spacetime.

To set the scene, recall that a black hole is periodic in imaginary time (1.85) and hence

43

thermal. Hawking [23] argued this is not only a curious formal analogy, but that black holes emit a blackbody spectrum of *Hawking radiation* from the near-horizon region, at inverse temperature given by the period. To prove this, Hawking determined ladder operators for field modes of a constant-radius observer far from the black hole $a_\infty, a_\infty^\dagger$, as well as the *Boulware vacuum* $|0_\infty\rangle$ annihilated by all a_∞, and similarly for a free-falling observer near the horizon, with operators $a_H, a_H^\dagger$ and *Kruskal vacuum* $|0_H\rangle$. He found using the methods of Boguliobov and Valatin [68, 69] that $|0_\infty\rangle$ is not annihilated by the a_H, but rather obeys a canonical Einstein-Bose distribution, so the near-horizon observer sees a thermal bath of particles:[24]

$$\langle 0_\infty | a_H^\dagger(\omega) a_H(\omega) | 0_\infty \rangle = \frac{1}{e^{\beta E} - 1}, \tag{1.124}$$

where ω labels the energy of field modes. See [71] for a pedagogical review.

From far away, the black hole glows like a lump of coal. This glow is powered by the energy of the black hole itself, and in flat space, it will shrink and eventually disappear. We say that the black hole has *evaporated*. But suppose our black hole is formed from the collapse of a star in a pure state $|\psi\rangle_i$. If the post-evaporation cloud of thermal radiation is in a mixed state ρ_f, we have apparently violated *unitarity*, one of the basic principles of quantum mechanics, which states that pure states evolve to pure states via a unitary time evolution operator $U(t)$. Put differently, we cannot run time backwards on the thermal cloud using $U(-t)$ and determine what collapsed. Information has been lost from the universe, a disturbing conclusion dubbed the *information paradox*. Since then, physicists have struggled to rescue unitarity from the clutches of black hole thermodynamics.

We can formulate the information paradox more precisely in terms of entropy. Recall the generalized entropy (1.106), the sum of horizon area and von Neumann entropy of fields in the exterior. This is the entropy measured by a low-energy observer outside the black hole who cannot distinguish different black hole microstates. For that reason, it is also called the *coarse-grained entropy* S_{coarse}. Bekenstein and Hawking separately showed

---

[24]All near-horizon field modes, not just photons, are in a thermal state. However, by considering the effect of the centrifugal barrier on transmission, called *greybody factors*, it can be shown that light dominates the emitted spectrum far from the black hole [70].

[72, 73] that even as the black hole area reduces, the entropy of emitted radiation more than compensates, in accord with the generalized second law $\mathrm{d}S_{\mathrm{coarse}}/\mathrm{d}t \geq 0$.

But suppose we have a microscopic description of the black hole (BH) and radiation (R) systems. Morally, to evade the information paradox, it must be the case that evaporation is not a truly random process, but rather a unitary (if highly chaotic) reorganization of black hole degrees of freedom into radiation which only looks random to a low-energy observer. To measure this, we define the entanglement entropy of a *microscopic* state of the black hole, also called the *fine-grained entropy S_{fine}*:

$$S_{\mathrm{fine}} = S[\rho_{\mathrm{BH}}] = -\operatorname{Tr}[\rho_{\mathrm{BH}} \log \rho_{\mathrm{BH}}]. \tag{1.125}$$

We expect that, if evaporation is unitary but chaotic, S_{fine} will increase as the black hole becomes entangled with the radiation, and at about the halfway point, begin decreasing to zero as the system size limits the possible entanglement. This graph of the fine-grained entropy is called the *Page curve*, and can be proved formally by taking the unitary evolution as Haar random [74]. The information paradox can thus be restated as a homework problem: find a way to compute fine-grained entropy in gravity which gives the Page curve and not the monotonically increasing coarse-grained answer.

In principle, AdS/CFT does our homework for us, since black holes are dual to thermal states in a closed, manifestly unitary system. There are two problems with this purported resolution. First, AdS black holes do not evaporate, but are in equilibrium with the Hawking radiation bouncing back in from the boundary. Second, our sophisticated methods for calculating entropy, namely FLM (1.104) and QES (1.105), are sums of area terms and bulk entanglement entropy, and therefore appear to be computing coarse-grained rather than fine-grained entropy. In [75, 76], both problems are elegantly resolved. To make black holes evaporate, the conformal boundary of AdS/CFT is attached to a flat space reservoir into which the Hawking quanta can permanently escape. Secondly, in this setup it can be shown that the quantum extremal surface moves an $O(G)$ distance inside the horizon at late times. This is sufficient to reproduce the Page curve and other expected features of unitary evaporation.[25]

---

[25]Appropriately, information is saved due to bulk discounts.

However, the question remains: how does the information get out when it is stuck behind a horizon? In toy models, the escape is beautifully geometrized by an emergent higher dimension. In the AMMZ model [6], a 2d black hole is dual to a 1d system, which is itself the boundary of a 2d holographic BCFT. The BCFT thus provides a flat-space bath and 3d bulk spacetime, as in Fig. 1.10. Quantum extremal surfaces are replaced by ordinary RT surfaces in the 3d bulk which can end on the lower-dimensional black hole or a "Cardy brane", introduced by hand to model the evaporation. When the minimal surface for a half-infinite interval (Fig. 1.10, middle) hits the interior. The region of intersection is called a *quantum extremal island* [6], and provides a channel for the information to escape.
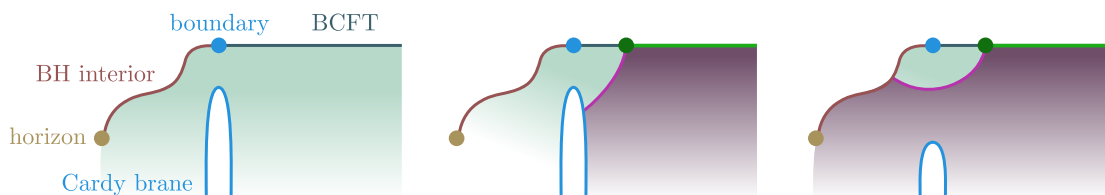
Figure 1.10: *Left.* Time slice of AMMZ [6]. *Middle.* At early times, the Cardy brane obstructs the minimal surface for a half-infinite region of the BCFT, so it does not include any of the black hole interior. *Right.* Like a lowering sluice, the Cardy brane opens up a channel to the interior.

In Chapter 4 we will discuss how to repurpose the boundary state black hole to provide a simple time-dependent black hole with explicit microscopic control. The basic idea is to map the half-plane BCFT to the plane with a disk removed, the Euclidean geometry for the thermofield double state of a half-line. Analytically continuing to real time gives a boundary theory of two half-lines, accelerating away from each other on Rindler trajectories, and joined in the 3d bulk by a brane (Fig. 1.11, left). The brane itself has causal horizons and can therefore be regarded as a black hole.

Instead of computing minimal surfaces for a single half-line, we have two *symmetric* half-lines, $A = (-\infty, -x] \cup [x, \infty]$, and can compute their entanglement entropy as a function of time. Although these minimal surfaces initially skirt around the interior (Fig. 1.11, bottom right), they inevitably transition to form an island (Fig. 1.11, top right). Even though there is no energy loss, there is nevertheless a dynamical transition in the entanglement wedge to include a portion of the interior, a phenomenon we call *information*

radiation. We also consider a genuinely evaporating example, built from a more compli-
cated BCFT model, which exhibits qualitatively similar behaviour.
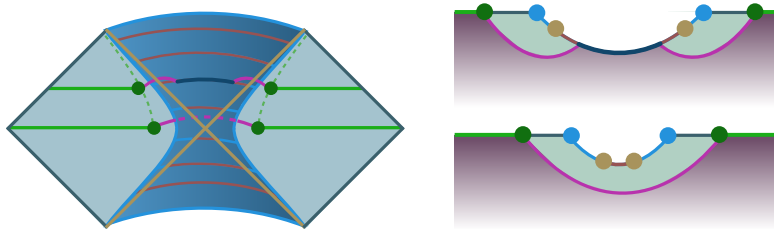
Figure 1.11: *Left.* A BCFT with boundaries on accelerating Rindler trajectories. *Right.*
The formation of an island, with the same coloring scheme as Fig. 1.10.

1.5   Tasks with branes

It seems that, once the extremal surface falls into the horizon, a channel forms in the
higher-dimensional bulk, allowing information to escape. But how can information ac-
tually travel through this channel? One way to make this sharp is to consider a class of
bulk scattering problems called *quantum tasks* [77, 78]. The basic idea is to consider
a distributed quantum computation in the CFT. Information-theoretic constraints on the
achievability of these tasks can teach us about the bulk spacetime. Conversely, the bulk
strategies suggest that there are quantum algorithms for these computations which dramat-
ically outperform the state-of-the-art.

In Chapter 5, we will consider a distributed computation naturally associated to a CFT
with boundary. A CFT observer starting at the *call point* C is require to determine the
boundary condition $g_q \in \{g_0, g_1\}$, and send the bit q to two *return points* R_1 and R_2 on
the CFT boundary.[26] We work in the Lorentzian BCFT on an interval so that we can
have return points on opposite edges. There are two strategies for a boundary observer.
The naive strategy is simply to travel to the boundary, determine g_q, and then if causality

---

[26]We can cast this in terms a *monogamy task* [79] by concealing a qubit $|b\rangle, b \in \{0, 1\}$, and handing the
observer $H^q|b\rangle$ at C. They are required to produce b at the return points with probability $p > \cos^2(\pi/8)$.

allows it, send q to the call points. We show a case where strategy is viable in Fig. 1.12 (left), with red lines indicating the path of the observer and their messages.

Define the *decision region* as the intersection of the future light cone of C and past light cone of the call points, all on the boundary:

$$\hat{\mathcal{V}} = \hat{J}^+(C) \cap \hat{J}^-(R_1) \cap \hat{J}^-(R_2). \tag{1.126}$$

This is the domain of dependence of a boundary region A, shown in Fig. 1.12. The "boundary-local" approach will work when $\hat{\mathcal{V}}$ (or equivalently A) intersects the CFT boundary. But even when it doesn't, the task can still be achieved with sufficient amounts of entanglement, as shown formally (in a slightly different setting) in [80]. Here, the entanglement is between $\hat{\mathcal{V}}$ and the boundary itself, [27] as depicted in Fig. 1.12 (right). In the context of holography, we can ask about the *duals* of these strategies. Heuristically, we expect that the boundary-local strategy corresponds to an observer with control of the causal wedge, and the entanglement-based strategy to the entanglement wedge.
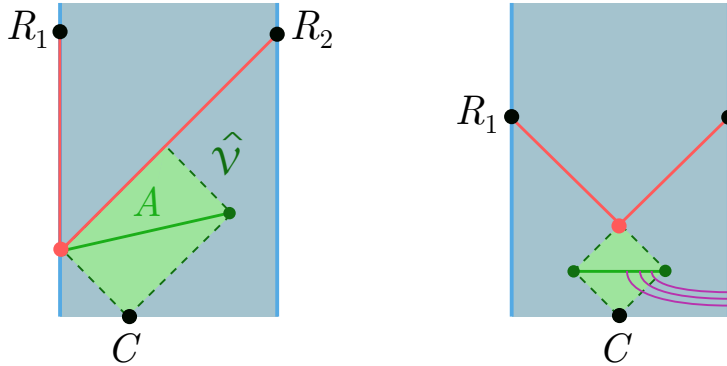
Figure 1.12: *Left.* A marginally viable boundary-local strategy. *Right.* With sufficient entanglement between the decision region $\hat{\mathcal{V}}$ and the boundary, the task is still achievable even when the local strategy doesn't work.

We can make this more precise by consider a bulk-local strategy, where our BCFT has a semiclassical dual cut off by a brane. The observer starts off at the call point, but now

---

[27]Technically, we entangle the quantum system Q containing q and a reference system $\bar{Q}$. If the mutual information $I(\hat{\mathcal{V}}, \bar{Q}) = 0$, the observer cannot succeed with the required probability.

travels into the bulk, where they can learn the boundary condition g_q by visiting the brane. They then propagate light rays with the value q along the brane, as shown in Fig. 1.13 (left). Using methods from general relativity, we prove for arbitrary dimension and bulk matter that, if the bulk-local strategy is viable, then the entanglement wedge Ξ_A intersects the brane, where as above, A is any Cauchy slice of the decision region $\hat{\mathcal{V}}$. This is precisely what we expect from entanglement wedge reconstruction.[28] This situation is shown in Fig. 1.13 (middle lower). Taking the contrapositive, if Ξ_A is not connected (Fig. 1.13, middle upper), the bulk-local strategy does not work.
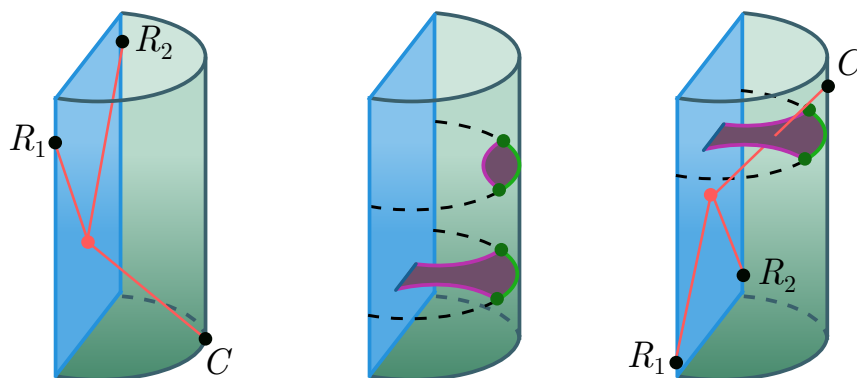
Figure 1.13: *Left.* The bulk-local strategy. *Middle.* The bulk local strategy works only if the entanglement wedge of $\hat{\mathcal{V}}$ is attached to the brane. *Right.* Applying the theorem in reverse for lower-dimensional black holes connects islands to bulk signal propagation.

Our results provide insight into the role of islands as channels for information escape. Focusing on the kinematics of bulk scattering, we can run our main result in reverse. Suppose that the return points generate the horizons of a black hole on the brane itself, and the CFT acts as our auxiliary flat space into which information can escape, in a similar spirit to Chapter 4. Consider a call point C in the future of both R_1 and R_2. We can form a time-reversed decision region $\hat{\mathcal{V}}$, and find that if a signal can travel through the bulk from the "bifurcation point" on the brane to C, then the entanglement wedge for $\hat{\mathcal{V}}$ attaches to the brane, as shown in Fig. 1.13 (right). Put simply, if information can

---

[28]We do not expect the "if" implication because light rays in the bulk are generically delayed by matter [81]. But for pure AdS$_3$ cut off by an ETW brane, there is no delay and we have an equivalence.

propagate causally through the higher dimension to C, the associated decision region has an island. This provides a sharp relation between islands and signal propagation in the higher-dimensional bulk.

1.6 Looking for a brane

In Chapter 3, we investigate microscopic conditions which ensure the Ryu-Takayagani formula holds for the bulk dual of 2d BCFT. This is what lets us peer behind the horizon in the boundary microstates of Chapter 2, and track information radiation in the dynamic black holes of Chapter 4. We also use this in Chapter 5 to explore the connection between islands and bulk signal propagation. But the propagation of bulk signals does not obviously follow from the same microscopic properties as entanglement. To see why, note that we can recast our quantum task as a correlator $\langle \mathcal{O}(R_1)\mathcal{O}(R_2)\mathcal{O}(C)\rangle$ for some operator $\mathcal{O}$. superposition of frequencies, shoot them into the bulk, and expect singularities when there is a bulk scattering vertex [82]. This is manifest in the bulk picture, but unexpected from a pure BCFT perspective. We would like to understand what this tells us about the BCFT.

In fact, there are singularities in this three-point function since the R_i lie on the edge, and it is simpler to consider the two-point function

$$\langle \mathcal{O}(C)\mathcal{O}(R)\rangle, \tag{1.127}$$

with a single return point R in the CFT interior. This is pictured in Fig. 1.14 (left). Although a single return point does not have all the information-theoretic properties of the task in Chapter 5,[29] it is still a nontrivial quantum task (start at C, determine q, send to R) where bulk-local strategies work when boundary-local ones do not, or equivalently, where there can be "surprise" singularities in the BCFT.

From the doubling trick, we expect the kinematics to be similar to a 4-point function in a full CFT, as in Fig. 1.14 (right). The suprise singularities in this correlator were

---

[29]This is more intuitive for a related "pizza delivery" quantum task in which the concealed bit $b \in \{0, 1\}$ must be sent to the output region R_b only. This problem becomes trivial with a single region, since we can always deliver the pizza!
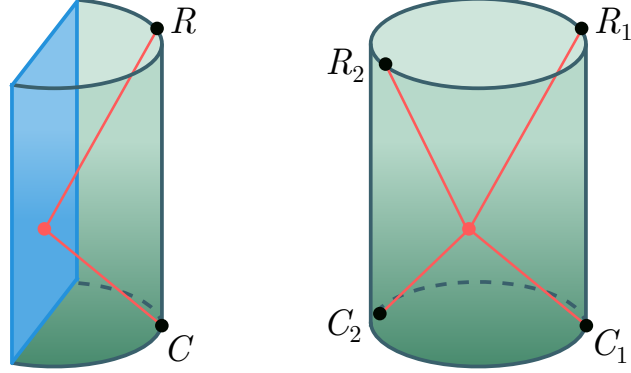
Figure 1.14: *Left.* A simple quantum task, with bulk scattering vertex on the brane. *Right.* The analogous correlator without a brane.

studied by Heemskerk, Polchinski, Penedones and Sully (HPPS) [17], who established the conditions listed at the end of §1.1.3 for a CFT with semiclassical bulk dual. In particular, these conditions guarantee *sub-AdS locality*, with the 4-point function exhibiting "suprise" singularities in bulk perturbation theory. Hartman [65] found that these same conditions guaranteed the RT formula (1.101) in a 2d CFT. Maldacena, Simmons-Duffin and Zhiboedov [83] reconsidered the problem. They used the apparent bulk singularties to place microscopic constraints on the spectrum and OPE coefficients appearing in the 4-point function. They also argued that at finite N, the "surprise" singularities should be smeared out into resonances, and were able to prove this rigorously in a 2d CFT.

Taking inspiration from [17, 83], in Chapter 6 we initiate the study of microscopic constraints on holographic BCFTs dual to spacetimes with geometric branes. In particular, using the sliced metric (1.117) and solutions (1.10) on each AdS_d slice, we are able to constrain the boundary operator spectrum in a fashion analogous to [83]. We find that, in order to have a "surprise" singularity in the BCFT correlator $\langle \mathcal{O}(R)\mathcal{O}(C)\rangle$, we need unrelated constraints for each boundary primary. Each boundary operator can backreact on the brane in different ways, and we need to tune them separately to prevent a breakdown of the geometry. This suggests that bulk causal structure is fragile, and BCFTs with good holographic duals are non-generic in the space of boundary states. Similarly, even when these conditions are satisfied we do not expect true singularities at finite N, a fact we are able to prove for 2d BCFTs.

Finally, unlike a CFT, the conditions required for Lorentzian bulk causal structure with a brane seem unrelated to constraints on entanglement entropy. This makes sense if we view entanglement entropy as arising from the behaviour of the bulk/boundary identity operator (and its descendants), as discussed in Chapter 3, and causal structure as an independent alignment of high-energy boundary primaries so as not to backreact on the geometry in different ways. Although symmetries (specifically, the conformal bootstrap program for boundary CFTs [84]) relate the high and low energy spectrum, these do not appear to be sufficiently constraining to guarantee a good bulk brane from conditions on entanglement entropy.

This does not negate the results of earlier chapters. We already know that CFTs with semiclassical duals are non-generic in the space of CFTs (even at large N), and boundary states in a given CFT are non-generic in the space of boundary conditions. The combination of the two—boundary states with semiclassical duals—is unsurprisingly non-generic in the space of boundary states. This does not make our results invalid, any more than the non-genericity of holographic CFTs makes AdS/CFT invalid. And like AdS/CFT, these special boundary states give us a framework in which some of the problems of quantum gravity and black holes may be profitably, and explicitly, addressed. However, we must bear in mind that they are atypical, and more work is required to understand the full structure of the black hole Hilbert space.

Chapter 2

Boundary Microstates

2.1 Introduction

In this chapter, following [85] and [86], we will explore the possibility that for certain CFT states, the corresponding black hole geometry is captured by the Penrose diagram in Fig. 2.1. Here, the geometry on the right side is the AdS-Schwarzschild black hole exterior. On the left, instead of the full second asymptotic region that would be present in the maximally extended black hole geometry, we have a finite region terminating on an end-of-the-world (ETW) brane (shown in red in Fig. 2.1). In the microscopic description, this brane could involve some branes from string/M theory theory or could correspond to a place where the spacetime effectively ends due to a degeneration of the internal space (as in a "bubble of nothing" geometry [87]).

The basic strategy will be to take a *boundary state*, roughly speaking an $\mathrm{SO}(d+1,1)$-invariant state of a CFT, and evolve it in Euclidean time. We then analytically continue from a moment-of-time symmetry to obtain a Lorentzian black hole. We call these configurations *boundary microstates*, since they provide a microscopic description of a state of a black hole, i.e. with some exterior Schwarzschild geometry.

The chapter is structured as follows:

- In the remainder of §2.1, we introduce some background material on black holes and AdS/BCFT in higher dimensions.
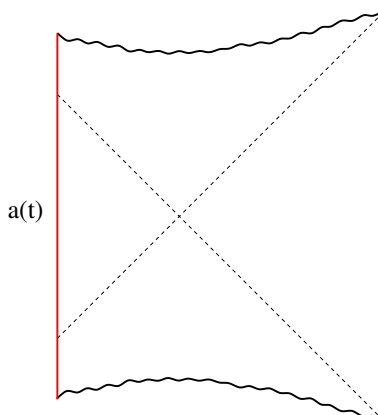
Figure 2.1: Penrose diagram for spacetimes associated with boundary microstates for black holes. The spacetime terminates on the left with an ETW brane (shown in red on the left).

- In §2.2, we discuss the construction of boundary microstates from the perspective of the Euclidean path integral on a cylinder. We derive an equation of motion for the ETW brane, and compute the analogue of the Hawking-Page transition between the thermal geometry and Schwarzschild black hole. We provide explicit solutions for the brane trajectories in $d = 2$.

- In §2.3, we discuss entanglement entropy in boundary microstates, and show that for a suitably large interval, the RT surface falls through the horizon and intersects the brane. This grants us in-principle access to physics behind the horizon. Again, we compute the results explicitly for $d = 2$.

- In §2.4, we point out a Rindler analogue of our construction in 2+1 dimensions, where the maximally extended black hole geometry is replaced with empty AdS space divided into complementary Rindler wedges and the microstates are particular states of a CFT on a half-sphere with BCFT boundary conditions.

- Finally, §2.5 discusses various open questions about this construction.
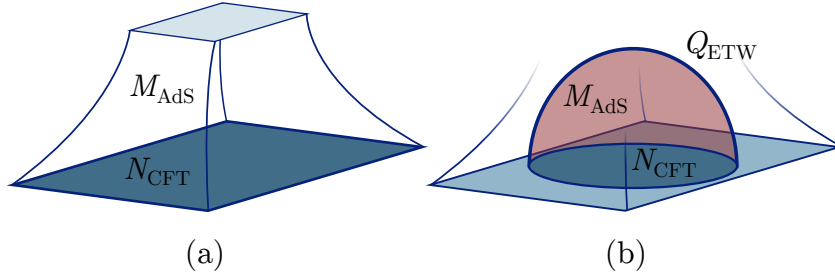
Figure 2.2: (a) The AdS/CFT correspondence, with an asymptotically AdS bulk M_{AdS} and an asymptotic boundary $N_{\text{CFT}} = \partial M_{\text{AdS}}$. (b) The AdS/BCFT correspondence. We add a boundary to the CFT, whose holographic "image" is the ETW brane Q.

2.1.1 AdS/BCFT in general dimensions

Consider a d-dimensional Euclidean CFT on $\mathbb{R}^d = \{(\tau, x_1, \ldots, x_{d-1})\}$, with conformal symmetry group $\text{SO}(d+1, 1)$. If we place a boundary at $\tau = 0$ and restrict the CFT to the half-space $\tau > 0$, we obtain a *boundary conformal field theory* (BCFT) with symmetry group $\text{SO}(d, 1)$, since conformal symmetry is only broken in the τ direction [88, 89]. Similarly, we can start with a finite temperature CFT ($T = 1/\beta$) on $\mathbb{R}^{d-1} \times \mathbb{S}^1_\beta$, and obtain a BCFT by restricting to a subinterval of the thermal circle. Once again, this breaks the symmetry to $\text{SO}(d, 1)$. A *boundary state* is just a state of the BCFT preserving the remaining $\text{SO}(d, 1)$-symmetry.

An important motivation for AdS/CFT is that the symmetries on both sides match, with the conformal symmetry group $\text{SO}(d+1, 1)$ equal to the isometry group of AdS_{d+1}. By analogy, we expect that a boundary state will be dual to a codimension-1 object with $\text{SO}(d, 1)$-symmetry, as proposed in [90] and [59, 91]. Different boundary states will give rise to different stress-energy content on the brane (to be discussed below), while the interior of the CFT will be dual to the interior of an asymptotically AdS spacetime, as per usual. For simplicity, the physics of this boundary was modelled by an ETW brane, as depicted in Fig. 2.2.

The physics of the bulk spacetime and ETW brane can be encoded in an action $I = I_{\text{bulk}} + I_{\text{ETW}}$. The first term I_{bulk} is the usual Einstein-Hilbert term, regularized by a

Gibbons-Hawking term at the asymptotic boundary:

$$I_{\text{bulk}} = -\frac{1}{16\pi G} \int_{M_{\text{AdS}}} \mathrm{d}^{d+1}x \, \sqrt{-g}(R - 2\Lambda) + I_{\text{bulk}}^{\text{matter}} + I_{\text{GHY}}. \tag{2.1}$$

The action on the ETW brane Q is a Gibbons-Hawking term, but for a dynamical boundary metric:

$$I_{\text{ETW}} = -\frac{1}{8\pi G} \int_{Q_{\text{ETW}}} \mathrm{d}^d y \, \sqrt{-h} K + I_{\text{ETW}}^{\text{matter}}, \tag{2.2}$$

where y^a are intrinsic coordinates on the brane, h_{ab} is the intrinsic brane metric, and K_{ab} is the extrinsic curvature.

More precisely,

$$K_{ab} = n_{\mu;\nu} e_a^\mu e_b^\nu, \quad K = K_{ab} h^{ab} \quad e_a^\mu = \frac{\partial x^\mu}{\partial y^a}. \tag{2.3}$$

Stress-energy on the brane is defined as the variational derivative of the brane matter action with respect to the intrinsic metric:

$$T_{ab}^{\text{ETW}} = \frac{2}{\sqrt{-h}} \frac{\delta I_{\text{ETW}}^{\text{matter}}}{\delta h^{ab}}. \tag{2.4}$$

Varying with respect to $g^{\mu\nu}$ and h^{ab} [58], we obtain Einstein's equation in the bulk and the Neumann condition on the brane:

$$R_{\mu\nu} - \frac{1}{2} R g_{\mu\nu} = 8\pi G T_{\mu\nu}^{\text{bulk}} - \Lambda g_{\mu\nu} \tag{2.5}$$

$$K_{ab} - K h_{ab} = 8\pi G T_{ab}^{\text{ETW}}. \tag{2.6}$$

We will focus on branes of *constant tension* T (or equivalently, constant extrinsic curvature), where T is defined by

$$8\pi G T_{ab}^{\text{ETW}} = \frac{(1 - d)}{L_{\text{AdS}}} T h_{ab} , \tag{2.7}$$

where the prefactor on the right hand side is chosen for convenience.

For general holographic BCFTs, we expect that the boundary action would be more complicated; it could include general terms involving intrinsic and extrinsic curvatures, sources for various bulk fields, and additional fields localized to the boundary. However, for this this chapter, we will focus on studying the simple one-parameter family of models as proposed in [90, 59].

Tension is a "phenomenological" parameter, but is related to the central charges of the BCFT. We can see this most explicitly for $d = 2$. Recall the boundary entropy g which appears in the expression for the vacuum entanglement entropy (1.119). Using the holographic prescription, [59] computed both the disk partition function and the entanglement entropy for intervals on a half line, showing that in both cases, the holographic calculation matches with the CFT result if the tension parameter is related to the boundary entropy by

$$g = \frac{L_{\text{AdS}}}{4G} \text{arctanh}(L_{\text{AdS}}T) \ . \tag{2.8}$$

Thus, larger values of the tension correspond to larger boundary entropy, or more degrees of freedom associated with the boundary. We expect that this qualitative relationship also holds in higher dimensions.

2.1.2 Schwarzschild AdS black holes

Eternal AdS black holes are dual to thermal states of the CFT [24]. In $d + 1$ dimensions, the Schwarzschild-AdS metric (SAdS$_{d+1}$) in Schwarzschild coordinates is

$$\mathrm{d}s^2 = -f(r)\,\mathrm{d}t^2 + \frac{\mathrm{d}r^2}{f(r)} + r^2\,\mathrm{d}\Omega_{d-1}^2 \tag{2.9}$$

$$f(r) = 1 + \frac{r^2}{L_{\text{AdS}}^2} - \frac{\mu}{r^{d-2}} \tag{2.10}$$

for AdS radius L_{AdS} and horizon radius r_H obeying $f(r_H) = 0$. For $d + 1 = 3$, the parameter $\mu = 1 + (r_H/L_{\text{AdS}})^2$, but in higher dimensions

$$\mu = r_H^{d-2}\left(\frac{r_H^2}{L_{\text{AdS}}^2} + 1\right). \tag{2.11}$$

Smoothness of the geometry relates r_H and the Hawking temperature $1/\beta$:

$$\beta = \frac{4\pi}{|f'(r_H)|} = \frac{4\pi r_H L_{\mathrm{AdS}}^2}{(d-2)L_{\mathrm{AdS}} + dr_H^2}. \tag{2.12}$$

For the moment, we set $L_{\mathrm{AdS}} = 1$.

For $r \gg 1$, the "blackening factor" $f(r) \approx r^2$, so the metric (2.9) reduces to the Poincaré patch of empty AdS (blue wedge in Fig. 2.3). However, the maximal extension of SAdS$_{d+1}$ has *two* such asymptotic regions. We can describe the full geometry using
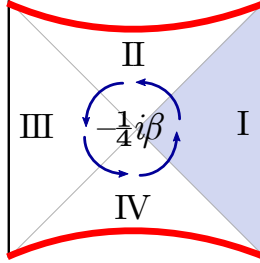
Figure 2.3: The eternal AdS black hole SAdS$_{d+1}$. For $d + 1 > 3$, the singularities (in red) are "bowed in" [7]. Crossing horizons counter-clockwise results in an imaginary increment to Schwarzschild time by $\Delta\tau = \beta/4$.

complexified Schwarzschild time $t = t_L + i\tau$, including this second exterior region. Each time we cross a horizon, starting in the right Poincaré patch and going around the Penrose diagram counter-clockwise, the Schwarzschild time is incremented by $-i\beta/4$ [7]. We can think of this as thermal time evolution by $\Delta\tau = \beta/4$.

2.2 Microstate geometries

In this section, we define boundary microstates and explore the dual geometries, assuming the simple constant-tension ansatz. These states were suggested and studied in the context of the SYK model by [85], and later studied directly in the context of holographic CFTs in [86]. Simple specific examples of these states and the corresponding geometries have been discussed earlier, for example in [92, 30, 65]. The microstate geometries will be time-

dependent and hence "non-equilibrium"; for a different construction of non-equilibrium microstates with geometry behind the horizon, see [93]. We will review and generalize those discussions, starting with the definition of the CFT states and then moving to the geometrical interpretation.

2.2.1 CFT states

The states we consider, suggested in [85], have two equivalent descriptions. First, consider the thermofield double state of two CFTs (on $\mathbb{S}^d$),

$$|\Psi_{\mathrm{TFD}}^{\beta}\rangle = \frac{1}{Z[\beta]} \sum e^{-\beta E_i/2} |E_i\rangle_L \otimes |E_i\rangle_R \ . \tag{2.13}$$

For high enough temperatures, this corresponds to the maximally extended AdS-Schwarzschild black hole geometry [30]. Now consider projecting this state onto some particular pure state $|B\rangle$ of the left CFT. This could be the result of measuring the state on the left. We will be more specific about the pure state $|B\rangle$ later on. The result is a pure state of the right CFT given by

$$|\hat{\Psi}_B^{\beta}\rangle = \frac{1}{Z[\beta]} \sum e^{-\beta E_i/2} \langle B|E_i\rangle |E_i\rangle \ . \tag{2.14}$$

We can think of this state as the result of measuring the state of the left CFT. If this measurement corresponds to looking at the state of local (UV) degrees of freedom, we might expect that the effects on the corresponding geometry propagate inwards causally (forward and backward, since we will be considering time-symmetric states) from near the left boundary, so that the geometry retains a significant portion of the second asymptotic region. This motivates considering states $|B\rangle$ with no long-range entanglement.

We can also consider a closely related state $|\Psi_B^{\beta}\rangle$ obtained by complex conjugation of the coefficients in the superposition,

$$\begin{aligned}
|\Psi_B^{\beta}\rangle &= \frac{1}{Z[\beta]} \sum e^{-\beta E_i/2} \langle E_i|B\rangle |E_i\rangle \\
&= \frac{1}{Z[\beta]} \sum e^{-\beta E_i/2} |E_i\rangle \langle E_i|B\rangle
\end{aligned}$$

59
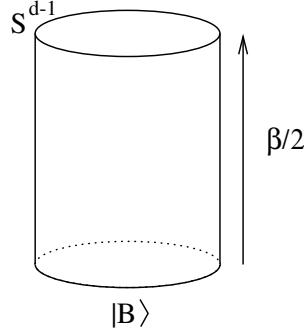
Figure 2.4: Path integral description of black hole microstates $|\Psi_B^\beta\rangle$.

$$= \frac{1}{Z[\beta]} e^{-\beta H/2} |B\rangle \ . \tag{2.15}$$

We recall that the operation $|\hat{\Psi}_B^\beta\rangle \to |\Psi_B^\beta\rangle$ is anti-linear and anti-unitary and corresponds to the operation of time-reversal. For example, given any Hermitian $\mathcal{O}$ we have that

$$\langle \Psi_B^\beta(t)|\mathcal{O}|\Psi_B^\beta(t)\rangle = \langle \hat{\Psi}_B^\beta(-t)|\mathcal{O}|\hat{\Psi}_B^\beta(-t)\rangle \ . \tag{2.16}$$

In our case, we will consider states which are time-reversal symmetric, so the two definitions are equivalent.

We see from (2.15) that the states $|\Psi_B^\beta\rangle$ correspond to starting from a state $|B\rangle$ and having a finite amount of Euclidean evolution. These states are naturally defined by a Euclidean path integral as shown in Fig. 2.4. Since the CFT path integral for holographic theories maps onto the gravity path integral, we will be able to make use of the AdS/CFT correspondence to deduce the corresponding geometries if we can choose states $|B\rangle$ for which we can understand a gravity prescription for dealing with the boundary condition at the initial Euclidean time.

2.2.2 Euclidean geometries

This CFT path integral is the key to constructing the microstates of interest. For a holographic CFT, we can compute the correlator *gravitationally* using the extrapolate dictionary [94] as a limit of bulk correlators in a Euclidean geometry with boundary $\mathbb{S}^{d-1} \times$

$[-\tau_0, \tau_0]$. The appropriate bulk geometry is determined by extremizing the gravitational action with appropriate boundary terms for the ETW brane. This geometry is time-reversal symmetric if we insert operators at $\tau = 0$ (or symmetrically around it). To find the Lorentzian geometry associated with our state, we take the $\tau = 0$ bulk slice as the initial data for our Lorentzian solution (which will also be time-reversal symmetric), also known as the Skenderis-van Rees prescription [20].

From the AdS/BCFT correspondence described above, we expect the bulk geometry dual to the Euclidean path integral to be an asymptotically AdS spacetime, with a dynamical ETW brane that forms an extension of the CFT boundary into the bulk. We wrote the equations of motion with a dynamical brane above, (2.5) and (2.6), with the constant tension condition (2.7). Since the boundary states obeys $SO(d, 1)$ symmetry, so does the ETW brane, and in particular it is spherically symmetric. The bulk geometry is also spherically symmetric, with some emergent radial direction r, and we can assume the Euclidean geometry of the brane depends only on r and the Euclidean time τ [91].
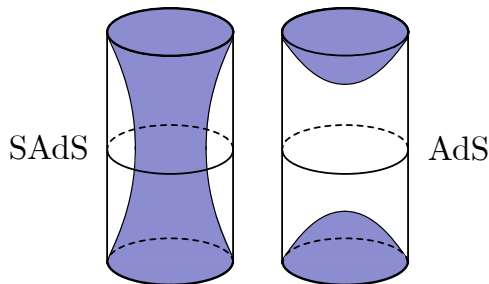
Figure 2.5: Euclidean gravity solutions "filling in" the boundary geometry. The phase with a connected ETW brane configuration (left), dominant for small β, is a Euclidean black hole geometry, while the disconnected brane (right) is thermal AdS.

Since the boundary is disconnected, there are two options for the topology of the ETW brane, a connected and a disconnected brane, depicted in Fig. 2.5. In fact, from spherical symmetry and Birkhoff's theorem, there are two possible bulk geometries: a Schwarzschild-AdS black hole, and thermal AdS, which is simply pure AdS with a periodic Euclidean time. There is a Hawking-Page phase transition between them depending on their Euclidean action, which we will compute explicitly in a moment [25, 91, 59].

Before moving onto the technicalities, we can in fact identify the topologies of Fig. 2.5 with geometries based on simple physical considerations. Since tension is essentially energy density, the energetic cost of a brane is proportional to its area. Thus, the connected phase will be favoured for "short" cylinders, corresponding to high temperatures, and hence the black hole phase. Similarly, the disconnected phase wil be favoured for "long" cylinders, which are at low temperatures and hence thermal AdS.

The approach to finding the brane trajectory is the same in both phases, and we outline the calculation briefly. It will turn out that both the Euclidean black hole and thermal AdS have metrics of the form

$$\mathrm{d}s^2 = f(r)\,\mathrm{d}\tau^2 + \frac{\mathrm{d}r^2}{f(r)} + r^2\mathrm{d}\Omega_{d-1}^2, \tag{2.17}$$

for some function $f(r)$ and spherical coordinates

$$\mathrm{d}\Omega_{d-1}^2 := \sum_i \vartheta_i\,(\mathrm{d}\theta^i)^2, \tag{2.18}$$

with ϑ_i functions of the angular variables θ^i, satisfying $\sum_i \vartheta_i^2 = 1$. If we parameterize our brane embedding by $r(\tau)$, the induced metric is

$$\mathrm{d}s_{\mathrm{ETW}}^2 = \left[f(r) + \frac{r'^2}{f(r)}\right]\mathrm{d}\tau^2 + r^2\mathrm{d}\Omega_{d-1}^2,$$

where $r' = \mathrm{d}r/\mathrm{d}\tau$. We set $L_{\mathrm{AdS}} = 1$ in the rest of the derivation.

For intrinsic coordinates $y^a := (\tau, \vec{\theta})$, we can immediately read off $h_{ii} = r^2\vartheta_i$. The unit normal is

$$n_\mu = \gamma(r', 1, \vec{0}), \quad \gamma := \sqrt{\frac{f(r)}{f(r)^2 + r'^2}}. \tag{2.19}$$

The ii component of the extrinsic curvature is

$$K_{ii} = n_{\mu;\nu}e_i^\mu e_i^\nu = n_{i;i} = \Gamma_{ii}^\mu n_\mu = \gamma r f(r)\vartheta_i. \tag{2.20}$$

Taking the trace of the Neumann condition (2.6) and using (2.7), we find $K = dT$. Hence,

62

the ii component of (2.6) combined with (2.20) yields

$$K_{ii} = T h_{ii} \quad \implies \quad \gamma r f(r) \vartheta_i = T r^2 \vartheta_i. \tag{2.21}$$

Rearranging, we deduce the equation of motion for the brane with respect to Euclidean time,

$$\frac{\mathrm{d}r}{\mathrm{d}\tau} = \frac{f(r)}{Tr} \sqrt{f(r) - T^2 r^2}. \tag{2.22}$$

We now discuss the two phases in more detail, and compute their actions in order to see when the phase transition occurs.

Black hole phase

We start with the black hole phase. We can Wick rotate the Lorentzian Schwarzchild coordinates (2.9) to obtain the Euclidean metric

$$\mathrm{d}s^2 = f(r)\, \mathrm{d}\tau^2 + \frac{\mathrm{d}r^2}{f(r)} + r^2\, \mathrm{d}\Omega_{d-1}^2, \quad f(r) = 1 + \frac{r^2}{L_{\mathrm{AdS}}^2} - \frac{\mu}{r^{d-2}}, \tag{2.23}$$

with $\mu = 1 + (r_H / L_{\mathrm{AdS}})^2$ in $d = 2$, and for $d > 2$,

$$\mu = r_H^{d-2} \left(\frac{r_H^2}{L_{\mathrm{AdS}}^2} + 1 \right).$$

Solutions of (2.22) that are symmetric about $\tau = 0$ will have $\mathrm{d}r/\mathrm{d}\tau = 0$ for $\tau = 0$, with r equal to some minimum value r_0 determined in terms of T and r_H by

$$f(r_0) = T^2 r_0^2 . \tag{2.24}$$

This gives the maximum ETW brane radius in the Lorentzian solution. As we increase T, the ratio r_0 / r_H increases monotonically from 1 at $T = 0$. In $d = 2$, we have simply

$$\frac{r_0}{r_H} = \frac{1}{\sqrt{1 - T^2}} , \tag{2.25}$$

63
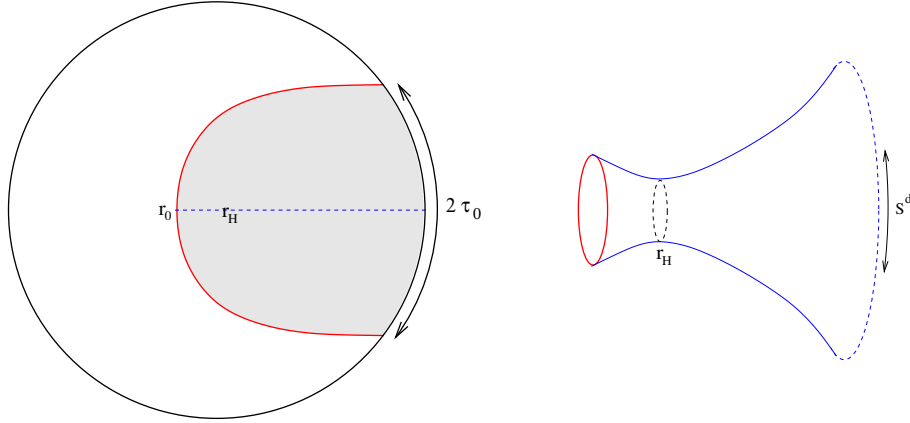
Figure 2.6: Euclidean geometry associated with a $T > 0$ state. *Left.* ETW brane trajectory on r, τ plane, with $r = r_H$ at the center and $r = \infty$ represented as the boundary of the disk. We have a S^d of radius r associated with each point. *Right.* Spatial geometry fixed by time-reflection symmetry (blue dashed line on the left). This provides the initial data for the Lorentzian solution.

while in higher dimensions, we will see below that this ratio reaches a finite maximum value. Integrating (2.22), the brane locus obeys

$$
\tau(r) = \int_{r_0}^{r} d\hat{r} \frac{T\hat{r}}{f(\hat{r})\sqrt{f(\hat{r}) - T^2\hat{r}^2}} \ . \tag{2.26}
$$

A typical solution for $T > 0$ is depicted in Fig. 2.6. On the left, the full disk represents the r, τ coordinates of the Euclidean Schwarzschild geometry, with r ranging from r_H at the center to infinity at the boundary. We have an $\mathbb{S}^d$ of radius r associated with each point. The ETW brane bounds a portion of the spacetime (shaded) that gives the Euclidean geometry associated with our state. This has a time-reflection symmetry about the horizontal axis. The invariant co-dimension one surface (blue dashed line) gives the $t = 0$ geometry (depicted on the right) that we will analytically continue to obtain the associated Lorentzian solution In this picture, the minimum radius sphere corresponds to the black hole horizon, so we see that the ETW brane is behind the horizon. For $T < 0$, we obtain the same trajectories, but the geometry corresponds to the unshaded part, and the ETW brane from the initial data slice is outside the horizon.

For a given r_H and T, the Euclidean preparation time τ_0 associated with the solution corresponds to half the range of τ bounded by the ETW brane at the AdS boundary. This is given explicitly by

$$\tau_0 = \frac{2\pi r_H}{dr_H^2 + (d-2)} - \int_{r_0}^{\infty} \mathrm{d}r \frac{Tr}{f(r)\sqrt{f(r) - T^2 r^2}} \; . \tag{2.27}$$

For a specified tension T and preparation time τ_0, the temperature of the corresponding black hole is determined implicitly by this equation. There can be more than one pair r_H that gives the same τ_0 for fixed T, but in this case, the solution with smaller r_H is never the minimum action solution.

For $d = 2$, we find that for every value of T and r_H, the ETW brane trajectory meets the boundary of the (r, τ) disc at antipodal points, so the black hole temperature is very simply related to the Euclidean preparation time,

$$\tau_0 = \frac{\beta}{4} = \frac{\pi}{2r_H} \; . \tag{2.28}$$

In this case, the ETW brane radius on the initial data slice is

$$r_0 = \frac{r_H}{\sqrt{1 - T^2}} \; , \tag{2.29}$$

so the region behind the horizon can become arbitrarily large as we take $T \to 1$. This is consistent with the thermalization of boundary states in $d = 2$ [63].

For $d > 2$ we find that Euclidean solutions in this phase exist only for a portion of the $\tau_0 - T$ plane. In particular, we have some maximum value $T_{\max}$ above which there are no Euclidean solutions with a connected ETW brane (corresponding a black hole geometry). For $T > T_*(r_H)$, the corresponding Euclidean solutions are not sensible since the ETW brane overlaps itself, as shown on the left in Fig. 2.7. In this case, the thermal AdS geometry (with disconnected ETW branes bounding the Euclidean past and future in the Euclidean solution) is apparently the only possibility. However, it may be possible that in a more complete holographic model, repulsive self-interactions for fields on the brane prevent the trajectory from overlapping itself, as depicted in Fig. 2.7 (right).
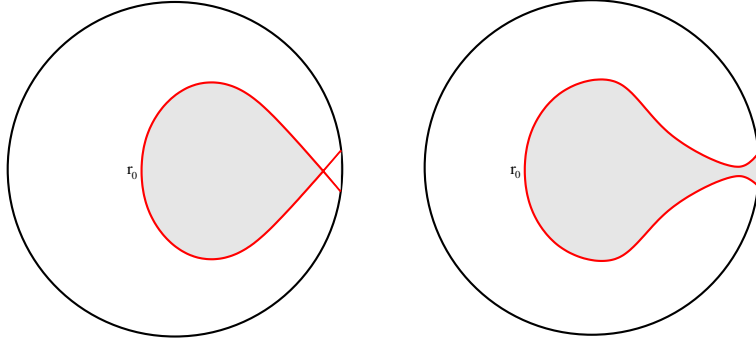
Figure 2.7: *Left.* Euclidean ETW brane trajectories for $d > 2$ and $T_*(r_H) < T$ in the regime where the classical brane trajectory overlaps itself. *Right.* A possible alternative picture in a more complete holographic model with self-interactions of the ETW brane.

Thermal AdS phase

Thermal AdS has a metric of the form (2.17), with

$$f(r) = r^2 + L_{\text{AdS}}^2.$$

Again, we set $L_{\text{AdS}} = 1$. For any value of τ_0 and $T > 0$, there exists a Euclidean solution where the ETW brane has two disconnected components as shown on the right in Fig. 2.5. We can parameterize the brane embedding by $\tau(r)$ with $\tau(\infty) = \pm\tau_0$ for the upper and lower brane respectively. From (2.22), the brane embedding is given by

$$\tau(r) - \tau_0 = \int_r^\infty \mathrm{d}\hat{r} \frac{T\hat{r}}{f(\hat{r})\sqrt{f(\hat{r}) - T^2\hat{r}^2}} \ , \tag{2.30}$$

with $f(r) = r^2 + 1$. Integrating, we find (in any dimension)

$$\tau(r) - \tau_0 = \text{arcsinh}\left(\frac{T}{\sqrt{r^2 + 1}\sqrt{1 - T^2}}\right) \tag{2.31}$$

The negative τ component of the ETW brane is obtained via $\tau \to -\tau$.

Comparing actions

In order to determine which type of solution leads to the classical geometry associated with our state for given (τ_0, T), we need to compare the Euclidean gravitational action for the two phases. Recall that this action is a sum of bulk and boundary contributions,

$$I_E = I_{\text{bulk}} + I_{\text{ETW}} = -\frac{1}{16\pi G} \int \mathrm{d}^{d+1}x\sqrt{g}(R - 2\Lambda) - \frac{1}{8\pi G} \int \mathrm{d}^d y\sqrt{h}(K - (d-1)T) \ . \tag{2.32}$$

For the solutions we consider, the bulk and boundary equations of motion (2.5), (2.6), and (2.7) imply that $R - 2\Lambda = -2d$ and $K - (d-1)T = T$. We also note that for geometries of the form (2.17), we have

$$\sqrt{g} = r^{d-1}, \tag{2.33}$$

while from (2.22), the determinant of the induced metric is

$$\sqrt{h} = \pm\frac{1}{T}r^{d-2}f(r)\frac{\mathrm{d}\tau}{\mathrm{d}r}, \tag{2.34}$$

where we have the $+$ or $-$ depending on whether τ is an increasing or decreasing function of r. Finally, integrating over all of space will produce infinities which we must regularize. For both phases, we will integrate up to $r = r_{\text{max}}$, corresponding to $z = \epsilon$ in Fefferman-Graham coordinates [95], then take the limit $\epsilon \to 0$ after subtracting the actions for the two phases.

Let us warm up with the pure AdS calculation. The bulk action gives

$$I_{\text{bulk}} = \frac{\omega_{d-1}}{8\pi G} \int_0^{r_{\text{max}}} \mathrm{d}r \, dr^{d-1} \cdot 2\tau(r), \tag{2.35}$$

where $\omega_{d-1} = \text{vol}(\mathbb{S}^{d-1})$, and $\tau(r)$ obeys (2.31). Each component of the boundary action gives

$$I_{\text{ETW}} = \frac{\omega_{d-1}}{8\pi G} \int_0^{r_{\text{max}}} \mathrm{d}r \, \frac{r^{d-2}f(r)}{\mathrm{d}r/\mathrm{d}\tau} \ . \tag{2.36}$$

Combining these, we have

$$I_E^{\text{AdS}} = \frac{\omega_{d-1}}{4\pi G} \left\{ r_{\max}^d \tau(r_{\max}) + \int_0^{r_{\max}} \mathrm{d}r \, \frac{r^{d-2}}{\mathrm{d}r/\mathrm{d}\tau} \right\}$$

where $\mathrm{d}r/\mathrm{d}\tau$ can be read off from (2.22).

For the black hole phase, we integrate up to $r = \hat{r}_{\max}$ and subtract the action for the excised part. This gives

$$I_{\text{bulk}} = \frac{\omega_{d-1}}{8\pi G} \int_{r_H}^{\hat{r}_{\max}} \mathrm{d}r \, dr^{d-1}\beta - \int_{r_0}^{\hat{r}_{\max}} \mathrm{d}r \, dr^{d-1} 2\tau(r), \tag{2.37}$$

where $\tau(r)$ obeys (2.22), with

$$f(r) = r^2 + 1 - \frac{r_H^{d-2}}{r^{d-2}}(1 + r_H^2). \tag{2.38}$$

The brane action has the same form as for pure AdS, but integrated up to $\hat{r}_{\max}$. Combining everything, we get

$$I_E^{\text{BH}} = \frac{\omega_{d-1}}{4\pi G} \left\{ \frac{\beta}{2} r^d \Big|_{r_H}^{\hat{r}_{\max}} - r^d \tau(r) \Big|_{r_0}^{\hat{r}_{\max}} - \int_{r_0}^{\hat{r}_{\max}} \mathrm{d}r \frac{(r^{d-2}f(r) - r^d)}{\mathrm{d}r/\mathrm{d}\tau} \right\}.$$

In order to compare the actions, we choose both $r_{\max}$ and $\hat{r}_{\max}$ to each correspond to the surface $z = \epsilon$ in Fefferman-Graham coordinates. The z coordinate is related to the r coordinate by

$$\frac{\mathrm{d}z}{z} = \frac{\mathrm{d}r}{\sqrt{f(r)}}, \tag{2.39}$$

with the integration constant fixed by demanding that $r \sim 1/z$ at leading order for small z. For the pure AdS case, this gives in any dimension

$$r_{\max} = \frac{1}{\epsilon} - \frac{\epsilon}{4}. \tag{2.40}$$

while the expression for the Euclidean black hole depends on the dimension. For $d = 2$,
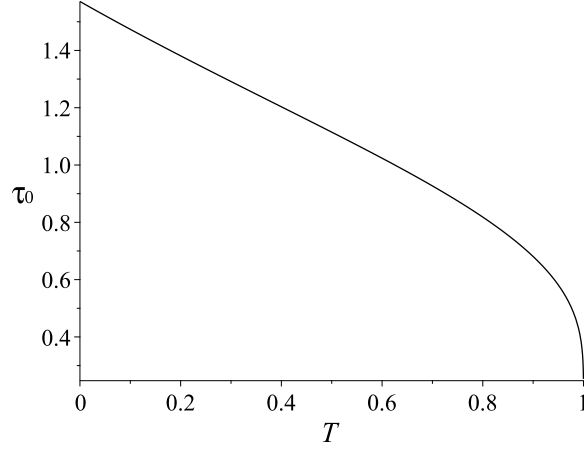
Figure 2.8: Critical value of τ_0 vs T for $d = 2$.

for instance, we have

$$\hat{r}_{\max}^{d=2} = \frac{1}{\epsilon} + \frac{\pi^2 \epsilon}{16\tau_0^2} + O(\epsilon^3).$$ (2.41)

For any choice of d, we can evaluate the difference

$$\Delta I_E = I_E^{\text{AdS}}(T, \tau_0, \epsilon) - I_E^{\text{BH}}(T, \tau_0, \epsilon)$$ (2.42)

and take the limit $\epsilon \to 0$ in order to determine which solution has smaller action and gives rise to the classical geometry associated with the state.

Since this difference does not have a simple expression for general d, we will content ourselves with an example. For $d = 2$, we can plug in the explicit formulas for $\tau(r)$ and $\mathrm{d}r/\mathrm{d}\tau$ to obtain

$$\lim_{\epsilon \to 0}(I_E^{\text{AdS}}(T, \tau_0, \epsilon) - I_E^{\text{BH}}(T, \tau_0, \epsilon)) = \frac{1}{2G}\left[-\text{arctanh}(T) - \frac{\tau_0}{2} + \frac{\pi^2}{8\tau_0}\right].$$ (2.43)

Thus, our states (for a CFT on a unit circle) correspond to bulk black holes when

$$\tau_0 < -\text{arctanh}(T) + \sqrt{\frac{\pi^2}{4} + \text{arctanh}^2(T)}\,.$$ (2.44)

69

This phase boundary is shown in Fig. 2.8. Our result agrees with the calculation of [58] (reinterpreted for our context).

2.2.3 Lorentzian geometries

To find the Lorentzian geometries associated with our states, we use the $\tau = 0, \pi$ slice of the Euclidean geometry as initial data for Lorentzian evolution. The resulting geometry is a portion of the maximally extended black hole geometry, with one side truncated by a dynamical ETW brane. These Lorentzian geometries parallel earlier results on domain walls and thin shells in AdS [96, 7, 97].[1] For $T > 0$, we will see that the brane emerges from the past singularity, expands into the second asymptotic region and collapses again into the future singularity. For $T < 0$ we have an equivalent ETW brane trajectory but on the other side of the black hole, so that the brane emerges from the horizon, enters the right asymptotic region, and falls back into the horizon.

Using Schwarzschild coordinates to describe the portion of the ETW brane trajectory in one of the black hole exterior regions, the brane locus is given by the analytic continuation of the Euclidean trajectory. To achieve this, we simply set $\tau = -it$. We can absorb this into the square root in (2.22), so it becomes

$$\frac{\mathrm{d}r}{\mathrm{d}t} = \frac{f(r)}{Tr}\sqrt{T^2 r^2 - f(r)}.$$
(2.45)

Integrating gives

$$t(r) = \int_{r_0}^{r} \mathrm{d}\hat{r} \frac{T\hat{r}}{f(\hat{r})\sqrt{T^2\hat{r}^2 - f(\hat{r})}} \ .$$
(2.46)

For example, in $d = 2$, we obtain

$$\cosh(tr_H)\sqrt{\frac{r^2}{r_H^2} - 1} = \frac{T}{\sqrt{1 - T^2}} \ .$$
(2.47)

To understand the behaviour of the brane in the full spacetime, it is convenient to

---

[1]Indeed, the Neumann condition reduces to the thin shell junction condition where the extrinsic curvature on the "excised" side of the brane vanishes.

rewrite the equation in terms of the proper time λ on the brane, related to Schwarzschild time by

$$\frac{\mathrm{d}t}{\mathrm{d}\lambda} = \gamma = \sqrt{\frac{f(r)}{f(r)^2 - \dot{r}^2}} \; . \tag{2.48}$$

We then find that the coordinate-independent equation of motion for the brane relating the proper radius r to the proper time λ is simply

$$\dot{r}^2 = T^2 r^2 - f(r) \; , \tag{2.49}$$

where now the dot indicates a derivative with respect to proper time. In terms of $L = \log(r)$, this becomes simply

$$\dot{L}^2 + V(L) = T^2 \tag{2.50}$$

where

$$V(L) = \frac{f(r)}{r^2} = 1 + e^{-2L} - e^{-d(L - L_H)}(1 + e^{-2L_H}) \; . \tag{2.51}$$

So the trajectory $L(\lambda)$ is that of a particle in a one-dimensional potential $V(L)$ with energy T^2. These potentials take the form shown in Fig. 2.9.

Considering general values of T, we can have five classes of trajectories (two for $d = 2$), as shown on the right in Fig. 2.9. However, all of our time-symmetric Euclidean solutions in the black hole phase correspond to values $T < 1$ (corresponding to case **a**) in Fig. 2.9) for which the Lorentzian trajectory starts at $r = 0$, increases to $r = r_0$ and decreases back to $r = 0$. Thus, the brane emerges from the past singularity, reaches a maximum size r_0, and shrinks again to $r = 0$ at the future singularity.

General tension

In this subsection, we discuss the Lorentzian solutions corresponding to general values of the parameter T. We recall that in terms of the proper time and the variable $L = \log(r)$ (where r is the proper radius of the brane), the equation for the brane trajectory is

$$\dot{L}^2 + V(L) = T^2 \tag{2.52}$$
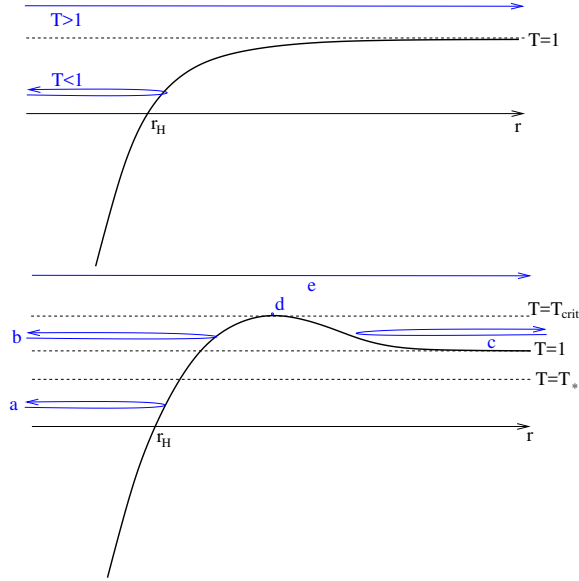
Figure 2.9: Effective potential $V(L)$ and types of Lorenzian ETW brane trajectories for $d = 2$ (above) and $d > 2$ (below).

where

$$V(L) = \frac{f(r)}{r^2} = 1 + e^{-2L} - e^{-d(L-L_H)}(1 + e^{-2L_H}) \ . \tag{2.53}$$

So the trajectory $L(\lambda)$ is that of a particle in a one-dimensional potential $V(L)$ with energy T^2.

For $d = 2$, the potential is monotonically increasing and asymptotes to 1. The Lorentzian trajectories for $|T| < 1$ all correspond to time-symmetric configurations where the brane emerges from the past singularity at $r = 0$, reaches a maximum size $r_0 = r_H/\sqrt{1 - T^2}$, and shrinks again to $r = 0$ at the future singularity. These all have analytic continuations to Euclidean solutions as discussed above. For $T > 1$, there are no time-symmetric trajectories; the ETW brane size either increases from $r = 0$ to $r = \infty$ or shrinks from $r = \infty$ to $r = 0$. These do not come from analytically continued time-symmetric geometries, and we expect that they do not correspond to the types of states we have been discussing.

For $d > 2$, the potential is monotonically increasing to some value $T_{\text{crit}}^2 > 1$, where

$$T_{\text{crit}} = 1 + \left(\frac{2}{d}\right)^{\frac{2}{d-2}} \left(1 - \frac{2}{d}\right) \frac{1}{r_H^2(1 + r_H^2)^{\frac{2}{d-2}}} . \tag{2.54}$$

We have five classes of trajectories, as shown below in Fig. 2.9. The corresponding spacetimes are shown in Fig. 2.10.
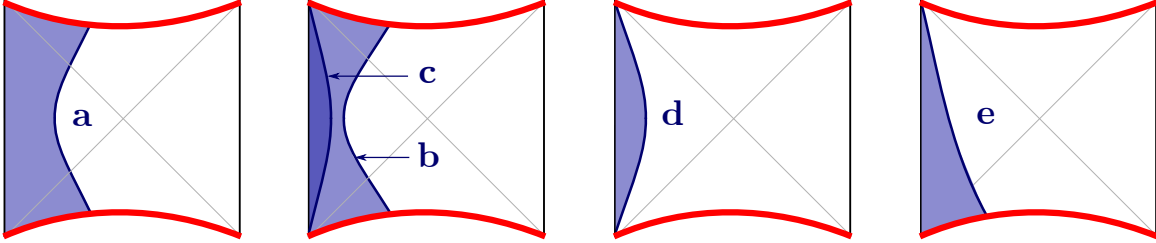
Figure 2.10: Lorentzian ETW branes for various values of T.

- **Case a**: $0 < T < T_*$

  For this case, we have time-symmetric solutions which have analytic continuations to good Euclidean solutions corresponding to some finite positive Euclidean preparation time. These are the geometries that are most plausibly providing a holographic picture of the microstate geometries for some legitimate CFT states. The Lorentzian geometry takes the form in Fig. 2.1. The brane emerges from the past singularity, expands and enters the second asymptotic region and then shrinks, eventually falling into the future horizon. The maximum radius of the ETW brane is r_0 (the minimal radius in the Euclidean solution), realized at the time-symmetric point $t = 0$.

- **Case b**: $1 < T < T_{\text{crit}}$, small r branch

  For this case, we have Lorentzian trajectories that are qualitatively similar to the previous case, but we recall that here the corresponding Euclidean solutions are not sensible (at least without some improvement of the model). It is possible that these

Lorentzian solutions still correspond to some CFT states, but we do not have a clear argument for this.

- **Case c**: $1 < T < T_{\mathrm{crit}}$, large r branch

For these solutions the ETW brane starts and ends at infinite size, shrinking to a minimum size at the time-symmetric point. We have an infinitely large portion of the second asymptotic region both in the past and the future, so it is unlikely these geometries correspond to pure states of a single CFT.

- **Case d**: $T = T_{\mathrm{crit}}$

In this case, we have Lorentzian brane trajectories at a constant radius, and the ETW brane geometry is the Einstein static universe. Here, the solutions retain the isometry present in the maximally extended black hole geometry and the physics of the CFT is time-independent. The Euclidean solutions in this case also have the brane at a constant radius, so the trajectory does not intersect the Euclidean boundary and does not seem likely to correspond to the class of states we have been discussing. However, it is interesting that the spacetime picture we have been discussing is similar to the proposal of [93] for the geometries dual to typical states, so perhaps the Lorentzian geometries in this case can serve as a model of the typical states. It is intriguing that we are constrained to have the brane at one specific radius,

$$\frac{r}{r_H} = \left(\frac{d}{2}\right)^{\frac{1}{d-2}} (1 + r_H^2)^{\frac{1}{d-2}} \ . \tag{2.55}$$

- **Case e**: $T > T_{\mathrm{crit}}$

For this case, there are no time-symmetric ETW brane trajectories, and we have an infinitely large portion of the second asymptotic region either in the past or the future. It seems unlikely that these geometries correspond to pure states of a single CFT.

74
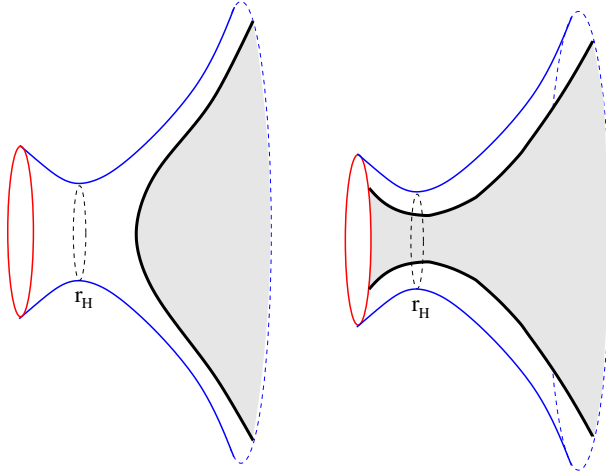
Figure 2.11: Two possibilities for extremal surfaces and associated entanglement wedges (shaded) for ball-shaped boundary regions. The extremal surface on the right has the topology of S^{d-2} times an interval, so is connected for $d > 2$.

2.3 Probing behind the horizon with entanglement

In this section, we consider the holographic calculation of entanglement entropy for CFT states whose dual geometries are captured by Fig. 2.1. We will continue to use the simple model of a spacetime terminating with an ETW brane, but we expect the same qualitative conclusions when the ETW brane is replaced by a more complete microscopic description. We begin by considering a general behind-the-horizon ETW brane trajectory $r(t)$ symmetric about $t = 0$ with maximum radius $r(0) = r_0$.

We will consider the entanglement entropy for ball-shaped regions on the sphere as a function of size and of CFT time. As depicted in Fig. 2.11, we have extremal surfaces that stay outside the horizon, but we can also have extremal surfaces that enter the horizon and end on the ETW brane.[2] Depending on the value of time and the ball size, we can

---

[2]We recall that the topological constraint on the extremal surfaces is that they are homologous to the boundary region under consideration. This means that the surface together with the boundary region form the boundary of some portion of a spatial slice of the bulk spacetime. The relevant regions in the two cases are shown as the shaded regions in Fig. 2.11. In the case where the extremal surfaces go behind the horizon and terminate on the ETW brane, this region includes part of the ETW brane. We emphasize that

have transitions between which type of surface has least area. In the phase where the exterior surface has less area, the CFT entanglement entropy will be time-independent (at leading order in large N), while in the other phase, we will have time dependence inherited from the time-dependent ETW brane trajectory. In our examples below, we will find that in favorable cases, the minimal area surface for sufficiently large balls goes behind the horizon during some time interval $[-t_0, t_0]$ which increases with the size of the ball.

2.3.1 A tale of two surfaces

We now turn to the details of the holographic calculation of entanglement entropy given some ETW brane trajectory $r(t)$. This was calculated for the $T = 0$ case in [65]. Similar methods were used in slightly more exotic geometries, and reaching different conclusions, in [98].

Exterior extremal surfaces

First, consider the exterior extremal surfaces, working in Schwarzschild coordinates. Let θ_0 be the angular size of the ball, such that $\theta_0 = \pi/2$ corresponds to a hemisphere.

Since the exterior geometry is static, the extremal surface lives in a constant t slice, and we can parameterize it by $r(\theta)$. In terms of this, the area is calculated as

$$\text{Area}_{\text{ext}} = \omega_{d-2} \int \mathrm{d}\theta \, r^{d-2} \sin^{d-2}\theta \sqrt{r^2 + \frac{1}{f(r)}(r')^2}. \tag{2.56}$$

Extremizing this action, we obtain equations of motion that can be solved numerically, or analytically in the $d = 2$ case discussed in §2.3.2.

To obtain a finite result for entanglement entropy, we use a similar strategy to compute the action, first regulating by integrating up to some fixed r_{max} corresponding to $z = \epsilon$ in Fefferman-Graham coordinates. We then subtract off the vacuum entanglement entropy, calculated in the same way but with pure AdS, i.e. $f(r) = r^2 + 1$. Finally, we take $\epsilon \to 0$.

this is not part of the extremal surface and its area should not be included in the holographic calculation of entanglement entropy.

Interior extremal surfaces

To study extremal surfaces that pass through the horizon, it is convenient to work in a set of coordinates that cover the entire spacetime. In this case, we parameterize the surfaces by a time coordinate and a radial coordinate, which are both taken to be functions of an angle θ on the sphere.

The only new element here is that the extremal surfaces intersect the ETW brane, and we need to understand the appropriate boundary conditions here. Since we are extremizing area, our extremal surfaces must intersect the ETW brane normally, so that a variation in the intersection locus does not change the surface area to first order.

Criterion for seeing behind the horizon with entanglement

When the behind-the-horizon extremal surfaces have less area, the CFT entanglement is detecting a difference between our state and the thermal state. We expect that this is most likely to happen for $\theta = \pi/2$, where we are looking at the largest possible subsystem, and for $t = 0$, since at other times the state will become more thermalized.

For this case $\theta_0 = \pi/2$, $t = 0$, the behind-the-horizon extremal surface remains at $\theta = \pi/2$ and $t = 0$, extending all the way to the ETW brane on the far side of the horizon. This intersects the ETW brane normally by the time-reflection symmetry. In this case, we can calculate the regulared areas explicitly as

$$\text{Area}_{\text{int}}(\theta = \pi/2, t = 0, r_0) = \omega_{d-2} \int_{r_H}^{r_{\text{max}}} \mathrm{d}r \frac{r^{d-2}}{\sqrt{f(r)}} + \omega_{d-2} \int_{r_H}^{r_0} \mathrm{d}r \frac{r^{d-2}}{\sqrt{f(r)}} \ . \quad (2.57)$$

When this area is greater than the area of the exterior extremal surface corresponding to $\theta = \pi/2$, we expect that the entanglement entropy will always be calculated in terms of the exterior surfaces. Thus, we have a basic condition

$$\text{Area}_{\text{ext}}(\pi/2) > \text{Area}_{\text{int}}(\theta = \pi/2, t = 0, r_0) \quad (2.58)$$

for when entanglement will tell us something about the geometry behind the horizon. This is more likely to be satisfied for smaller values of r_0 (ETW brane not too far past the

horizon). It can fail to be satisfied even for $r_0 = r_H$ if the black hole is too small, so below some minimum value $r_H^{\min}$, all minimal area extremal surfaces probe outside the horizon.

2.3.2 Analytics in $d = 2$

In this section, we work out the explicit results for $d = 2$ where the CFT lives on a circle. We will restore L_{AdS} to facilitate a later comparison to the microscopic result. We calculate the entanglement entropy $S(\Delta\theta, t)$ for an interval of angular size $\Delta\theta$ on the circle, as a function of CFT time t. We find that having access to large enough subsystem of the CFT allows us to probe behind the horizon, and thus renders the microstates distinguishable, in broad qualitative agreement with [99].

Exterior extremal surfaces

First consider the exterior surfaces, which we parameterize by $r(\theta)$. Since the integrand $\mathcal{L}$ in (2.56) does not depend explicitly on θ, the extremizing surfaces must satisfy

$$r' \frac{\delta\mathcal{L}}{\delta r'} - \mathcal{L} = \text{constant}. \tag{2.59}$$

Calling this constant r_0 (this represents the minimum value of r on the trajectory, where $r' = 0$), we get

$$r' = \pm \frac{r}{r_0 L_{\mathrm{AdS}}} \sqrt{(r^2 - r_H^2)(r^2 - r_0^2)} . \tag{2.60}$$

The solution, taking $\theta = 0$ to be the point where $r = r_0$, is given implicitly by

$$\theta = -\frac{L_{\mathrm{AdS}}}{2 r_H} \ln \left[\frac{-2 r_H^2 r_0^2 + r_H^2 r^2 + r^2 r_0^2 - 2 r_0 r_H \sqrt{(r^2 - r_0^2)(r^2 - r_H^2)}}{r^2 (r_0^2 - r_H^2)} \right] . \tag{2.61}$$

We will only need that

$$\theta(r = \infty) = \frac{L_{\mathrm{AdS}}}{2 r_H} \ln \left(\frac{r_0 + r_H}{r_0 - r_H} \right) , \tag{2.62}$$

78

so that

$$\frac{r_0}{r_H} = \coth\left(\frac{r_H \Delta\theta}{2L}\right) . \tag{2.63}$$

The area of such a surface, regulating by integrating only up to $r_{\max} = L/\epsilon$ is

$$\text{Area}(\Delta\theta) = 2L_{\text{AdS}} \ln\left(\frac{2L_{\text{AdS}}}{\epsilon r_H} \sinh\left(\frac{r_H \Delta\theta}{2L_{\text{AdS}}}\right)\right), \tag{2.64}$$

where we have dropped terms of order ϵ.

Using the *Brown-Henneaux relation* $c = 3L_{\text{AdS}}/2G$ for the central charge c [18], this gives entropy $S = \text{Area}/(4G)$ of

$$S = \frac{c}{3} \ln\left(\frac{2L_{\text{AdS}}}{\epsilon r_H} \sinh\left(\frac{r_H \Delta\theta}{2L_{\text{AdS}}}\right)\right) . \tag{2.65}$$

In terms of the CFT effective temperature β, we have $r_H/L_{\text{AdS}} = 2\pi L_{\text{CFT}}/\beta$, where L_{CFT} is the size of the circle on which the CFT lives. Thus, the result in terms of CFT parameters is

$$S = \frac{c}{3} \ln\left(\frac{\beta}{\epsilon\pi L_{\text{CFT}}} \sinh\left(\frac{\pi L_{\text{CFT}} \Delta\theta}{\beta}\right)\right) . \tag{2.66}$$

This agrees with the CFT result for finite temperature [62]. Since the exterior has the geometry of a Schwarzschild black hole, dual to a thermal state, it is natural for the exterior geodesics to reproduce this thermal entanglement entropy.

For comparison, the area of a disconnected surface with two parts extending from the interval boundaries to the horizon via the geodesic path at constant θ and t gives

$$\text{Area}_0 = 2\int_{r_H}^{r_{\max}} \frac{\mathrm{d}r}{\sqrt{f(r)}} = 2L_{\text{AdS}} \ln\left(\frac{2L_{\text{AdS}}}{\epsilon r_H}\right) . \tag{2.67}$$

This shows that regardless of what happens behind the horizon, the entanglement entropy of an interval with size $\Delta\theta$ will be calculated by an extremal surface outside the horizon if

$$\sinh\left(\frac{r_H \Delta\theta}{2L_{\text{AdS}}}\right) \leq 1 . \tag{2.68}$$

79

This will hold even for the largest interval $\Delta\theta = \pi$ if

$$\frac{r_H}{L_{\text{AdS}}} \leq \frac{2}{\pi}\text{arcsinh}(1) \ . \tag{2.69}$$

Thus, we must have a sufficiently large black hole if the CFT entanglement entropy is going to have any chance of seeing behind the horizon.

Interior extremal surfaces

Now we consider the extremal surfaces that enter the horizon and end on the ETW brane. Here, it is most convenient to use coordinates for which the maximally extended black hole spacetime takes the form

$$\text{d}s^2_{\text{BTZ}} = \frac{1}{\cos^2(y)}\left(-\text{d}s^2 + \text{d}y^2 + r_H^2\cos^2(s)\,\text{d}\phi^2\right) \tag{2.70}$$

where the coordinate ranges are $-\pi/2 \leq s, y \leq \pi/2$, with the horizons at $y = \pm s$. The coordinate transformations relating this to Schwarzschild coordinates are given in the following supplementary section, §2.3.2. Using these parameters, the ETW brane trajectory is found to be simply

$$y = -\arcsin(L_{\text{AdS}}T) \ . \tag{2.71}$$

We also find that the general spacelike geodesics in this geometry take the form

$$\sin(s_B - s_0)\sin(y) = \sin(s - s_0) \tag{2.72}$$

where the geodesic passes through s_0 at $y = 0$ and ends on the AdS boundary ($y = \pi/2$) at s_B.

The geodesics with fixed s_B and different s_0 all end on the same point at the AdS boundary, but different points on the ETW brane. However, requiring that the surface extremize area also with respect to variations of this boundary point on the ETW brane implies that the geodesic should be normal to the ETW brane worldvolume. This gives the
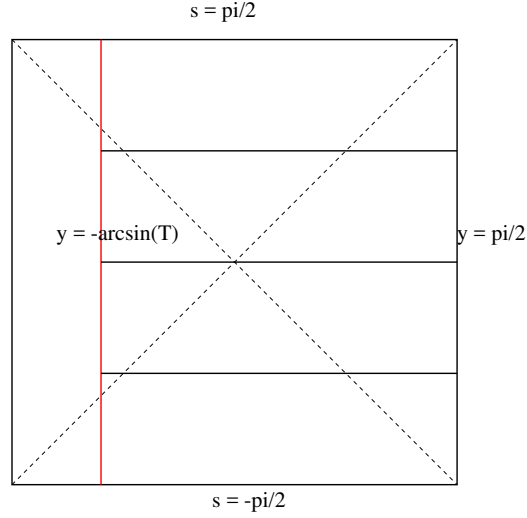
Figure 2.12: BTZ black hole in s-y coordinates, showing ETW brane (red) and various geodesics orthogonal to it. Geometry to the left of the ETW brane is excised.

very simple class of geodesics

$$s = s_0 \tag{2.73}$$

which sit at fixed θ and s. The black hole geometry together with these geodesics is depicted in Fig. 2.12.

We can now evaluate the area of these extremal surfaces. We will evaluate the area up to the same regulator point $r_{\max} = L_{\mathrm{AdS}}/\epsilon$. This gives a maximum y of

$$y_{\max} = \arctan\left(e^{-r_H t_0}\sqrt{\frac{r_{\max}/r_H - 1}{r_{\max}/r_H + 1}}\right) + \arctan\left(e^{r_H t_0}\sqrt{\frac{r_{\max}/r_H - 1}{r_{\max}/r_H + 1}}\right), \tag{2.74}$$

Note that this depends on the Schwarzschild time t_0. We have then

$$
\begin{aligned}
\mathrm{Area}_{\mathrm{int}}(\Delta\theta) &= 2\int_{-\arcsin(L_{\mathrm{AdS}}T)}^{y_{\max}} \frac{\mathrm{d}y}{\cos(y)} \\
&= 2L_{\mathrm{AdS}}\ln\left(\frac{2L_{\mathrm{AdS}}}{\epsilon r_H}\right) + 2L_{\mathrm{AdS}}\ln\left(\cosh\left(\frac{t_0 r_H}{L_{\mathrm{AdS}}^2}\right)\sqrt{\frac{1 + L_{\mathrm{AdS}}T}{1 - L_{\mathrm{AdS}}T}}\right) \tag{2.75}
\end{aligned}
$$

The regulated entanglement entropy is then

$$S = \frac{c}{3} \ln \left(\frac{2L_{\mathrm{AdS}}}{\epsilon r_H} \cosh \left(\frac{t_0 r_H}{L_{\mathrm{AdS}}^2} \right) \sqrt{\frac{1 + L_{\mathrm{AdS}}T}{1 - L_{\mathrm{AdS}}T}} \right) . \qquad (2.76)$$

In terms of CFT parameters, this gives

$$S = \frac{c}{3} \ln \left(\frac{\beta}{\epsilon \pi L_{\mathrm{CFT}}} \cosh \left(\frac{2\pi t_{\mathrm{CFT}}}{\beta} \right) \sqrt{\frac{1 + L_{\mathrm{AdS}}T}{1 - L_{\mathrm{AdS}}T}} \right) . \qquad (2.77)$$

If we use the relation (2.8) and the Brown-Henneaux relation $c = 3L_{\mathrm{AdS}}/2G$, this becomes

$$S = \frac{c}{3} \ln \left(\frac{\beta}{\epsilon \pi L_{\mathrm{CFT}}} \cosh \left(\frac{2\pi t_{\mathrm{CFT}}}{\beta} \right) \right) + 2g.$$

This is twice the entanglement entropy associated with each endpoint of the interval, considered as a half-interval in a BCFT [62, 63]. (We will explain how this arises, from a CFT perspective, in Chapter 3.)

The interior surfaces gives less area than the exterior surface when

$$\sinh \left(\frac{r_H \Delta\theta}{2L_{\mathrm{AdS}}} \right) \geq \cosh \left(\frac{t_0 r_H}{L_{\mathrm{AdS}}^2} \right) \sqrt{\frac{1 + L_{\mathrm{AdS}}T}{1 - L_{\mathrm{AdS}}T}} . \qquad (2.78)$$

When this is satisfied, the entanglement entropy (times $4G$) is given by the expression (2.76) and is time-dependent but independent of the interval size. Otherwise, the entanglement entropy is time-independent but depends on the interval size and given by (2.65).

The entanglement entropy as a function of interval size for various times is shown in Fig. 2.14. The entanglement entropy as a function of time for various interval sizes is shown in Fig. 2.13. The fact that the entanglement entropies are independent of angle when the minimal-area extremal surfaces probe behind the horizon is a special feature of the $d = 2$ case arising from the fact that these extremal surfaces have two disconnected parts, each at a constant angle. In higher dimensions, the corresponding surfaces are connected and we have non-trivial angular dependence for all angles.
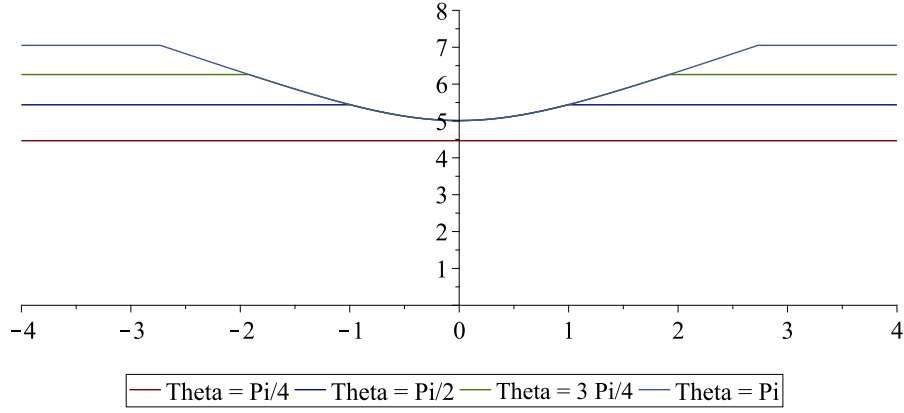
Figure 2.13: Regulated entanglement entropy as a function of time for various interval sizes for $T = 0.5$, $r_H = 2L_{\mathrm{AdS}}$, $\epsilon = 0.01$. Plots from bottom to top show $\Delta\theta = \pi/16, \pi/4, \pi/2, 3\pi/4, \pi$.
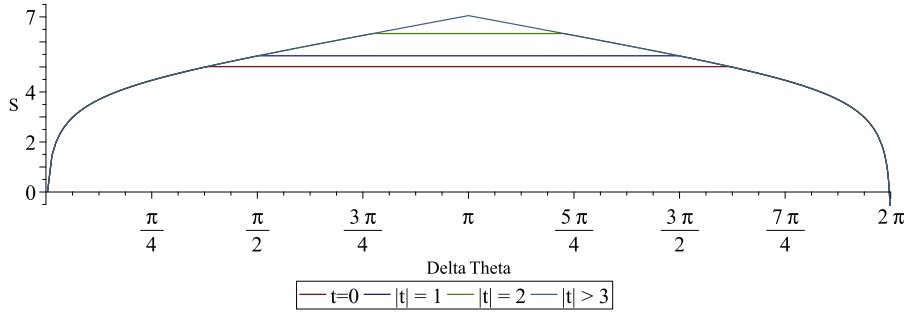
Figure 2.14: Regulated entanglement entropy as a function of interval size for $T = 0.5$, $r_H = 2L_{\mathrm{AdS}}$, $\epsilon = 0.01$. Plots from bottom to top show successively later times starting at $t = 0$.

Coordinate systems for $d = 2$

In this section, we give the coordinate transformations relating s-y coordinates in (2.70) which cover the full maximally extended black hole geometry to the Schwarzschild coordinates. We first go to Kruskal-type coordinates by defining

$$r = r_H \left(\frac{1 - uv}{1 + uv} \right) , \qquad t = \frac{1}{2r_H} \ln \left(-\frac{u}{v} \right) . \tag{2.79}$$

Setting $L_{\text{AdS}} = 1$, the metric becomes

$$ds^2_{\text{BTZ}} = -\frac{4 du \, dv}{(1 + uv)^2} + r_H^2 \frac{(1 - uv)^2}{(1 + uv)^2} d\phi^2 . \tag{2.80}$$

These coordinates cover the whole extended spacetime. The two boundaries are at $uv = -1$, the singularities are at $uv = 1$, and the horizons are at $uv = 0$. The relation to Schwarzschild coordinates in the second asymptotic region is given by (2.79) with the replacement $u \leftrightarrow v$.

To obtain the metric (2.70), we further define

$$u = \tan(\alpha) \qquad v = \tan(\beta) \qquad s = \beta + \alpha \qquad y = \alpha - \beta . \tag{2.81}$$

From (2.46), the Lorentzian ETW brane trajectory in Schwarzschild coordinates for the second asymptotic region is given (in the case for $0 < T < 1$) by

$$t = \frac{1}{r_H} \text{arctanh} \left(\frac{\sqrt{r_H^2 - r^2(1 - T^2)}}{T r_H} \right) . \tag{2.82}$$

In the u-v coordinates, we find that this becomes

$$T = \frac{v - u}{\sqrt{1 + u^2}\sqrt{1 + v^2}} . \tag{2.83}$$

In the s-y coordinates we get simply

$$y = -\arcsin(L_{\text{AdS}} T) , \tag{2.84}$$

as claimed above.

2.4 Pure AdS analogue

There is a close analogy between the maximally extended AdS-Schwarzschild black hole spacetime and pure AdS space divided into complementary Rindler wedges [100], where the two exterior regions correspond to the interiors of the two Rindler wedges, as shown in Fig. 2.16. In this section, we extend this analogy to describe states of a CFT on a half-sphere that are analogous to the black hole microstates considered above. We specialize to 2+1 dimensions for simplicity.

In the black hole story, the full geometry is described by two entangled CFTs, each in a thermal state. Our microstates are pure states of just one of these CFTs. For pure AdS, the geometry is described by a state in which the CFT degrees of freedom on two halves of a circle are entangled. The analogue of a black hole microstate is a pure state of the CFT on a half circle (i.e. an interval). To ensure this is well defined, we can place boundary conditions on the two ends of the interval, so that our CFT on a circle is replaced by a pair of BCFTs each on an interval. As discussed in [101], we can define an entangled state of this pair of BCFTs whose dual geometry is a good approximation to the geometry of the original CFT state (inside a Wheeler-deWitt patch). The black hole microstates are now pure state of one of these BCFTs that we can define using a path integral, as shown in Fig. 2.15.

The path integral in Fig. 2.15(d) is equivalent via a conformal transformation to the path integral that defines the vacuum state of the BCFT on an interval. For this state, the corresponding geometry was described in [59] and can be represented as a portion of the global AdS geometry ending on a static ETW brane, as shown in Fig. 2.16. Also shown are the Rindler wedges analogous to the two exterior regions in the maximally extended black hole geometry. We can see that (in the $T > 0$ case) the ETW brane emerges from the past Rindler horizon in the second asymptotic region, reaches some maximum distance from the horizon, and then falls back in.
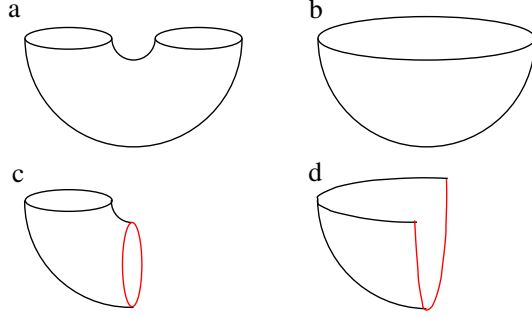
Figure 2.15: Euclidean path integral geometries defining (a) thermofield double state of two CFTs (b) the vacuum state of a single CFT (c) a black hole microstate (d) a microstate for a half space. The red curves indicate BCFT boundary conditions.

Explicit geometry

To find the geometry associated with the BCFT vacuum state, it is simplest to consider a conformal frame where the interval on which the BCFT lives is $(-\infty, 0]$. In this case, we recall from §2.1.2 that in Poincaré coordinates

$$ds^2_{\text{Rind}} = \frac{L^2_{\text{AdS}}}{z^2}(-dt^2 + dz^2 + dx^2) \,, \tag{2.85}$$

the vacuum geometry corresponds to the region $x/z < L_{\text{AdS}}T/\sqrt{1 - L_{\text{AdS}}T^2}$ terminating with an ETW brane, as shown in Fig. 2.16. Passing to global coordinates via the transformations

$$\frac{L_{\text{AdS}}}{z} = \cosh(\rho)\cos(\tau) - \sinh(\rho)\sin(\theta), \qquad \frac{x}{z} = \sinh(\rho)\cos(\theta), \qquad \frac{t}{z} = \cosh(\rho)\sin(\tau) \,, \tag{2.86}$$

the ETW brane locus becomes

$$\sinh(\rho)\cos(\theta) = \frac{L_{\text{AdS}}T}{\sqrt{1 - L_{\text{AdS}}T^2}} \tag{2.87}$$

in coordinates where the metric is

$$ds^2_{\text{Rind}} = L^2_{\text{AdS}}\left[-\cosh^2\rho \, d\tau^2 + d\rho^2 + \sinh^2\rho \, d\theta^2\right] \,. \tag{2.88}$$

86

Here, the brane is static in the global coordinates, extending to antipodal points at the boundary of AdS, as shown in Fig. 2.16.

To make the analogy with the black hole more clear, we can now describe the ETW brane trajectory for $T > 0$ in a Rindler wedge, the analog of the second asymptotic region in the black hole case. Defining coordinates (χ, ζ, r) from the Poincaré coordinates by

$$\frac{t}{L_{\text{AdS}}} = e^{\chi} \sinh(\zeta)\sqrt{1 - \frac{1}{r^2}}, \qquad \frac{x}{L_{\text{AdS}}} = e^{\chi} \sinh(\zeta)\sqrt{1 - \frac{1}{r^2}}, \qquad \frac{z}{L_{\text{AdS}}} = e^{\chi}\frac{1}{r} , \tag{2.89}$$

the Rindler wedge corresponding to the second asymptotic region takes the form of a Schwarzschild metric with non-compact horizon [102],

$$\mathrm{ds}^2_{\text{Rind}} = L^2_{\text{AdS}} \left[-(r^2 - 1)\mathrm{d}\zeta^2 + \frac{\mathrm{d}r^2}{r^2 - 1} + r^2 \mathrm{d}\chi^2 \right] , \tag{2.90}$$

and the brane locus is simply

$$\cosh(t)\sqrt{r^2 - 1} = \frac{L_{\text{AdS}}T}{\sqrt{1 - L_{\text{AdS}}T^2}} . \tag{2.91}$$

Note that, setting $r_H = 1$, this is precisely the same as the result (2.47). The reason is that the black hole geometry we considered previously is simply obtained from the present case by periodically identifying the χ direction. Thus, as in that case, for each time t, the ETW brane sits at a constant r in the Schwarzschild picture, with $r(t)$ reaching a maximum at $t = 0$.

Entanglement calculations

In analogy to the earlier result for BTZ black holes, the entanglement entropy of sufficiently large intervals in the BCFT can provide information about the geometry behind the Rindler horizon. Using the standard CFT time in a conformal frame where we have a fixed distance between the two boundaries, the entanglement entropy for a connected boundary region is time-independent. However, to better parallel our earlier calculations, we can instead consider the entanglement entropy of an interval of fixed width in the Schwarzschild
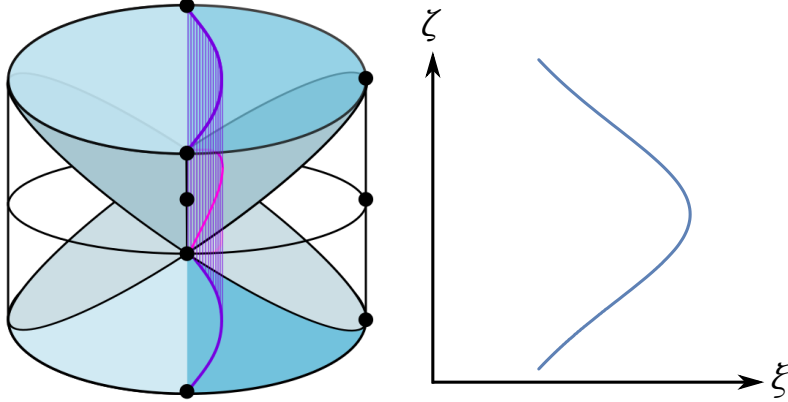
Figure 2.16: *Left.* The ETW brane in global AdS. For $T > 0$ we have the geometry on the left of the brane. For $T > 0$, we have the geometry on the right of the brane. Diagonal planar surfaces are Rindler horizons dividing the spacetime into complementary Rindler wedges plus past and future regions. *Right.* Dependence of the radial position parameter $\xi = \sqrt{r^2 - 1}$ on Schwarzschild time ζ.

spatial coordinate χ, as shown in Fig. 2.17.

We have seen that the geometry and the brane trajectory in the present case is mathematically identical to the black hole case for $r_H = 1$ except that the χ coordinate is now non-compact. The compactness of θ did not enter into the previous calculations of entanglement entropy, so all the calculations in §2.3.2 apply here as well. We can immediately conclude that the entangling surface will probe behind the horizon when

$$\sinh\left(\frac{\Delta\chi}{2}\right) \geq \cosh(\zeta_0)\sqrt{\frac{1 + L_{\text{AdS}}T}{1 - L_{\text{AdS}}T}} \ . \tag{2.92}$$

Since χ is noncompact now, we have that for any time ζ_0 and any T, we can always choose a large enough interval $\Delta\chi$ so that the entangling surface probes behind the horizon. Thus, if we unwrap the compact direction of the BTZ black hole, the ETW branes will be dual to boundary states on a spatial interval of pure AdS$_3$. Our BTZ entanglement calculations carry over, implying that control of a suitably large boundary subregion should allow an observer to probe behind the Rindler horizon.
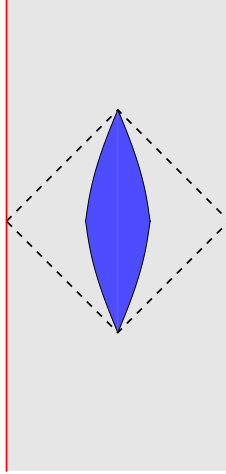
Figure 2.17: Interval of fixed width in Schwarzschild time (blue shaded region) in the BCFT world-volume geometry.

2.5 Discussion

For the specific examples in this chapter, we have considered geometries obtained from a simple holographic ansatz, where the ETW brane is a placeholder for some more detailed microscopic physics. This might involve branes or orientifold planes of string/M theory, or geometrical features such as the degeneration of an internal manifold. A more realistic model might require additional terms in the brane action or couplings to additional bulk fields. As a particular example, scalar operators in a BCFT can have one-point functions growing as $1/|x|^{2\Delta}$ as the distance x to the boundary decreases. This would correspond to having some extra scalar fields in the bulk, sourced by the ETW brane.[3]

In our context, this would lead to matter outside the black hole that falls into the horizon. Thus, the explicit geometries we have utilized should be viewed as simple examples that may elucidate the basic physics of more precise holographic duals for Euclidean-time-evolved boundary states. It would be interesting to flesh out the AdS/CFT correspondence for BCFTs more fully and explore the microstate geometries emerging from more general bulk effective actions.

---

[3]Some particular top-down examples of complete geometries dual to supersymmetric BCFT states have already been understood: see [103, 104, 105].

Another interesting generalization would be to consider states constructed in a similar way, but with boundary conditions that do not preserve conformal invariance. For example, we can have boundary conditions that correspond to boundary RG flows from one conformally invariant boundary condition to another. These may be represented by a more general class of ETW brane actions, and give rise to a wider variety of geometries. Finally, we can consider similar constructions in holographic theories which are not conformal, for example in holographic RG flow theories or in holographic theories derived from low-energy Dp-brane actions. For all these cases, we expect that the basic idea of probing behind-the-horizon physics via time-dependence of subsystem entanglement remains valid.

2.6   Conclusion

Taking states of a holographic CFT on a sphere and evolving them in Euclidean time gives a high-energy state dual to a black hole. When the state is a highly symmetric boundary state, the AdS/BCFT corresponds suggests that the corresponding black hole geometry ends on a brane exhibiting the same symmetries. Here, we constructed the trajectories for these branes in AdS black holes of arbitrary dimension. We also determined the conditions under which the entanglement entropy of a ball-shaped region on the boundary can fall through the horizon and probe the interior region, with explicit calculations in $d = 2$. Finally, we saw an analogous phenomenon in flat space, where the horizon of the black hole is replaced by the Rindler horizon governing an accelerating observer.

Given our bulk result, it is natural to attempt a direct calculation of entanglement entropy for boundary microstates on the CFT side. This would also act as a consistency check on the modification of the homology condition for the RT surface, where we allow it to end on the brane. In the next chapter, we will perform such a computation in the $d = 2$ case, corroborating the bulk results on boundary microstates, and allowing us to generalize using conformal symmetry to other two-dimensional settings of interest. In particular, we are able to derive the RT formula given a set of reasonably natural assumptions about the CFT and boundary state under consideration.

Chapter 3

BCFTs at Large c

3.1 Introduction

In this chapter, we use the doubling trick and standard results for semiclassical Virasoro blocks to prove that in sparse, large c BCFTs, the entanglement entropy for any number of disjoint boundary intervals is correctly given by this modified RT formula. Our results can be viewed as specifying an auxiliary geometry (or class of geometries) using symmetry and universal properties of ground state entanglement.

Here is a brief outline of the chapter:

- In the remainder of §4.1, we review background material on boundary conformal field theory, and provide a formal argument for the doubling trick.

- In §3.2, we describe holographic predictions for entanglement entropy which follow from the RT formula. In particular, we will confirm the bulk calculations of entanglement entropy provide in Chapter 2 from the CFT side.

- In §3.3, we compute the entanglement entropy for a single interval on the field theory side using the replica trick and semiclassical Virasoro blocks. We use this to specify the set of BCFTs in which the field theory calculation agrees at leading order in c with holographic prediction. Roughly speaking, these BCFTs enjoy vacuum dominance in both bulk and boundary channels of their correlation functions.

- In §3.4, we extend the calculation to an arbitrary union of intervals.

3.1.1 Review of boundary conformal field theory

In this section, we start with a brief review of boundary conformal field theories.[1] Given a CFT, we can define the theory on a manifold with boundary by making a choice of boundary conditions for the fields, and possibly adding boundary degrees of freedom coupled to the bulk CFT fields. For the theory defined on half of $\mathbb{R}^d$ or $\mathbb{R}^{d-1,1}$ (e.g. the region $x \geq 0$ for some spatial coordinate x), certain choices of the boundary physics give a theory that preserves the subset of the global conformal group mapping the half-space to itself, $SO(d, 1) \subset SO(d + 1, 1)$ for the Euclidean case.[2] These choices define a *boundary conformal field theory* (BCFT).[3] There are typically many choices of conformally invariant boundary condition for a given bulk CFT. We label the choice by an index b.

In this chapter, we focus on BCFTs defined starting from two-dimensional conformal field theories. In this case, there is a natural boundary analog of the central charge, known as the *boundary entropy* g_b. This may be defined by considering the CFT on a half-space $x \geq 0$ with boundary condition b at $x = 0$. As we review below, the entanglement entropy of an interval $[0, L]$ including the boundary is

$$S = \frac{c}{6} \log \left(\frac{2L}{\epsilon} \right) + g_b \; . \tag{3.1}$$

Thus, the boundary entropy gives a boundary contribution to the entanglement entropy.

Boundary states

For any BCFT, there is a natural family of states $|b, \tau_0\rangle$ that we can associate to the parent CFT defined on a unit circle. The wavefunctional $\langle \phi_0|b, \tau_0\rangle$ is defined as the Euclidean path integral for the CFT on a cylinder of height τ_0, with boundary condition b at Euclidean time

---

[1]For more detailed reviews of BCFTs, see e.g. [88, 12, 89, 62, 84, 63].

[2]More generally, there can be boundary RG flows between such theories.

[3]We can also consider the same theory with different boundary geometries; in this chapter, we will only consider geometries that can be mapped to a half-space via a conformal transformation.

$-\tau_0$ and CFT field configuration ϕ_0 at $\tau = 0$.[4] We can formally define a *boundary state* $|b\rangle$ associated with boundary condition b via

$$|b\rangle = |b, \tau_0 \to 0\rangle . \tag{3.2}$$

In terms of $|b\rangle$, we have

$$|b, \tau_0\rangle = e^{-\tau_0 H}|b\rangle , \tag{3.3}$$

since adding $\delta\tau$ to the height of the cylinder corresponds to acting on our state with Euclidean time evolution $e^{-\delta\tau H}$. The boundary state itself has infinite energy expectation value, but the Euclidean evolution used to define $|b, \tau_0\rangle$ suppresses the high-energy components so that $|b, \tau_0\rangle$ is a finite energy state.[5] In general, this state is time-dependent.

The overlap of the boundary state $|b\rangle$ with the vacuum state is computed via the path integral on a semi-infinite cylinder. This can be mapped to the disk via a conformal transformation, so the result is the disk partition function:

$$\langle 0|b\rangle = e^{g_b} . \tag{3.4}$$

Boundary operators

In addition to the usual CFT bulk operators, a BCFT has a spectrum of local boundary operators $\hat{O}_J(x)$, each with a dimension $\hat{\Delta}_J$. Via the usual radial quantization (taking the origin to be a point on the boundary), these may be understood to be in one-to-one correspondence with the states of the BCFT on an interval with the chosen boundary condition at each end. The boundary operator dimension is equal to the energy of the corresponding state on the strip.

---

[4]With this definition, the norm of the states is not equal to 1.

[5]This is a version of the *global quench* considered in the condensed matter literature [63], but we have compactified the space on which the CFT is defined.

Symmetries and correlators

A two-dimensional BCFT defined on the upper-half plane (UHP) preserves one copy of the Virasoro symmetry algebra, corresponding to transformations

$$\delta z = \epsilon(z) \qquad \delta\bar{z} = \bar{\epsilon}(\bar{z}) \qquad \bar{\epsilon}(\bar{z}) = \epsilon(\bar{z}^*) \tag{3.5}$$

that map the boundary to itself.[6] These correspond to a set of generators

$$\tilde{L}_n = L_n + \bar{L}_n \ . \tag{3.6}$$

In this case, the conformal Ward identity becomes

$$
\left\langle \tilde{T}(z) \prod_i \mathcal{O}_{h_i \bar{h}_i}(z_i, \bar{z}_i) \right\rangle
$$
$$
= \sum_i \left[\frac{h_i}{(z - z_i)^2} + \frac{1}{z - z_i} \frac{\partial}{\partial z_i} + \frac{\bar{h}_i}{(\bar{z} - \bar{z}_i)^2} + \frac{1}{\bar{z} - \bar{z}_i} \frac{\partial}{\partial \bar{z}_i} \right] \left\langle \prod_i \mathcal{O}_{h_i \bar{h}_i}(z_i, \bar{z}_i) \right\rangle ,
$$

where $\tilde{T}(z) = \sum_n z^{-n-2} \tilde{L}_n$.

The Virasoro symmetry algebra of a BCFT is thus the same as that of a chiral CFT on the whole plane. A consequence is that the kinematics (i.e. the functional form of correlators given the operator dimensions) of the BCFT in the UHP is directly related to that of a chiral CFT on the whole plane. Correlators

$$\langle \mathcal{O}_{h_1 \bar{h}_1}(z_1, \bar{z}_1) \cdots \mathcal{O}_{h_n \bar{h}_n}(z_n, \bar{z}_n) \rangle^b_{\text{UHP}} \tag{3.7}$$

of bulk CFT operators $\mathcal{O}_{h_k \bar{h}_k}$ with conformal weights $(h_k, \bar{h}_k)$ in the UHP are constrained

---

[6]Here, we recall that it is standard to treat z and $\bar{z}$ as independent coordinates and consider a complexified version of the symmetry algebra for which the infinitesimal transformations are $\delta z = \epsilon(z)$ and $\delta\bar{z} = \bar{\epsilon}(\bar{z})$. The non-complexified transformations correspond to taking $\bar{\epsilon}(\bar{z}) = \epsilon(\bar{z}^*)$ with $\epsilon(x)$ real for real x, or $\bar{\epsilon}(\bar{z}) = -\epsilon(\bar{z}^*)$ with $\epsilon(x)$ pure imaginary for real x. Of these, the first set preserves the upper half plane, acting explicitly as $\delta x = (\epsilon(x+iy) + \epsilon(x-iy))/2, \delta y = -i(\epsilon(x+iy) - \epsilon(x-iy))/2$ on the physical coordinates.

to have the same functional form as chiral CFT correlators

$$\langle \mathcal{O}_{h_1}(z_1) \cdots \mathcal{O}_{h_n}(z_n) \mathcal{O}_{\bar{h}_1}(\bar{z}_1) \cdots \mathcal{O}_{\bar{h}_n}(\bar{z}_n) \rangle \tag{3.8}$$

of fields $\mathcal{O}_{h_k}$ and $\mathcal{O}_{\bar{h}_k}$ with chiral weights h_k and $\bar{h}_k$ respectively.[7] More generally, we can include boundary operators $\hat{\mathcal{O}}_{\hat{\Delta}_I}(x_I)$ in (3.7), where x_I is real. In this case, the functional form is reproduced by adding chiral operators with $h_I = \hat{\Delta}_I$ at $z = x_I$ to the chiral correlator (3.8). See [106] for a more complete discussion of this constraint, often referred to as the "doubling trick".

We will later make use of this kinematic equivalence to relate conformal blocks for a BCFT on the UHP to chiral conformal blocks on the entire plane.

Bulk one-point functions

The doubling trick implies that a primary operator with weights $(h, \bar{h})$ is kinematically allowed to have a nonvanishing one-point function if $h = \bar{h}$ (i.e. for a scalar primary). In this case, the one-point function $\langle \mathcal{O}_{h,h}(z, \bar{z}) \rangle_{\text{UHP}}^b$ is constrained to have the same form as a chiral two-point function $\langle \mathcal{O}_h(z) \bar{\mathcal{O}}_h(z^*) \rangle$, so we have

$$\langle \mathcal{O}_{h,\bar{h}}(z, \bar{z}) \rangle_{\text{UHP}}^b = \frac{\mathcal{A}_{\mathcal{O}}^b}{|z - z^*|^{2h}} = \frac{\mathcal{A}_{\mathcal{O}}^b}{|2y|^{\Delta_{\mathcal{O}}}}, \tag{3.9}$$

where we take $z = x + iy$ here and below. Once the normalization of the operators is fixed by choosing the normalization of the two-point function in the parent CFT, the coefficient $\mathcal{A}_{\mathcal{O}}^b$ in the one-point function is a physical parameter that depends in general on both the operator and the boundary condition.

Here and everywhere in this chapter we will take the expectation value $\langle \cdot \rangle_{\text{UHP}}^b$ to be normalized by the UHP partition function so that

$$\langle \mathbf{1} \rangle_{\text{UHP}}^b = 1. \tag{3.10}$$

---

[7]Here, the original theory is defined on the slice where $\bar{z} = z^*$, so the operators $\mathcal{O}_{\bar{h}_i}(\bar{z}_i)$ live on the lower half-plane.

Bulk-boundary two-point functions

The correlation function

$$\langle \mathcal{O}_i(z, \bar{z}) \hat{\mathcal{O}}_I(x') \rangle^b_{\text{UHP}} \tag{3.11}$$

of bulk and boundary primary operators is constrained to have the functional form of a chiral three-point function

$$\langle \mathcal{O}_{h_i}(z) \mathcal{O}_I(x') \mathcal{O}_{\bar{h}_i}(\bar{z}) \rangle . \tag{3.12}$$

For a scalar operator $\mathcal{O}_i$, this gives

$$\langle \mathcal{O}_i(z, \bar{z}) \hat{\mathcal{O}}_I(x') \rangle^b_{\text{UHP}} = \frac{\mathcal{B}^b_{iI}}{(2y)^{\Delta_i - \Delta_I}(y^2 + (x - x')^2)^{\Delta_I}} , \tag{3.13}$$

where $\mathcal{B}^b_{iI}$ forms part of the basic data of our BCFT. Taking $\hat{\mathcal{O}}_I$ to be the identity operator, we have from the previous section that $\mathcal{B}^b_{i1} = \mathcal{A}^b_i$.

Boundary operator expansion and OPEs

In the same way that a pair of bulk operators at separated points can be expanded as a series of local operators via the OPE, a bulk operator can be expanded in terms of boundary operators via a *boundary operator expansion (BOE)*.[8] For a scalar primary operator, symmetries constrain the general form of this expansion to be

$$
\begin{aligned}
\mathcal{O}_i(z, \bar{z}) &= \sum_J \frac{\mathcal{B}^{bJ}_i}{(2y)^{\Delta_i - \Delta_I}} \tilde{C}[y, \partial_x] \hat{\mathcal{O}}_J(x) \\
&= \sum_J \frac{\mathcal{B}^{bJ}_i}{(2y)^{\Delta_i - \Delta_I}} \hat{\mathcal{O}}_J(x) + \text{desc.} ,
\end{aligned} \tag{3.14}
$$

where the sum is over boundary primary operators. The differential operator $\tilde{C}$ determines the contribution of descendant operators and depends only on the conformal weights of $\mathcal{O}_i$ and $\hat{\mathcal{O}}_J$. The coefficients $\mathcal{B}^{bJ}_i$ are related to the ones appearing in the bulk-boundary two-

---

[8]This follows by the same logic of the state-operator mapping and OPE in a CFT. The state produced by a bulk operator can be mapped by an infinite dilation to a local operator at the origin on the boundary. And, as in the OPE, we choose to expand this local operator in terms of a basis of dilation eigenstates.

point function by raising the index with the metric g_{IJ} appearing in the boundary two-point function

$$\langle \hat{\mathcal{O}}_I(x_I)\hat{\mathcal{O}}_J(x_I)\rangle = \frac{g_{IJ}}{|x_I - x_J|^{2\Delta_I}}\,, \tag{3.15}$$

though we will generally assume that we are working with a basis of boundary operators for which $g_{IJ} = \delta_{IJ}$.

Below, we will also make use of the ordinary OPE for bulk scalar operators,[9]

$$\begin{aligned}
\mathcal{O}_i(z_1,\bar{z}_1)\mathcal{O}_j(z_2,\bar{z}_2) &= \sum_k \frac{\hat{\mathcal{C}}_{ij}^k}{|z_1 - z_2|^{\Delta_i+\Delta_j-\Delta_k}}C_{\Delta_i\Delta_j;\Delta_k}[z_{12},\partial_z]\mathcal{O}_k(z_2,\bar{z}_2) \\
&= \sum_k \frac{\hat{\mathcal{C}}_{ij}^k}{|z_1 - z_2|^{\Delta_i+\Delta_j-\Delta_k}}\mathcal{O}_k(z_2,\bar{z}_2) + \text{desc.} \tag{3.16}
\end{aligned}$$

Finally, there is also an OPE for boundary fields, but we will not need this in our calculations below.

Two-point functions and conformal blocks

We now consider the bulk two-point function. Here, we restrict to scalar primary operators of equal dimension Δ since that is what we will need below. However, in general, bulk two-point functions in a BCFT can be non-vanishing for any conformal weights $(h_1,\bar{h}_1)$ and $(h_2,\bar{h}_2)$. We discuss the general case in detail in §3.1.2.

By the doubling trick, the BCFT two-point function

$$\langle \mathcal{O}_1(z_1,\bar{z}_1)\mathcal{O}_2(z_2,\bar{z}_2)\rangle_{\text{UHP}}^b \tag{3.17}$$

of scalar operators with dimension Δ has the same functional form as a four-point function of chiral operators

$$\langle \mathcal{O}_1(z_1)\mathcal{O}_2(z_2)\mathcal{O}_3(\bar{z}_2)\mathcal{O}_4(\bar{z}_1)\rangle\,, \tag{3.18}$$

---

[9]To see that this should still be valid in the presence of a boundary, note that in a conformal frame where the upper-half-plane is mapped to the exterior of a circle surrounding the origin, the presence of the boundary is equivalent to the insertion of an operator at the origin (specifically, the operator associated with the state $|b,\tau_0\rangle$ described above).

where each operator has chiral weight $h = \Delta/2$. Making use of (3.23) for the general form of such a correlator, we have that

$$\langle \mathcal{O}_1(z_1, \bar{z}_1) \mathcal{O}_2(z_2, \bar{z}_2) \rangle^b_{\text{UHP}} = \left[\frac{\eta}{4y_1 y_2} \right]^{\Delta} F(\eta) \tag{3.19}$$

where $F(\eta)$ is some function of the cross-ratio

$$\eta = \frac{(z_1 - \bar{z}_1)(z_2 - \bar{z}_2)}{(z_1 - \bar{z}_2)(z_2 - \bar{z}_1)} . \tag{3.20}$$

The function F can be written more explicitly by making use of either the BOE or the bulk OPE for the operators in (3.19). Using the BOE for each operator in (3.19), the bulk two-point functions can be expressed as a sum of boundary two-point functions. In this way, the function $F(\eta)$ in (3.19) may be expressed as

$$F(\eta) = \sum_I \mathcal{B}^{bI}_{\mathcal{O}_1} \mathcal{B}^b_{\mathcal{O}_2 I} \mathcal{F}(c, \Delta_I, \Delta/2 \,|\, \eta) \tag{3.21}$$

for a sum over boundary primary operators, while $\mathcal{F}(c, \Delta_I, \Delta/2|\eta)$ gives the contribution of a single boundary primary operator and all of its Virasoro descendants. We show in §3.1.2 that this function is the usual conformal block appearing in the expansion of a chiral four-point function of operators with equal conformal weight $h = \Delta/2$.[10]

We can alternatively use the bulk OPE to reduce the BCFT two-point function (3.19) to a sum of one-point functions. This leads to an alternative expression for $F(\eta)$,

$$F(\eta) = \sum_i \mathcal{C}^i_{\mathcal{O}_1 \mathcal{O}_2} \mathcal{A}^b_i \mathcal{F}(c, \Delta_I, \Delta/2 \,|\, 1 - \eta) . \tag{3.22}$$

Here, $\mathcal{F}$ is the same chiral conformal block as in (3.21), as we show in §3.1.2. The equivalence of the expressions (3.21) and (3.22) is a BCFT version of the usual crossing symmetry constraints; in this case, we have a relation between bulk OPE coefficients and

---

[10]In general, the conformal block depends on four external weights; here and below, we will use the shorthand $\mathcal{F}(c, h_{\text{int}}, h|\eta) \equiv \mathcal{F}(c, h_{\text{int}}, [h, h, h, h]|\eta)$ where the latter is the general expression for the chiral conformal block used in §3.1.2.

boundary operator expansion coefficients.

3.1.2 BCFT two-point functions from Virasoro conformal blocks*

In this section, we briefly review the structure of four-point functions of chiral operators and their expansion in terms of Virasoro conformal blocks, and then argue that the same objects form the building blocks of two-point functions in boundary conformal field theories.

Chiral four-point functions and conformal blocks

In a 2D CFT, for operators ϕ_i with chiral dimensions h_i, the global conformal symmetry implies that the four-point function takes the form

$$\langle \phi_1(z_1)\phi_2(z_2)\phi_3(z_3)\phi_4(z_4) \rangle = \left(\frac{z_{24}}{z_{14}} \right)^{h_1-h_2} \left(\frac{z_{14}}{z_{13}} \right)^{h_3-h_4} \frac{\eta^{h_1+h_2}}{(z_{12})^{h_1+h_2}(z_{34})^{h_3+h_4}} F(\eta) \,,$$

(3.23)

where $z_{ij} = z_i - z_j$ and F is some function of the single cross-ratio $\eta = z_{12}z_{34}/(z_{13}z_{24})$. We can define F as

$$F(\eta) = \lim_{z_\infty \to \infty} (-1)^{h_1+h_2+h_3+h_4} z_\infty^{2h_4} \langle \phi_1(0)\phi_2(\eta)\phi_3(1)\phi_4(z_\infty) \rangle \,.$$

(3.24)

We can express $\mathcal{F}$ in terms of the OPE data for the CFT and a standard set of functions by expanding the products $\phi_1(z_1)\phi_2(z_2)$ and $\phi_3(z_3)\phi_4(z_4)$ using (3.16). In this case, the four point function reduces to a sum of two-point functions of intermediate operators,

$$F(\eta) = \sum_i C_{12}^i C_{34}^i \mathcal{F}(c, h; [h_1, h_2, h_3, h_4]|\eta) \,.$$

(3.25)

The conformal blocks $\mathcal{F}(c, h; [h_1, h_2, h_3, h_4]|\eta)$ are specific functions which depend only on the central charge, the dimensions h_i of the external operators, and the "internal" dimension h. These give the contribution to the four-point function from a primary operator of weight h and all of its Virasoro descendants. The block has a simple behavior in the

limit $\eta \to 0$, where we have

$$\mathcal{F}(c, h; [h_1, h_2, h_3, h_4]|\eta \to 0) \sim \eta^{h-h_1-h_2}. \tag{3.26}$$

BCFT two-point function

We now consider the two-point function of bulk operators in a BCFT defined on the upper-half-plane

$$\langle \mathcal{O}_1(z_1, \bar{z}_1) \mathcal{O}_2(z_2, \bar{z}_2) \rangle^b_{\text{UHP}} . \tag{3.27}$$

As we discussed in §3.1.1, this has the kinematics of a chiral four-point function. We will show this somewhat more carefully here, and see that we can expand the two-point function in either a bulk channel or a boundary channel in terms of the chiral conformal blocks defined above.

One-point functions for scalar Virasoro descendants

To begin, it will be useful to compute one-point functions for scalar global primaries that are themselves Virasoro descendants. Consider, in particular, a Virasoro primary operator $\mathcal{O}_{h,\bar{h}}(z, \bar{z})$ and state $|h, \bar{h}\rangle$ for the CFT on $\mathbb{S}^1$ associated to it by the state-operator correspondence. We denote an operator $\mathcal{O}^{\alpha,\beta}_{h,\bar{h}}(0)$ which creates the Virasoro descendants of this state $V^h_\alpha \bar{V}^{\bar{h}}_\beta |h, \bar{h}\rangle$. Here, V^h_α and $V^{\bar{h}}_\beta$ are polynomials in L_{-n} and $\bar{L}_{-n}$ respectively chosen so that these states give an orthonormal basis of the Verma module:[11]

$$\langle \mathcal{O}^{\alpha',\beta'}_{h,\bar{h}}(\infty) \mathcal{O}^{\alpha,\beta}_{h,\bar{h}}(0) \rangle = \langle h, \bar{h}| V^{h,\dagger}_{\alpha'} \bar{V}^{\bar{h},\dagger}_{\beta'} V^h_\alpha \bar{V}^{\bar{h}}_\beta |h, \bar{h}\rangle = \delta_{\alpha\alpha'} \delta_{\beta\beta'} . \tag{3.28}$$

We can re-express the same operators in terms of local operators $\mathcal{O}^{\alpha_i,\beta_i}_{h,\bar{h}}(z_i, \bar{z}_i)$ at arbitrary points z_1, z_2 by the use of a global conformal transformation that maps $(\infty, 0)$ to (z_1, z_2). We then have

$$\langle \mathcal{O}^{\alpha_1,\beta_1}_{h,\bar{h}}(z_1, \bar{z}_1) \mathcal{O}^{\alpha_2,\beta_2}_{h,\bar{h}}(z_2, \bar{z}_2) \rangle = \delta_{\alpha_1\alpha_2} \delta_{\beta_1\beta_2} . \tag{3.29}$$

---

[11]Recall that the conjugation operation used to define the dual operator at infinity is an inversion in radial quantization, and so the operator is rescaled by the conformal transformation. We keep the rescaling implicit.

Note that the form of each local descendant operator depends explicitly on both points z_1, z_2, and not just implicitly on one point through the local primary. These operators are only orthogonal precisely at the points z_1, z_2 (and form an orthogonal basis of operators in the 'North-South' quantization between these two points).

Next, we require a somewhat more refined version of the doubling trick. We have seen that a correlator

$$\langle \mathcal{O}_{h_1 \bar{h}_1}(z_1, \bar{z}_1) \cdots \mathcal{O}_{h_n \bar{h}_n}(z_n, \bar{z}_n) \rangle^b_{\text{UHP}} \tag{3.30}$$

of bulk CFT operators $\mathcal{O}_{h_k \bar{h}_k}$ with conformal weights $(h_k, \bar{h}_k)$ is constrained to have the same functional form as chiral CFT correlators

$$\langle \mathcal{O}_{h_1}(z_1) \cdots \mathcal{O}_{h_n}(z_n) \mathcal{O}_{\bar{h}_1}(\bar{z}_1) \cdots \mathcal{O}_{\bar{h}_n}(\bar{z}_n) \rangle \tag{3.31}$$

Similarly, a correlator of descendants

$$\langle \mathcal{O}^{\alpha_1, \beta_1}_{h_1 \bar{h}_1}(z_1, \bar{z}_1) \cdots \mathcal{O}^{\alpha_n, \beta_n}_{h_n \bar{h}_n}(z_n, \bar{z}_n) \rangle^b_{\text{UHP}} \tag{3.32}$$

takes the same functional form as

$$\langle \mathcal{O}^{\alpha_1}_{h_1}(z_1) \cdots \mathcal{O}^{\alpha_n}_{h_n}(z_n) \mathcal{O}^{\beta_1}_{\bar{h}_1}(\bar{z}_1) \cdots \mathcal{O}^{\beta_n}_{\bar{h}_n}(\bar{z}_n) \rangle . \tag{3.33}$$

Then, taking $\mathcal{O}_h(z)$ to be a primary operator in some CFT such that[12]

$$\langle \mathcal{O}_{h,h}(z, \bar{z}) \rangle^b_{\text{UHP}} = \mathcal{A}^b_h \langle \mathcal{O}_h(\bar{z}) \mathcal{O}_h(z) \rangle = \frac{\mathcal{A}^b_h}{|z - \bar{z}|^{2h}} , \tag{3.34}$$

we have that

$$\begin{aligned} \langle \mathcal{O}^{\alpha, \beta}_{h,h}(z, \bar{z}) \rangle^b_{\text{UHP}} &= \mathcal{A}^b_h \langle \mathcal{O}^{\alpha}_h(z) \mathcal{O}^{\beta}_h(\bar{z}) \rangle \\ &= \delta_{\alpha\beta} \mathcal{A}^b_h , \end{aligned} \tag{3.35}$$

where here the descendant indices are labeling the orthogonal basis of states for the pair

---

[12]Note that it's not necessary for such a CFT to exist, since we are only making statements about kinematics.

of points $z, \bar{z}$.

Bulk channel expression for the two-point function

We can now derive a bulk-channel expression for the two-point function (3.27). First we will use the bulk state-operator map (bulk OPE) to insert a complete set of bulk states (in this 'North-South' quantization between z_3 and $\bar{z}_3$)

$$\langle \mathcal{O}_1(z_1, \bar{z}_1) \mathcal{O}_2(z_2, \bar{z}_2) \rangle_{\text{UHP}}^b = \sum_{i,\alpha,\beta} \langle \mathcal{O}_1(z_1, \bar{z}_1) \mathcal{O}_2(z_2, \bar{z}_2) \mathcal{O}_i^{\alpha,\beta}(\bar{z}_3, z_3) \rangle \langle \mathcal{O}_i^{\alpha,\beta}(z_3, \bar{z}_3) \rangle_{\text{UHP}}^b .$$
(3.36)

Using the form of the boundary one-point function (3.35), we can rewrite this as

$$\langle \mathcal{O}_1(z_1, \bar{z}_1) \mathcal{O}_2(z_2, \bar{z}_2) \rangle_{\text{UHP}}^b = \sum_{\{i|h_i=\bar{h}_i\},\alpha,\beta} \hat{\mathcal{C}}_{12}^i \mathcal{A}_i^b \times \langle \mathcal{O}_{h_1}(z_1) \mathcal{O}_{h_2}(z_2) \mathcal{O}_{h_i}^\alpha(\bar{z}_3) \rangle$$
$$\times \langle \mathcal{O}_{h_i}^\alpha(z_3) \mathcal{O}_{\bar{h}_1}(\bar{z}_1) \mathcal{O}_{\bar{h}_2}(\bar{z}_2) \rangle , \quad (3.37)$$

where we have pulled out the dynamical information in the OPE coefficients and expectation values.

The three-point functions, as written, are now purely kinematic, i.e. they represent the functional dependence of such a three-point function where the overall coefficient is taken to be one. Each sum over Virasoro descendants now can be seen to give a standard chiral Virasoro conformal block $\mathcal{F}(c, h; [h_1, h_2, \bar{h}_1, \bar{h}_2]|z)$, so that the two-point function can be expanded in this *bulk channel* as

$$\langle \mathcal{O}_1(z_1, \bar{z}_1) \mathcal{O}_2(z_2, \bar{z}_2) \rangle_{\text{UHP}}^b = \left(\frac{z_{21^*}}{z_{11^*}} \right)^{h_1-h_2} \left(\frac{z_{11^*}}{z_{12^*}} \right)^{\bar{h}_2-\bar{h}_1} \frac{z^{h_1+h_2}}{(z_{12})^{h_1+h_2}(z_{2^*1^*})^{\bar{h}_1+\bar{h}_2}}$$
$$\times \sum_i \hat{\mathcal{C}}_{12}^i \mathcal{A}_i^b \mathcal{F}(c, h_i; [h_1, h_2, \bar{h}_1, \bar{h}_2]|z) , \quad (3.38)$$

and where we have written the conformal block in terms of the cross-ratio

$$z = \frac{z_{12} z_{2^*1^*}}{z_{12^*} z_{21^*}} . \quad (3.39)$$

102

Boundary channel expression for the two-point function

We can similarly expand the two-point function in the *boundary channel*. Here we insert a complete set of states corresponding to the expansion of the bulk operators in terms of the boundary operator expansion. The boundary state-operator mapping gives a complete set of states in terms of boundary operators which appear in representations of the surviving diagonal Virasoro symmetry. We thus insert a complete set of orthonormal states of the form

$$\langle \mathcal{O}_1(z_1, \bar{z}_1) \mathcal{O}_2(z_2, \bar{z}_2) \rangle_{\mathrm{UHP}}^b = \sum_{I,\alpha} \langle \mathcal{O}_1(z_1, \bar{z}_1) \tilde{V}_\alpha^{\hat{h}_I} | \hat{h}_I \rangle_{\mathrm{UHP}}^b \langle \hat{h}_I | \tilde{V}_\alpha^{\hat{h}_I \dagger} \mathcal{O}_2(z_2, \bar{z}_2) \rangle_{\mathrm{UHP}}^b \, . \tag{3.40}$$

Using the doubling trick to account for the representation of bulk operators under the boundary Virasoro operators, we can rewrite this as

$$\langle \mathcal{O}_1(z_1, \bar{z}_1) \mathcal{O}_2(z_2, \bar{z}_2) \rangle_{\mathrm{UHP}}^b = \sum_{I,\alpha} \mathcal{B}_{1h}^b \mathcal{B}_{2h}^b \langle \mathcal{O}_{h_1}(z_1) \mathcal{O}_{\bar{h}_1}(z_1^*) V_\alpha^{\hat{h}_I} | \hat{h}_I \rangle$$
$$\times \langle \hat{h}_I | V_\alpha^{\hat{h}_I \dagger} \mathcal{O}_{h_2}(z_2) \mathcal{O}_{\bar{h}_2}(z_2^*) \rangle \, , \tag{3.41}$$

where we have pulled out the dynamical information in the coefficients. The remaining three-point functions, as written, are now purely kinematic. Again we recognize that this sum over Virasoro descendants is the standard bulk chiral Virasoro conformal block $\mathcal{F}(c, h; [h_1, \bar{h}_1, h_2, \bar{h}_2]|\eta)$, giving

$$\langle \mathcal{O}_1(z_1, \bar{z}_1) \mathcal{O}_2(z_2, \bar{z}_2) \rangle_{\mathrm{UHP}}^b = \left(\frac{z_{1^*2}}{z_{12}} \right)^{h_1 - \bar{h}_1} \left(\frac{z_{12}}{z_{12^*}} \right)^{\bar{h}_2 - h_2} \frac{\eta^{h_1 + \bar{h}_1}}{(z_{11^*})^{h_1 + \bar{h}_1} (z_{22^*})^{h_2 + \bar{h}_2}}$$
$$\times \sum_I \mathcal{B}_{1I}^b \mathcal{B}_{2I}^b \mathcal{F}(c, h; [h_1, \bar{h}_1, h_2, \bar{h}_2]|\eta) \tag{3.42}$$

where we have used the cross-ratio

$$\eta = 1 - z \, . \tag{3.43}$$

3.2 Holographic BCFT entanglement entropies

In this section, we review the holographic calculation of entanglement entropies for sub-systems of BCFTs with gravitational duals, or for states of holographic CFTs defined via Euclidean BCFT path integrals. These are the results that we will try to understand via direct CFT calculations in the next section.

3.2.1 Holographic BCFTs

Certain BCFTs have a dual gravitational description. These correspond to holographic CFTs defined on a space M with boundary ∂M, and a boundary condition perhaps obeying additional constraints so that the theory remains holographic. The dual geometries are asymptotically AdS with boundary geometry M, but the bulk physics associated with ∂M can be different depending on the choice of boundary condition.

For a d-dimensional CFT, we can have an effective "bottom up" description of the gravity dual as a $(d+1)$-dimensional asypmtotically AdS spacetime with an end-of-the-world (ETW) brane extending from ∂M [107, 59, 58, 108]. However, in "top down" microscopic examples (see for instance [103, 104, 109, 110, 111, 112]), the dual can be a smooth higher-dimensional geometry. In this case, the ETW brane in the lower-dimensional description represents the smooth degeneration of an internal dimension.

The simplest possible gravitational dual has an ETW brane coupling only to the bulk metric field. Its action is taken to include a boundary cosmological constant (interpreted as the brane tension) and a Gibbons-Hawking term involving the trace of the extrinsic curvature. The details of the action and equation of motion, and all the solutions that we will require in this chapter, can be found in Chapter 2. A more general ansatz is an ETW brane action with coupling to additional bulk fields, e.g. light scalars.

3.2.2 Entanglement entropies for holographic BCFTs

We can use the Ryu-Takayanagi (RT) formula [37] to holographically calculate the entanglement entropy for spatial subsystems. As usual, the entropy (at leading order in the $1/c$

expansion) is given as

$$S_A = \frac{1}{4G}\mathrm{Area}(\tilde{A}) \,, \tag{3.44}$$

where $\tilde{A}$ is the minimal area extremal surface in the dual geometry homologous to the boundary region A.

A new feature of entanglement entropy for holographic BCFTs is that the RT surfaces can end on the ETW brane [59]. Here, we should keep in mind that the ETW brane itself represents a part of the bulk geometry. The homology condition says that the RT surface $\mathcal{X}_A$ for a region A on the boundary, together with the region A itself, should be the boundary of a region Ξ_A of the bulk spacetime: $\partial\Xi_A = A \cup \mathcal{X}_A$. But when applying this condition, the ETW brane should be considered as part of this bulk spacetime region Ξ_A, rather than an additional contribution to the boundary. As a result, we can have a disconnected RT surface for a connected boundary region, as shown in figure 3.

BCFT vacuum state on a half space

As an example, consider the vacuum state of a two-dimensional BCFT on a half-space $x > 0$. Here, the $SO(1,2)$ symmetry preserved by the BCFT should be reflected in the dual geometry. Generally, this gives a warped product of AdS_2 and an internal space, such that the full geometry has an asymptotic region that is locally AdS_3 times some internal space, with boundary geometry equal to the half-space on which the CFT lives. In general, we can write the metric as

$$ds_{\mathcal{M}}^2 = \ell_{\mathrm{AdS}}^2 \left[\hat{g}_{ij}(\mu)\mathrm{d}\mu_i\mathrm{d}\mu_j + \frac{f(\mu)}{z^2}(\mathrm{d}z^2 - \mathrm{d}t^2) \right]. \tag{3.45}$$

Microscopic solutions of this type were constructed in [103, 104].

We can also give a lower dimensional description (at least in the vicinity of the boundary), where we reduce on the internal space so that the internal metric is represented via scalars and vectors. In this case, we can write

$$ds_{\mathcal{M}}^2 = \ell_{\mathrm{AdS}}^2 \left[\mathrm{d}\mu^2 + \frac{f(\mu)}{z^2}(\mathrm{d}z^2 - \mathrm{d}t^2) \right], \tag{3.46}$$

105
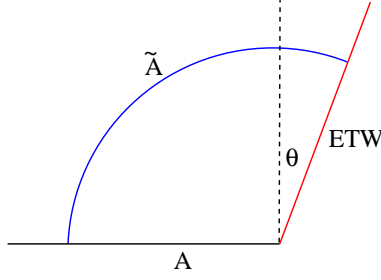
Figure 3.1: Holographic calculation of entanglement entropy for an interval A containing the boundary. The RT surface $\tilde{A}$ sits at a fixed location on the AdS$_2$ fibers of the dual geometry. Here A is homologous to $\tilde{A}$ since the ETW brane represents a smooth part of full microscopic geometry.

where $f(\mu) \to \cosh^2(\mu/\ell_{\text{AdS}})$ as we approach the asymptotic boundary at $\mu = -\infty$ so that the metric is asymptotically AdS$_3$. In general, the scalar fields in the geometry can be functions of the coordinate μ.

In the simplest effective bulk theory, there is an ETW brane with stress-energy tensor $8\pi G T_{ab} = -T g_{ab}/\ell_{\text{AdS}}$ [107, 59], and bulk geometry pure AdS, with $f(\mu) = \cosh^2(\mu/\ell_{\text{AdS}})$. The brane sits at $\mu_{\max} = \text{arctanh}(T)$. Here, the coordinate μ is related to the angular coordinate θ in a polar-coordinate description of Poincaré-AdS by $1/\cos(\theta) = \cosh(\mu)$, so the brane goes into the bulk at a constant angle $\theta = \arcsin(T)$, as shown in Fig. 3.1.

Entanglement entropy for an interval including the boundary

We now consider the entanglement entropy for an interval in the half-space. In the case of an interval $[0, L]$ containing the boundary, we expect the universal form (3.1) for the entanglement entropy. In the holographic calculation with the general metric (3.45), the RT surface sits at a constant position on the AdS$_2$ fiber, so the entanglement entropy is

$$S = \frac{1}{4G} \int_{z > \epsilon} \mathrm{d}^{d+1}x \sqrt{\hat{g}} \,, \tag{3.47}$$

where z is the Fefferman-Graham radial coordinate and d is the dimension of the internal space. We can regulate this by subtracting off half the area of the entangling surface of an

106
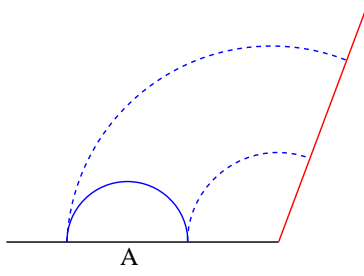
Figure 3.2: Holographic calculation of entanglement entropy for an interval A away from the boundary. The RT surface has two possible topologies, a connected (solid curve) and disconnected (dashed curves).

interval of length $2L$ in vacuum AdS, so

$$
S = \left[\frac{\ell_{\text{AdS}}^{d+1}}{4G} \int_{z>\epsilon} \mathrm{d}^d \mu_i \sqrt{\hat{g}} - \frac{\ell_{\text{AdS}}^{d+1}}{4G} \int_{z>\epsilon, x>0} \mathrm{d}^d x \sqrt{\hat{g}_{\text{AdS}}} \right] + \frac{\ell_{\text{AdS}}^{d+1}}{4G} \int_{z>\epsilon, x>0} \mathrm{d}^d x \sqrt{\hat{g}_{\text{AdS}}} ,
\tag{3.48}
$$

where $\hat{g}_{\text{AdS}}$ is the metric for pure AdS. In this expression, the term in square brackets has a finite limit as $\epsilon \to 0$, independent of L, while the second term gives $\frac{c}{6} \log\left(\frac{2L}{\epsilon}\right)$. Thus, we reproduce (3.1), with the identification

$$
g_b = \lim_{\epsilon \to 0} \left[\frac{\ell_{\text{AdS}}^{d+1}}{4G} \int_{z>\epsilon} \mathrm{d}^d x \sqrt{\hat{g}} - \frac{\ell_{\text{AdS}}^{d+1}}{4G} \int_{z>\epsilon, x>0} \mathrm{d}^d x \sqrt{\hat{g}_{\text{AdS}}} \right] .
\tag{3.49}
$$

As an example, with a constant tension ETW brane, we have

$$
g_b = \frac{\ell_{\text{AdS}}}{4G} \int_0^{\mu_{\max}} \mathrm{d}\mu = \frac{\ell_{\text{AdS}}}{4G} \text{arctanh}(T) = \frac{c}{6} \text{arctanh}(T) .
\tag{3.50}
$$

This is the result of Takayanagi [59] relating the boundary entropy to brane tension.

Entanglement entropy for an interval away from the boundary

Now consider the holographic calculation of entanglement entropy for an interval $[x_1, x_2]$ away from the boundary. In general, the CFT result for this entanglement entropy does not have a universal form. In the holographic calculation, we can have a phase transition

between two different possible RT surface topologies: a connected RT surface or a discon-
nected surface with both components ending on the ETW brane. The two topologies are
shown in Fig. 3.2.

Let us consider these phases in more detail. In the disconnected case, the RT surface
computing the entanglement entropy of an interval $[x_1, x_2]$ is the union of the RT surfaces
associated with $[0, x_1]$ and $[0, x_2]$. Thus, to leading order in large N, we have that

$$S_{[x_1,x_2]}^{\text{disc}} = S_{[0,x_1]} + S_{[0,x_2]} = \frac{c}{6} \log \left(\frac{2x_1}{\epsilon} \right) + \frac{c}{6} \log \left(\frac{2x_2}{\epsilon} \right) + 2g_b \ . \tag{3.51}$$

This result makes use only of the disconnected topology of the RT surface, so is a univer-
sal result for the disconnected phase in any holographic theory. In the connected phase
(expected to apply when the interval is sufficiently far from the CFT boundary), there is
in general no simple universal result for the entanglement entropy. We need to find an RT
surface in the dual geometry, and the calculation of this surface will depend on the details
of the metric $\hat{g}$ appearing in (3.45).

For certain boundary conditions, it may be that the dual gravitational theory is well-
described by an ETW brane with only gravitational couplings. In this case, the dual ge-
ometry is locally AdS$_3$, and the calculation of entanglement entropy for the interval will
be the same as the holographic calculation of vacuum entanglement entropy for the same
interval in the CFT without a boundary. Thus, we have

$$S_{[x_1,x_2]}^{\text{conn}} = \frac{c}{3} \log \left(\frac{x_2 - x_1}{\epsilon} \right) \ . \tag{3.52}$$

Below, we will try to understand what conditions must be satisfied in the BCFT in order
that this result is correct.

In cases where (3.51) and (3.52) give the correct results for the two possible RT-surface
topologies, the actual entanglement entropy will be computed by taking the minimum of
these two results. We find that the disconnected surface gives the correct result for the

entanglement entropy when

$$\log\left[\frac{1}{2}\left(\sqrt{\frac{x_2}{x_1}} - \sqrt{\frac{x_1}{x_2}}\right)\right] > \frac{6g_b}{c} , \tag{3.53}$$

so that for a fixed interval size, we have a phase transition as the location of the interval relative to the boundary is varied. In the more general case where the bulk geometry is not locally AdS, there is no explicit result for the entanglement entropy in the connected phase and (3.53) does not apply. However, we expect that the qualitative behavior of the entanglement entropy is similar, with a transition to the disconnected phase as the interval approaches the boundary. We can view this as a prediction for the behavior of entanglement entropy in holographic BCFTs. One of our main goals below will be to understand the existence of this transition via a direct CFT calculation.

Before turning to the machinery of CFTs, we review a closely related holographic calculation involving a black hole. The transition in RT surfaces takes us between phases where the entanglement wedge of the CFT region under consideration does or does not include a portion of the black hole interior.

In more detail, consider a CFT on $\mathbb{S}^1$, in the state $|b, \tau_0\rangle$ defined via the Euclidean path integral (3.3). We can consider the entanglement entropy for an interval of angular size $\Delta\theta$ in this state, at some fixed Lorentzian time. As described in [86, 1], for small enough τ_0, this is a high-energy pure state of the CFT and the dual geometry is expected to be black hole. Assuming that the bulk effective gravitational theory for the BCFT involves a purely gravitational ETW brane of tension T, it was shown in [86, 1] that the dual geometry for $T > 0$ is a portion of the maximally-extended AdS-Schwarzchild geometry. The black hole interior terminates on a spherically-symetric ETW brane with a time-dependent radius, as shown in Fig. 4.14.

In this case, the geometry outside the horizon is pure AdS-Schwarzchild. In the connected phase, which dominates for small enough $\Delta\theta$, the RT surface lies entirely outside the horizon and gives a time-independent entanglement entropy

$$S^{\mathrm{conn}} = \frac{c}{3}\log\left[\frac{4\tau_0}{\pi\epsilon}\sinh\left(\frac{\pi\Delta\theta}{4\tau_0}\right)\right] , \tag{3.54}$$

109
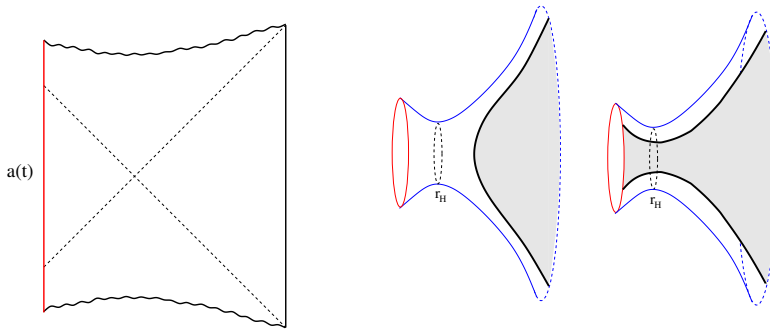
Figure 3.3: The dual geometry for $|b, \tau_0\rangle$ for sufficiently small τ_0 is a portion of the maximally-extended AdS-Schwarzchild geometry, cut off by a spherically symmetric ETW brane. The pictures on the right show the spatial slice at $t = 0$ and the connected and disconnected topologies for the RT surface corresponding to a large interval on the boundary circle.

where we take the circumference of the CFT circle to be 1.

For small enough τ_0, large-enough interval size $\Delta\theta$, and time t sufficiently close to 0 (when the state is prepared) we also have a disconnected phase, where the RT surface is a union of two surfaces at fixed angular position that enter the horizon and terminate on the ETW brane. Here, we find that

$$S^{\text{disc}} = \frac{c}{3} \log \left[\frac{4\tau_0}{\epsilon\pi} \cosh \left(\frac{\pi t}{2\tau_0} \right) \right] + 2g_b \ . \tag{3.55}$$

This is smaller than the connected result (and thus represents the actual entanglement entropy) when

$$\sinh \left(\frac{\pi\Delta\theta}{4\tau_0} \right) \geq \cosh \left(\frac{\pi t}{2\tau_0} \right) e^{\frac{6g_b}{c}} \ . \tag{3.56}$$

When this condition is satisfied, the entanglement wedge of the interval includes a portion of the black hole interior, and hence the entanglement entropy probes the interior geometry. For late times, the connected phase always dominates. This is consistent with the expectation that the state will thermalize, so that the entanglement entropy for a subsystem gives the thermal result.[13]

---

[13]This is similar to the behaviour of correlators in microscopic models of black hole collapse based on

3.3 BCFT calculation of entanglement entropies

In this section, we move on to our central task: performing a direct CFT calculation of entanglement entropy for one or more intervals in the vacuum state of a BCFT on a half-line, for the thermofield double state of two BCFTs, or for the CFT state $|b, \tau_0\rangle$ generated by a Euclidean BCFT path integral. We will argue that with certain assumptions, we can directly reproduce the holographic results described in the previous section.

3.3.1 Entanglement entropy from correlation functions of twist operators

We begin by briefly recalling the CFT calculation of entanglement entropy (for more details, see [114]). We consider a CFT or BCFT on a spatial geometry M in some state $|\Psi\rangle$, defined by a Euclidean path integral on a geometry H with boundary M. We would like to calculate the entanglement entropy $S_A = -\operatorname{tr}(\rho_A \log \rho_A)$ for a region $A \subset M$.

The entanglement entropy can be obtained from a limit of n-*Rényi entropies* $S_A^{(n)}$:

$$S_A = \lim_{n \to 1} S_A^{(n)} , \quad S_A^{(n)} := \frac{1}{1-n} \log \operatorname{Tr}[\rho_A^n] . \tag{3.57}$$

The matrix elements $\langle \phi_A^- | \rho_A | \phi_A^+ \rangle$ are calculated from the path integral on a space $(\bar{H}H)_A$ formed from gluing two copies of H along the complement of A in M,[14] where we set boundary conditions $\phi(x, \tau = \pm\epsilon) = \phi_A^\pm$ on either side of a cut A. The proper normalization is obtained by dividing by the same path integral without a cut along A.

The trace $\operatorname{Tr}[\rho_A^n]$ is then obtained by the path integral on a *replica geometry* $\mathcal{R}_n$ obtained by gluing n copies of $(\bar{H}H)_A$ across the cut A, with the lower half of the cut on each copy glued to the upper half of the cut on the next copy, as shown in Fig. 3.4. Includ-

---

approximate global quenches of Vaidya type [113]. A phase transition in channel dominance leads to a shift in the gravitational saddle computing entanglement entropy, which in turn is responsible for maintaining unitarity. We thank Tarek Anous for discussion of this point.

[14]More precisely, the path integral corresponding to the second copy is the one associated with $\langle\Psi|$; any complex sources in the action should be conjugated.
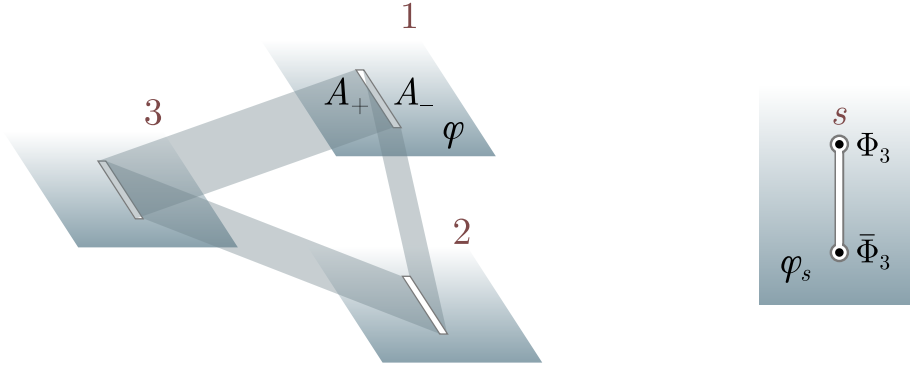
Figure 3.4: *Left*. Three-replica geometry, $\mathcal{R}_3$, with a local field φ. *Right*. Individual copies s, with boundary conditions for φ_i implemented by twists $\Phi_3, \bar{\Phi}_3$.

ing the proper normalization in the path integral expression for the density matrix gives

$$\mathrm{Tr}[\rho_A^n] = \frac{Z_n}{Z_1^n} \ , \tag{3.58}$$

where Z_n is the partition function for the CFT on $\mathcal{R}_n$.

The ratio Z_n/Z_1^n can be expressed as a correlation function of *twist operators* for a CFT/BCFT defined to be the product of n copies of the original theory. A twist operator $\Phi_n(z)$ inserted at z is defined via the path integral by inserting a branch cut ending at z, across which the fields in the kth copy of the (B)CFT are identified with fields in the $(k+1)$-st copy as we move clockwise around the branch point. Similarly, an anti-twist operator $\bar{\Phi}_n(z)$ inserts a branch cut ending at z across which fields in the kth copy of the CFT/BCFT are identified with fields in the $(k-1)$-st copy as we move clockwise around the branch point.

In a CFT, every twist operator must come with an anti-twist operator, with the branch cut running between the two. For a BCFT, in contrast, we can have an *unpaired* twist operator, with the branch cut running between the operator insertion and the boundary. For both the CFT and BCFT, deforming the branch cut simply corresponds to changing the fundamental domain of the replica Riemann surface $\mathcal{R}_n$, as in Fig. 3.5.
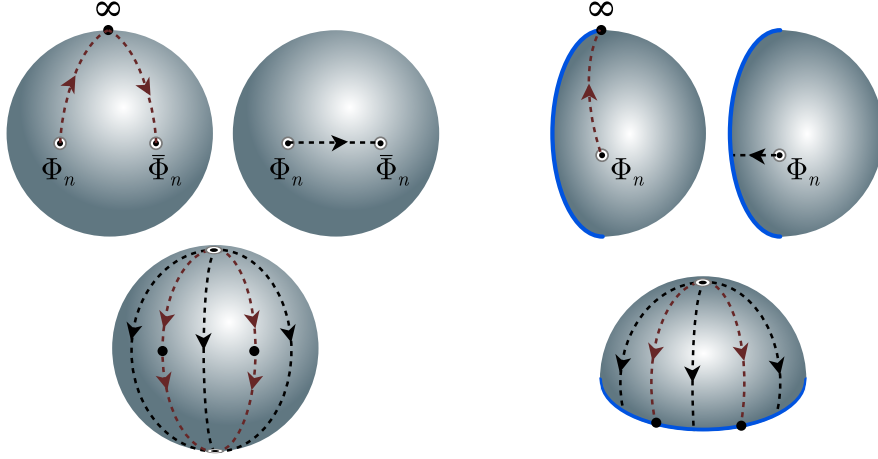
Figure 3.5: *Left*. Deforming the contour of the fundamental domain of $\mathcal{R}_n$ for a CFT. *Right*. Performing the equivalent deformation on $\mathcal{R}_n$ for a BCFT.

Two-point function of the twist operators in a CFT

The correlator $\langle \bar{\Phi}_n(x_1)\Phi_n(x_2) \rangle$ for the n-copy CFT on the real line with a branch cut running between x_1 and x_2 exactly computes the right-hand side of (3.58) for the case where A is the interval $[x_1, x_2]$. The two point function takes a simple form, since as shown in [62], the twists fields Φ_n, $\bar{\Phi}_n$ act like scalar primaries with scaling dimension

$$d_n := \frac{c}{12}\left(n - \frac{1}{n}\right) \tag{3.59}$$

and weights $h_n = \hat{h}_n = d_n/2$. Thus, we have

$$\langle \bar{\Phi}_n(x_1)\Phi_n(x_2) \rangle \sim |x_1 - x_2|^{-2d_n} \ , \tag{3.60}$$

as we will derive again below.

To say more about the coefficient, we need to define the twist operators more precisely by specifying the behavior of the CFT at the branch points. As a specific regularization, we can consider instead the n-copy theory defined on a space obtained by removing a disk of radius ϵ centered at each branch point and placing boundary condition labelled by a_i at

113

the ith resulting circular boundary [67].[15] The resulting path integral geometries for Z_n (and Z_1) are then smooth. A conformal transformation

$$z \mapsto i \log \left(\frac{z - x_2}{z - x_1} \right) \tag{3.61}$$

maps the original plane to a cylinder defined by the complex plane with identification $z \sim z + 2\pi$, and the branch cut $[x_1, x_2]$ mapping to $\mathrm{Re}\,(z) = \pi$.

For small ϵ, the boundaries surrounding the branch points map to $z = \pm i \log[(x_2 - x_1)/\epsilon]$ up to corrections of order ϵ. Thus, the path integral geoemtry is a cylinder of length $\tau = 2 \log[(x_2 - x_1)/\epsilon]$, with boundary condition a_1, a_2 at the two ends. The replica geometry is defined by gluing n copies of this cylinder along the vertical branch cut, so corresponds to a cylinder with circumference $2\pi n$. We can write the path integral on this space using boundary states as[16]

$$Z_n = \langle a_2 | e^{-\frac{\tau}{2\pi n} H} | a_1 \rangle \tag{3.62}$$

where H is the Hamiltonian for the CFT on a circle of unit length. For large τ, the operator inside approaches a projector to the vacuum state

$$e^{-\frac{\tau}{2\pi n} H} \to e^{-\frac{\tau}{2\pi n} E_0} |0\rangle \langle 0| \ , \tag{3.63}$$

where $E_0 = -\pi c/6$ is the vacuum energy for a CFT on a circle of unit length.

Thus, we get

$$(Z_n)_{\epsilon \to 0} = \left(\frac{|x_2 - x_1|}{\epsilon} \right)^{\frac{c}{6n}} \langle a_2 | 0 \rangle \langle 0 | a_1 \rangle \ . \tag{3.64}$$

Finally,

$$\langle \bar{\Phi}_n(x_1) \Phi_n(x_2) \rangle = \frac{Z_n^{a,\epsilon}}{(Z_1^{a,\epsilon})^n} = (\langle a_2 | 0 \rangle \langle 0 | a_1 \rangle)^{(1-n)} \left(\frac{|x_1 - x_2|}{\epsilon} \right)^{-2d_n} \ . \tag{3.65}$$

---

[15]It will be convenient for our discussion below to allow different boundary conditions to regulate the different twist operators, but generally we can choose the same one for each.

[16]We recall that the boundary state was defined using a circle of length 1. Scaling the cylinder to have this circumference, the length becomes $\tau/2\pi n$.

Making use of this in (3.57) and (3.58) gives the standard result for the entanglement entropy of an interval. With our original definition of ϵ, we have $c/3 \log(L/\epsilon) + g_{a_1} + g_{a_2}$, however, it will be convenient to take $a_1 = a_2 = a$ and absorb the last two terms here into the definition of ϵ.

One-point function of the twist operator on a half space

In a BCFT, the twist operators also have a non-vanishing one-point function, related to the Rényi entropies for an interval $[0, x]$ in the vacuum state of the BCFT on a half-space $x \geq 0$. We can calculate this using the regularization defined above.

We will consider a BCFT on the UHP with boundary condition b at $\text{Im}\,(z) = 0$, with the twist operator at $z_1 = x_1 + iy_1$ regulated by boundary condition a. The conformal transformation

$$z \mapsto i \log \left(\frac{z - z_1^*}{z - z_1} \right) \tag{3.66}$$

maps the upper half-plane to a cylinder defined by the complex plane with identification $z \sim z + 2\pi$, where the boundary along the real axis maps to the interval $[0, 2\pi]$ on the real axis. The circle of radius ϵ regulating the twist operator maps (in the limit of small ϵ) to a second end of the cylinder at $\text{Im}\,(z) = \log(2y_1/\epsilon)$.

Thus, the one-point function is $Z_n/(Z_1)^n$, where Z_n is the partition function on a cylinder of circumference $2\pi n$ and height $\tau = \log(2y_1/\epsilon)$. Using the second equation in (3.65), we have that

$$\langle \Phi_n(z_1, \bar{z}_n) \rangle = \frac{Z_n}{(Z_1)^n} = (\langle a|0\rangle \langle 0|b\rangle)^{(1-n)} \left| \frac{2y_1}{\epsilon} \right|^{-d_n}, \tag{3.67}$$

Interpreting the $\text{Re}\,(z)$ direction as Euclidean time, this gives $\text{tr}(\rho^n)$ for an interval $[0, y_1]$ in the vacuum state of a BCFT on a half-space. From (3.57), the entanglement entropy associated with this density matrix is

$$S = \frac{c}{6} \log \left(\frac{2y_1}{\epsilon} \right) + g_a + g_b . \tag{3.68}$$

The term g_a in the regulator can be absorbed by a redefinition of ϵ to give the result (3.1).[17] On the other hand, boundary entropy term g_b is physical. It is equal to the difference between the BCFT entanglement entropy and the half the entanglement entropy in the parent CFT for an interval of length $2y_1$, with twist regularization fixed.

3.3.2 Two-point function of twist operators on a half-space

We are now ready for our main calculation. We consider the correlator on the UHP of a twist operator at z_1 and an anti-twist operator at z_2. As discussed in §3.1.1, we can express the two-point function here either as a sum of bulk one-point functions (the *bulk channel*), or as a sum of boundary two-point functions (the *boundary channel*), using the bulk OPE or the BOE respectively. We now consider these expressions explicitly.

Boundary channel for the two-point function

The boundary channel for the BCFT two-point function is obtained by first expanding each operator using the BOE, so that the bulk two-point function becomes a sum of boundary two-point functions. The contribution of two-point functions involving all the operators in a multiplet of the Virasoro symmetry sums to a conformal block. Using the general result (3.19) with (3.21), we find

$$\langle \Phi_n(z_1, \bar{z}_1) \bar{\Phi}_n(z_2, \bar{z}_2) \rangle^b_{\text{UHP}} = \left[\frac{\eta}{4y_1 y_2} \right]^{d_n} \sum_I \mathcal{B}^b_{\Phi I} \mathcal{B}^b_{\bar{\Phi} I} \mathcal{F}(c, \Delta_I, d_n/2 | \eta) \tag{3.69}$$

where

$$\eta = \frac{(z_1 - \bar{z}_1)(z_2 - \bar{z}_2)}{(z_1 - \bar{z}_2)(z_2 - \bar{z}_1)} , \tag{3.70}$$

and where I indexes untwisted boundary operators in the n-fold product theory. As we reviewed in §3.3.3, the BOE coefficients here can be expressed in terms of correlators of boundary operators in the original BCFT.[18] Writing the cross ratio explicitly in terms of

---

[17] Note that this is the same redefinition as the previous subsection.

[18] To avoid cluttering our notation further, we will generally leave n implicit in our BOE coefficients $\mathcal{B}$.

real coordinates, we have

$$\eta = \frac{4y_1y_2}{(x_1 - x_2)^2 + (y_1 + y_2)^2} = 1 - \frac{(x_1 - x_2)^2 + (y_1 - y_2)^2}{(x_1 - x_2)^2 + (y_1 + y_2)^2} \,, \qquad (3.71)$$

so we see that η is a real number in $[0, 1]$, with $\eta \to 1$ in the limit where z_1 and z_2 are much closer to each other than the boundary and $\eta \to 0$ in the limit where z_1 and z_2 are much closer to the boundary than to each other.

Consider the contribution from the term where only the boundary identity operator is kept in each BOE (3.14). This is equal to the disconnected term in the two-point function that factorizes into the product of one-point functions, and hence

$$
\begin{aligned}
\langle \Phi_n(z_1, \bar{z}_1)\bar{\Phi}_n(z_2, \bar{z}_2)\rangle^b_{\text{UHP},\mathbf{1}} &= \frac{\mathcal{B}^b_{\Phi\mathbf{1}}\mathcal{B}^b_{\bar{\Phi}\mathbf{1}}}{[4y_1y_2]^{d_n}} \\
&= \frac{e^{2g_b(1-n)}\epsilon^{2d_n}}{[4y_1y_2]^{d_n}} \,,
\end{aligned}
\qquad (3.72)
$$

where we have read off $\mathcal{B}^b_{\Phi\mathbf{1}}$ from (3.67). In general, this contribution should dominate the correlator in the limit $\eta \to 0$, where the two operators approach the boundary.

Bulk channel for the two-point function

We can obtain an alternative expression for the two-point function using the bulk OPE to express the product $\Phi_n(z_1, \bar{z}_1)\bar{\Phi}_n(z_2, \bar{z}_2)$ as a sum of bulk operators. This reduces the two-point function to a sum of one-point functions.

Using the general result (3.19) with (3.22) for this bulk-channel expression for the two-point function, we obtain

$$
\begin{aligned}
\langle \Phi_n(z_1, \bar{z}_1)\bar{\Phi}_n(z_2, \bar{z}_2)\rangle^b_{\text{UHP}} &= \left[\frac{\eta}{4y_1y_2}\right]^{d_n} \sum_i C^i_{\Phi_n\bar{\Phi}_n}\mathcal{A}^b_i\mathcal{F}(c, h_i, d_n/2|1-\eta) \\
&= \left[\frac{1-\eta}{|z_1 - z_2|^2}\right]^{d_n} \sum_i C^i_{\Phi_n\bar{\Phi}_n}\mathcal{A}^b_i\mathcal{F}(c, h_i, d_n/2|1-\eta) \,(3.73)
\end{aligned}
$$

where i indexes untwisted operators in the n-fold product CFT. Again, it will be useful

below to note the contribution where we keep only the bulk identity operator term in the OPE (3.16):

$$\langle \Phi_n(z_1, \bar{z}_1)\bar{\Phi}_n(z_2, \bar{z}_2)\rangle_{\text{UHP},\mathbf{1}}^b = \frac{C_{\Phi_n\bar{\Phi}_n}^{\mathbf{1}}\mathcal{A}_{\mathbf{1}}^b}{|z_1 - z_2|^{2d_n}}$$

$$= \frac{\epsilon^{2d_n}}{|z_1 - z_2|^{2d_n}} , \qquad (3.74)$$

where we have used $\mathcal{A}_{\mathbf{1}}^b = 1$ and $C_{\Phi_n\bar{\Phi}_n}^{\mathbf{1}} = \epsilon^{2d_n}$ from (3.65). This contribution should dominate the correlator in the limit $\eta \to 1$, where the two operators approach each other away from the boundary.

3.3.3 Boundary operator expansion for twist operators*

In this section, we relate the boundary operator expansion of the twist operator Φ_n in an n-copy BCFT to n-point functions of boundary operators in the original BCFT. Our discussion here is directly parallel to the discussion in §4 of [115] on contributions to the OPE coefficients of CFT twist operators.

Via radial quantization, a twist operator inserted at z into an n-copy BCFT can be understood to give rise to some entangled state of this n-copy BCFT on an interval. By the state-operator correspondence, the same state can be obtained by the insertion of some operator at the origin. A basis of boundary operators for the n-copy BCFT may be written as $\mathcal{O}_{I_1} \otimes \cdots \otimes \mathcal{O}_{I_n}$, where $\mathcal{O}_I$ are a basis of boundary operators in the original BCFT. Thus, we can write that

$$\Phi_n(x + iy) = \sum_{\{I_k\}} \frac{1}{|2y|^{d_n - \sum_k \Delta_{I_k}}} B_{I_1 \cdots I_n}^{\Phi_n} \mathcal{O}_{I_1} \otimes \cdots \otimes \mathcal{O}_{I_n}(x) . \qquad (3.75)$$

When the operators $\mathcal{O}_{I_1}$ are primary, the coefficient $B_{I_1 \cdots I_n}^{\Phi_n}$ can be defined according to (3.13) via the bulk-boundary two-point function as

$$B_{I_1 \cdots I_n}^{\Phi_n} = 2^{d_n - \sum_k \Delta_{I_k}} \langle \Phi_n(z = i)\mathcal{O}_{I_1} \otimes \cdots \otimes \mathcal{O}_{I_n}(0)\rangle$$

$$= 2^{d_n - \sum_k \Delta_{I_k}} \langle \Phi_n(i)\rangle \frac{\langle \Phi_n(i)\mathcal{O}_{I_1} \otimes \cdots \otimes \mathcal{O}_{I_n}(0)\rangle}{\langle \Phi_n(i)\rangle}$$

118

$$= 2^{-\sum_k \Delta_{I_k}} \epsilon^{d_n} e^{g_b(1-n)} \frac{\langle \Phi_n(i) \mathcal{O}_{I_1} \otimes \cdots \otimes \mathcal{O}_{I_n}(0) \rangle}{\langle \Phi_n(i) \rangle} \; .$$

To compute the ratio of correlators in the last line, consider the conformal transformation

$$w(z) = i \left(\frac{(z+i)^n + (z-i)^n}{(z+i)^n - (z-i)^n} \right) \; . \tag{3.76}$$

This takes the UHP to the n-sheeted UHP associated with the insertion of our twist operator. The points

$$x_k \equiv \cot \left(\pi \frac{2k-1}{2n} \right) \qquad k = 1, \ldots, n \tag{3.77}$$

map to the origin on the various sheets. By this conformal transformation, we have that

$$\frac{\langle \Phi_n(i) \mathcal{O}_{I_1} \otimes \cdots \otimes \mathcal{O}_{I_n}(0) \rangle}{\langle \Phi_n(i) \rangle} = \prod_k \left(\frac{dw}{dz}(x_k) \right)^{-\Delta_{I_k}} \left\langle \prod_k \mathcal{O}_{I_k}(x_k) \right\rangle \tag{3.78}$$

For the points x_k where $w(z) = 0$, we have that

$$\frac{dw}{dz}(x_k) = \frac{n}{x_k^2 + 1} = n \sin^2 \left(\pi \frac{2k-1}{2n} \right) \; . \tag{3.79}$$

Combining everything, we have that

$$B^{\Phi_n}_{I_1 \cdots I_n} = 2^{-\sum_k \Delta_{I_k}} \epsilon^{d_n} e^{g_b(1-n)} \prod_k \left[n \sin^2 \left(\pi \frac{2k-1}{2n} \right) \right]^{-\Delta_{I_k}} \left\langle \prod_k \mathcal{O}_{I_k}(x_k) \right\rangle \; . \tag{3.80}$$

It is useful to note that the explicit dependence on c appears as a universal prefactor,

$$B^{\Phi_n}_{I_1 \cdots I_n} = \epsilon^{d_n} e^{g_b(1-n)} \bar{B}^{\Phi_n}_{I_1 \cdots I_n} \; . \tag{3.81}$$

For $n = 2$, we see that the correlator vanishes unless $I_1 = I_2$, and we have that

$$\bar{B}^{\Phi_2}_{II} = \frac{1}{16^{\Delta_I}} \; . \tag{3.82}$$

For $n = 3$, we have that

$$\bar{B}^{\Phi_3}_{IJK} = \frac{C_{IJK}}{3^{\frac{3}{2}(\Delta_I + \Delta_J + \Delta_K)}} \ , \tag{3.83}$$

where we have used the standard result for a CFT three-point function.

3.3.4 Rényi entropy

We now use our results to calculate the Renyi entropy for an interval $A = [y_1, y_2]$ for the vacuum state of a BCFT on a half space $y > 0$. This is related to the two-point function of twist operators on the upper half-plane as

$$e^{(1-n)S_A^{(n)}} = \langle \Phi_n(z_1, \bar{z}_1) \bar{\Phi}_n(z_2, \bar{z}_2) \rangle^b_{\text{UHP}} \ , \tag{3.84}$$

where we take $z_1 = (0, y_1)$ and $z_2 = (0, y_2)$.

Bulk and boundary limits

First, consider the Rényi entropy in the limits $\eta \to 0$ and $\eta \to 1$, where the twist operator two-point function is given by (3.72) and (3.74) respectively. In this case, we find that

$$S_A^{(n)} = \begin{cases} \dfrac{c}{12}\dfrac{n+1}{n} \log\left(\dfrac{2y_1}{\epsilon}\right) + \dfrac{c}{12}\dfrac{n+1}{n} \log\left(\dfrac{2y_2}{\epsilon}\right) + 2g_b & \eta \to 0 \\[3mm] \dfrac{c}{6}\dfrac{n+1}{n} \log\left(\dfrac{|y_2 - y_1|}{\epsilon}\right) & \eta \to 1 \ . \end{cases} \tag{3.85}$$

Taking the $n \to 1$ limit, these give entanglement entropies

$$S_A = \begin{cases} \dfrac{c}{6} \log\left(\dfrac{2y_1}{\epsilon}\right) + \dfrac{c}{6} \log\left(\dfrac{2y_2}{\epsilon}\right) + 2g_b & \eta \to 0 \\[3mm] \dfrac{c}{3} \log\left(\dfrac{|y_2 - y_1|}{\epsilon}\right) & \eta \to 1 \ . \end{cases} \tag{3.86}$$

We see that these precisely match the holographic results (3.51) and (3.52).

The result (3.51) is expected to be valid for any holographic CFT in some finite interval around $\eta = 0$ where the RT surface is disconnected, while the result (3.52) is expected to

be valid in a finite interval around $\eta = 1$ in the case where the holographic theory can be modelled by a purely gravitational ETW brane. Thus, the results (3.86) have a much larger range of validity than we would naively expect from the CFT point of view. We would now like to understand from the CFT perspective how this larger range of validity for the vacuum results can arise.

Entropies at large c

We begin with the general expressions (3.69) and (3.73) for the twist operator two-point function. General closed-form expressions for the conformal blocks are not known, but in the *semiclassical limit* $c \to \infty$, the chiral conformal blocks exponentiate [116]:[19]

$$\mathcal{F}(c, h_{\text{int}}, h | \eta) \overset{c \to \infty}{=} \exp\left[-\frac{c}{6} f\left(\frac{h_{\text{int}}}{c}, \frac{h}{c}, \eta \right) \right] . \tag{3.87}$$

The exponent f is called the *semiclassical block*.[20] In our case of identical external weights, recursion relations for the block allow one to commute the limits $c \to \infty$ and $h_{\text{int}}/c, h/c \to 0$ [119, 65]. Hence, the semiclassical blocks associated to *light* internal operators $h_{\text{int}} = O(c^0)$ are just the vacuum (semiclassical) block:

$$f_0\left(\frac{h}{c}, \eta \right) \equiv f\left(0, \frac{h}{c}, \eta \right) . \tag{3.88}$$

We can apply these results to our two-point function of twist operators, for which all of the external dimensions are $d_n/2$, and the central charge of the replicated CFT is nc.

We find that the $c \to \infty$ limit of the expressions (3.69) and (3.73) for the twist operator

---

[19]There is a beautiful but non-rigorous argument for exponentiation from Liouville theory, using the explicit structure constants [117, 118] and the path integral. We refer the interested reader to the clear account in [70].

[20]In general, this depends on the set of external weights, but our notation takes into account that all of the external weights are identical.

two-point function in the boundary and bulk channels become

$$
\langle \Phi_n(z_1,\bar{z}_1)\bar{\Phi}_n(z_2,\bar{z}_2)\rangle^b_{\mathrm{UHP}}
$$

$$
= \left(\frac{\eta}{4y_1 y_2}\right)^{d_n}\left[\hat{\mathcal{D}}_{\mathrm{L}}e^{-\frac{nc}{6}f_{\hat{0}}\left(\frac{d_n}{2nc},\eta\right)} + \sum_{J_{\mathrm{H}}}\mathcal{B}^b_{\Phi J}\mathcal{B}^b_{\bar{\Phi}J}e^{-\frac{nc}{6}f\left(\frac{\hat{\Delta}_J}{nc},\frac{d_n}{2nc},\eta\right)}\right] \tag{3.89}
$$

$$
= \left(\frac{\eta}{4y_1 y_2}\right)^{d_n}\left[\mathcal{D}_{\mathrm{L}}e^{-\frac{nc}{6}f_0\left(\frac{d_n}{2nc},1-\eta\right)} + \sum_{j_{\mathrm{H}}}C^j_{\Phi_n\bar{\Phi}_n}\mathcal{A}^b_j e^{-\frac{nc}{6}f\left(\frac{h_j}{nc},\frac{d_n}{2nc},1-\eta\right)}\right], \tag{3.90}
$$

where $J_{\mathrm{H}}, j_{\mathrm{H}}$ range over heavy internal operators, and $\hat{\mathcal{D}}_{\mathrm{L}}$ and $\mathcal{D}_{\mathrm{L}}$ are degeneracy factors multiplying the vacuum channel:

$$
\hat{\mathcal{D}}_{\mathrm{L}} = \sum_{J_{\mathrm{L}}}\mathcal{B}^b_{\Phi J}\mathcal{B}^b_{\bar{\Phi}J}, \quad \mathcal{D}_{\mathrm{L}} = \sum_{j_{\mathrm{L}}}C^j_{\Phi_n\bar{\Phi}_n}\mathcal{A}^b_j . \tag{3.91}
$$

As $c \to \infty$, the sums (3.89) and (3.90) should be dominated by the exponential with smallest exponent, if the coefficients of the exponential in the sum are not too large. More precisely, let us now make two assumptions:

1. The contribution of all heavy internal operators, in a neighbourhood around $\eta = 0$ or $\eta = 1$ in the respective channel, is exponentially suppressed in c. We will take heavy to mean any operators whose dimension scales as $O(c)$ or greater.

2. The degeneracy factors $\hat{\mathcal{D}}_{\mathrm{L}}, \mathcal{D}_{\mathrm{L}}$ are given by the vacuum contribution times some multiplicative correction that does not change the leading exponential in c behaviour.

If the neighborhoods described in the first assumption meet at some point η^n_*, so that they cover the entire interval $\eta \in [0,1]$, we can conclude that large-c behaviour of the correlator is given by the larger of the vacuum block contribution in the boundary channel or the vacuum block contribution in the bulk channel for the entire interval $\eta \in [0,1]$. This behaviour is commonly known as *vacuum block dominance*.

Under our first assumption of vacuum block dominance, the Rényi entropy for an

interval $[y_1, y_2]$ is given by

$$
S_A^{(n)} = \begin{cases}
\dfrac{c}{6}\dfrac{n+1}{n}\log(y_1 + y_2) + \dfrac{c}{6}\dfrac{n}{n-1}f_0\left(\dfrac{1}{24}\left(1 - \dfrac{1}{n^2}\right), \dfrac{4y_1 y_2}{(y_1 + y_2)^2}\right) + \dfrac{1}{1-n}\log\hat{\mathcal{D}}_{\mathrm{L}} & \eta < \eta_*^n \\[3mm]
\dfrac{c}{6}\dfrac{n+1}{n}\log(y_1 + y_2) + \dfrac{c}{6}\dfrac{n}{n-1}f_0\left(\dfrac{1}{24}\left(1 - \dfrac{1}{n^2}\right), \dfrac{(y_1 - y_2)^2}{(y_1 + y_2)^2}\right) + \dfrac{1}{1-n}\log\mathcal{D}_{\mathrm{L}}, & \eta > \eta_*^n
\end{cases}
\tag{3.92}
$$

where η_*^n is the value of η at which the lower expression becomes larger than the upper one. In the limit $n \to 1$, the behavior of the semiclassical vacuum block follows from the result that for small $\alpha = (n-1)/12$ [65],

$$
f_0(\alpha, \eta) = 12\alpha \log \eta + \mathcal{O}(\alpha^2) ,
\tag{3.93}
$$

as we derive in §3.4.2.

Under our second assumption of vacuum block dominance, we have that (at order c)

$$
\begin{aligned}
\lim_{n\to 1}\frac{1}{1-n}\log\hat{\mathcal{D}}_{\mathrm{L}} &= \lim_{n\to 1}\frac{1}{1-n}\log\left(\mathcal{B}^b_{\Phi \mathbf{1}}\mathcal{B}^b_{\bar{\Phi}\mathbf{1}}\right) \\
&= -\frac{c}{3}\log \epsilon + 2g_b \\
\lim_{n\to 1}\frac{1}{1-n}\log\mathcal{D}_{\mathrm{L}} &= \lim_{n\to 1}\frac{1}{1-n}\log\left(C^{\mathbf{1}}_{\Phi_n \bar{\Phi}_n}\mathcal{A}^b_{\mathbf{1}}\right) \\
&= -\frac{c}{3}\log \epsilon
\end{aligned}
$$

up to contributions $O(c^0)$. Note that, by keeping the boundary entropy term, we are assuming that it, too, is $O(c)$.

Using these results and the results for the semiclassical blocks gives

$$
S_A = \lim_{n\to 0}S_A^{(n)} = \begin{cases}
\dfrac{c}{6}\log\left(\dfrac{2y_1}{\epsilon}\right) + \dfrac{c}{6}\log\left(\dfrac{2y_2}{\epsilon}\right) + 2g_b & \eta < \eta_* \\[3mm]
\dfrac{c}{3}\log\left(\dfrac{|y_2 - y_1|}{\epsilon}\right) & \eta > \eta_*
\end{cases}
\tag{3.94}
$$

where η_* is the value of η where the two expressions coincide. These are exactly the results (3.86) we obtained keeping only the contributions from boundary and bulk identity operators. Thus, we see that the assumption of vacuum block dominance provides the extended

123

range of validity for the formulas in (3.86), so that the results match our gravitational calculation with a purely gravitational ETW brane.

3.3.5 BCFT requirements for vacuum block dominance

Our expression in (3.94) now matches precisely the gravitational calculation, (3.51) and (3.52) for all η, at leading order in c. Following the previous work for bulk CFTs [65, 115], let us now explore what constraints our vacuum block dominance assumptions place on the spectrum and OPE data of the BCFT.

Boundary channel

We begin with the disconnected phase in the boundary channel that dominates in a neighbourhood of $\eta = 0$. Our first assumption held that the contribution of heavy boundary operators was exponentially suppressed in c and does not contribute at leading order. We will examine this claim in a cascading series of steps, from heaviest to lightest operators.

First, looking at operators of dimension $O(c^\alpha)$ for $\alpha > 1$, we find that agreement with the gravity calculation seems to place rather weak constraints on the BCFT. In particular, the convergence of the boundary OPE can be used in an exactly analogous manner to the convergence of the bulk OPE [120] to show that the contribution of all operators of dimension $\hat{\Delta} > O(c)$ is exponentially suppressed in the central charge.

We then need only worry about operators up to dimension $O(c)$. Define $\rho_{b,n}(\delta)\,\mathrm{d}\delta$ to be the number of untwisted n-fold product boundary operators with dimensions $\hat{\Delta} \in c[\delta, \delta + \mathrm{d}\delta]$, and define a measure of the average twist-operator BOE coefficients by

$$|B_n(\delta)|^2 = \frac{\sum_{\hat{\Delta}_I \in c[\delta, \delta + \mathrm{d}\delta]} \bar{\mathcal{B}}^b_{\Phi I} \bar{\mathcal{B}}^b_{\bar{\Phi}I}}{\sum_{\hat{\Delta}_I \in c[\delta, \delta + \mathrm{d}\delta]} 1} \ , \tag{3.95}$$

where we have introduced $\bar{\mathcal{B}}^b_{\Phi I} = \epsilon^{-d_n} e^{g_b(n-1)} \mathcal{B}^b_{\Phi I}$ to remove a universal prefactor that appears in all the BOE coefficients (see §3.3.3). We can use the known small η expansion

of the semiclassical block [65],

$$f(h_{\text{int}}, h_{\text{ext}}, \eta) = 6(2h_{\text{ext}} - h_{\text{int}}) \log \eta - \frac{h_{\text{int}}}{2}\eta + O(\eta^2) \,, \tag{3.96}$$

to write the bracketed expression in (3.89) as

$$e^{-\frac{nc}{12}\left(1-\frac{1}{n^2}\right) \log \eta/\epsilon + 2(1-n)g_b} \int_0^{O(1)} \mathrm{d}\delta \, \rho_{b,n}(\delta)|B_n(\delta)|^2 e^{c\delta \log \eta + c\delta \eta + O(\eta^2)} \,. \tag{3.97}$$

In this expression, the heavy operators will not contribute to the order c entanglement entropy if the integral over of any region bounded away from zero is exponentially suppressed in c as compared to the integral near zero. This constrains the product of the density of operators appearing in the twist OPE and their OPE coefficients so as not to grow so quickly as to overcome the suppression from the block. For $\eta \ll 1$, this requires

$$\log\left(\rho_{b,n}(\delta)|B_n(\delta)|^2\right) < c\delta \log\left(\eta^{-1}\right) \quad \text{for} \quad \delta \gtrsim 0 \,. \tag{3.98}$$

In particular, requiring the CFT calculation to agree with the gravity result in an interval $0 < \eta < \hat{\eta} \ll 1$ implies that $\rho_{b,n}(\delta)|B_n(\delta)|^2$ grows more slowly than $\exp(c\delta \log(1/\hat{\eta}))$. Extending to a larger range with $\hat{\eta}$ not necessarily much less than 1 gives a stronger constraint, but the exact form requires more detailed knowledge of the semiclassical block.

Let us then focus on the lower limit of this integral and consider only operators of dimension less than $O(c^\alpha)$ for $\alpha < 1$, where we can approximate the semiclassical block by the vacuum block for all operators, up to $O(c^{\alpha-1})$ corrections. The gravity calculation predicts that the leading exponential in c behavior of the result matches the vacuum channel contribution, so we require that

$$\sum_{I_L} \bar{\mathcal{B}}^b_{\Phi_n I} \bar{\mathcal{B}}^b_{\bar{\Phi}_n I} \tag{3.99}$$

is subexponential in c.[21] In §3.3.3, we recall that the coefficients $\bar{\mathcal{B}}^b_{\Phi_n I}$ can be expressed in

---

[21]It is also interesting to consider the constraints on the CFT assuming that we have a conventional gravitational theory with a usual semiclassical expansion. In this case, the corrections to the entropy are expected to be of order c^0 (as opposed to some larger power of c or $\log c$). In this case, we would obtain stronger constraints on the BCFT. However, for this chapter, we focus on the constraints arising from demanding that

125

terms of n-point correlations functions of light boundary operators in the original BCFT, so this constraint can be translated into a constraint on the spectrum and n-point functions of the original BCFT. We consider the case $n = 2$ in more detail below.

Bulk channel

We can largely repeat the above analysis in the bulk channel. Again, we find only weak constraints on operators of dimension $O(c^\alpha)$ for $\alpha > 1$. The convergence of the bulk OPE can be used now precisely as in [120] to show that the contribution of all operators of dimension $\Delta > O(c)$ is exponentially suppressed in the central charge. We then need only worry about operators up to dimension $O(c)$.

Define $\rho_n(\delta) \, \mathrm{d}\delta$ to be the number of bulk untwisted n-fold product operators with dimensions $\Delta \in c[\delta, \delta + \mathrm{d}\delta]$ and

$$AC_{b,n}(\delta) = \frac{\sum_{\Delta_i \in c[\delta, \delta + \mathrm{d}\delta]} \bar{C}^i_{\Phi\bar{\Phi}} \mathcal{A}^b_i}{\sum_{\Delta_i \in c[\delta, \delta + \mathrm{d}\delta]} 1} \, , \tag{3.100}$$

where $\bar{C}^i_{\Phi\bar{\Phi}} = \epsilon^{-2d_n} C^i_{\Phi\bar{\Phi}}$. Then in this channel, we have

$$e^{-\frac{nc}{12}\left(1 - \frac{1}{n^2}\right)\log(1-\eta)/\epsilon} \int_0^{O(1)} \mathrm{d}\delta \, \rho_n(\delta) AC_{b,n}(\delta) e^{c\delta \log(1-\eta) + c\delta(1-\eta) + O((1-\eta)^2)} \, . \tag{3.101}$$

For heavy operators to not contribute to the order c entanglement entropy when $1 - \eta \ll 1$, we require

$$\log\left(\rho_n(\delta) AC_{b,n}(\delta)\right) < c\delta \log(1 - \eta)^{-1} \quad \text{for} \quad \delta \gtrsim 0 \, . \tag{3.102}$$

This is analogous to the boundary channel condition, but with $\eta \to 1 - \eta$.

For operators with dimension $O(c^\alpha)$ for $\alpha < 1$, assumption 2 must hold in order to match with from gravity with a purely gravitational ETW brane. This requires that for the light operators, the sum

$$\sum_{i_L} \bar{C}^i_{\Phi\bar{\Phi}} \mathcal{A}^b_i \tag{3.103}$$

---

the order c terms in the entropies match with the classical gravity calculation.

should be sub-exponential in c.

3.3.6 Constraints on holographic BCFTs

We have now spelled out explicitly a set of conditions on a BCFT that will ensure that the direct BCFT calculation of entanglement entropy matches with the gravity results in the holographic model with a purely gravitational ETW brane. However, we recall that the disconnected phase result (3.51) is universally valid for any holographic BCFT. Assuming that entanglement entropy has such a disconnected phase for some interval $\eta \in [0, \eta_*]$, as it does for the simple model, suggests that vacuum block dominance should hold for any holographic BCFT in an interval $\eta \in [0, \eta_n]$, where the upper end of the interval may depend on the Renyi index n.

From the results in the previous subsection, this implies a constraint

$$\log\left(\rho_{b,n}(\delta)|B_n(\delta)|^2\right) < c\beta^*\delta + O(c^a)\,, \quad a < 1\,, \tag{3.104}$$

where the quantities in the left side were defined in (3.95) and the preceeding paragraph. Here our knowledge of the semiclassical block was not sufficient to fix the $O(1)$ coefficient β^* in this bound. In addition, we have a constraint (3.99) on the light operators. We take these bounds to be novel constraints on which BCFTs can possibly have a gravitational dual.

Although we found an analogous bound

$$\log\left(\rho_n(\delta)AC_{b,n}(\delta)\right) \lesssim c\gamma^*\delta + O(c^a)\,, \quad a < 1 \tag{3.105}$$

in the bulk channel, this should not be viewed as a constraint on the boundary expectation values $\mathcal{A}_i^b$. While the disconnected phase is universal and depends only on the boundary entropy, the connected phase depends on the gravitational background (e.g. whether we have backreacting scalars in the solution dual to the BCFT vacuum). The vacuum solution for the bulk CFT is unique, but in contrast, there is no unique gravitational solution consistent with the symmetries of the BCFT.

A useful diagnostic for the non-universal behaviour of entropy and the bulk back-

ground is when light operators have large, $O(c)$, expectation values that backreact on the gravitational solution:

$$\langle \mathcal{O}_i(x, y) \rangle^b_{\text{UHP}} = \frac{\mathcal{A}_i^b}{(2y)^\Delta} \, , \quad \mathcal{A}_i^b \sim c \, . \tag{3.106}$$

Consistency with the large-c factorization in the bulk then implies there is a large family of "multi-trace" operators of the schematic form $\mathcal{O}^m$ with expectation values $\langle \mathcal{O}^m \rangle^b_{\text{UHP}} \sim c^m$. When calculating the twist correlation function, this tower of operators must be resummed into a new semiclassical block, just as with the gravitational Virasoro descendants. For a BCFT, the form of the semiclassical block is theory-dependent and hence non-universal.

Thus, in the bulk channel vacuum-block dominance is not required by the theory. We must choose to restrict to those boundary states without semiclassical expectation values where non-universal contributions can be ignored.[22]

Constraints on the BCFT base theory

The constraint (3.104) involves both the spectrum of boundary operators in the n-copy theory and the BOE coefficients for twist operators in this theory. As we review in §3.3.3, both of these can be related to the spectrum and OPE data for boundary operators in the single-copy BCFT; we can make use of these relations to convert the constraint (3.104) to a direct statement about the single-copy BCFT.

In particular, consider the case of $n = 2$, where the branched geometry (including a regulator boundary for the twist operator as above) is conformal to the annulus. The Virasoro primaries appearing in the the $n = 2$ twist BOE, analogously to the bulk CFT case in [115, 121, 122], contain products of base primaries of the form

$$\mathcal{O}_I = \mathcal{O}_i \otimes \mathcal{O}_i \, , \tag{3.107}$$

___
[22]The same limitation holds for previous bulk CFT calculations. When light bulk operators have large expectation values that backreact on the geometry, the entanglement entropy of a region is no longer universal and is not determined by vacuum block dominance.

For these operators, as we show in §3.3.3, the BOE coefficients are

$$\bar{\mathcal{B}}^b_{\Phi_2 I} \bar{\mathcal{B}}^b_{\Phi_2 I} = 16^{-2\hat{\Delta}_i} \,, \tag{3.108}$$

identical to the bulk case in [115, 121, 122] up to the non-standard normalization of the twist operators induced by the boundary. Taking into account only these primaries, we have a constraint from (3.99) that

$$\sum_{i_L} 16^{-2\hat{\Delta}_i} \,, \tag{3.109}$$

is sub-exponential in c, where the sum is over light boundary primary operators in the original BCFT. This will be true if the number of light boundary primaries in the base theory is also sub-exponential in c.

Note that the BOE also contains primaries composed of products of descendants in the base theory, such as

$$\mathcal{O}_i \otimes L^2_{-1}\mathcal{O}_i - 2\left(\frac{h_i + 1/2}{h_i}\right) L_{-1}\mathcal{O}_i \otimes L_{-1}\mathcal{O}_i + L^2_{-1}\mathcal{O}_i \otimes \mathcal{O}_i \,. \tag{3.110}$$

These are primaries with respect to the orbifold Virasoro generators:

$$L_m \otimes 1 + 1 \otimes L_m \,, \tag{3.111}$$

but are generated by even powers of the antisymmetric linear combinations

$$L_m \otimes 1 - 1 \otimes L_m \,. \tag{3.112}$$

To estimate the number of such primaries, we use the Hardy-Ramanujan Formula [123], which gives an asymptotic estimate for the number of descendants (partitions $p(k)$) at a given level k:

$$p(k) \sim e^{2\pi\sqrt{k/6}} \,. \tag{3.113}$$

If the density of light primaries for a single BCFT is sub-exponential, as above, including the contribution of the extra primaries in the 2-copy BCFT not of the form (3.107) gener-

129

ates no new contributions exponential in c. Thus, we do not get a substantially stronger constraint from their inclusion.

3.4 Multiple intervals

The generalization of our BCFT results from a single interval to multiple intervals closely parallels the generalization of the CFT result from two intervals to multiple intervals [65]. We start with the holographic calculation, and then discuss how to obtain the results from the monodromy method in the BCFT.

3.4.1 Holographic results for multiple intervals

Consider a collection of k disjoint intervals $A = \sqcup_i A_i$, $A_i = [x_{2i-1}, x_{2i}]$, in the vacuum state of a BCFT on the half-space $x \geq 0$, with an associated minimal surface $\mathcal{X}_A$. A given topology for $\mathcal{X}_A$ geodesically (and without intersection) pairs each endpoint x_i to either (a) another endpoint x_j, or (b) the brane. Morally, we can view the latter as pairing x_i to an image point x_i^* placed on a mirror image of the bulk theory across the brane.

Thus, the possible topologies $\mathrm{top}(\mathcal{X}_A)$ can equally be described by *symmetric* geodesic pairings of $2k$ intervals, of which there are $\binom{2k}{k}$.[23] Assuming that the gravity dual theory is described via a purely gravitational ETW brane, so that the local geometry is pure AdS, the two types of geodesics have (regulated) lengths

$$\frac{\ell_{ij}}{4G_{\mathrm{N}}} = \frac{c}{3} \log\left(\frac{x_{ij}}{\epsilon}\right), \quad \frac{\ell_{mm^*}}{4G_{\mathrm{N}}} = \frac{c}{6} \log\left(\frac{2x_m}{\epsilon}\right) + g_b .$$

---

[23] Arbitrary non-intersecting geodesic pairings of n intervals are counted by Catalan numbers $\binom{2k}{2}/(k+1)$. Each yields $k+1$ symmetric pairings on $2k$ intervals, giving our result. We thank Chris Waddell for discussion of this point.

Hence, the holographic result is

$$S_A = \min_{\text{top}(\mathcal{X}_A)} \frac{1}{4G_{\text{N}}} \left[\sum_{(ij)} \ell_{ij} + \sum_{(mm^*)} \ell_{mm^*} \right]$$

$$= \min_{\text{top}(\mathcal{X}_A)} \left[\sum_{(ij)} \frac{c}{3} \log \left(\frac{x_{ij}}{\epsilon} \right) + \sum_{(mm^*)} \frac{c}{6} \log \left(\frac{2x_k}{\epsilon} \right) + g_b \right] , \qquad (3.114)$$

where (ij) denotes paired endpoints in the half-space and (mm^*) image-paired endpoints.

As a concrete example, take the interval $A = [x_1, x_2]$. The explicit expression for holographic entanglement entropy is then

$$S_A = \min \left\{ \frac{c}{3} \log \left(\frac{x_2 - x_1}{\epsilon} \right) , \frac{c}{6} \log \left(\frac{4x_1 x_2}{\epsilon^2} \right) + 2g^b \right\}$$

$$= \min \left\{ S_A^{\text{conn}}, S_A^{\text{disc}} \right\} ,$$

recovering our results from §3.2.2. The calculation is similar in other vacuum geometries. We can also include a boundary-centred interval $[0, x_0]$, which forces at least one image-paired geodesic.[24]

3.4.2 BCFT calculation for multiple intervals

To calculate the entanglement entropy of $A = \sqcup A_i$ in the BCFT on a half-space, we can simply calculate a correlator of k twist and anti-twist operators on the Euclidean UHP and analytically continue. We will therefore focus on the UHP calculation. As above, we can use kinematic doubling to write the correlator as

$$\left\langle \prod_{i=1}^k \Phi_n(z_{2i-1}, \bar{z}_{2i-1}) \bar{\Phi}_n(z_{2i}, \bar{z}_{2i}) \right\rangle_{\text{UHP}}^b = \left\langle \prod_{i=1}^k \Phi_n(z_{2i-1}) \bar{\Phi}_n(\bar{z}_{2i-1}) \bar{\Phi}_n(z_{2i}) \Phi_n(\bar{z}_{2i}) \right\rangle .$$

$$(3.115)$$

---

[24]When $A = [0, x_0] \sqcup A_1 \sqcup \cdots \sqcup A_{k-1}$, $\mathcal{X}_A$ has $\binom{2k+1}{k}$ possible topologies. This can established by similar combinatorics to the non-boundary case.

As in the single interval case, we have some choice about the order in which we perform bulk OPE or BOE expansions of the twist correlator. We can regard this sequence of choices as a fusion channel $\mathcal{E}$, analogous to the s- and t-channels in the single interval case. A given fusion channel has a natural expansion in terms of a set of cross-ratios, $\vec{\eta}$, and higher-point conformal blocks:

$$\left\langle \prod_{i=1}^{k} \Phi_n(z_{2i-1})\bar{\Phi}_n(\bar{z}_{2i-1})\bar{\Phi}_n(z_{2i})\Phi_n(\bar{z}_{2i}) \right\rangle_{\text{UHP}}^{b} = N(\vec{\eta}) \sum_{\vec{h},\vec{\Delta}} \mathcal{C}^{\mathcal{E},\vec{h},\vec{\Delta}} e^{-\frac{nc}{6}f(\vec{h},d_n/2nc,\vec{\eta})} ,$$

(3.116)

where we have taken the semiclassical limit, and $\mathcal{C}^{\mathcal{E},\vec{h},\vec{\Delta}}$ is a product of OPE and BOE coefficients depending on the internal weights $\vec{h}, \vec{\Delta}$. Here $N(\vec{\eta})$ is just a standard prefactor.

Having related the UHP correlator to a chiral correlator, the higher-point blocks can be obtained from the standard monodromy method. We briefly summarize this method here, following [65]. We discuss the method in slightly more detail in §3.4.3. Readers familiar with the monodromy method may freely jump ahead to (3.123).

The monodromy method begins with a powerful trick: instead of the desired $2k$-point function, consider a $(2k + 1)$-point function, where we have added an additional operator, $\chi_{(1,2)}(z)$, which is taken to be a null descendant of a primary operator $\theta(z)$.[25] The null operator must decouple and the correlator must vanish. The vanishing of the correlator is expressed as the differential equation (writing $\chi(z)$ as a differential operator acting on $\theta(z)$)

$$\Theta''(z) + T(z)\Theta(z) = 0 ,$$

(3.117)

where $\Theta(z)$ is the correlator

$$\Theta(z) = \left\langle \theta(z) \prod_i \Phi_n(z_{2i-1})\bar{\Phi}_n(\bar{z}_{2i-1})\bar{\Phi}_n(z_{2i})\Phi_n(\bar{z}_{2i}) \right\rangle ,$$

(3.118)

---

[25]Strictly speaking, this operator is only guaranteed to exist in Liouville theory. However, as the block is a kinematic object, we expect the form not to depend on whether this operator exists in our theory or not.

and $T(z)$ is

$$T(z) = \sum_i \left\{ \frac{6h_n/c}{(z-z_i)^2} + \frac{6h_n/c}{(z-\bar{z}_i)^2} + \frac{\partial_{z_i}}{z-z_i} + \frac{\partial_{\bar{z}_i}}{z-\bar{z}_i} \right\} \ . \qquad (3.119)$$

For a given channel $\mathcal{E}$, in an appropriate limit of the cross ratios $\eta \to \eta_0^{\mathcal{E}}$, we expect this to be dominated by the exchange of the lightest possible operator, generally the identity and its descendants. We thus make the ansatz that the correlator is given by

$$\Theta(z) \approx \psi(z|z_i, \bar{z}_i) e^{-\frac{nc}{3} f_0^{\mathcal{E}}} \ , \qquad (3.120)$$

to leading order in c. Here $f_0^{\mathcal{E}}$ is the semiclassical vacuum block for the original $2k$-point function and $\psi(z|z_i, \bar{z}_i)$ is thought of as a 'wavefunction' for the inserted operator. In this case, we can rewrite $T(z)$

$$T(z) = \sum_i \left\{ \frac{6h_n/c}{(z-z_i)^2} + \frac{6h_n/c}{(z-\bar{z}_i)^2} - \frac{c_i}{z-z_i} - \frac{\bar{c}_i}{z-\bar{z}_i} \right\} \ , \qquad (3.121)$$

where the c_i are *accessory parameters*:

$$c_i = \frac{\partial f_0^{\mathcal{E}}}{\partial z_i}, \quad \bar{c}_i = \frac{\partial f_0^{\mathcal{E}}}{\partial \bar{z}_i} = \overline{c_i} \ . \qquad (3.122)$$

If we know the accessory parameters, we can integrate (3.122) to find the block $f_0^{\mathcal{E}}$. To determine these parameters, the monodromy method then uses the fact that a solution of the differential equation must have monodromies around any set of points that is consistent with the corresponding operator being exchanged in the block. This constraint can be used to fix the accessory parameters. In general, this cannot be done analytically. However, it is possible to find the parameters explicitly for twist operators in the $n \to 1$ limit, when we can break the problem down into a sum of independent monodromy constraints.

Solving the monodromy constraints and integrating the accessory parameters near $n =$
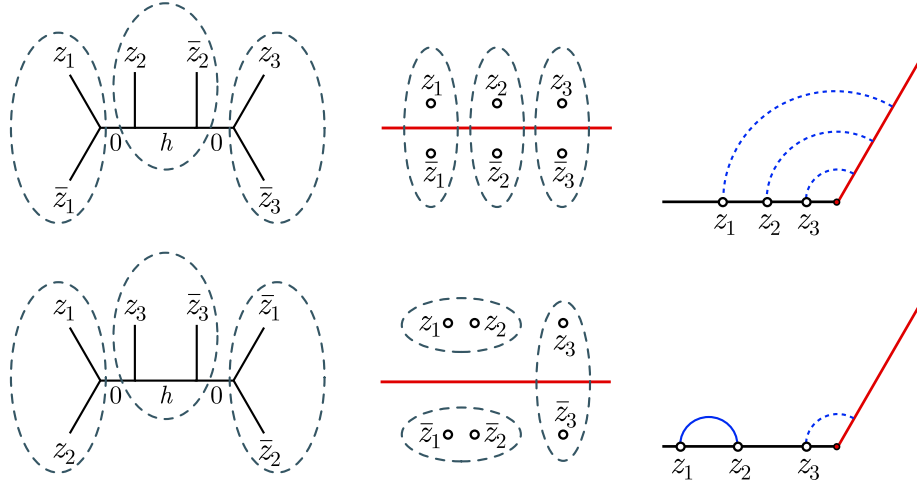
Figure 3.6: *Left.* Vacuum exchange in two different channels for $k = 3$ twists on the UHP. Trivial cycles cut through identities. *Middle.* The monodromy cycles to be trivialized in the doubled picture of the BCFT. *Right.* The corresponding RT topologies in the bulk with an ETW brane.

1, one finds

$$f_0^{\mathcal{E}} = \sum_{(ij)} 12\alpha \log |z_{ij}|^2 + \sum_{(mm^*)} 12\alpha \log z_{mm^*} + O(\alpha^2) \,. \tag{3.123}$$

Here, the channel $\mathcal{E}$ pairs some twists to anti-twists on the same half-plane, and some twists to their images on the opposite half-plane. We have denoted the pairs by (ij) and (mm^*) respectively, and note that (as expected from the CFT case [65]) channels biject with the topologies of §3.4.1, so we can view $\mathcal{E} \in \mathrm{top}(\mathcal{X}_A)$. We illustrate the correspondence between channels, trivial cycles, and the bulk RT surfaces in Fig. 3.6.

To calculate the entanglement entropy, we also need to compute $\mathcal{C}_0^{\mathcal{E}}$. This is easily done, since the OPE coefficients for vacuum exchange are always unity, while the BOE always gives the one-point function of twists (3.67). If there are M image pairs (mm^*), we have

$$\mathcal{C}_0^{\mathcal{E}} = [e^{g_b(1-n)}]^M = e^{-12\alpha M g_b} \,. \tag{3.124}$$

134

We can recover the factors of ϵ from the one-point functions (3.64) and (3.67). From (3.120), the entanglement entropy in the limit $\eta \to \eta_0^{\mathcal{E}}$ is then

$$S_A = \lim_{\alpha \to 0} \left(\frac{c}{36\alpha} f_0^{\mathcal{E}} - \frac{1}{12\alpha} \log \mathcal{C}_0^{\mathcal{E}} \right)$$

$$= \sum_{(ij)} \frac{c}{3} \log \left(\frac{|z_{ij}|}{\epsilon} \right) + \sum_{(mm^*)} \left\{ \frac{c}{6} \log \left(\frac{z_{mm^*}}{\epsilon} \right) + g_b \right\} . \tag{3.125}$$

The corrections to (3.130) are in α^2 and not in z_{ij}. It follows that in *finite* regions around $\eta_0^{\mathcal{E}}$, expression (3.125) is the full entanglement entropy to leading order in c.

If we make the assumption of vacuum block dominance as in §3.3.4, we can upgrade (3.125) to precisely reproduce (3.114):

$$S_A = \min_{\text{top}(\mathcal{X}_A)} \left[\sum_{(ij)} \frac{c}{3} \log \left(\frac{|z_{ij}|}{\epsilon} \right) + \sum_{(mm^*)} \left\{ \frac{c}{6} \log \left(\frac{z_{mm^*}}{\epsilon} \right) + g_b \right\} \right] . \tag{3.126}$$

This follows because vacuum dominance in a channel $\mathcal{E}$ implies the vacuum contribution is larger in other channels. Thus, we have a derivation of the full RT formula in a BCFT dual to AdS with an ETW brane, to the same level of generality as the CFT case [65].

3.4.3   Monodromy method*

Here we continue the discussion of accessory parameters from (3.122) in the main text to give a more complete description of the calculation of the semiclassical blocks. There are only $2k - 3$ independent accessory parameters, since global $\mathrm{SL}(2, \mathbb{R})$ invariance imposes three (real) constraints. Explicitly, these constraints are

$$\sum_i \mathrm{Re} \, (c_i) = \sum_i \mathrm{Re} \left(c_i z_i - \frac{6h_n}{c} \right) = \sum_i \mathrm{Re} \left(c_i z_i^2 - \frac{12h_n z_i}{c} \right) = 0 ,$$

the real part of the usual $\mathrm{SL}(2, \mathbb{C})$ constraints.

If we know the accessory parameters, we can integrate to find the block $f_0^{\mathcal{E}}$. To determine these parameters, we transport a pair of solutions $\vec{\Theta}(z) = [\Theta^+(z), \Theta^-(z)]^T$ around a

point z_c where an OPE or BOE is to be performed. The null decoupling equation (3.117) applied to the three-point function implies that the 2×2 monodromy matrix M performing the transport, $\vec{\Theta}(z) \mapsto M\vec{\Theta}(z)$, gives[26]

$$\mathrm{tr}M = -2\cos(\pi\Lambda_c), \quad \Lambda_c = \sqrt{1 - \frac{24h_n}{c}}. \tag{3.127}$$

The number of independent monodromies to tune equals the number of internal primaries, $2k - 3$,[27] so we have the right number of monodromy constraints to fix our accessory parameters c_i.

In general, we cannot analytically solve for the accessory parameters. Luckily, however, it is possible to find them explicitly for twist operators in the $n \to 1$ limit. As above, we define $\alpha = (n - 1)/12$. Entanglement entropy is obtained from Rényi entropies in the limit $\alpha \to 0$, and since $h_n = c(n + 1)\alpha/2n = c\alpha \to 0$ in this limit, the function (3.121) vanishes away from the singular points $z_i, \bar{z}_i$. As a result, the equation (3.117) decouples into a sum of independent monodromy equations, depending on which cycles the channel $\mathcal{E}$ trivializes.

To illustrate, suppose $\mathcal{E}$ involves a pairing between twists $\Phi_n(z_i)$ and $\bar{\Phi}_n(z_j)$. We must choose the accessory parameters to make the monodromy around z_i, z_j trivial. Since this decouples from the other problems as $\alpha \to 0$, we can simply focus on the contribution

$$\begin{aligned} T_{ij}(z) &= \frac{6h_n}{c} \left[\frac{1}{(z - z_i)^2} + \frac{1}{(z - z_j)^2} \right] - \frac{c_i}{z - z_i} - \frac{c_j}{z - z_j} + \text{c.c.} \\ &= 6\alpha \left[\frac{1}{(z - z_i)^2} + \frac{1}{(z - z_j)^2} - \frac{2}{z_j(z - z_i)} \right] - \frac{c_i}{z - z_i} + \frac{c_i z_i}{z_j(z - z_j)} + \text{c.c.} , \end{aligned} \tag{3.128}$$

where "c.c" stands for complex conjugate terms, and in (3.128), we used the constraint

---

[26]To see this, we suppose the leading term in $\Theta(z) \sim (z - z_c)^\kappa$. Plugging this into (3.117), we find that $\kappa(\kappa - 1) = -6h_n/c$, with two solutions $\kappa_\pm$. These pick up factors $e^{2\pi i \kappa_\pm}$ after traversing a loop $z = z_c + \epsilon e^{i\theta}$, leading to (3.127). See [65] for details.

[27]An exchange channel $\mathcal{E}$ is a cubic tree with $2k$ leaves and $2k - 2$ internal nodes in the doubled picture. The total number of edges is one less than the number of nodes, $E = 4k - 3$, and hence the number of internal edges is $E - 2k = 2k - 3$.

$\text{Re}\,(c_i z_i + c_j z_j) = 6\alpha$. To obtain a trivial monodromy around z_i, z_j (and the image cycle enclosing $\bar{z}_i$, $\bar{z}_j$), it is sufficient for $T_{ij}(z)$ to be regular at infinity. This is equivalent to the sum of residues at simple poles vanishing, and hence

$$c_i + \bar{c}_i = \frac{12\alpha}{|z_{ij}|^2} + O(\alpha^2) \,, \tag{3.129}$$

where $O(\alpha^2)$ corrections arise because the equations only strictly decouple for $\alpha = 0$. The calculation is analogous for a twist paired with its image, but the contribution $T_{mm^*}(z)$ involves only two insertions at z_m and $\bar{z}_m$. If we integrate the accessory parameters defined in (3.129) (and the image-paired counterparts), we find

$$f_0^{\mathcal{E}} = \sum_{(ij)} 12\alpha \log |z_{ij}|^2 + \sum_{(mm^*)} 12\alpha \log z_{mm^*} + O(\alpha^2) \tag{3.130}$$

as required.

3.5 Conclusion

Starting with the vacuum state of a 1+1-dimensional CFT, the geometry of a putative bulk dual is fixed by symmetry to be AdS$_3$, up to internal dimensions. We can also fix AdS$_3$ using the RT formula: it is the unique bulk geometry whose minimal surfaces correctly reproduce the universal result for the entanglement entropy of a single interval. The RT formula makes *non-universal* predictions for two or more intervals, so we can go in the other direction and determine the class of *holographic CFTs* which reproduce these non-universal gravitational results. As shown in [65], vacuum block dominance guarantees that the twist-antitwist correlators used to calculate entanglement entropy agree with the holographic value for any number of intervals. Vacuum dominance places explicit constraints on the spectrum and OPE coefficients of a holographic CFT.

The logic for a CFT with boundary is similar. Symmetry, or the universal result for the entanglement entropy of a boundary-centred interval, restricts us to a class of $SO(1,2)$-invariant geometries. These can include warping in the bulk and compact internal dimen-

sions as before. The simplest bulk geometry is a portion of AdS$_3$ cut off by an ETW brane with purely gravitational couplings [59], though we emphasize this is not the most general bulk dual consistent with ground-state symmetry.

In this chapter, we have taken the next step of transforming non-universal gravitational predictions from these geometries with a purely gravitational ETW brane into a constraint on holographic BCFTs. To match the holographic predictions for a non-centred interval, or indeed any number of intervals, vacuum dominance in both the BCFT bulk and boundary channels is necessary and sufficient. From a kinematic perspective, this follows from the doubling trick and the remaining copy of the Virasoro algebra. But the implications for the BCFT spectrum and OPE coefficients are more subtle. We have made some precise statements above, but expect there is more juice to be squeezed from this particular lemon. For instance, it might be possible to finesse the spectral constraints along the lines of [124], though the CFT machinery required is potentially quite different. It would also be interesting to investigate the additional constraints that arise from assuming not only that the BCFT calculations reproduce the leading $O(c)$ entropies, but also that the subleading corrections to the entropies are order c^0 as we expect from a conventional gravitational theory with a semiclassical expansion.

We have argued that the expression (3.51) for the small η entanglement entropy is universal in holographic CFTs (assuming that the RT surface is disconnected in some interval $[0, \eta_d]$ as in the simple model), so the constraints associated with vacuum block dominance for an interval around $\eta = 0$ should be expected to hold much more generally, for any holographic BCFT with a disconnected RT surface phase at small η. It seems plausible that any holographic BCFT should have such a phase, though it would be interesting to find a direct argument.

Our results have several interesting consequences and applications. First, they put the AdS/BCFT proposal of [59] on firmer microscopic footing, exhibiting explicit conditions on a BCFT under which a locally AdS geometry with a purely gravitational ETW brane captures the microscopic ground-state entanglement entropies. The gravity calculations allow the RT surface to end on an ETW brane, so our results also confirm this aspect of Takayanagi's proposal.[28]

---

[28]From the lower-dimensional perspective, this is a modification of the usual homology condition, though

Our work also has direct applications to the physics of black holes. As discussed in Chapter 2, for black holes dual to CFT states prepared by a Euclidean path integral on the cylinder with conformally invariant boundary conditions, the phase transition in entanglement entropy for a non-centred interval leads to a period of Lorentzian time where boundary observers with access to suitably large boundary regions can see behind the horizon. In the next two chapters, we will exploit these results to gain insight into the dynamics of evaporating black holes.

---

no modification is required if we take the higher-dimensional perspective that the ETW brane represents a smooth part of the full bulk geometry.

Chapter 4

Information Radiation

4.1 Introduction

In this chapter, we introduce and study various holographic systems which capture the dynamics of evaporating black holes. In particular, we consider BCFTs in which the number of local degrees of freedom on the boundary (c_{bdy}) is large compared to the number of local degrees of freedom in the bulk CFT (c_{bulk}). We consider states where the boundary degrees of freedom on their own would describe an equilibrium black hole, but the coupling to the bulk CFT degrees of freedom allows this black hole to evaporate. Put simply, the bulk CFT acts as a bath for the boundary.

If this process is unitary, then as we monitor the entanglement entropy between black hole and bath, it should initially increase, peak when the two systems are close to maximally entangled, and then decrease as the black hole fritters away its remaining degrees of freedom. The time at which it peaks is called the *Page time*. In the bulk/boundary CFT setup, the Page time for the black hole is controlled by the ratio $c_{\mathrm{bdy}}/c_{\mathrm{bulk}}$. Using both holographic calculations and direct CFT calculations, we study the evolution of the entanglement entropy for the subset of the radiation system (i.e. the bulk CFT) at a distance $d > a$ from the boundary. We find that the entanglement entropy for this subsystem increases until time $a + t_{\mathrm{Page}}$ and then undergoes a phase transition after which the entanglement wedge of the radiation system includes the black hole interior.

Remarkably, we will see that this occurs even if the radiation system is initially at the same temperature as the black hole so that the two are in thermal equilibrium. In this case, even though the black hole does not lose energy, it "radiates" information through interaction with the radiation system until the radiation system contains enough information to reconstruct the black hole interior.

The chapter is structured as follows:

- The remainder of this section provides background material on the black hole information problem, holographic approaches to black hole evaporation, evaporation timescales, and how these apply in the presence of a brane.

- In §4.2, we consider a simple 2d BCFT, dual to a black hole which is not evaporating, but in which information "radiates" from the boundary into the bulk CFT nonetheless.

- Finally, §4.3 generalizes the toy model of §4.2 to slightly more realistic single-sided and evaporating black holes.

4.1.1   Black hole evaporation in holography

Within the context of holographic models of quantum gravity, the formation and evaporation of black holes is a manifestly unitary process in the sense that the underlying quantum system evolves through conventional Schrödinger evolution with a Hermitian Hamiltonian. However, in the gravity picture, the physics of the black hole interior and the mechanism through which information about the microstate of the black hole emerges in the Hawking radiation are still not fully understood.

A crucial piece of physics to understand is the evolution of the density matrix for the black hole radiation. Hawking's original calculation [125] suggests that the entropy of this density matrix continues to increase throughout the black hole's evaporation. But unitary evolution predicts that this entropy should begin decreasing at the "Page time" when the black hole's (macroscopic) entropy has been reduced to half of its original value [74, 126] and the remaining black hole becomes maximally entangled with the radiation system. The specific increasing and then decreasing behavior of the entropy of the radiation system as

141

a function of time is known as the *Page curve*. Understanding how this curve comes about from the gravity picture is a key challenge.

A further mystery appeared in the work [127, 128, 129, 130, 131], in which the authors argued that assuming a unitary picture of black hole evaporation leads to the conclusion that there cannot be a smooth region of spacetime behind the horizon of an evaporating black hole past the Page time. The argument was based on an apparent inconsistency between having maximal entanglement between the black hole and its early Hawking radiation after the Page time and having entanglement between field theory degrees of freedom on either side of the black hole horizon, as required by smoothness. The proposed alternative is that the old black hole develops a "firewall" at its horizon.

A fascinating suggestion [35] to avoid this firewall conclusion, making use of the general idea that the connectivity of spacetime is related to quantum entanglement between underlying degrees of freedom [30, 34], is that the entanglement between the black hole and its early radiation past the Page time is actually responsible for the existence of a smooth geometry behind the black hole horizon, in the same way that the entanglement between two conformal field theories (CFTs) in the thermofield double state gives rise to a smooth wormhole geometry connecting the two black hole exteriors.[1] In this picture, the behind-the-horizon degrees of freedom are the radiation degrees of freedom, so there is no contradiction that both are entangled with outside-the-horizon modes of the black hole.

Recently, a series of papers [75, 76, 6] have provided more detailed insight into how the black hole radiation can be seen to have an entropy described by a Page curve yet avoid the firewall paradox by the mechanism of [35] (see also [133]). The examples in these papers make use of an auxiliary radiation system coupled to a system that would otherwise describe an equilibrium black hole[2]. The new insights come by making use of the quantum version [44, 45] of the Ryu-Takayanagi formula [38, 41], which gives the gravity interpretation of entanglement entropies for subsystems of a holographic quantum

---

[1]Along similar lines, it was suggested in [132] that this analogy could be made precise by coupling a holographic CFT to an auxiliary "radiation" system consisting of another copy of the holographic CFT. In this case, an initial pure-state black hole described by the first CFT would evolve to an entangled state of the two CFTs which could be dual to a two-sided black hole. In this case, the radiation system manifestly describes the region behind the horizon of the original black hole.

[2]See [134] for an early application of this idea.

system.

For a subsystem A of a holographic system, the *quantum Ryu-Takayanagi* surface $\tilde{A}$ in the dual gravitational picture is a bulk surface which encloses a region corresponding to A at the boundary of the dual spacetime and has the minimum value of the functional

$$S_{\text{grav}}(A) = \frac{\text{Area}(\tilde{A})}{4G} + S_{\text{bulk}}(\Sigma_A) \tag{4.1}$$

among extrema of this functional. Here $S_{\text{bulk}}(\Sigma_A)$ is the entanglement entropy of bulk fields in the bulk region Σ_A enclosed by $\tilde{A}$. Importantly, the prescription for calculating these entropies in the gravity picture requires the identification of a "quantum extremal surface" on which the functional (4.1) is evaluated to calculate the entanglement entropy. A central observation of [75, 76, 6] is that during the evaporation of a black hole, the quantum extremal surface that computes the entanglement entropy of the radiation system can jump, leading to a first-order transition in the entanglement entropy that provides the necessary switch from increasing to decreasing behavior.

Further insights in [75, 76, 6] make use of the notion of the "entanglement wedge" of a subsystem of a holographic system, which is the portion of the full spacetime that is dual to or reconstructable from the density matrix for the subsystem, and is understood to be the bulk region enclosed by the quantum extremal surface [48, 43, 53, 135, 49, 50, 51]. In the examples of [75, 76, 6], it is seen that after the transition in the quantum extremal surface, the entanglement wedge of the radiation system actually includes a portion of the black hole interior. Thus, the underlying degrees of freedom for this interior region after the transition are understood to be the degrees of freedom of the radiation system, in accord with the proposal of [35].

In this chapter, our first motivation is to further elucidate the observations of [75, 76, 6] by studying the evolution of black holes in a new class of models where the evolution of entanglement entropy and the entanglement wedge can be studied very explicitly through direct holographic calculations. Our models are similar to and motivated by the one in [6] in that they have a holographic description in one higher dimension than the original black hole of interest, and the full dynamics of entanglement entropy for the basic degrees of freedom is captured geometrically through the behaviour of classical Hubeny-
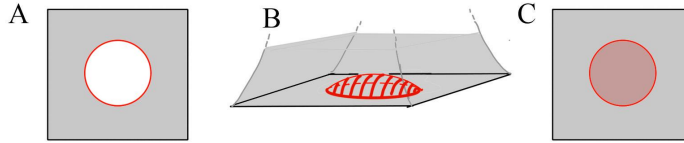
Figure 4.1: Basic setup. (A) Our thermal system, dual to a bulk black hole, is the red boundary. It interacts with a bulk CFT which can serve as an auxiliary system to which the black hole can radiate. (B) Higher-dimensional bulk picture: the red surface is a dynamical 'end-of-the-world' (ETW) brane whose tension is monotonically related to the number of local degrees of freedom in the boundary system. For large tension, this ETW brane moves close to the boundary and behaves like a Randall-Sundrum Planck brane. (C) The Planck-brane picture suggests an effective lower-dimensional description where a part of the CFT in the central region is replaced with a cutoff CFT coupled to gravity, similar to the setup in [6].

Rangamani-Takayanagi (HRT) surfaces. However, our systems are described somewhat more explicitly than the one in [6] and have an additional parameter that controls the Page time for the black hole.

A schematic of our basic setup is shown in Fig. 4.1(A). We imagine starting with a holographic system on $\mathbb{S}^{d-1}$ whose high-energy states or high-temperature thermal states describe black holes in a dual gravitational picture. In these systems, the black hole is in equilibrium with its Hawking radiation, which reflects off the boundary of the spacetime.

Next, following [75, 76, 6] we augment our holographic model with additional degrees of freedom which will serve as an auxiliary radiation system, allowing the black hole to evaporate. As in [76, 6], our auxiliary degrees of freedom will take the form of a higher-dimensional CFT living on a space with boundary $\mathbb{S}^{d-1}$, such that the original system now serves as a set of boundary degrees of freedom for the higher-dimensional CFT. We will denote by c_{bulk} the local number of bulk CFT degrees of freedom and by c_{bdy} the local number of boundary degrees of freedom. We have in mind that $c_{\text{bdy}} \gg c_{\text{bulk}} \gg 1$. This will allow the full system to be holographic, but as we show below, will give a parametrically large evaporation time.

4.1.2 Evaporation timescales

We now discuss some heuristic expectations for the Page time in our setup, guided by dimensional analysis and thermodynamics. We first discuss the evaporation time in terms of CFT parameters, and then compare to the calculation of [136] for an AdS black hole with absorbing boundary conditions.

Suppose we have some initial energy M in the boundary degrees of freedom such that the energy corresponds to a temperature above the Hawking-Page transition for that system. The relation between temperature, energy, and entropy is

$$E \sim c_{\text{bdy}} R^{d-1} T^d \qquad\qquad S \sim c_{\text{bdy}} R^{d-1} T^{d-1} \ , \tag{4.2}$$

for a boundary system of size R. If this system is coupled to a higher-dimensional CFT with c_{bulk} local degrees of freedom, we expect that the energy will be radiated away at a rate

$$\frac{\mathrm{d}E}{\mathrm{d}t} \sim -e c_{\text{bulk}} R^{d-1} T^{d+1} \tag{4.3}$$

where we are using a Boltzmann law, with emissivity e that presumably depends on the nature of the coupling. The factor of c_{bulk} can be understood from a weak-coupling picture where we have c_{bulk} light fields that can carry away the energy.

Using these results, we have that

$$\frac{\mathrm{d}T}{\mathrm{d}t} = -\hat{e} \frac{c_{\text{bulk}}}{c_{\text{bdy}}} T^2 \ , \tag{4.4}$$

where $\hat{e}$ is defined to absorb any numerical coefficients we are ignoring. Solving, we have

$$T = \left(\frac{1}{T_0} + \hat{e} t \frac{c_{\text{bulk}}}{c_{\text{bdy}}} \right)^{-1} \ . \tag{4.5}$$

The Page time is when half the (macroscopic) entropy of the black hole has been radiated. This corresponds to a temperature

$$T_p = 2^{-1/(d-1)} T_0 \ . \tag{4.6}$$

Ignoring factors of order 1, we find that

$$t_{\text{Page}} \sim \frac{c_{\text{bdy}}}{c_{\text{bulk}}} \frac{1}{\hat{e} T_0} \tag{4.7}$$

or

$$\frac{t_{\text{Page}}}{R} \sim \frac{1}{c_{\text{bulk}} \hat{e}} \frac{c_{\text{bdy}}^{1+\frac{1}{d}}}{(MR)^{\frac{1}{d}}} \ . \tag{4.8}$$

Since the initial energy is of order c_{bdy}, it is also illustrative to write $MR = x c_{\text{bdy}}$, so that

$$\frac{t_{\text{Page}}}{R} \sim \frac{c_{\text{bdy}}}{c_{\text{bulk}} \hat{e}} \frac{1}{x^{\frac{1}{d}}} \ . \tag{4.9}$$

We see that the Page time is proportional to $c_{\text{bdy}}/c_{\text{bulk}}$. Thus, we can make the black hole evaporation take a long time by choosing $c_{\text{bdy}} \gg c_{\text{bulk}}$.

We can compare this to the calculation in [136] of Page (see also [137]), who considers perfectly absorbing boundary conditions for a large black hole in AdS. Using those results, one finds a Page time

$$t_{\text{Page}} \sim \frac{L_{\text{AdS}}^{d+1-\frac{2}{d}}}{G^{1+\frac{1}{d}}} \frac{1}{M^{\frac{1}{d}}} \ , \tag{4.10}$$

where we have omitted some numerical factors. An energy of $1/R$ in the field theory corresponds to energy $1/L_{\text{AdS}}$ on the gravity side, while field theory entropy $c_{\text{bdy}} R^{d-1} T^{d-1}$ corresponds on the gravity side to $r_H^{d-1} = T^{d-1} L_{\text{AdS}}^{2d-2}$. Hence, we can relate

$$c_{\text{bdy}} R^{d-1} = \frac{L_{\text{AdS}}^{2d-2}}{G} \ . \tag{4.11}$$

Rewriting (4.10) in terms of field theory parameters, we get

$$\frac{t_{\text{Page}}}{R} \sim \frac{c_{\text{bdy}}^{1+\frac{1}{d}}}{(MR)^{\frac{1}{d}}} \ . \tag{4.12}$$

Comparing with the expression (4.8) above, we see that the expressions have the same dependence on c_{bdy} and M; to match the gravity calculation, we should take $c_{\text{bulk}} \hat{e}$ to be of order 1, at least in terms of scaling with c_{bdy}. In order that the full system is holographic,

146

we want to take $c_{\text{bdy}} \gg c_{\text{bulk}} \gg 1$.

4.1.3 Black holes and branes

In this section, we briefly review the gravitational dual description of holographic BCFTs and explain how the dual of a BCFT with large $c_{\text{bdy}} \gg c_{\text{bulk}}$ can give rise to the physics of a Planck brane whose geometry is the geometry of the black hole we are studying.

In their vacuum state, BCFTs preserve the conformal invariance of a CFT in one lower dimension. Thus, the gravity dual of a d-dimensional CFT with boundary in its vacuum state will generally correspond to a spacetime that is a warped product of AdS_d with some internal space, but which has an asyptotically AdS_{d+1} region with boundary geometry equal to the half space. For various supersymmetric examples, gravitational dual solutions corresponding to the vacuum state are known explicitly [103, 104]. For example, there is a family of half-supersymmetric solutions to type IIB supergravity that correspond to the vacua of $\mathcal{N} = 4$ SYM theory living on half-space with the various boundary conditions preserving half supersymmetry (see e.g. [109, 110, 111, 112]).

In general it is difficult to work with the fully microscopic examples and to find solutions of the ten- or eleven-dimensional supergravity equations that would correspond to various BCFT states. Thus, rather than employing this top-down approach, we will consider bottom-up models of BCFT duals, introduced in [90, 59, 58][3]. Here, the bulk dual of a d-dimensional CFT with boundary is taken to be a $d + 1$-dimensional gravitational theory on a space which has a dynamical boundary extending from the CFT boundary into the bulk. Just as we can consider various possibilities for the bulk gravitational effective action, we can choose various terms for the boundary effective action. We expect that for appropriate choices of the bulk and boundary effective actions, we can accurately capture the physics of various holographic CFTs.[4] In this chapter, we consider the simple situation where the ETW brane couples only to the bulk metric field; its action is taken to include a boundary cosmological constant (interpreted as the brane tension) and a Gibbons-Hawking

---

[3]Note that other bottom-up constructions for the bulk dual of a BCFT have been proposed, e.g. [108].

[4]We note that in the top-down models, there is generally not an explicit ETW brane; instead, the spacetime can "end" by a smooth degeneration of the internal space. The ETW brane in the bottom-up model captures some of this higher-dimensional behavior.
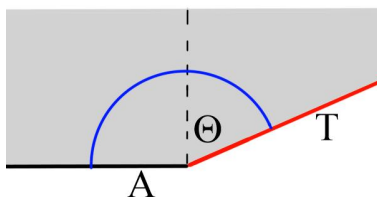
Figure 4.2: An ETW brane with tension parameter T enters the bulk at coordinate angle Θ in Fefferman-Graham coordinates. Larger T gives a larger angle Θ. Shown in blue is the RT surface computing the entanglement entropy of the subsystem A which includes the boundary. The area to the right of the dashed line is proportional to the boundary entropy.

term involving the trace of the extrinsic curvature. The details of the action and equation of motion, and all the solutions that we will require her may be found in Chapter 2.

The work of [59] established a connection between the tension of the ETW brane and the boundary entropy (or higher-dimensional generalizations), which can be understood as a measure of the number of degrees of freedom associated with the boundary. One simple calculation that indicates this relation is the holographic calculation of entanglement entropy for a region of the BCFT that is the interior of a half-sphere centred on the boundary. Holographically, this is computed via the area of an extremal surface anchored to the half-sphere which extends into the bulk and ends on the ETW brane. For larger tension of the ETW brane, this brane enters the bulk at a larger coordinate angle from the vertical in Fefferman-Graham coordinates for the asymptotic region, as shown in Fig. 4.2. As a result, the area of the extremal surface becomes larger, indicating a larger boundary entropy.

In our application, we would like to consider the case where the number of local boundary degrees of freedom is large compared with the number of local bulk degrees of freedom. In this case, there is an independent way to motivate the ETW brane picture. Since we are considering the bulk CFT degrees of freedom to be much fewer than the boundary degrees of freedom, we expect that in some sense, they act as a small perturbation. Over short time scales (much shorter than the Page time), the physics of the boundary degrees of freedom is not significantly affected by the bulk CFT degrees of freedom.

We can think of the d-dimensional geometry of the ETW brane as the usual holographic

dual of the $d - 1$-dimensional boundary system in its state at a particular time. The $d +$ 1-dimensional system dual to the bulk CFT-degrees of freedom couples to this system, and this corresponds to adding in the bulk $d + 1$-dimensional geometry coupled to the d-dimensional brane. Over long time scales, the bulk CFT degrees of freedom can have a significant impact (e.g. when the black hole evaporates). Thus, over long time scales, the full geometry of the ETW brane can be affected significantly by its coupling to the bulk gravity modes, so it is important to consider the full $d + 1$-dimensional system when understanding the long-time dynamics of the system.

As we have reviewed above, a large number of boundary degrees of freedom corresponds to a large tension for the ETW brane and in this case, the ETW brane enters the bulk at a very large angle to the AdS boundary. For the case of a single sphere-topology boundary, the resulting dual gravity solutions have ETW branes that stay close to the boundary in some sense (e.g. they correspond to a cutoff surface in a complete AdS spacetime for which light signals can propagate out to the AdS boundary and back in small proper time).

In this and similar cases, the ETW brane behaves as a "Planck brane" in the Randall-Sundrum sense [138], cutting off a portion of the asymptotic region of the geometry so that this part of the spacetime now terminates with a dynamical brane.[5] This point of view suggests a third description of the physics of our situation: from the CFT point of view, the addition of a Planck brane to a region of the bulk corresponds to cutting off the CFT in some spatial region and coupling to gravity in this region. The cutoff goes to infinity at the boundary of the region. This picture corresponds to the "2D gravity with holographic matter" picture of [6]. This latter picture most closely aligns with the model in [76]. The three pictures are summarized in Fig. 4.1. Note that it is this last picture, Fig. 4.1(C), where the coupling between the black hole system and the radiation system is strictly at the boundary of the gravitational system.

---

[5]It is interesting that BCFTs can provide a microscopic realization of Randall-Sundrum models; this idea manifested itself in a different way in the recent work [1, 139].
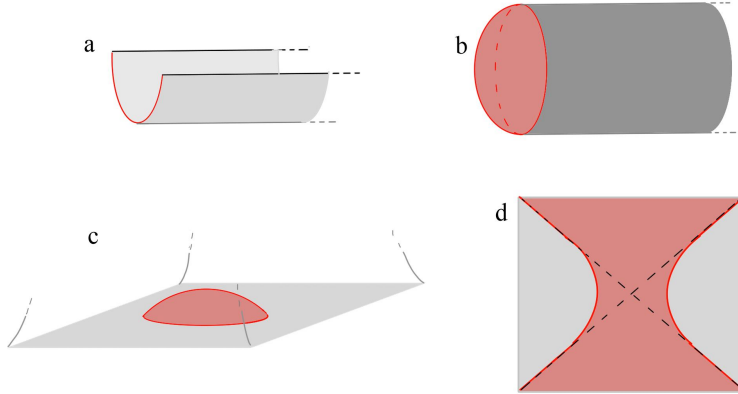
Figure 4.3: (a) BCFT path integral defining the thermofield double state of two 1+1 dimensional BCFTs. (b) Euclidean geometry dual to the BCFT thermofield double. The red surface is an ETW brane. (c) The same geometry represented as part of Euclidean Poincaré-AdS. (d) Lorentzian geometry of the original state, viewed along the z axis, coordinates (x, t). Dashed lines represent horizons on the ETW brane, corresponding to the horizons of the two-sided black hole represented by the boundary system.

4.2   Radiation without evaporation

In this section, we will consider a very simple system that already exhibits all of the key features of the entanglement dynamics described in [75, 76, 6]. The system we consider is not an evaporating black hole, but one where the auxiliary radiation system has the same initial temperature as the black hole, so that the two systems are in equilibrium. The system we look at has a static energy density (in a particular conformal frame), but the entanglement entropy for various subsystems still evolves with time and the entanglement wedge exhibits a phase transition similar to the ones discussed in [75, 76, 6].

4.2.1   Building the model

Specifically, we consider a 1+1 dimensional BCFT which is in the thermofield double state with a second copy of this system. This can be constructed via a path integral on a quarter-cylinder $y \leq 0$, $0 \leq \theta \leq \pi$, where θ is the Euclidean time direction, and the boundary of each CFT is at $y = 0$. This is shown in Fig. 4.3(a).

To understand the gravity dual, we use the bottom-up prescription where the boundary system leads to a bulk ETW brane. For 1+1 dimensional CFTs, it is convenient to define

$$c_{\text{bdy}} = 6g, \tag{4.13}$$

where g is the usual boundary entropy. Then, defining

$$F = \frac{c_{\text{bdy}}}{c_{\text{bulk}}} , \tag{4.14}$$

the tension parameter T (defined explicitly in [1]) for the ETW brane is related to F and to the angle Θ in Fig. 4.2 by

$$T = \tanh F = \sin \Theta . \tag{4.15}$$

The dual Euclidean solution corresponding to our state is a portion of Euclidean AdS, which we may describe using metric (setting $L_{\text{AdS}} = 1$)

$$ds^2 = (\rho^2 + 1)dy^2 + \frac{d\rho^2}{\rho^2 + 1} + \rho^2 d\phi^2 . \tag{4.16}$$

The specific solution we need was already constructed in [58, 1]. The bulk Euclidean solution terminates on an ETW brane with locus

$$y(\rho) = -\text{arcsinh} \left(\frac{\tan \Theta}{\sqrt{\rho^2 + 1}} \right) , \tag{4.17}$$

where Θ is related to the brane tension and the number of boundary degrees of freedom by (4.15). The Euclidean geometry is depicted in Fig. 4.3(b). The Lorentzian geometry dual to our state is obtained by taking the geometry of the $\phi = 0, \pi$ slice of the Euclidean solution as our initial data.

To analyze the extremal surfaces in the Lorentzian version of this geometry, it will be convenient to change coordinates to Poincaré coordinates, via the transformations

$$y = \ln(r), \qquad \rho = \tan(\theta), \tag{4.18}$$

151

which bring us to spherical Poincaré coordinates. We then perform the substitutions

$$z = r \cos \theta, \qquad x = r \sin \theta \cos \phi, \qquad \tau = r \sin \theta \sin \phi \tag{4.19}$$

which bring us to the usual Cartesian Poincaré coordinates in which the metric is

$$ds^2 = \frac{1}{z^2}(dz^2 + dx^2 + d\tau^2) . \tag{4.20}$$

In these coordinates, the CFT boundary is at $x^2 + \tau^2 = 1$, while the ETW brane is the surface

$$x^2 + \tau^2 + (z + \tan \Theta)^2 = \sec^2 \Theta , \tag{4.21}$$

as shown in Fig. 4.3(c).

We obtain the Lorentzian solution by analytic continuation $\tau \to it$. This gives

$$ds^2 = \frac{1}{z^2}(dz^2 + dx^2 - dt^2) , \tag{4.22}$$

the CFT boundary at $x^2 - t^2 = 1$, and the ETW brane at

$$x^2 - t^2 + (z + \tan \Theta)^2 = \sec^2 \Theta . \tag{4.23}$$

This is shown in Fig. 4.3(d). This completes the explicit construction of the solution, but the connection to black holes and causal structure remains to be seen.

Consider the ETW brane in the Lorentzian picture, where it is described as the surface (4.23) in the metric (4.22). We would like to find the future horizon for this surface, i.e. the boundary of the set of points from which it is possible to reach the right ETW brane boundary on a lightlike curve. The lightlike curves on the ETW brane satisfy

$$x(t)^2 - t^2 + (z(t) + \tan \Theta)^2 = \sec^2 \Theta \tag{4.24}$$

and

$$\left(\frac{dx}{dt}\right)^2 + \left(\frac{dz}{dt}\right)^2 = 1 . \tag{4.25}$$

We find that they are given by

$$x(t) = vt \pm \frac{\sqrt{1 - v^2}}{\cos \Theta}, \qquad z(t) = |\sqrt{1 - v^2}t \pm v \sec \Theta| - \tan \Theta \qquad (4.26)$$

for $|v| < 1$.

The right and left boundaries of the ETW brane are described by $x = \pm\sqrt{t^2 + 1}$. The future horizons are the lightlike curves that asymptotes to this for $t \to \infty$. These are the trajectories

$$x = \pm t, \qquad z = \frac{1 - \sin \Theta}{\cos \Theta} \, . \qquad (4.27)$$

Thus, independent of Θ, we have horizons on the ETW brane located at $x = \pm t$ and these lie at constant z. The black hole interior can be identified with the region $|x| < t$ or alternatively $z > (1 - \sin \Theta)/\cos \Theta$.

4.2.2 Holographic entanglement entropy

We would now like to investigate the HRT surfaces which calculate the entanglement entropy associated with the spacetime region spacelike separated from the interval $[-x_0, x_0]$ at $t = t_0$ (equivalently, the union of intervals $[\pm x_0, \pm\infty)$ at $t = t_0$). In general, there are two possibilities for this HRT surface. First, we have the connected surfaces described by the semicircle

$$t = t_0, \qquad z^2 + x^2 = x_0^2 \, . \qquad (4.28)$$

We can also have disconnected surfaces that end on the ETW brane. We need to compare the areas to find out which one is the minimal area extremal surface that computes the entanglement entropy.

Extremal surfaces

It will be somewhat simpler to perform our calculations in the Euclidean picture and then analytically continue the results to the Lorentzian case. That is, we will look at geodesics in the Euclidean geometry, evaluate their length and the length difference between the

153
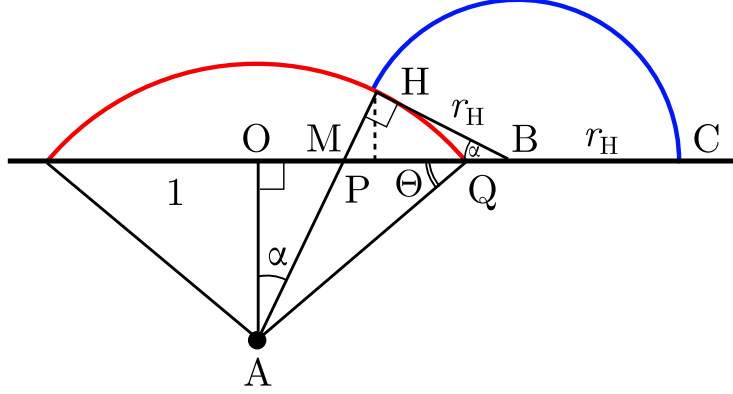
Figure 4.4: Geometry of the ETW brane and half of the disconnected RT surface in the plane of the RT surface.

two cases, and find the phase boundary for transitions between the two surfaces. The Lorentzian version of all of these quantities can be obtained by analytic continuation.

To find the areas, we note that the area of a geodesic semicircle of coordinate radius R from the point $z = R$ of maximum z to some $z_{\min}$ is

$$
\begin{aligned}
A(R, z_{\min}) &= \operatorname{arccoth}\left(\frac{1}{\sqrt{1 - z_{\min}^2/R^2}}\right) \\
&= \frac{1}{2}\ln\left(\frac{1 + \sqrt{1 - z_{\min}^2/R^2}}{1 - \sqrt{1 - z_{\min}^2/R^2}}\right).
\end{aligned}
\tag{4.29}
$$

For $z_{\min} = \epsilon$ with infinitesimal ϵ, this reduces to $\ln(2R/\epsilon)$. From this, the area of the connected extremal surface is

$$
A_c = 2\ln\left(\frac{2x_0}{\epsilon}\right).
\tag{4.30}
$$

For the disconnected surface, each part is the arc of a circle which lies at constant θ, intersecting the ETW brane orthogonally and intersecting one of the the points $(\pm x_0, \tau_0)$.[6] This is shown in Fig. 4.4.

---

[6]In the Lorentzian picture, the disconnected RT surfaces lie at constant x/t and are related by a boost to the circle arc from the point $(x = \sqrt{x_0^2 - t_0^2}, t = 0)$ to the ETW brane.

We can use basic geometry to determine the coordinate radius of the extremal surface. Referring to Fig. 4.4, we have $OQ = 1$ and $OA = \tan\Theta$. Thus, $AQ = AH = \sec\Theta$. Also $HB \perp AH$ so $AH^2 + HB^2 = OA^2 + OB^2$. Thus, we find that the extremal surface has coordinate radius

$$r_H = \frac{r^2 - 1}{2r}. \tag{4.31}$$

Now $OM = OA\tan\alpha = \tan\Theta\tan\alpha$ and $AM = OA\sec\alpha = \tan\Theta\sec\alpha$. So

$$HM = HA - MA = \sec\Theta - \tan\Theta\sec\alpha.$$

Finally, $HM/HB = \tan\alpha$ gives

$$r_H = \sec\Theta\cot\alpha - \tan\Theta\csc\alpha,$$

while $HP = HB\sin\alpha$ gives $z = r_H\sin\alpha$. Combining the foregoing, we learn that extremal surface intersects the ETW brane at z coordinate

$$z_c = \frac{\cos\Theta}{\frac{r^2+1}{r^2-1} + \sin\Theta}, \tag{4.32}$$

where $r^2 = x_0^2 + \tau_0^2$.

Setting $z_{\min} = z_c$ in (4.29), we find that the area of the disconnected surface (including both parts) is

$$A_d = 2\ln\left(\frac{r^2 - 1}{\epsilon} \cdot \frac{1 + \sin\Theta}{\cos\Theta}\right). \tag{4.33}$$

The difference in areas between the two possible extremal surfaces is therefore

$$A_d - A_c = 2\ln\left(\frac{x_0^2 + \tau_0^2 - 1}{2x_0} \cdot \frac{1 + \sin\Theta}{\cos\Theta}\right). \tag{4.34}$$

From this, we see that there will be a transition when

$$\tau_0^2 + \left(x_0 - \frac{1 - \sin\Theta}{\cos\Theta}\right)^2 = \frac{2}{1 + \sin\Theta}. \tag{4.35}$$

155

In the Lorentzian picture, this gives the trajectory of the phase boundary as

$$\left(x_0 - \frac{1 - \sin\Theta}{\cos\Theta}\right)^2 = t^2 + \frac{2}{1 + \sin\Theta} , \qquad (4.36)$$

using $t^2 = -\tau_0^2$.

We can now map back to the original conformal frame (corresponding to Fig. 4.3(a)) where the energy density is time-independent. Using the coordinate transformations

$$x = e^y \cos\phi, \qquad \tau = e^y \sin\phi \qquad (4.37)$$

we have that the phase boundary in Euclidean coordinates is

$$e^F \sinh y = \cos\phi . \qquad (4.38)$$

Here, ϕ is the Euclidean time, so in Lorentzian coordinates (where η is the time coordinate), this phase boundary becomes

$$e^F \sinh y = \cosh\eta . \qquad (4.39)$$

Finally, if we consider an interval $[y_0, \infty)$ (together with the equivalent interval in the other BCFT), we find that the entanglement wedge for this subsystem makes a transition to include geometry behind the black hole horizon when

$$\eta = \operatorname{arccosh}(e^F \sinh y_0) \sim F + y_0, \qquad (4.40)$$

where the last relation holds for large y_0 and F.

Thus, for intervals that include most of the radiation system (when y_0 is some small order 1 number), we see a transition at the Page time after which the black hole interior can be reconstructed from the radiation system. For large y_0 the time is increased by an amount which is the time taken for the radiation to reach y_0. The behavior of the transition time is shown in Fig. 4.5. In this frame, the entanglement entropy is constant after the transition, since each part of the disconnected extremal surface in this case is just a boosted version
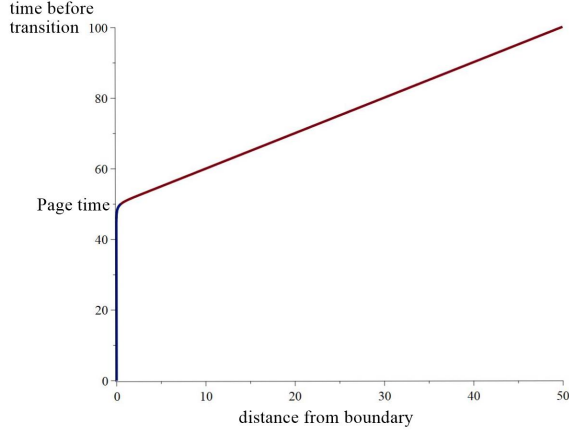
Figure 4.5: Time at which the subsystem of the radiation system greater than some distance from the BCFT boundary exhibits a transition in its entanglement entropy, for the case $c_{\text{bnd}}/c_{\text{bulk}} \sim 50$.

of the extremal surface for earlier times. It follows that the entanglement entropy increases from the initial time and then remains constant after the transition. From the results above, the precise expression for entropy as a function of time is[7]

$$
S = \begin{cases} \frac{c_{\text{bulk}}}{3} \ln\left(\frac{2}{\epsilon}\cosh\eta\right) & \eta < \text{arccosh}(e^F \sinh y) \\ 2g + \frac{c_{\text{bulk}}}{3} \ln\left(\frac{2}{\epsilon}\sinh y_0\right) & \eta > \text{arccosh}(e^F \sinh y), \end{cases} \tag{4.41}
$$

so we have an approximately linear increase before the transition and a constant entropy afterwards.

Let us explore the physics of this phase transition in the behavior of the entanglement. We have that the energy density in both BCFTs is completely time-independent. However, the entanglement entropy for the union of regions $x > x_0$ in the two CFTs increases with time, then undergoes a first order phase transition after which it is constant. The entanglement wedge initially does not include the black hole system, but after the transition

---

[7]Here, we use that the cutoff surface $\rho = 1/\epsilon$ maps to the cutoff surface $z = \epsilon r$ in the Poincaré coordinates. This cutoff surface is also employed in the equations (4.30) and (4.33) to calculate the entanglement entropies in the original y-coordinates.

157

includes a portion of the interior of the black hole. Thus, while everything is static from an energy point of view, the state is evolving in such a way that information about the black hole interior eventually becomes accessible in the auxiliary radiation system.

To understand this better, it is helpful to recall that for a free field theory in the thermofield double state, each mode in one copy of the system is purified by the corresponding mode in the other copy of the system. In our present case, we expect similarly that the boundary system is initially purified to a large extent by the other copy of the boundary system, while the bulk system is purified by the other copy of the bulk system.[8] However, as we evolve forward in time, the entanglement structure evolves, and the information initially contained within the boundary system (describing our black hole initial state) leaks out into the bulk degrees of freedom, eventually leading to the transition we observe.

Let us now compute where the boundary of the entanglement wedge lies on the ETW brane after the transition. Consider a point (x_0, τ_0) on the Euclidean transition surface (4.35). Just after the transition to a disconnected minimal area extremal surface, the part of the surface originating at (x_0, τ_0) will end on the ETW brane at a point $(x_c, \tau_c) = \lambda(x_0, \tau_0)$. From Fig. 4.4 we see that the distance $r_c = \sqrt{x_c^2 + \tau_c^2}$ from the origin for this point will satisfy

$$r = r_c + r_H + \sqrt{r_H^2 - z_c^2} \,. \tag{4.42}$$

This gives

$$r_c = \frac{2r}{r^2(1 + \sin \Theta) + (1 - \sin \Theta)} \,, \tag{4.43}$$

so we have

$$
\begin{aligned}
\lambda &= \frac{r_c}{r} \\
&= \frac{2}{(x_0^2 + \tau_0^2)(1 + \sin \Theta) + (1 - \sin \Theta)} \\
&= \frac{1}{x_0 \cos \Theta + 1},
\end{aligned}
$$

where we have used (4.35) in the last line.

---

[8]Here, we are describing the situation relative to the vacuum case. Of course, there is always an infinite entanglement entropy between the boundary system of one CFT and the bulk of that CFT.

158

Thus, we have

$$x_c = \frac{x_0}{x_0 \cos \Theta + 1}, \qquad \tau_c = \frac{\tau_0}{x_0 \cos \Theta + 1} . \tag{4.44}$$

Inverting these relations and plugging the resulting expressions for x_0 and τ_0 in (4.35), we find that the points (x_c, τ_c) lie on a curve

$$[1 + (1 - \sin \Theta)^2]x_c^2 + 2 \tan \Theta (1 - \sin \Theta)x_c + \tau_c^2 = 1 . \tag{4.45}$$

For the Lorentzian version of the problem, this becomes

$$[1 + (1 - \sin \Theta)^2]x_c^2 + 2 \tan \Theta (1 - \sin \Theta)x_c = t_c^2 + 1 . \tag{4.46}$$

Note that $x_0 > \sqrt{t_0^2 + 1} > t_0$, so from (4.44), we see that we will also have $x_c > t_c$. Thus, while the curve (4.46) crosses the horizon, the part beyond the horizon isn't relevant to us. The extremal surface always ends at a point on the brane that is outside the horizon.

Let's now calculate the proper distance to the horizon from the intersection point (x_c, t_c, z_c) on the ETW brane. The ETW brane lies in the plane containing the origin and the point (x_0, t_0) and extending directly inward in the z direction. In this plane, the geometry is as in Fig. 4.4, where the outermost point is at distance $r = \sqrt{x_0^2 - t_0^2}$. This is the proper distance along the blue curve in Fig. 4.4 from H to the top of the blue arc, which lies at

$$z_{\max} = \sec \Theta - \tan \Theta . \tag{4.47}$$

The distance is

$$d = \int_{z_c}^{z_{\max}} \frac{dz}{z} \sqrt{dz^2 + dr^2}. \tag{4.48}$$

Using

$$r^2 + (z + \tan \theta)^2 = \sec^2 \theta , \tag{4.49}$$

we find that

$$d = \frac{1}{\cos \Theta} \ln \left(\frac{r + 1}{r - 1} \right) . \tag{4.50}$$

159

In the y_0 coordinates and in terms of F, this is

$$d = \cosh(F) \ln \left(\frac{1 + e^{-y_0}}{1 - e^{-y_0}} \right) . \tag{4.51}$$

We see that for large y_0 the location of the HRT surface intersection with the ETW brane after the transition is very close to the horizon.

Finally, we can look at the trajectory of the intersection point as a function of time after the transition. For the interval with left boundary y_0 in the y-coordinates, the initial intersection point is at

$$x_c = \sec \Theta \left(1 + \frac{2}{(1 + \sin \Theta)(e^{2y_0} - 1)} \right)^{-1} \tag{4.52}$$

on the curve (4.46), while the later trajectory follows the curve

$$x_c^2 - t_c^2 = e^{2y_0} (1 - x_c \cos \Theta)^2 . \tag{4.53}$$

At late times, independent of y_0, this approaches the point

$$x = t = \sec \Theta = \cosh(F) \tag{4.54}$$

on the horizon.

The outgoing lightlike curve along the ETW brane from this point is $x = t$, while the ingoing lightlike curve along the ETW brane from this point is simply $x = \sec \Theta$ for all t, using the result (4.26). We note that the corresponding lightlike curve $x = -\sec \Theta$ on the other side of the black hole does not intersect this curve, but the ingoing lightlike curve from any closer point does intersect this curve. Thus, the points $t = \pm x = \sec \Theta$ are a distinguished pair of points on the horizon for which the ingoing lightlike curves barely meet at the future singularity. The late-time intersection between the entanglement wedge for the radiation system and the black hole geometry is shown in Fig. 4.6.
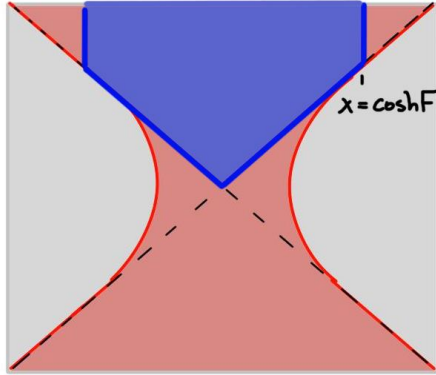
Figure 4.6: The blue shaded region is the portion of the black hole interior that is included in the late-time entanglement wedge of any subsystem $|x| > a$ for any a, of the radiation system (for Poincaré coordinates).

4.2.3 Entanglement entropy from the CFT

The calculations of the previous section relied on holographic calculations of the entanglement entropy in a bottom-up holographic model where the number of boundary degrees of freedom on our BCFT is related to the tension of an ETW brane. While bottom-up models in AdS/CFT are widely studied and known to produce qualitative results that agree with those in systems that can be studied using a top-down approach, the bottom-up approach for BCFTs is less well studied, and one might thus worry whether our holographic results correctly capture the physics of genuine holographic CFTs. We will alleviate these concerns by reproducing our results for the entanglement entropies using the CFT methods of Chapter 3.

Recall that entanglement entropy can be calculated from Rényi entropies using the replica trick:

$$S_A = \lim_{n \to 1} S_A^{(n)} = \lim_{n \to 1} \frac{1}{1-n} \ln \mathrm{Tr}[\rho_A^n].$$

The operator ρ_A^n can be related to the partition function of the n-fold branched cover, or *replica manifold*, of the original geometry. This, in turn, can be calculated for 2D CFTs by introducing certain *twist operators* Φ_n at the entangling points of A [61]. The partition

function is given by a correlator of these twists. For $A = [z_1, z_2]$ for instance, we have

$$\text{Tr}[\rho_A^n] = \langle \Phi_n(z_1) \Phi_{-n}(z_2) \rangle.$$

In holographic theories, these correlation functions are dominated by the identity block in some channel. A change in dominance will lead to a phase transition in entanglement entropy. In an ordinary two-dimensional holographic CFT, this exchange causes a sudden shift from the disconnected to the connected entanglement wedge for two disjoint intervals. In a holographic BCFT, this exchange can occur for a *two-point* correlator of twists, corresponding to the entanglement entropy of a single interval. This is analogous to the four-point result in a CFT since the two-point function in a BCFT has the same symmetries as the four-point function, and can be evaluated using the method of images.

Consider a BCFT with boundary condition b on the upper half-plane (UHP), $\{\text{Im}\,(z) \geq 0\}$. We can perform a global transformation to the complement of the disk of radius R via

$$w = R \left(\frac{1}{z - i/2} - i \right). \tag{4.55}$$

For simplicity, we also define $\vartheta := w + iR$. We then have

$$z = \frac{R}{\vartheta} + \frac{i}{2}, \quad \text{Im}\,[z(w)] = \frac{|w|^2 - R^2}{2|\vartheta|^2}, \quad w'(z) = -\frac{1}{R}\vartheta^2. \tag{4.56}$$

Since we have performed a global transformation, the energy density vanishes:

$$\langle T(w) \rangle = \frac{c}{12}\{z; w\} = \frac{c}{12}\frac{z'''z' - (3/2)(z'')^2}{(z')^2} = 0. \tag{4.57}$$

Consider a two-point function of twist operators, $\Phi_n(w_1)$, $\Phi_{-n}(w_2)$, introducing an n-fold branched cover with branch cut from w_1 to w_2. The twists are primary by definition,

so the correlation function transforms as

$$\langle \Phi_n(w_1)\Phi_{-n}(w_2)\rangle_{\overline{\text{disk}}} = |w'(z_1)w'(z_1)|^{-d_n}\langle \Phi_n(z_1)\Phi_{-n}(z_2)\rangle_{\text{UHP}}$$

$$= \left|\frac{(\vartheta_1\vartheta_2)^2}{R^2}\right|^{-d_n}\langle \Phi_n(z(w_1))\Phi_{-n}(z(w_2))\rangle_{\text{UHP}}. \qquad (4.58)$$

For holographic BCFTs, the correlator of twists on the UHP can be evaluated using vacuum block dominance and an appropriate sparsity condition on the density of states, in a similar vein to [65]. Using this correlator and the replica trick, the entanglement entropy of the interval $A = (-\infty, w_1] \cup [w_2, \infty)$ is calculated by

$$S_A = \lim_{n\to 1}\frac{1}{1-n}\ln\langle \Phi_n(w_1)\Phi_{-n}(w_2)\rangle_{\overline{\text{disk}}}$$

$$= \frac{c}{6}\left[2\ln\left|\frac{\vartheta_1\vartheta_2}{R}\right| + \min\left\{\frac{12}{c}g + \ln\left|\frac{(|w_1|^2 - R^2)(|w_2|^2 - R^2)}{(\vartheta_1\vartheta_2\epsilon)^2}\right|, \ln\left|\frac{Rw_{12}}{\vartheta_1\vartheta_2\epsilon}\right|^2\right\}\right]$$

$$(4.59)$$

where $g := -\ln\langle 0|b\rangle$ is the boundary entropy, and F is given by (4.14). We note the relations

$$e^F = \frac{1+T}{\sqrt{1-T^2}} = \frac{1+\sin\Theta}{\cos\Theta}, \quad 1 - e^{-2F} = \frac{2\sin\Theta}{1+\sin\Theta}, \qquad (4.60)$$

which we will use momentarily. The UV regulator ϵ is chosen in the physical conformal frame, namely the complement of the disk.

We now specialize to the symmetric interval A at some fixed time $\text{Im}(w) = \tau_0$, with $w_{1,2} = \pm x_0 + i\tau_0$. Exponentiating (4.59), a phase transition occurs at

$$\left(x_0^2 - e^{-F}R\right)^2 + \tau_0^2 = R^2(1 - e^{-2F}) \qquad (4.61)$$

$$\implies \quad \left(x_0^2 - \frac{\cos\Theta}{1+\sin\Theta}R\right)^2 + \tau_0^2 = \frac{2R\sin\Theta}{1+\sin\Theta}, \qquad (4.62)$$

using (4.60). In Lorentzian signature, $\tau_0^2 \to -t_0^2$, and we obtain

$$\left(x_0^2 - \frac{\cos\Theta}{1+\sin\Theta}R\right)^2 = t_0^2 + \frac{2R\sin\Theta}{1+\sin\Theta}. \qquad (4.63)$$

163
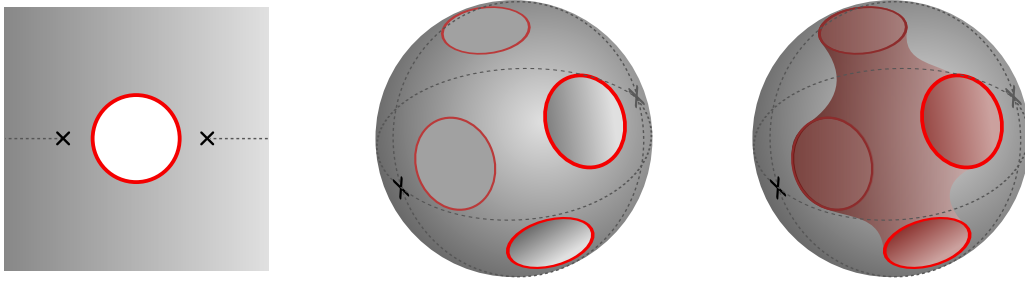
Figure 4.7: Replica calculation of entanglement entropy.

These phase boundaries precisely match (4.35) and (4.36) for $R = 1$.

4.2.4 Holographic replica calculation

It is interesting to ask if the replicas used in the previous section have a natural gravitational avatar. According to [140, 141], the entanglement wedge phase transition is dual to the dominance of new saddles in the gravitational path integral for the bulk dual of the replica geometries used to calculate entanglement entropy. We will make some brief qualitative remarks on how this insight plays out in the current setting.

In calculating the entanglement entropy, we evaluated the Rényi entropies by calculating the BCFT partition function on a replica manifold obtained by gluing n copies of the Euclidean space, shown in Fig. 4.7, across the cut. The topology of the replica manifold is a sphere with n boundaries, as shown in the second figure. Considering a larger and smaller portion of the radiation system corresponds to enlarging or shrinking the size of the boundaries relative to the size of the sphere.

Now we can consider performing this path-integral calculation holographically, using the bottom-up approach where the boundaries extend into the bulk as ETW branes. In the case of a smaller portion of the radiation system, the holes in the second picture will be small, and we will have a set of disconnected ETW branes of disk topology that "cap off" the boundary holes. On the other hand, as we consider a larger portion of the radiation system, the circles become large in the second picture, and we expect that the dominant saddle in the gravitational calculation will correspond to the topology shown in the pic-

ture on the right where we have a single connected ETW brane with multiple boundary components.

It seems plausible that the transition to this new bulk topology is directly related to the transition of HRT surfaces in our original calculation, since the two calculations must agree. However, it is also confusing: the CFT calculation correctly reproduces the disconnected bulk HRT surface from the disconnected contribution to the twist correlation function alone, while this bulk saddle is a complicated connected geometry involving both twist operators. However, the same issue crops up when calculating the entanglement entropy of two (or multiple) intervals in the vacuum of a 2d CFT [65], or a 2d BCFT as discussed in Chapter 3. The higher Rényi entropies are also computed by a connected bulk geometry [142], but the entanglement entropy is a sum of disconnected contributions. This is consistent because the semi-classical Virasoro block describing the connected geometry reduces to the identity exchange in the limit $n \to 1$.

Thus, taking into account the second HRT surface that correctly sees the decreasing branch of entanglement entropy corresponds in the gravity version of the replica calculation to including non-trivial topologies. Had we stuck with the original topology (as we would do if treating gravity perturbatively) it seems that we would get an answer which misses the transition, and is perhaps more akin to Hawking's original calculation, as suggested in [140, 141].

4.3 2D evaporating and single sided examples

In this section, we continue focusing on two-dimensional models, but generalize the simple example of the previous section to a case where we have a pure state of a single-sided black hole, and to cases with a dynamical energy density (as in the example of [6]) that more closely models the physics of a genuine evaporating black hole.[9]

---

[9]Of course, there are many examples that we can obtain from the previous case via local conformal transformations which would have non-trivial evolution of the energy density and may look more like an evaporating black hole. However, in this section, we focus on examples that are not conformally related to the one in the previous section.
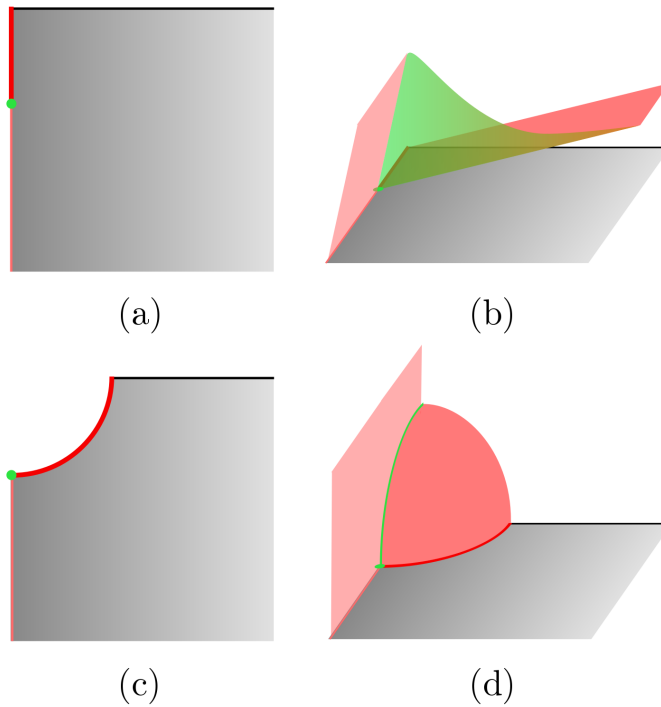
Figure 4.8: BCFT models for single-sided black holes.

4.3.1 Single-sided case

It is straightforward to come up with BCFT examples of single-sided black holes. For example, Fig. 4.8(a) shows a path-integral defining the state of a BCFT with some boundary system (fat red line) with many degrees of freedom. Here, instead of evolving the full BCFT from $\tau = -\infty$ to define the vacuum state of this system, we only evolve the boundary system from some finite past Euclidean time, as for the SYK states in [85]. For prior Euclidean times, we have a different boundary condition (thin red line) that we take to be associated with a small number of boundary degrees of freedom. At the transition between these two boundaries we have an appropriate boundary condition changing operator.

This construction should place the boundary system in a high-energy state, while the bulk CFT degrees of freedom should be in a lower-energy state (through they are also affected by the change of boundary conditions in the Euclidean past). In this case, the

166

dual gravity solution will involve ETW branes with different tensions, and some junction between branes dual to the boundary-condition changing operator. This may simply be a codimension-two surface, or something smoother, as depicted in Fig. 4.8(b).

It would be interesting to analyze this example in detail. For now, we point out that we can understand the physics of a similar example using the results of the previous section. Fig. 4.8(c) shows almost the same setup, but with a different geometry for the path-integral. This picture is similar to a $\mathbb{Z}_2$ identification of our setup from the previous section. If we choose the lower boundary condition to correspond to a $T = 0$ ETW brane in the bulk and we choose the boundary-condition changing operator appropriately (so that the equation of motion at the codimension-two brane gives a constraint that the two-types of ETW branes should meet orthogonally), then the dual geometry for this setup will be precisely a $\mathbb{Z}_2$ identification of the bulk geometries from the previous section, with a zero-tension ETW brane at the $\mathbb{Z}_2$ fixed point, as shown in Fig. 4.8(d). In this case, all of our calculations and qualitative conclusions go through almost unchanged. The only significant difference is that the connected RT surface from the previous section is now replaced by its $\mathbb{Z}_2$ identification, which ends on the $T = 0$ brane.

4.3.2 Dynamical case

We can also modify our two-sided example in order to introduce time evolution of the energy density more characteristic of an evaporating black hole. We would like to have a situation where our auxiliary system starts out in a state that is closer to the vacuum state, so that the energy in the initial black hole state will radiate into this system.

A simple construction (similar to that discussed in [6]) is shown in Fig. 4.9. The left picture shows a state of four quantum systems. The outer systems are BCFTs with some boundary condition (denoted by a dark red boundary) that we imagine has a small boundary entropy. The path integrals shown place these systems into their vacuum state. The remaining part of the path integral constructs a thermofield double state of two systems, each of which is a BCFT living on a small interval with different boundary conditions on the two ends. The dark red boundary condition is the same as before, but the semicircular boundary (shown bright red) corresponds to a boundary system with many degrees of
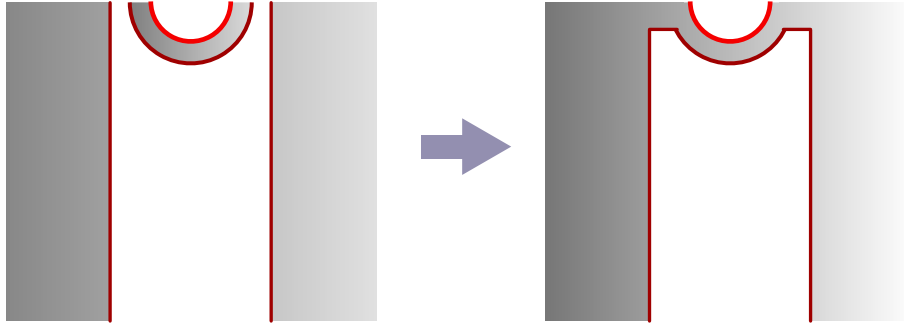
Figure 4.9: 2D model for an evaporating black hole.

freedom as in the example of the previous section.

In order to make the two-sided black hole evaporate, we consider a modified system where we glue the systems together as shown on the right side of Fig. (4.9). In the final path integral, shown on the right, we are describing a state of the same system that we considered in the earlier part of this section. However, since our Euclidean path integral is in some sense a small modification of the picture on the left, we expect that far away from the black hole, the local physics of the reservoir system will be similar to the vacuum. In this case, the energy in the (bright red) boundary degrees of freedom will gradually leak out into the reservoir system. The dual gravitational picture will be that of an evaporating black hole.

In studying the dual system explicitly using the bottom-up approach, we will now have two types of branes, one with a larger tension corresponding to the bright red boundary condition, and one with a smaller tension corresponding to the dark red boundary condition. The latter is what [6] refer to as the Cardy brane. We expect that the behaviour of this system should match the qualitative picture described in [6], but now it should be possible to study everything quantitatively. Since the branes only couple to the metric and we are in three dimensions, the local geometry of the holographic dual will be that of AdS, and the dynamics of the system will be reflected in the trajectories of the ETW branes.

Phase Boundaries on the Annulus

In order to study situations like the previous section, we can apply the methods of [143, 144] who were making use of a similar Euclidean setup (without the middle boundary) to study local quenches in a holographic CFT. For any specific shape of the boundaries in (4.9), it is possible to map the doubled picture describing the full CFT path integral conformally to an annulus, where the circular boundary maps to the inner edge of the annulus and the other boundaries (shown in dark red) together map to the outer boundary of the annulus. We can also map the annulus to a finite cylinder, so we see that the physics will be related to the physics of the thermofield double state of a pair of CFTs on a finite interval with different boundary conditions on the two ends.

We can again start with the global AdS metric (4.16) in which we know the ETW trajectories explicitly. Here, though, we consider a finite segment of the boundary cylinder, with a boundary condition corresponding to tension T at $y = -L$ and a boundary condition corresponding to tension $T = 0$ (or some other tension) at $y = 0$. Changing to Poincaré coordinates as in §4.2, the CFT region becomes an annulus with inner radius $R = e^{-L}$ and outer radius 1, centred at the origin. Also as in that section, the location of the ETW brane corresponding to the inner boundary is

$$x^2 + \tau^2 + (z + R \tan \Theta)^2 = R^2 \sec^2 \Theta \, , \qquad \Theta = \arcsin(T) \, , \qquad (4.64)$$

while that corresponding to the outer boundary is

$$x^2 + \tau^2 + z^2 = 1 \, . \qquad (4.65)$$

For sufficiently large L, the two BCFT boundaries are far apart and the phase boundaries for the transition between connected and disconnected HRT surfaces are those found previously for the case of a single boundary; the phase boundary for the transition between a connected surface and a disconnected surface ending on the inner ETW brane has locus

$$\left[x - \frac{R(1 - \sin \Theta)}{\cos \Theta} \right]^2 + \tau^2 = \frac{2R^2}{1 + \sin \Theta} \, , \qquad (4.66)$$

while that for the outer ETW brane is

$$(x+1)^2 + \tau^2 = 2 \,. \tag{4.67}$$

Note these are the phase boundaries in the region $x > 0$; the $x < 0$ phase boundaries are given by symmetry about $\tau = 0$.

As L is decreased to some critical value

$$L_{\text{c}} \equiv -\ln\left[\frac{(-1+\sqrt{2})\cos\Theta}{(1-\sin\Theta) + \sqrt{2(1-\sin\Theta)}}\right] \,, \tag{4.68}$$

the phase boundaries will osculate within the annulus at $\tau = 0$. For smaller L, a direct transition between disconnected HRT surfaces ending on the higher tension brane and surfaces ending on the lower tension brane can occur. The phase boundary between these disconnected phases is given by

$$x^2 + \tau^2 = R\left[\frac{(1-\sin\Theta) + R\cos\Theta}{R(1-\sin\Theta) + \cos\Theta}\right] = \ell^2 \,, \tag{4.69}$$

where we have defined ℓ for later convenience. This is pictured in Fig. 4.10.

We can now map to a new conformal frame with the desired dynamical Cardy brane. The phase boundaries should simply be pushed forward using the appropriate conformal transformation, then analytically continued to Lorentzian signature. Following [143], if we start from Poincaré coordinates

$$\mathrm{d}s^2 = \frac{\mathrm{d}\eta^2 + \mathrm{d}\zeta\mathrm{d}\bar{\zeta}}{\eta^2}, \tag{4.70}$$

a map $\zeta = f(w)$ corresponds to a coordinate transformation

$$
\begin{aligned}
\zeta &= f(w) - \frac{2z^2(f')^2(\bar{f}'')}{4|f'|^2 + z^2|f''|^2} \\
\eta &= \frac{4z|f'|^3}{4|f'|^2 + z^2|f''|^2}
\end{aligned}
$$
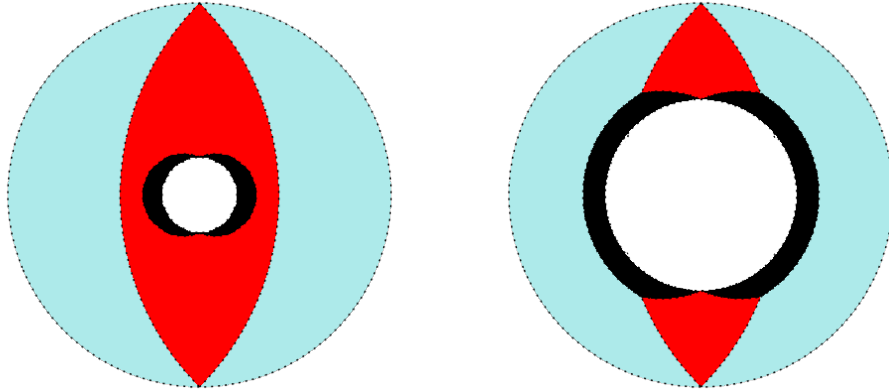
Figure 4.10: Phase diagram for annulus with supercritical L (left) and subcritical L (right). The point (x, y) belongs to one of three regions, depending on whether the RT surface anchored at points $\{(x, y), (-x, y)\}$ is connected (red), disconnected and ending on the inner ETW brane (black), or disconnected and ending on the outer ETW brane (light blue).

in the dual asymptotically AdS geometry. The new metric is

$$\mathrm{d}s^2 = \frac{1}{z^2} \left(\mathrm{d}z^2 + \mathrm{d}w\mathrm{d}\bar{w} + z^2(T(w)\mathrm{d}w^2 + \bar{T}(\bar{w})\mathrm{d}\bar{w}^2) + z^4 T(w)\bar{T}(\bar{w})\mathrm{d}w\mathrm{d}\bar{w} \right) , \quad (4.71)$$

where the holographic stress tensors (corresponding to the stress tensors in the CFT state) are given by

$$T(w) = \frac{3(f'')^2 - 2f'f'''}{4(f')^2}, \qquad \bar{T}(\bar{w}) = \frac{3(\bar{f}'')^2 - 2\bar{f}'\bar{f}'''}{4(\bar{f}')^2} . \qquad (4.72)$$

Conformal mapping

As a specific example, we can take the "single joining quench" geometry of [143] and add to it another boundary centered at the origin. This second boundary is taken to be the image of the inner boundary of the annulus under the conformal transformation

$$w(\zeta) = \frac{2\zeta}{1 - \zeta^2} , \qquad (4.73)$$

171
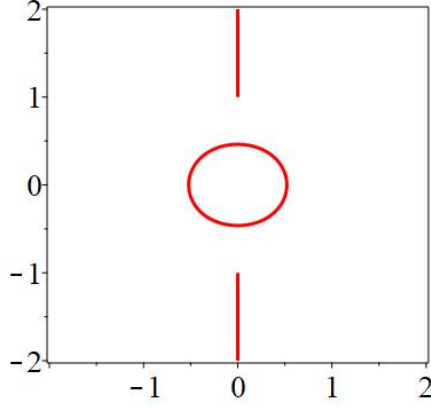
Figure 4.11: Example path-integral geometry generating a BCFT state corresponding to a two-sided black hole system with dynamical energy density.

which takes us from the unit disk (with complex coordinate $\zeta = x + i\tau$) to the single joining quench geometry (with coordinate $w = \hat{x} + i\hat{\tau}$). An example of the resulting path-integral geometry is shown in Fig. 4.11.

We note a few important features of such a map. Firstly, the symmetry $x \to -x$ translates to a symmetry $\hat{x} \to -\hat{x}$, and likewise symmetry $\tau \to -\tau$ translates to symmetry $\hat{\tau} \to -\hat{\tau}$. Secondly, the outer annular boundary $|\zeta| = 1$ maps to the intersection of the slits $i[1, \infty)$ and $-i[1, \infty)$, while the inner boundary maps to

$$\hat{x}^2 + \hat{\tau}^2 = \frac{1}{2\cosh^2(L)} \left[1 + \sqrt{1 + \frac{4\hat{x}^2}{\tanh^2(L)}} \right] . \tag{4.74}$$

Finally, we note that the energy density with respect to Euclidean time $\hat{\tau}$ is defined by

$$T(w) + \bar{T}(\bar{w}) = \frac{3}{4(1+w^2)^2} + \frac{3}{4(1+\bar{w}^2)^2} = \frac{3}{2} \left[\frac{\hat{\tau}^4 - 2(3\hat{x}^2 + 1)\hat{\tau}^2 + (\hat{x}^2 + 1)^2}{((1 + \hat{x}^2 - \hat{\tau}^2)^2 + 4\hat{x}^2\hat{\tau}^2)^2} \right] . \tag{4.75}$$

The Lorentzian analogue decays as we move away from the boundary which represents the black hole.

In the new coordinates, the phase boundary between connected HRT surfaces and dis-

connected surfaces ending on the outer ETW brane is $\hat{x}^2 + \hat{\tau}^2 = 1$, while the phase boundary between connected surfaces and disconnected surfaces ending on the inner ETW brane is

$$\left(\alpha(\hat{x}^2 + \hat{\tau}^2) - \beta\hat{x} - \sin\Theta \right)^2 = (\hat{x}^2 + \hat{\tau}^2 + 1)^2 - 4\hat{\tau}^2 \,, \tag{4.76}$$

with

$$\begin{aligned} \alpha &= \frac{(1 + R^2)^2(1 + \sin\Theta) - 4R^2}{4R^2} = \cosh^2(L)(1 + \sin\Theta) - 1 \\ \beta &= \frac{(1 + R^2)}{R}\cos\Theta = 2\cosh(L)\cos\Theta \,. \end{aligned} \tag{4.77}$$

If a transition between the two disconnected phases is present, the phase boundary has locus

$$\hat{x}^2 + \hat{\tau}^2 = \frac{2\ell^2}{(1 + \ell^2)^2}\left[1 + \sqrt{1 + \frac{4\hat{x}^2(1 + \ell^2)^2}{(1 - \ell^2)^2}} \right], \tag{4.78}$$

where we recall ℓ from (4.69). This transition is pictured in Fig. 4.12.

We can analytically continue $\hat{t} = -i\hat{\tau}$ to determine the BCFT boundaries and phase boundaries in Lorentzian signature. For $L > L_c$, the phase boundaries now meet at the point

$$\hat{x}_0 = \frac{\alpha - \sin\Theta}{2 + \beta} \,, \qquad \hat{t}_0 = \sqrt{\hat{x}_0^2 - 1} \,. \tag{4.79}$$

For $|\hat{t}| < \hat{t}_0$ we have three distinct phases, while for $|\hat{t}| > \hat{t}_0$ we just have the two disconnected phases. For $L < L_c$, we just have the two disconnected phases. The various phase configurations are shown in Fig. 4.13.

One can now determine the time-dependence of the entanglement entropy along any desired trajectory. Recall from previous sections that, on the annulus, the HRT surfaces for symmetrically situated intervals (with inner endpoints $(\pm x, \tau)$) are circular arcs. The
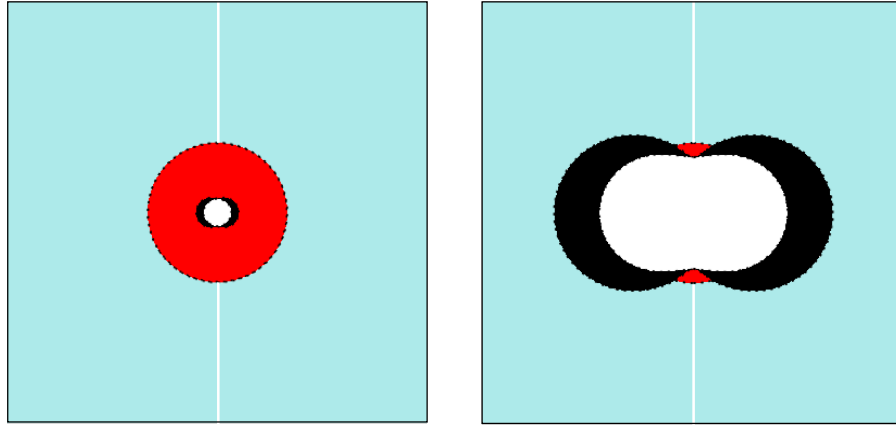
Figure 4.12: Phase diagram for Euclidean modified (two boundary) single joining quench geometry with supercritical L (left) and subcritical L (right). As before, the point (x, y) belongs to one of three regions, depending on whether the RT surface anchored at points $\{(x, y), (-x, y)\}$ is connected (red), disconnected and ending on the inner ETW brane (black), or disconnected and ending on the outer ETW brane (light blue).
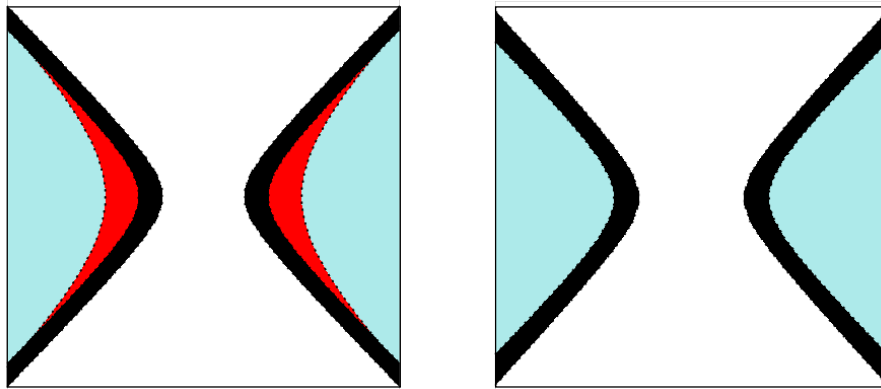
Figure 4.13: Phase diagram for Lorentzian modified (two boundary) single joining quench geometry with supercritical L (left) and subcritical L (right). We have simply analytically continued the phase boundaries from the Euclidean case.

corresponding entanglement entropy is given by

$$S(x,\tau) = \begin{cases} \ln\left[\frac{2x}{\tilde{\epsilon}(x,\tau)}\right], & \text{connected} \\ \ln\left[\frac{(x^2+\tau^2-R^2)(1+\sin\Theta)}{\tilde{\epsilon}(x,\tau)R\cos\Theta}\right], & \text{disconnected } T > 0 \\ \ln\left[\frac{1-x^2-\tau^2}{\tilde{\epsilon}(x,\tau)}\right], & \text{disconnected } T = 0. \end{cases} \tag{4.80}$$

Here, we have recalled [144] that the UV regulator ϵ in the physical setup requires a position dependent regulator $\tilde{\epsilon}(x,\tau) = |\zeta'(w)|\epsilon$ in the annular setup. It is a simple matter to apply the appropriate conformal transformation and Wick rotate to Lorentzian signature, whence we recover the expression for the entanglement entropy of symmetrically situated intervals in the Lorentzian modified local quench geometry.

4.4   Discussion

In this section, we present a few additional observations and some directions for future work.

4.4.1   Connection to boundary microstates

The transitions in entanglement entropy observed in this chapter are directly related to the transitions in entanglement entropy discussed in Chapter 2. There, we considered black hole microstates for a holographic CFT on $\mathbb{S}^d$ defined via a Euclidean path-integral on a finite cylinder, with a boundary at time τ_0 in the Euclidean past. This corresponds to the evolution of a boundary state $|B\rangle$ by Euclidean time τ_0. In the 2D CFT case for small enough τ_0, this state corresponds to a single-sided black hole at temperature $4/\tau_0$, with a time-dependent ETW brane behind the horizon providing an inner boundary for the black hole.

For these states, the entanglement entropy for an interval can exhibit a phase transition as the interval size is increased, such that after the transition, the entanglement wedge of the interval includes a region behind the black hole horizon (terminating on the ETW
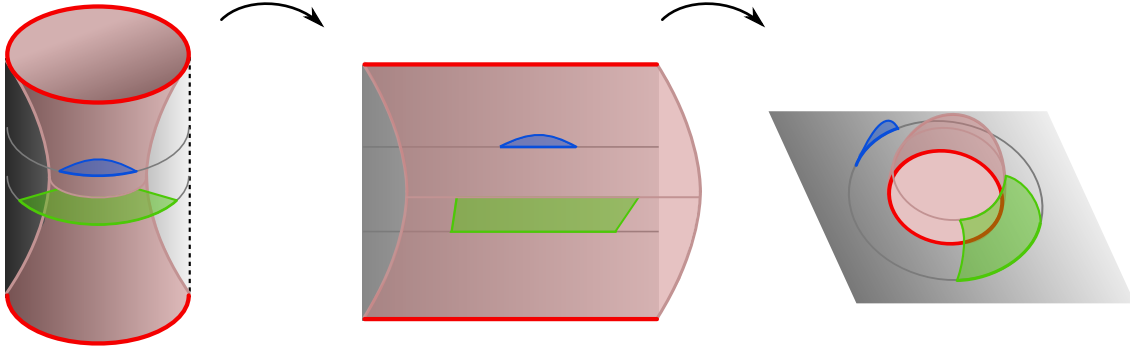
Figure 4.14: BTZ black hole microstates have the same brane profile and hence entanglement entropy as the planar black hole dual to a global quench. The quench geometry is obtained from a local conformal transformation of the excised disk, so the transition in entanglement entropy for the static case described above, and the BTZ microstates in Chapter 2, are controlled by the same CFT correlator.

brane). This is somewhat reminiscent of the entanglement wedge transition discussed in this chapter. However, the connection can be made precise.

If we unwrap the circle on which the CFT lives, we obtain a planar black hole dual (above the Hawking-Page transition [145]) to the global quench geometry [63]. The holographic results for entanglement entropy in this situation are the same as in the compact case, since the gravity dual for the compact case is just a periodic identification of the gravity dual for the non-compact case. The CFT calculation of entanglement entropy in the non-compact case is carried out via a correlation function of twist operators on an infinite strip. But a local conformal transformation maps this calculation to exactly the CFT calculation in §4.2.3 used to deduce the phase transition in this chapter.

We visual this connection in Fig. 4.14. In the single-sided microstates, there is a transition in the extremal surfaces as the boundary region is increased (blue and green regions in Fig. 4.14). In the CFT, this can be calculated by a correlator of twists in the large-c limit and simple spectral constraints, as described in Chapter 3.

4.4.2   Higher-dimensional evaporating black holes

In future work, it would be interesting to study explicitly some higher-dimensional ana-
logues of the constructions considered in this chapter. We describe a few specific con-
structions in this final section. For these higher-dimensional examples, a detailed study
will likely require some numerics as the bulk geometry will no longer be locally AdS.
However, as the geometries depend on only two variables, such a study should be quite
feasible.

BCFT microstate construction

Fig. 4.15 shows on the left a Euclidean path integral for a high-energy CFT state obtained
by placing some boundary conditions in the Euclidean past (at the red sphere). This corre-
sponds to a black hole with some time-dependent behind-the-horizon physics, as described
in Chapter 2. We have in mind that the red boundary corresponds to a boundary condition
with a large boundary entropy, so that the holographic description involves a brane with
large tension.

Now we couple this system to a bulk CFT as shown on the right. Here, we need to
introduce an additional boundary component (shown in green) into the Euclidean path
integral. Two possible choices for the topology of this boundary component are shown.
We have in mind that this boundary has a small boundary entropy, perhaps corresponding
to a $T = 0$ brane. This setup is the precise higher-dimensional analogue of the single-sided
setup of §4.3.

In the dual holographic theory, using the bottom-up approach, we will have a bulk
$d+1$-dimensional gravity action, but also two different types of d-dimensional ETW branes
corresponding to the two different boundary conditions. Finally, there will be another $d-1$
dimensional brane that serves as the interface between the two types of d-dimensional
branes. This can have its own tension parameter independent of the others.
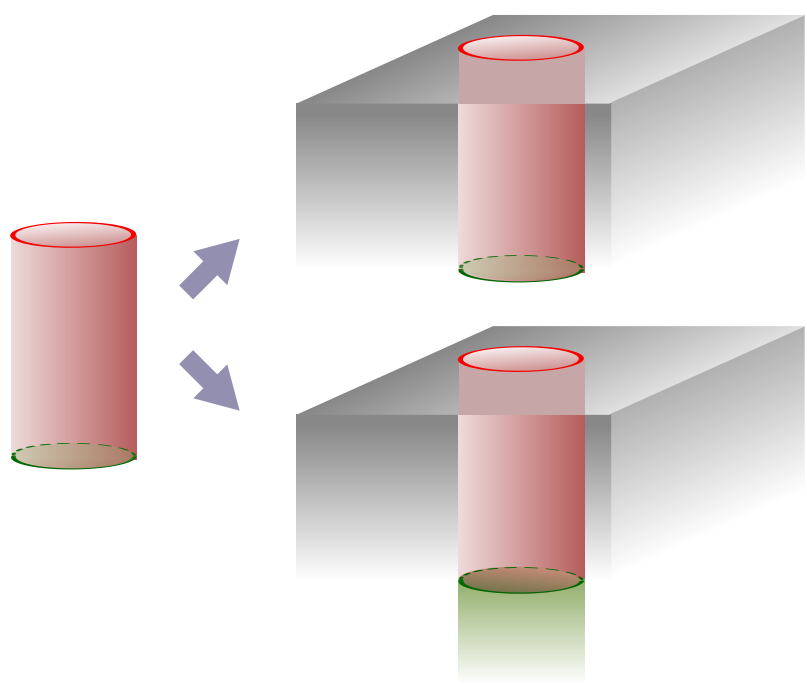
Figure 4.15: Higher dimensional construction based on BCFT microstates.
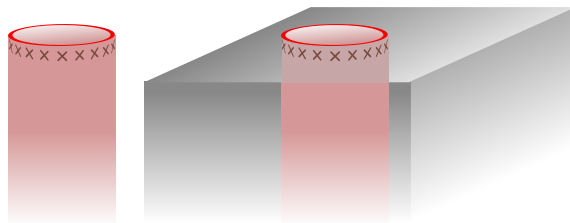
Figure 4.16: Higher-dimensional construction based on CFT-Vaidya states.

Vaidya-type construction

Another interesting case makes use of the setup of [113]. Fig. 4.16 shows on the left a Euclidean path integral for a CFT state dual to a shell of matter that collapses to form a black hole. We have insertions of many operators at some small time in the Euclidean past. Alternatively, we could consider a smooth source for some operator, again localized around some particular time $\tau = -\epsilon$. We can take a limit where $\tau \to 0$ but the sources/insertions are chosen such that we end up with a finite energy state.

Now we couple this system to a bulk CFT as shown on the right. Without the sources, this path-integral would give the vacuum state of the BCFT. We expect that the sources mainly excite boundary degrees of freedom, so the bulk part of the CFT is still nearly in the vacuum state. In this case, we expect that the state is dual to a shell that collapses to form a black hole but then evaporates.

4.5 Conclusion

In this chapter, we constructed simple holographic models in which the dynamics of evaporating black holes could be studied quantitatively. Our first model does not involve any lost degrees of freedom, but rather "information radiation" leaving the black hole. The signature of escape is a transition in the entanglement surface at the Page time, after which we are able to construct some portion of the interior region. We were able to verify our holographic computations using the microscopic techniques of Chapter 3. We also considered single-sided and genuinely evaporating examples, and discussed generalizations

to higher dimensions.

In the next chapter, we will consider a related transition in entanglement surface, but from the perspective of quantum information processing in spacetime. This will give us an alternative way to understand how information emerges from black holes.

Chapter 5

Quantum Tasks on the Brane

5.1   Introduction

In this chapter, we prove a theorem relating extremal surfaces and causal features of asymptotically AdS spacetimes which are ended by branes. These spacetimes are described by a manifold with boundary, along with a Lorentzian metric. The metric satisfies Einstein's equations and a boundary condition set at the brane, which we call the end-of-the-world (ETW) brane. Holographically, such spacetimes are proposed to be dual to conformal field theories with a boundary [59, 91], and are relevant to the emergence of spacetime [101, 146, 147], holographic approaches to cosmology [1, 139, 148], and to the black hole information problem [3, 6, 76, 149, 150, 151, 152, 153].

We will be most interested in the application of our theorem in the context of the black hole information problem. In particular, in the previous chapter (see also[6, 76, 149, 150, 151, 152, 153]) we viewed the brane as a black hole, and subregions of the CFT as the radiation which has escaped the black hole. To understand if the radiation system, call it R, reconstructs the black hole interior the standard approach is to find the minimal extremal surface anchored to R. The region enclosed by R and this extremal surface, called the entanglement wedge of R, is the portion of the bulk which can be recovered from R [100, 53, 43, 49, 50, 52]. Consequently by studying whether bulk extremal surfaces are brane-attached or detached one can understand when information that has fallen into the

black hole can be recovered from the radiation.

In this work we give an alternative approach to understanding when it is possible to reconstruct the black hole interior from a given radiation system. Our approach begins by recalling the connected wedge theorem [77, 78, 154], which relates the location of the entanglement wedge to the existence of causally defined regions in the bulk. We adapt the connected wedge theorem to the context of asymptotically AdS spacetimes which are ended by branes. Rather than find extremal surfaces, this theorem instructs us to check for the existence of a light ray from the black hole interior to the radiation system through the higher dimensional AdS geometry.[1] If this light ray exists, then the black hole interior can be recovered from the radiation.

Here is a brief chapter outline:

- In the remainder of this section, we preview the main result, the $1 \rightarrow 2$ *connected wedge theorem*, and briefly discuss the AdS/BCFT correspondence.

- In §5.2, we give the quantum information-based argument for the $1 \rightarrow 2$ theorem.

- In §5.3, we prove the $1 \rightarrow 2$ theorem from the bulk gravity perspective, making use of the null energy condition.

- In §5.4, we study bulk gravity solutions in $2 + 1$ dimensions that have a constant tension brane and are locally pure AdS, and verify the theorem explicitly.

- In §5.5, we take up the discussion of islands. We study in particular island formation in BCFT models of black holes, following the set-up of Chapter 4 closely.

- In §5.6 we conclude with some open questions and remarks.

5.1.1   Preview of the $1 \rightarrow 2$ connected wedge theorem

To arrive at our theorem, we employ the operational perspective on AdS/CFT initiated in [77] and elaborated in [78, 154]. In particular, the authors of [77, 78, 154] considered a

---

[1]This is an apparently impossible statement, since light rays should not escape black hole interiors. The light ray under discussion however is defined in a global geometry, which includes the black hole geometry as a coordinate patch. This is explained in detail in §5.5.

quantum computation with inputs given at two boundary spacetime locations and outputs at two other boundary locations. Viewing this computation from a bulk and boundary perspective leads to the connected wedge theorem. Here we use a similar construction that applies to the context of AdS spacetimes ended by branes. Specifically, we take quantum computations with one input location and two output locations. Additional information involved in the computation is localized to the brane. We refer to the present result as the $1 \to 2$ connected wedge theorem, and the earlier result of [78, 154] as the $2 \to 2$ connected wedge theorem, based on the number of input and output points involved.

To state the $1 \to 2$ connected wedge theorem, consider one 'input' region $\hat{\mathcal{C}}_1$ and two 'output' regions $\hat{\mathcal{R}}_1, \hat{\mathcal{R}}_2$. Note that we use hatted letters to denote regions in the boundary. We choose $\hat{\mathcal{R}}_1, \hat{\mathcal{R}}_2$ such that they touch the brane. The theorem is stated in terms of two additional spacetime regions constructed causally from $\hat{\mathcal{C}}_1, \hat{\mathcal{R}}_1, \hat{\mathcal{R}}_2$.

The first region is denoted $\hat{\mathcal{V}}_1$ and called the *decision region*. It is defined by

$$\hat{\mathcal{V}}_1 \equiv \hat{J}^+(\hat{\mathcal{C}}_1) \cap \hat{J}^-(\hat{\mathcal{R}}_1) \cap \hat{J}^-(\hat{\mathcal{R}}_2). \tag{5.1}$$

Here $\hat{J}^\pm(\hat{X})$ denotes the future and past of a region $\hat{X}$ taken in the boundary geometry.[2] We will restrict our attention to choices of region $\hat{\mathcal{C}}_i, \hat{\mathcal{R}}_i$ such that $\hat{\mathcal{C}}_i \subseteq \hat{\mathcal{V}}_i$.

The second region is called the *entanglement scattering region*. To define it, denote the entanglement wedge of a boundary region $\hat{X}$ by X, so that $X = \mathcal{E}_W(\hat{X})$. Further, denote the future and past of a region taken in the bulk geometry by $J^\pm(X)$. Then the entanglement scattering region is defined by

$$J^{\mathcal{E}}_{1 \to 12} \equiv J^+(\mathcal{C}_1) \cap J^-(\mathcal{R}_1) \cap J^-(\mathcal{R}_2) \cap \mathcal{B}, \tag{5.2}$$

where $\mathcal{B}$ denotes the end-of-the-world (ETW) brane. This and definition (5.1) are illustrated in Fig. 5.1.

Our main result is as follows.

Theorem 1. *($1 \to 2$ **connected wedge theorem**) Consider three boundary regions $\hat{\mathcal{C}}_1, \hat{\mathcal{R}}_1, \hat{\mathcal{R}}_2$*

---

[2]Note that $\hat{J}^\pm(\hat{X})$ is defined as the set of all points which are in the future of *any* point in X. In particular this means $\hat{X} \subseteq \hat{J}^+(\hat{X})$.
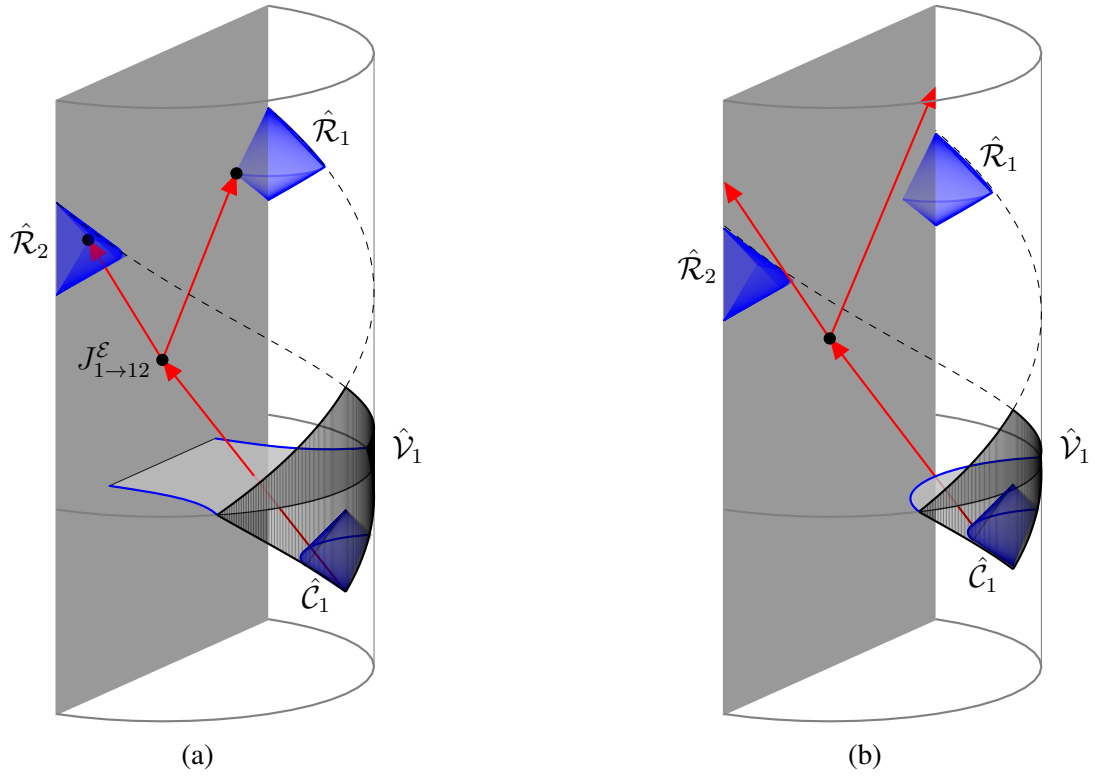
Figure 5.1: Illustration of Theorem 1, shown with a zero tension brane. The input region is $\hat{\mathcal{C}}_1$, shown in blue in the lower portion of the diagram, while the output regions are the light blue half diamonds attached to the edge. The decision region $\hat{\mathcal{V}}_1$ is shown in black. a) When a boundary point c_1 and two edge points r_1, r_2 have a bulk scattering region which intersects the brane, the entanglement wedge of an associated domain of dependence (black shaded region) attaches to the brane. b) When there is no such scattering region, the entanglement wedge need not be connected.

in an asymptotically AdS$_{2+1}$ spacetime with an end-of-the-world brane. Require that $\hat{\mathcal{C}}_1 \subseteq \hat{\mathcal{V}}_1$, and that $\hat{\mathcal{R}}_1, \hat{\mathcal{R}}_2$ touch the brane. Then if $J^{\mathcal{E}}_{1\rightarrow 12}$ is non-empty, the entanglement wedge of $\hat{\mathcal{V}}_1$ is attached to the brane.

Note that in some cases $\hat{\mathcal{V}}_1$ may attach to the brane in the boundary, in which case the theorem is trivially true. The converse to this theorem does not hold, and we give an explicit example in the main text.

To motivate our theorem, consider the following scenario. Suppose some classical information q is encoded in the brane, for instance in some brane-localized degrees of freedom. We leave unspecified at this stage in the argument where this corresponds to q being localized in the boundary. Alice, an observer, receives a quantum state $H^q |b\rangle$ in region $\hat{\mathcal{C}}_1$, where H is the Hadamard operator[3]. If $q = 0$, then $H^q = \mathcal{I}$ and this is $|0\rangle, |1\rangle$ for $b = 0, 1$. If $q = 1$, then $H^q = H$ and this is $|+\rangle, |-\rangle$ for $b = 0, 1$. Without knowing q, Alice is not able to measure in the correct basis and learn b. However, Alice's goal is to bring b to two regions $\hat{\mathcal{R}}_1$ and $\hat{\mathcal{R}}_2$, which will be attached to the CFT edge.

Causality requires that Alice can succeed in her task only when q is stored in the patch of spacetime formed from the overlap of the past of $\hat{\mathcal{R}}_1, \hat{\mathcal{R}}_2$ (since she needs to send b to both output regions) and the future of $\hat{\mathcal{C}}_1$ (since she needs the input $H^q |b\rangle$). We can consider this overlap in either the bulk or the boundary perspective. In the boundary we consider the future or past of the relevant boundary regions, $\hat{\mathcal{V}}_1 = \hat{J}^+(\hat{\mathcal{C}}_1) \cap \hat{J}^-(\hat{\mathcal{R}}_1) \cap J^-(\hat{\mathcal{R}}_2)$. In the bulk perspective it is appropriate to consider the future or past of the corresponding entanglement wedges, $J^+(\mathcal{C}_1) \cap J^-(\mathcal{R}_1) \cap J^-(\mathcal{R}_2)$. In either case if the overlap contains q, Alice can complete her task.

When the bulk overlap intersects the brane it contains q. This is just the statement that $J^{\mathcal{E}}_{1\rightarrow 12} = J^+(\mathcal{C}_1) \cap J^-(\mathcal{R}_1) \cap J^-(\mathcal{R}_2) \cap \mathcal{B}$ is non-empty. Then in the bulk picture Alice can complete her goal of bringing b to $\mathcal{R}_1$ and $\mathcal{R}_2$. Meanwhile, for a holographic BCFT, entanglement wedge reconstruction tells us that the information stored in $\hat{\mathcal{V}}_1$ is geometrized as bulk degrees of freedom in its entanglement wedge. Thus the entanglement wedge of $\hat{\mathcal{V}}_1$ should include the brane whenever $J^{\mathcal{E}}_{1\rightarrow 12}$ is non-empty, which is the claim of the theorem.

---

[3]The Hadamard operator is a unitary defined by $H|0\rangle = |+\rangle, H|1\rangle = |-\rangle$.

In earlier work [77, 78], the case where input and output regions consisted of single points was considered. For the applications of our theorem to islands discussed in §5.5 a point based version of Theorem 1 is appropriate. Partly this is because the statement in terms of regions is equivalent to the point based statement in the setting of pure AdS with an ETW brane. When not considering pure AdS spacetimes however the region based statement is stronger, so we have included the statement and proof of the more general theorem.

Notice that if we choose $\hat{\mathcal{C}}_i$ such that $\hat{\mathcal{C}}_i = \hat{\mathcal{V}}_i$ the theorem is not useful, in that finding the entanglement scattering region already involves determining the entanglement wedge of $\hat{\mathcal{V}}_i$. In this case however we can consider the minimal extremal surface which is not attached to the brane, call it $\gamma'_{\mathcal{V}_1}$, and define the region $W[\gamma'_{\mathcal{V}_1}]$ whose boundary is $\gamma'_{\mathcal{V}_1} \cup \mathcal{V}_1$. Note that $W[\gamma'_{\mathcal{V}_1}]$ is contained within the true entanglement wedge $W[\gamma_{\mathcal{V}_1}]$, which in general may be larger. In fact it will be larger whenever the minimal extremal surface $\gamma_{\mathcal{V}_1}$ is attached to the brane. Then Theorem 1 can be used to conclude that if

$$(J')^{\mathcal{E}}_{1 \to 12} \equiv J^+(W[\gamma'_{\mathcal{V}_1}]) \cap J^-(\mathcal{R}_1) \cap J^-(\mathcal{R}_2) \cap \mathcal{B} \neq \varnothing \tag{5.3}$$

then $W[\gamma'_{\mathcal{V}_1}]$ will not be the full entanglement wedge, and instead it is the brane attached extremal surface which is minimal.

5.1.2 Review of AdS/BCFT

The $1 \to 2$ theorem will be proven using the focusing theorem for asymptotically AdS spacetimes which feature an end-of-the-world (ETW) brane. In the context of our quantum information discussion however, and in the context of applying our theorem to islands, we have a particular holographic dual description of these spacetimes in mind. We describe this boundary picture in this section.

A BCFT is a conformal field theory living on a manifold with boundary, along with a conformally invariant boundary condition. For appropriate BCFTs, the AdS/BCFT [59, 91] correspondence suggests a bulk dual description, which consists of an asymptotically AdS region along with an extension of the CFT boundary into the bulk as an ETW brane.

186

To avoid confusion with the bulk-boundary language of the AdS/CFT correspondence, we will refer to the CFT boundary as the *edge*. The bulk spacetime and brane are described by an action

$$I_{\text{bulk}} + I_{\text{brane}} = \frac{1}{16\pi G_N} \int \mathrm{d}^{d+1}x \, \sqrt{g}(R - 2\Lambda + L_{\text{matter}})$$
$$+ \frac{1}{8\pi G_N} \int_{\mathcal{B}} \mathrm{d}^d y \, \sqrt{h}(K + L_{\text{matter}}^{\mathcal{B}}) \,, \tag{5.4}$$

where L_{matter} and $L_{\text{matter}}^{\mathcal{B}}$ are matter Lagrangians for fields in the bulk and brane respectively. As usual, R is the Ricci curvature and Λ the bulk cosmological constant, while K is the trace of the extrinsic curvature of the brane,

$$K_{ab} = \nabla_a n_b \,, \tag{5.5}$$

for outward normal n_j to $\mathcal{B}$, and a, b refer to brane coordinates y^a. This action leads to Einstein's equations in the bulk, along with the boundary condition

$$-\frac{1}{8\pi G_N}(K_{ab} - K h_{ab}) = T_{ab}^{\mathcal{B}} \,. \tag{5.6}$$

In AdS/BCFT, the Ryu-Takayanagi formula [38] and its covariant generalization the HRT formula [41] continue to calculate the entropy of boundary subregions, provided the homology condition is appropriately adapted [2]. In the context of AdS/CFT, and assuming the null energy condition, the HRT formula is equivalent to the maximin formula [43]. We will assume this remains the case in AdS/BCFT. The maximin formula states that, to leading order in $1/G_N$,

$$S(A) = \max_{\Sigma} \min_{\gamma_A} \left(\frac{\text{Area}[\gamma_A]}{4 G_N} \right). \tag{5.7}$$

The maximization is over Cauchy surfaces that include A in their boundary, and the minimization is over spacelike codimension-2 surfaces γ_A which are homologous to A. We will refer to the surface γ_A picked out by such a procedure, whose area computes the entropy, as an *entangling surface*. In spacetimes with an ETW brane we should understand

187

the homology constraint as

$$\partial S = \gamma_A \cup A \cup b \qquad (5.8)$$

for S a spacelike codimension-1 surface in the bulk, and where b is allowed to be any portion of the ETW brane. For a single interval in the CFT, this allows two qualitatively distinct classes of entangling surface: those which do not include a portion of the brane to satisfy the homology constraint, which we call brane-detached, and those which do, which we call brane-attached (see Fig. 5.1).

In addition to calculating the von Neumann entropy, the maximin formula has a second important meaning. In particular the maximin procedure defines the region S according to (5.8). The domain of dependence of S, $D(S)$, is known as the *entanglement wedge* and denoted E_A. The entanglement wedge is the portion of bulk that is completely described by the density matrix ρ_A. More precisely, any bulk operator with support on E_A can be written in the boundary with support on A.

In the BCFT description there are degrees of freedom which live at the edge and are associated with the choice of boundary condition. At least for constant, large tension branes these edge degrees of freedom are dual in the bulk to degrees of freedom living on the brane [138].

5.2 Quantum tasks argument

In this section, we give the quantum tasks argument for Theorem 1. Several aspects of the argument follow the argument of the $2 \rightarrow 2$ connected wedge theorem [78, 154], but we emphasize that the qualitative picture of how the boundary completes the task is distinct in the two cases. In particular, in the $2 \rightarrow 2$ theorem the boundary uses a quantum non-local computation to complete the task, whereas in the $1 \rightarrow 2$ theorem the boundary employs bulk reconstruction, as we will see below.
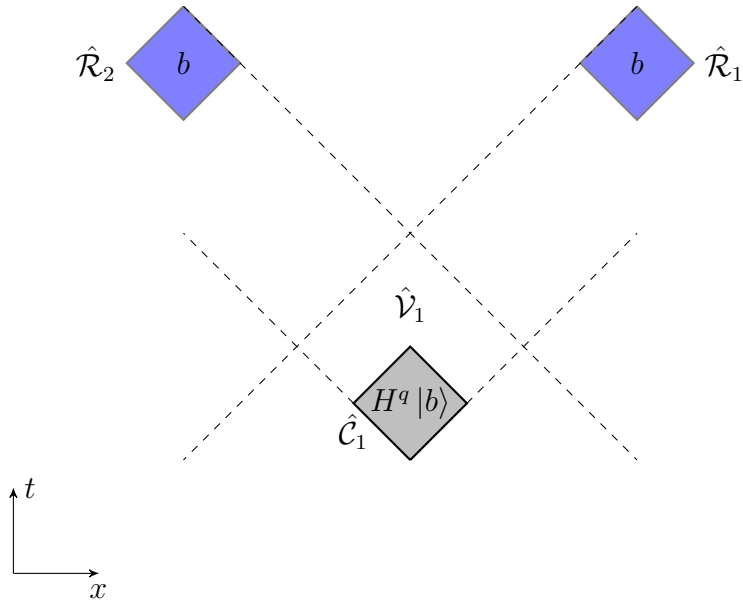
Figure 5.2: The **M** task, which we employ to argue for the $1 \rightarrow 2$ connected wedge theorem. In region $\hat{\mathcal{C}}_1$ (grey) the quantum system A is received which holds a state $H^q |b\rangle$. For the task to be completed successfully, b should be produced at both $\hat{\mathcal{R}}_1$ and $\hat{\mathcal{R}}_2$. We show that completing the task with a high success probability requires the bit q be available in the region $\hat{\mathcal{V}}_1 = \hat{J}^+(\hat{\mathcal{C}}_1) \cap \hat{J}^-(\hat{\mathcal{R}}_1) \cap \hat{J}^-(\hat{\mathcal{R}}_2)$.

5.2.1 The monogamy task

A quantum task is a quantum computation which has its inputs and outputs at specified spacetime locations. We will consider tasks which have inputs and outputs recorded into extended spacetime regions. To understand this more precisely, suppose the A system of a quantum state $|\Psi\rangle_{A\bar{A}}$ has been recorded into the degrees of freedom of a quantum field. We will say that A is *localized to region X relative to a channel* $\mathcal{M}_{X\to A}$ if $\mathcal{M}_{X\to A} \otimes \mathcal{I}_{\bar{A}}(\rho_{X\bar{A}}) = |\Psi\rangle\langle\Psi|_{A\bar{A}}$. If there exists a channel such that quantum system A is localized to a region X relative to that channel, we say just that A is localized to X[4]. If it is not possible to learn anything about A from X, we say A is *excluded* from X. For a review of quantum tasks as they are employed here, see [154].

For our particular example, there is one input region $\hat{\mathcal{C}}_1$ and two output regions $\hat{\mathcal{R}}_1, \hat{\mathcal{R}}_2$. System A is in one of the states $H^q |b\rangle_A$ and is localized to region $\hat{\mathcal{C}}_1$. H is the Hadamard operator, and $b, q \in \{0, 1\}$. There is an additional system Q which holds the bit q, and we leave unspecified for the moment where Q is located in spacetime. To complete the task the bit b should be localized to $\hat{\mathcal{R}}_1$ and $\hat{\mathcal{R}}_2$. We will momentarily leave the channels $\mathcal{M}_{\hat{\mathcal{C}}_1}, \mathcal{M}_{\hat{\mathcal{R}}_1}, \mathcal{M}_{\hat{\mathcal{R}}_2}$ unspecified. This task is illustrated in Fig. 5.2, and we refer to it as the M task or "monogamy task", for reasons that will become apparent.

We will need to introduce an equivalent formulation of M that we refer to as *purified* M. The purified task is modified in two ways: (1) a second system $\bar{Q}$ is introduced, and placed in the maximally entangled state with Q; and (2) the input qubit $H^q |b\rangle_A$ is replaced with the A system of a maximally entangled state $|\Psi^+\rangle_{A\bar{A}}$. We refer to the $\bar{Q}\bar{A}$ system as the reference system. Notice that Bob can now perform measurements on the reference system to return this to the original task. To do this, Bob first measures the $\bar{Q}$ system, and obtains some output q. Then, he measures $\bar{A}$ in the computational basis if $q = 0$, and in the Hadamard basis if $q = 1$. Bob obtains one bit b of output. Meanwhile, the post-measurement state on QA is $|q\rangle_Q \otimes H^q |b\rangle_A$, so that the inputs are as in the unpurified task. Alice's success probability is unaffected whether Bob performs these measurements before or after Alice returns her outputs, since the QA and $\bar{Q}\bar{A}$ systems never interact.

---

[4] An equivalent, possibly more familiar, way to define this is in terms of operators rather than states: A is localized to region X if the algebra of operators acting on A has support on subregion X.

Thus, the purified and unpurified tasks have the same success probability.

The three regions $\hat{\mathcal{C}}_1, \hat{\mathcal{R}}_1, \hat{\mathcal{R}}_2$ have a naturally associated spacetime region which we label $\hat{\mathcal{V}}_1$, defined according to

$$\hat{\mathcal{V}}_1 \equiv \hat{J}^+(\hat{\mathcal{C}}_1) \cap \hat{J}^-(\hat{\mathcal{R}}_1) \cap \hat{J}^-(\hat{\mathcal{R}}_2) \,. \tag{5.9}$$

and which we call the *decision region*. $\hat{\mathcal{V}}_1$ is natural to consider because it is where it is possible to act on A and reach both of $\hat{\mathcal{R}}_1$ and $\hat{\mathcal{R}}_2$. We will in particular be interested in two situations: (1) the setting where Q is localized to $\hat{\mathcal{V}}_1$ and (2) the setting where Q is excluded from $\hat{\mathcal{V}}_1$.

Let us consider first the case where Q is localized to $\hat{\mathcal{V}}_1$. For convenience, take the unpurified task. Then within $\hat{\mathcal{V}}_1$ Alice should apply H^q to A to obtain $(H^q)^2 |b\rangle_A = |b\rangle_A$, measure $|b\rangle_A$ in the $\{|0\rangle, |1\rangle\}$ basis, and then send the outcome to each of r_1 and r_2. Doing so, she can complete the task with high probability, say $p_{\text{suc}}(\mathbf{M}) = 1 - \epsilon$. We introduce the parameter ϵ to account for the effect of any noise present in carrying out this protocol.[5]

We can make a stronger statement by introducing a parallel repetition of the monogamy task, which we call $\mathbf{M}^{\times n}$. We consider n states $\{H^{q_i} |b_i\rangle\}_i$ being input at $\hat{\mathcal{C}}_1$, with the q_i and b_i drawn independently and at random. To complete the task, a fraction $1 - \delta$ of the b_i should be localized to both $\hat{\mathcal{R}}_i$. As discussed in the last paragraph, Alice can complete each of the n runs with a probability $p_{\text{suc}}(\mathbf{M}) = 1 - \epsilon$. For $\epsilon < \delta$, the probability that this leads to more than a fraction $1 - \delta$ of the runs being successful will be high. For concreteness take $\delta = 2\epsilon$. In this case we have, at large n,

$$p_{\text{suc}}(\mathbf{M}^{\times n}) = 1 - 2\epsilon^{2+n}. \tag{5.10}$$

In particular we see that the success probability converges to 1 exponentially in n.

Next, consider the case where q is excluded from $\hat{\mathcal{V}}_1$. More precisely, we consider

---

[5]One source of noise may be our assumption that Alice is working in a classical geometry. In the AdS/CFT context, at finite G_N, it seems plausible that small errors are inevitable.

purified $\mathbf{M}$ and state this assumption as

$$I(\hat{\mathcal{V}}_1 : \bar{Q}) = 0 \ . \tag{5.11}$$

Then Alice will be limited in her ability to complete the task, a fact we formalize in the following lemma.

Lemma 2. *Consider the* $\mathbf{M}$ *task [cf. Fig. 5.2] with* $I(\hat{\mathcal{V}}_1 : \bar{Q}) = 0$. *Then any strategy for completing the task has* $p_{suc}(\mathbf{M}) \leq \cos^2(\pi/8)$.

To see why this is true, consider that Alice holds the A subsystem of a maximally entangled state on $A\bar{A}$ in the region $\hat{\mathcal{V}}_1$. After applying a quantum channel to A, she will send part of the output, call it B_1, to $\hat{\mathcal{R}}_1$ and part of the output, call it B_2, to $\hat{\mathcal{R}}_2$. At best, Alice will learn Q in the regions $\hat{\mathcal{R}}_i$. At each of the R_i then she can use B_i along with q to produce a guess for b. This is exactly the guessing game analyzed in [79], known as the monogamy of entanglement game. The stated bound on success probability was proven there.

Notice that if B_1 and $\bar{A}$ are maximally entangled, Alice can measure in the q basis and produce an output at $\hat{\mathcal{R}}_1$ which is perfectly correlated with Bobs measurement outcome. Similarly if $B_2\bar{A}$ is maximally entangled she can produce the correct output at $\hat{\mathcal{R}}_2$. The monogamy of entanglement however ensures that there will be a trade-off, and no perfect strategy will exist.[6] The proof in [79] makes this rigorous.

We can also consider the parallel repetition of the task $\mathbf{M}^{\times n}$ in the case where $I(V : \bar{Q}) = 0$. Following the reasoning of Lemma 2, this can again be reduced to the guessing game discussed in [79], who proved that this parallel repetition of the task satisfies the following lemma.

Lemma 3. *Consider the* $\mathbf{M}^{\times n}$ *task with* $I(\hat{\mathcal{V}}_1 : \bar{Q}) = 0$, *and require that a fraction* $1 - \delta$ *of the individual* $\mathbf{M}$ *tasks are successful. Then any strategy for completing the task has*

$$p_{suc} \leq \left(2^{h(\delta)} \cos^2 \left(\frac{\pi}{8} \right) \right)^n \equiv \left(2^{h(\delta)} \beta \right)^n \tag{5.12}$$

---

[6]This explains our naming convention $\mathbf{M}$ for the task.

where $h(\delta)$ is the binary entropy function $h(\delta) \equiv -\delta \log \delta - (1 - \delta) \log(1 - \delta)$ and the second equality defines β.

For small enough δ we have that $2^{h(\delta)}\beta < 1$, so that with zero mutual information the success probability is small. Our next result will be to show that a large success probability implies a large mutual information.

In fact, this argument was already completed in [154], albeit in a changed setting.[7]

Lemma 4. *Suppose that the $\mathbf{M}^{\times n}$ task is completed with success probability $p_{suc} = 1 - 2\epsilon^{2+n}$, where we deem the $\mathbf{M}^{\times n}$ task successful if a fraction $1 - 2\epsilon$ of the individual $\mathbf{M}$ tasks are. Then the bound*

$$\frac{1}{2}I(\hat{\mathcal{V}}_1 : \bar{Q}) \geq n(-\log 2^{h(2\epsilon)}\beta) - 1 + O((\epsilon/\beta)^n) \tag{5.13}$$

holds.

This will be the key technical result in the argument from quantum tasks for the connected wedge theorem, which we present in the next section.

We should highlight an important assumption made in proving Lemma 4. In addition to the region $\hat{\mathcal{V}}_1$, there is also the spacelike complement, consisting of all points spacelike separated from every point in $\hat{\mathcal{V}}_1$. This is also given by the complement of the future and past of $\hat{\mathcal{V}}_1$, so that $\hat{X} = [\hat{J}^+(\hat{\mathcal{V}}_1) \cup \hat{J}^-(\hat{\mathcal{V}}_1)]^c$. Lemma 3, on which Lemma 4 relies, assumes that information from this region is not made use of in Alice's protocol. If it were, one could use protocols of the type considered in appendix B of [78] to perform the $\mathbf{M}^{\times n}$ task without entanglement between $\hat{\mathcal{V}}_1$ and $\bar{Q}$. As discussed in [78], it seems sensible to assume such strategies are not allowed. In particular they require large amounts of GHZ type entanglement in the CFT, which is not expected to exist [155].

5.2.2   Tasks argument for the $1 \to 2$ connected wedge theorem

With Lemma 4 in hand, we are ready to complete the tasks argument for the $1 \to 2$ connected wedge theorem. For convenience we repeat the theorem here.

---

[7]In particular the systems $\hat{\mathcal{V}}_1$ and $\bar{Q}$ play the role of systems $\hat{\mathcal{V}}_1$ and $\hat{\mathcal{V}}_2$ discussed in [154]. Our Lemma 4 is their Lemma 7 with this replacement made.

Theorem 1: *Consider three boundary regions $\hat{\mathcal{C}}_1, \hat{\mathcal{R}}_1, \hat{\mathcal{R}}_2$ in an asymptotically AdS_{2+1} spacetime with an end-of-the-world brane. Require that $\hat{\mathcal{C}}_1 \subseteq \hat{\mathcal{V}}_1$, and that $\hat{\mathcal{R}}_1, \hat{\mathcal{R}}_2$ touch the brane. Then if $J^{\mathcal{E}}_{1 \to 12}$ is non-empty, the entanglement wedge of $\hat{\mathcal{V}}_1$ is attached to the brane.*

Argument. Using our assumption that $J^{\mathcal{E}}_{1 \to 12} \neq \varnothing$, we have that there exist bulk points c_1, r_1, r_2 such that

$$J^+(c_1) \cap J^-(r_1) \cap J^-(r_2) \cap \mathcal{B} \neq \varnothing \tag{5.14}$$

with $c_1 \in \mathcal{C}_1, r_1 \in \mathcal{R}_1, r_2 \in \mathcal{R}_2$, where recall $X = \mathcal{E}_W(\hat{X})$, with $\hat{X}$ a boundary region. We will consider a $\mathbf{M}^{\times n}$ task in the bulk such that the input system $A = A_1....A_n$ is input near c_1, and each bit b_i should be brought near r_1 and r_2. Further, system Q will be recorded into the brane degrees of freedom.

It is easy to see that the $\mathbf{M}^{\times n}$ task can be completed in this case with high probability. To see this, note that a simple bulk strategy is to bring A to the brane, learn the q_i, and use them to recover the b_i. The b_i are then copied and sent to both r_1 and r_2. Doing so we can complete each $\mathbf{M}$ task with some probability $p = 1 - \epsilon$, leading to a success probability $p_{\text{suc}} = 1 - 2\epsilon^{2+n}$ for the $\mathbf{M}^{\times n}$ task. Since the boundary reproduces bulk physics, the boundary must also complete the task with the same probability. Lemma 4 then gives

$$\frac{1}{2}I(\hat{\mathcal{V}}_1 : \bar{Q}) \geq n(-\log 2^{h(2\epsilon)}\beta) - 1 + O((\epsilon/\beta)^n) \tag{5.15}$$

so that when the entanglement scattering region is non-empty, we have large mutual information.

This bound on mutual information actually requires the entanglement wedge of $\hat{\mathcal{V}}_1$ to attach to the brane. To see this, consider that in the purified $\mathbf{M}^{\times n}$ task there are n Bell pairs $|\Psi^+\rangle_{A_i \bar{A}_i}$ with $A = A_1...A_n$ input at $\mathcal{C}_1$, and $\bar{A} = \bar{A}_1...\bar{A}_n$ held by Bob. There are an additional n Bell pairs $|\Psi^+\rangle_{Q_i \bar{Q}_i}$, with $Q = Q_1...Q_n$ stored on the brane, and $\bar{Q} = \bar{Q}_1...\bar{Q}_n$ held by Bob. We can choose n to satisfy $O(1) < n < O(1/G_N)$, so that n grows as $G_N \to 0$ but does so more slowly than $1/G_N$.

Suppose that $\mathcal{E}_W(\hat{\mathcal{V}}_1)$ is not connected to the brane. Then the entropies of the region

194

$\hat{\mathcal{V}}_1$ and of system $\bar{Q}$ satisfy

$$S(\hat{\mathcal{V}}_1) = \frac{A_{\text{dis}}}{4G_N} + n + O(1),$$
$$S(\bar{Q}) = n,$$
$$S(\hat{\mathcal{V}}_1 \bar{Q}) = \frac{A_{\text{dis}}}{4G_N} + 2n + O(1). \tag{5.16}$$

The first statement is just our assumption: the disconnected surface calculates the entropy of $\hat{\mathcal{V}}_1$, and then we add the entropy of the n Bell pairs shared between $\hat{\mathcal{V}}_1$ and $\bar{A}$, along with any $O(1)$ contribution. The second statement is due to $Q\bar{Q}$ being in the maximally entangled state. The third statement follows from the disconnected surface being of minimal area along with our choice to take $n < O(1/G_N)$. This is because the other option, of having the connected surface calculate the entropy, would imply that the quantum extremal surface has moved to enclose the n qubits of Q, which would happen only if $n > (A_{\text{dis}} - A_{con})/G_N$. Using these statements about the entropy, the mutual information is

$$I(\bar{Q} : \hat{\mathcal{V}}_1) = S(\bar{Q}) + S(\hat{\mathcal{V}}_1) - S(\hat{\mathcal{V}}_1 \bar{Q}) = O(1), \tag{5.17}$$

so that in the disconnected phase the mutual information is $O(1)$. Since (5.15) implies the mutual information is $O(n) > O(1)$, we find that the entanglement wedge must attach to the brane. ∎

It is interesting to consider this result in the context of entanglement wedge reconstruction. We can observe that when the entanglement wedge connects to the brane Q is reconstructable from $\hat{\mathcal{V}}_1$. This clarifies how the boundary completes the task. Whenever the task can be completed in the bulk, the entanglement wedge connects to the brane, which means Q is available in $\hat{\mathcal{V}}_1$. Thus the boundary dynamics can recover the bits q_i and use them to decode the b_i, then forward the b_i to both output points.

We should contrast this boundary picture with the analogous feature of the connected wedge theorem in AdS/CFT. In that setting there are two decision regions $\hat{\mathcal{V}}_1$ and $\hat{\mathcal{V}}_2$, with $\hat{\mathcal{V}}_1$ associated with the input $H^q |b\rangle$ and $\hat{\mathcal{V}}_2$ associated with the input q. In that case, even

in the connected phase, $\hat{\mathcal{V}}_1$ does not reconstruct q. To complete the task then the boundary must make use of a different strategy. Indeed in [78] the authors argued that the boundary dynamics should be understood as a quantum non-local computation.

5.3 Proof from the focusing theorem

In this section we prove the $1 \to 2$ connected wedge theorem. Following [78, 154] closely, our main tools are the focusing theorem and the maximin statement of the HRRT formula [43]. We apply the focusing theorem to null congruences beginning on extremal surfaces. Doing so, new complications arise from the presence of the ETW brane. In particular additional boundary terms arise where the congruence meets the brane. In the next section, we review the usual statement of the focusing theorem, then treat these additional boundary terms.

5.3.1 The focusing theorem with boundaries

We will briefly review the focusing theorem without an ETW brane present.

Consider a null codimension-1 surface $\mathcal{N}$. We assume $\mathcal{N}$ is foliated by null geodesics which start on a spacelike codimension-2 surface Σ_1, and end on another spacelike codimension-2 surface Σ_2. Call the affine parameter along the null geodesics λ, which we scale so that $\lambda = 0$ on Σ_1 and $\lambda = 1$ on Σ_2. Then

$$A(\Sigma_2) - A(\Sigma_1) = \int dY \sqrt{h}_{\lambda=0} - \int dY \sqrt{h}_{\lambda=1} = \int_0^1 d\lambda \int dY \partial_\lambda \sqrt{h} \qquad (5.18)$$

where h is the determinant of the induced metric on a constant λ slice of $\mathcal{N}$, and $dY = dy^1 \wedge ... \wedge dy^{d-2}$.

Define the expansion, θ, and a $d - 1$ form ϵ by

$$\theta = \frac{1}{\sqrt{h}} \partial_\lambda \sqrt{h} \qquad \epsilon = \sqrt{h} \, d\lambda \wedge dY. \qquad (5.19)$$

Then the area difference can be written as

$$A(\Sigma_2) - A(\Sigma_1) = \int \epsilon \, \theta. \tag{5.20}$$

Expressing the area difference in this way is convenient, since the expansion is constrained in certain situations if we assume the null energy condition (NEC),

$$k^\mu k^\nu T_{\mu\nu} \geq 0. \tag{5.21}$$

In particular, consider an extremal surface γ. Then the boundary of the future or past of γ, $\partial J^\pm(\gamma)$, is generated by a congruence of null geodesics. Assuming the NEC, this congruence has non-positive expansion when moving away from γ, as can be shown using the Raychaudhuri equation. We will call surfaces with non-positive expansion *light sheets*. Considering $\mathcal{N}$ to be a portion of either $\partial J^+(\gamma)$ or $\partial J^-(\gamma)$ then allows us to conclude $A(\Sigma_2) \leq A(\Sigma_1)$. That is, the area of a cross section of the congruence decreases as we follow the geodesics.

Notice that there are various lightsheets we can define given an extremal surface γ, in particular the four surfaces $\partial J^\pm_{\text{in,out}}(\gamma)$. To specify it will be more convenient to define light sheets as the boundary of the future or past of a (codimension-0) entanglement wedge, $\partial J^\pm(X)$. Notice that $\partial J^\pm_{\text{in}}(\gamma_X) = \partial J^\pm(X)$, so that defining light sheets in this way chooses the inward pointing sheets.

Next, we consider the focusing theorem in the setting where $\mathcal{N}$ intersects the brane. The situation is shown in Fig. 5.3. The null surface $\mathcal{N}$ is still foliated by a null congruence, but some geodesics end or begin on an additional portion of the boundary, $\mathcal{N} \cap \mathcal{B}$. To prove an area theorem in this setting, we will need to assume the NEC holds both for the bulk stress tensor and for the branes stress tensor. This later statement is

$$\ell^a \ell^b T^\mathcal{B}_{ab} \geq 0, \tag{5.22}$$

where ℓ^a is a null tangent vector to the brane. This is satisfied with equality for constant tension branes. Using the boundary condition $8\pi G_N T_{ab} = -(K_{ab} - K h_{ab})$ we can also express this as $\ell^a \ell^b K_{ab} \leq 0$.

197
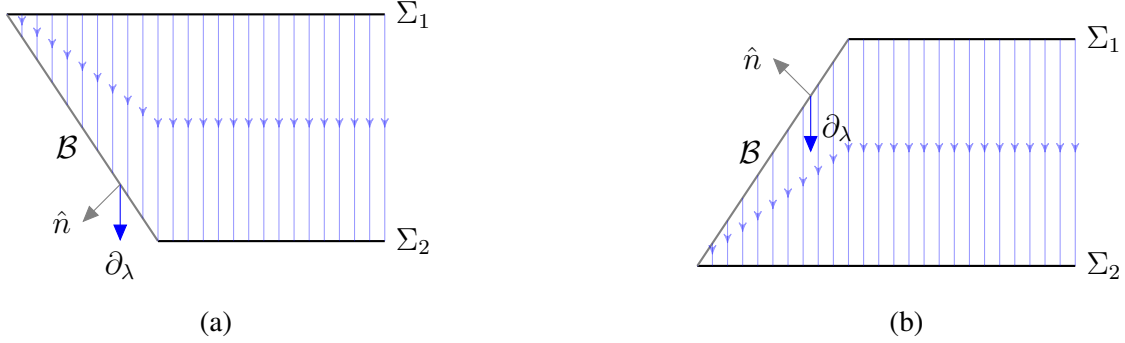
Figure 5.3: A portion of the boundary of the past $\partial J^-(\mathcal{R}_i)$, showing two cross sections Σ_1, Σ_2, and the end-of-the-world brane $\mathcal{B}$. Null geodesics generating the lightcone are shown in blue. The outward pointing normal to the brane is labelled $\hat{n}$, while the tangent vector to the null geodesics is labelled ∂_λ. (a) When $\hat{n} \cdot \partial_\lambda \geq 0$, the brane removes area. (b) When $\hat{n} \cdot \partial_\lambda \leq 0$, the brane adds area.

We will reconsider $\int \epsilon \, \theta$ and write this as a boundary integral. A simple application of the fundamental theorem of calculus sufficed to derive (5.20), but this was only because the null geodesics meet Σ_1 and Σ_2 normally. For the additional portion of the boundary we need to use Stokes theorem in a more general form. To begin, note that

$$\epsilon \, \theta = (\partial_\lambda \sqrt{h}) \, \mathrm{d}\lambda \wedge \mathrm{d}Y = \mathrm{d}(\sqrt{h}\mathrm{d}Y) \equiv \mathrm{d}\omega \tag{5.23}$$

so $\epsilon \, \theta$ is closed. The last equality defines ω. Now we will use Stokes theorem in the form

$$\int_M \mathrm{d}\omega = \int_{\partial M} \mathrm{d}^{d-2}x \sqrt{\gamma} n^\mu V_\mu \tag{5.24}$$

where γ is the induced metric on the boundary, n^μ is the normal vector to the boundary[8], and $V_\mu = (-1)^{d-1}(*\omega)_\mu$ where $*$ denotes the Hodge dual.

The one-form V in (5.24) is simple to compute, $V = (-1)^{d-1} * \omega = (-1)^{d-1}\mathrm{d}\lambda$. Along Σ_1 we have $n^\mu = -(\partial_\lambda)^\mu$, and along Σ_2 we have $n^\mu = (\partial_\lambda)^\mu$, which recovers the

---

[8]For spacelike boundaries we should choose the outward pointing normal, while for timelike boundaries we choose the inward pointing one.
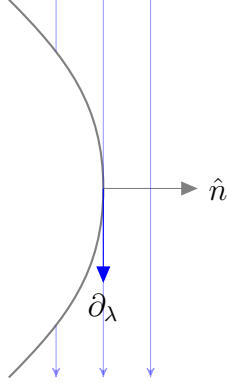
Figure 5.4: The lightsheet $\partial J^-(R_i)$ where it meets the brane. For $\hat{n} \cdot \partial_\lambda = n_\lambda \geq 0$ initially, a change in sign requires that the extrinsic curvature be positive somewhere along the brane (as shown here), which is ruled out by the NEC applied to the brane stress tensor.

two boundary terms appearing in (5.20). The boundary $\mathcal{B} \cap \mathcal{N}$ returns an additional term,

$$\int_{\mathcal{N}} \epsilon\, \theta = A(\Sigma_2) - A(\Sigma_1) + \int_{\Sigma \cap \mathcal{N}} \mathrm{d}^{d-2}x \sqrt{\gamma}\, n_\lambda. \tag{5.25}$$

We will need this more general statement when we focus backwards in the proof of Theorem 1.

For (5.25) to relate $A(\Sigma_2)$ and $A(\Sigma_1)$ we would like to fix the sign of n_λ. In particular, $n_\lambda \geq 0$ along with $\theta \leq 0$ would imply $A(\Sigma_2) \geq A(\Sigma_1)$, recovering the usual area theorem. This is illustrated in Fig. 5.3. In fact we can show $n_\lambda \geq 0$ in one particular but important situation. Suppose that $\mathcal{N}$ is a portion of $\partial J^-(\mathcal{R}_i)$, for $\mathcal{R}_i$ the entanglement wedge of an edge anchored region. Then we have that at $\lambda = 0$,[9]

$$n_\lambda = 0. \tag{5.26}$$

This holds because the entangling surface $\gamma_{\mathcal{R}_i}$ meets the brane normally, which means the normal vectors of $\gamma_{\mathcal{R}_i} \cap \mathcal{B}$ will be tangent to the brane.

We claim the NEC imposed on the brane stress tensor ensures $n_\lambda \geq 0$ everywhere. To

---

[9]More generally we need only that $n_\lambda \geq 0$. Thus the theorem may still hold in certain cases where $\hat{\mathcal{R}}_i$ is not attached to the edge, though its unclear when this occurs.

see this, study the derivative of n_λ as we move along the brane,

$$\ell^\mu \nabla_\mu (n_\lambda) = \ell^\mu \nabla_\mu (n_\sigma k^\sigma) = \ell^\mu k^\sigma \nabla_\mu n_\sigma + \ell^\mu n_\sigma \nabla_\mu k^\sigma \tag{5.27}$$

Using

$$\begin{aligned}
k^\sigma &= n_\lambda n^\sigma + \ell^\sigma, \\
0 &= n^\nu \nabla_\mu n_\nu, \\
0 &= k^\mu \nabla_\mu k^\nu,
\end{aligned} \tag{5.28}$$

this becomes

$$\ell^\mu \nabla_\mu (n_\lambda) = \ell^\mu \ell^\sigma \nabla_\mu n_\sigma - n_\lambda n^\mu n_\sigma \nabla_\mu k^\sigma. \tag{5.29}$$

Since initially $n_\lambda = 0$, if we establish that $\nabla_\lambda n_\lambda \geq 0$ whenever $n_\lambda = 0$, we are done. But when $n_\lambda = 0$ the above is just

$$\nabla_\lambda n_\lambda = \ell^\mu \ell^\sigma \nabla_\mu n_\sigma = -\ell^a \ell^b K_{ab} \geq 0 \tag{5.30}$$

where the minus sign in the second equality is introduced because K_{ab} is defined using the inward pointing normal vector, whereas the normal vector appearing in Stokes theorem was outward pointing. The inequality is just the NEC imposed on the brane. How the curvature in the brane prevents a sign change in n_λ is illustrated in Fig. 5.4.

5.3.2 Proof of the connected wedge theorem

In this section we prove the $1 \to 2$ connected wedge theorem for asymptotically AdS spacetimes with an ETW brane. Our proof follows the earlier proof for the $2 \to 2$ connected wedge theorem appearing in [78, 154] closely, since a minor modification of the proof given there suffices to prove our theorem. We repeat the full proof in order to explain this modification clearly, and to keep the chapter self-contained.

The proof relies on three assumptions: (i) that the null energy condition holds in the
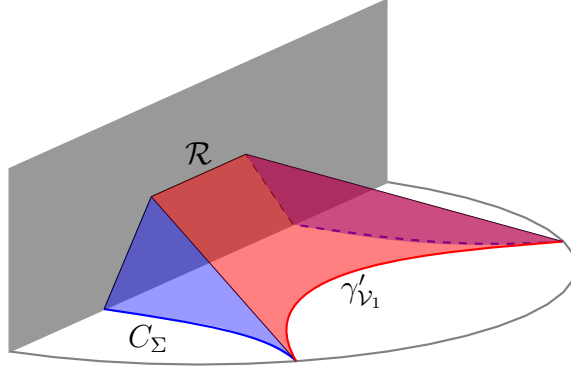
Figure 5.5: The null membrane. The red surface is the lift $\mathcal{L}$, the blue surfaces make up the slope. The ridge $\mathcal{R}$, is where the lift meets the brane.

bulk; (ii) that the null energy condition holds for the branes stress tensor; and (iii) that the maximin procedure [43, 156, 46] for finding HRRT surfaces is correct even in the context of AdS/BCFT.

Given these assumptions, the outline of the proof of Theorem 1 is as follows. We suppose, by way of contradiction, that $J_{1\to12} \neq \varnothing$ and the HRRT surface for region $\hat{\mathcal{V}}_1$ is brane-detached. Call this surface $\gamma'_{\mathcal{V}_1}$. According to the maximin procedure, this surface is minimal in some Cauchy slice Σ. We'll use the focusing theorem and the fact that $J^{\mathcal{E}}_{1\to12} \neq \varnothing$ to construct a smaller area surface in Σ which is brane-connected, called the *contradiction surface* C_Σ. This provides a contradiction with $\gamma'_{\mathcal{V}_1}$ having been the HRRT surface, showing the correct HRRT surface must be brane-attached.

To begin, we consider two cases, corresponding to the boundary scattering region

$$\hat{J}^{\mathcal{E}}_{1\to12} = \hat{J}^+(\hat{\mathcal{C}}_1) \cap \hat{J}^-(\hat{\mathcal{R}}_1) \cap \hat{J}^-(\hat{\mathcal{R}}_2) \cap \mathcal{B} = \hat{\mathcal{V}}_1 \cap \mathcal{B} \qquad (5.31)$$

being empty or non-empty. If it is non-empty, then $\hat{\mathcal{V}}_1$ is attached to the brane in the boundary, so its entanglement wedge is immediately brane attached and we are done. If it is empty, we proceed with the proof below.

Define the null surface

$$\mathcal{L} = \partial J^+(\mathcal{V}_1) \cap J^-(\mathcal{R}_1) \cap J^-(\mathcal{R}_2) \qquad (5.32)$$

201

which we call the *lift*. This is defined by taking the inward pointing null orthogonal vectors of $\gamma_{\mathcal{V}_1}$ as generators for a null congruence, and extending those geodesics until they reach the past of $\mathcal{R}_1$ or $\mathcal{R}_2$. Additionally, geodesics should not be extended past any caustic points — defining the lift in terms of $\partial J^+(\mathcal{V}_1)$ implements this for us, as geodesics leave the boundary of $J^+(\mathcal{V}_1)$ after developing a caustic.

There are two features of the lift that will be important. The first feature is that the lift has a non-empty intersection with the brane. To see this, recall that by assumption

$$J^{\mathcal{E}}_{1 \to 12} = J^+(\mathcal{C}_1) \cap J^-(\mathcal{R}_1) \cap J^-(\mathcal{R}_2) \cap \mathcal{B} \neq \varnothing. \tag{5.33}$$

Then, recall that since $\hat{\mathcal{C}}_i \subseteq \hat{\mathcal{V}}_i$, we have also $\mathcal{C}_i \subseteq \mathcal{V}_i$. Thus we learn

$$J^{\mathcal{E}}_{1 \to 12} \subseteq J^+(\mathcal{V}_1) \cap J^-(\mathcal{R}_1) \cap J^-(\mathcal{R}_2) \cap \mathcal{B} \neq \varnothing. \tag{5.34}$$

This gives that $J^+(\mathcal{V}_1)$ meets the brane while in the past of $\mathcal{R}_1$ and $\mathcal{R}_2$. In particular then the ridge, defined by

$$\mathcal{R} \equiv \mathcal{L} \cap \mathcal{B} \neq \varnothing \tag{5.35}$$

is non-empty.

The second important feature of the lift is that its boundary has a component $\mathcal{A}_1$ along $\partial J^-(\mathcal{R}_1)$ and a component $\mathcal{A}_2$ along $J^-(\mathcal{R}_2)$ which are separated by the ridge. The other possibility would be for the ridge to extend to one or more of the edges. This cannot occur however, which follows because the ridge is a subregion of the bulk scattering region, which by assumption does not extend to the boundary.

Next define a second null sheet which we call the *slope*,

$$\mathcal{S}_{\Sigma} = \partial[J^-(\mathcal{R}_1) \cap J^-(\mathcal{R}_2)] \cap J^-[\partial J^+(\mathcal{V}_1)] \cap J^+(\Sigma). \tag{5.36}$$

The slope is generated by past-directed null geodesics beginning as the inward, past directed null normals to $\gamma_{\mathcal{R}_1}$ and $\gamma_{\mathcal{R}_2}$, and extended until they reach Σ. We will be particu-

larly interested in

$$C_\Sigma \equiv S_\Sigma \cap \Sigma \tag{5.37}$$

which we introduced above as the contradiction surface. The lift, ridge, slope, and contradiction surface are shown in Fig. 5.5.

Now, we apply the focusing theorem in the form of equation (5.25) to the lift and to the slope. The lift is a portion of the boundary of the future of an extremal surface, $\partial J^+(\mathcal{V}_1)$, so focusing applies. We choose a parameterization such that the null generators begin on $\gamma_{\mathcal{V}_1}$ and end on $\mathcal{R} \cup \mathcal{A}_1 \cup \mathcal{A}_2 \cup B_{\mathcal{L}}$, where $B_{\mathcal{L}}$ is any caustics present in the lift. This leads to

$$\text{area}(\mathcal{A}_2) + \text{area}(\mathcal{A}_1) + 2\,\text{area}(B_{\mathcal{L}}) + \text{area}(\mathcal{R}) - \text{area}(\gamma'_{\mathcal{V}_1}) = \int \epsilon\,\theta \leq 0. \tag{5.38}$$

Similarly, we can apply (5.25) to the slope, which is a portion of $\partial[J^-(\mathcal{R}_1) \cap J^-(\mathcal{R}_2)]$. Choosing the parameterization such that generators begin on $\mathcal{A}_1 \cup \mathcal{A}_2$ and end on $C_\Sigma \cup B_{S_\Sigma}$, where B_{S_Σ} is any caustics present in the slope. We have then

$$\text{area}(C_\Sigma) + 2\,\text{area}(B_{S_\Sigma}) - \text{area}(\mathcal{A}_2) - \text{area}(\mathcal{A}_1) + \int_{S_\Sigma \cap \mathcal{B}} \mathrm{d}^{d-2}x\,\sqrt{\gamma}n_\lambda = \int \epsilon\,\theta \leq 0. \tag{5.39}$$

Adding these two inequalities and rearranging terms we obtain

$$\text{area}(\gamma'_{\mathcal{V}_1}) \geq \text{area}(C_\Sigma) + \text{area}(R) + \text{area}(B_{S_\Sigma}) + \text{area}(B_{\mathcal{L}}) + \int_{S_\Sigma \cap \mathcal{B}} \mathrm{d}^{d-2}x\,\sqrt{\gamma}n_\lambda,$$

$$\geq \text{area}(C_\Sigma) \tag{5.40}$$

where we've used that $n_\lambda \geq 0$, which follows when the NEC applied to the brane matter tensor holds, as shown at the end of the last section. This ensures that the brane-disconnected surface $\gamma'_{\mathcal{V}_1}$ is not of minimal area in the Cauchy slice Σ, so from the maximin procedure cannot be the correct HRRT surface, completing the proof.

We should highlight the modifications made from the similar proof of the $2 \rightarrow 2$

connected wedge theorem [78, 154]. In that case, there were four regions $\mathcal{C}_1, \mathcal{C}_2, \mathcal{R}_1$ and $\mathcal{R}_2$, and two decision regions $\mathcal{V}_1$ and $\mathcal{V}_2$. The lift was formed by a null congruence of geodesics starting on $\gamma_{\mathcal{V}_1} \cup \gamma_{\mathcal{V}_2}$. Points on the ridge corresponded to where a geodesic starting on $\gamma_{\mathcal{V}_1}$ collided with a geodesic starting on $\gamma_{\mathcal{V}_2}$, whereas in our setting the ridge is formed by generators from $\gamma'_{\mathcal{V}_1}$ colliding with the brane. Another distinction is the occurrence of the boundary $S_\Sigma \cap \mathcal{B}$ and associated term in (5.39). This is handled in our case by assuming the NEC holds for the brane stress tensor.

5.3.3   Comments on the $1 \to 2$ connected wedge theorem

The scattering region is inside the entanglement wedge

In the context of the $2 \to 2$ theorem, [78, 154] showed that the scattering region $J_{12 \to 12}$ is inside of the entanglement wedge of $\hat{\mathcal{V}}_1 \cup \hat{\mathcal{V}}_2$. It is straightforward to adapt either of the proofs given there to the $1 \to 2$ theorem, where the analogous statement is that $J^{\mathcal{E}}_{1 \to 12}$ is inside the entanglement wedge of $\hat{\mathcal{V}}_1$. Since $J^{\mathcal{E}}_{1 \to 12}$ lives in the brane, we can be more specific and say that $J^{\mathcal{E}}_{1 \to 12}$ is inside the island formed by $\hat{\mathcal{V}}_1 \cap \mathcal{B}$.

Relationship to $2 \to 2$ theorem and interface branes

It is possible to describe ETW brane geometries as a $\mathbb{Z}_2$ identification of an interface brane geometry. In particular, consider a spacetime $\mathcal{M}$ described by metric $g_{\mu\nu}(x^\mu)$ and satisfying the boundary condition

$$K_{ab} - K h_{ab} = -8\pi G_N T^{\mathcal{B}}_{ab} \tag{5.41}$$

at the ETW brane. Then we can define a doubled geometry featuring an interface brane, with metric $g_{\mu\nu}(x^\mu_+)$ on one side of the brane and a copy of that metric $g_{\mu\nu}(x^\mu_-)$ on the other. At the interface brane Einsteins equations require we satisfy the Israel junction

conditions

$$h_{ab}^+ = h_{ab}^-, \tag{5.42}$$

$$[K_{ab}^+ - K_{ab}^-] - [K^+ - K^-]h_{ab} = -8\pi G_N T_{ab}^I. \tag{5.43}$$

Setting $T_{ab}^I = 2T_{ab}^B$ satisfies this condition. Identifying points $x_+ = x_-$ then recovers the ETW brane geometry.

We can apply the $2 \to 2$ connected wedge theorem to this interface brane geometry, and in limited cases recover the $1 \to 2$ theorem. To do this choose $\hat{\mathcal{C}}_1$ and $\hat{\mathcal{C}}_2$ to be mirror images across the interface brane. Choose $\hat{\mathcal{R}}_1$ and $\hat{\mathcal{R}}_2$ to be intervals centered on the two CFT interfaces. Notice that the brane anchored scattering region $J_{1 \to 12}^{\mathcal{E}}$ is not empty if and only if the bulk scattering region $J_{12 \to 12}^{\mathcal{E}}$ in the interface geometry is not empty. Further, the entanglement wedge of $\hat{\mathcal{V}}_1 \cup \hat{\mathcal{V}}_2$ will be connected if and only if the entanglement wedge of $\hat{\mathcal{V}}_1$ connects to the brane in the ETW brane geometry. Thus, when the doubled geometry satisfies the conditions for the $2 \to 2$ theorem — in particular when the NEC holds in the doubled geometry — the $1 \to 2$ theorem follows from the $2 \to 2$ theorem.

Recall however the conditions for the $1 \to 2$ theorem: the bulk stress tensor and brane stress tensor should separately satisfy the NEC. There are many cases where these conditions hold, but in the associated interface brane geometry the NEC is violated. Consider for instance an ETW brane solution with

$$T_{\mu\nu} = 0,$$
$$T_{ab}^{\mathcal{B}} = -Th_{ab}. \tag{5.44}$$

Then in the interface brane geometry the stress tensor is

$$T_I^{\mu\nu} = -Th^{ab}e_a^\mu e_b^\nu \, \delta(x - x_0) \tag{5.45}$$

where the delta function is turned on at the interface. To study the NEC for $T_{\mu\nu}^I$, it's

convenient to rewrite this using the completeness relation,

$$g^{\mu\nu} = n^\mu n^\nu + h^{ab} e_a^\mu e_b^\nu \tag{5.46}$$

so that

$$T_I^{\mu\nu} \ell_\mu \ell_\nu = -T(g^{\mu\nu} - n^\nu n^\mu)\ell_\mu \ell_\nu = T(n^\mu \ell_\mu)^2 \tag{5.47}$$

We see that the NEC is satisfied if and only if $T > 0$. However, in the ETW brane geometry, the $1 \to 2$ theorem holds even for $T < 0$. Consequently we find that the $2 \to 2$ theorem applied to the interface geometry only recovers the $1 \to 2$ theorem in special cases.

Counterexample to the converse

We claimed in the introduction that the converse to Theorem 1 is false. In [78, 154], the authors constructed a counterexample to the converse of the $2 \to 2$ theorem. By taking a $\mathbb{Z}_2$ identification of the solution used in their example we can easily construct a counterexample to the converse of the $1 \to 2$ theorem. We do this in Fig. 5.6.

The out regions are not entangled

In the $2 \to 2$ connected wedge theorem, time reversal implies that in addition to the decisions regions having a connected entanglement wedge, an analogous pair of late time regions do as well, where the late time regions are defined by[10]

$$\hat{\mathcal{W}}_1 = J^-(\hat{\mathcal{R}}_1) \cap J^+(\hat{\mathcal{C}}_1) \cap J^+(\hat{\mathcal{C}}_2),$$
$$\hat{\mathcal{W}}_2 = J^-(\hat{\mathcal{R}}_2) \cap J^+(\hat{\mathcal{C}}_1) \cap J^+(\hat{\mathcal{C}}_2). \tag{5.48}$$

In the context of the $1 \to 2$ theorem one can define similar regions. To do so, we define points x_1, x_2 as the points where $\partial \hat{J}^+(\hat{\mathcal{C}}_1)$ reaches edge 1 and edge 2, respectively. Then

---

[10]We are interested here in the case where $\hat{\mathcal{W}}_i \subseteq \hat{\mathcal{R}}_i$, analogous to our condition $\hat{\mathcal{C}}_i \subseteq \hat{\mathcal{V}}_i$ on the input and decision regions.
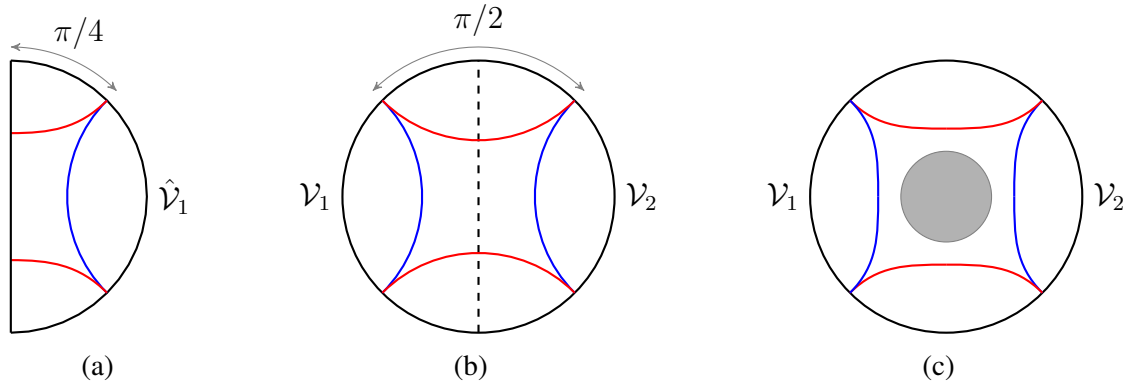
Figure 5.6: A counterexample to the converse of Theorem 1. (a) A constant time slice of a solution with a $T = 0$ brane sitting in pure AdS. These solutions are described in detail §5.4. We choose a region $\hat{\mathcal{V}}_1$ of size $\pi/2$ and which is centered between the two edges. This region sits exactly on the phase transition between brane-attached (red surface) and brane detached (blue surface), and the scattering region consists of a single point. (b) The $T = 0$ solution can be viewed as a $\mathbb{Z}_2$ identification of global AdS with the identification across $\rho = 0$. (c) In the unfolded geometry, we consider adding a spherically symmetric matter distribution (shown in grey). This delays light rays travelling from c_1 to the brane by some finite amount, closing the scattering region. Due to spherical symmetry, the region $\hat{\mathcal{V}}_1$ remains on the phase transition. Increasing its size infinitesimally then keeps the scattering region closed, while also ensuring the red, brane-attached surface is minimal.

we define

$$\hat{\mathcal{W}}_1' = \hat{J}^+(x_1) \cap J^-(\hat{\mathcal{R}}_1),$$
$$\hat{\mathcal{W}}_2' = \hat{J}^+(x_2) \cap J^-(\hat{\mathcal{R}}_2). \tag{5.49}$$

We can ask if $\hat{\mathcal{W}}_1'$ and $\hat{\mathcal{W}}_2$ must also be entangled when the entanglement scattering region is non-empty.

In fact, these regions do not need to be entangled. For an explicit counterexample, begin with the example shown in Fig. 5.6a, where $\hat{\mathcal{V}}_1$ consists of an interval of size $\pi/2$ centered between the two edges. Then the scattering region consists of a single point, and the minimal surface enclosing $\hat{\mathcal{W}}_1' \cup \hat{\mathcal{W}}_2'$ is on the transition from giving a connected and disconnected entanglement wedge. Now decrease the tension, moving the brane inward. This shortens the light travel time from $\hat{\mathcal{C}}_1$, so increases the size of the scattering region. Meanwhile, the disconnected surface enclosing $\hat{\mathcal{W}}_1' \cup \hat{\mathcal{W}}_2'$ loses area and becomes dominant, so that there is a non-empty scattering region but only $O(1)$ correlation between the $\hat{\mathcal{W}}_i$ regions.

$1 \to 1$ **theorem**

For completeness, we also point out a $1 \to 1$ connected wedge theorem, which follows from a simple tasks argument or from geometric observations. We consider two regions $\hat{\mathcal{C}}_1, \hat{\mathcal{R}}_1$, both in the AdS boundary, and define the scattering region,

$$J_{1\to 1}^{\mathcal{E}} = J^+(\mathcal{C}_1) \cap J^-(\mathcal{R}_1) \cap \mathcal{B}, \tag{5.50}$$

and the decision region,

$$\hat{\mathcal{V}}_1 = \hat{J}^+(\hat{\mathcal{C}}_1) \cap \hat{J}^-(\hat{\mathcal{R}}_1). \tag{5.51}$$

By analogy with the $1 \to 2$ theorem, we expect that $J_{1\to 1}^{\mathcal{E}}$ being non-empty implies the entanglement wedge of $\hat{\mathcal{V}}_1$ is brane-attached. To verify this, we can give both a tasks and geometric argument.

From tasks, we consider an input $H^q \left| b \right\rangle_A$ at $\mathcal{C}_1$ and output b at $\mathcal{R}_1$, with q recorded into the brane degrees of freedom. If $J^{\mathcal{E}}_{1 \to 1}$ is non-empty, then one can use a simple bulk strategy: travel to the brane, learn q, then send q to the output point where it can be used to undo H^q and recover b. In the bulk picture knowing q is necessary to successfully recover b, so $\hat{\mathcal{V}}_1$ must know q, so $\hat{\mathcal{V}}_1$ must have the brane in its entanglement wedge.[11].

To understand this from the geometric perspective, note that $J^+(\mathcal{C}_1) \cap J^-(\mathcal{R}_1)$ is inside the entanglement wedge of $\hat{\mathcal{V}}_1$, so $J^{\mathcal{B}}_{1 \to 1}$ non-empty means the brane is inside the entanglement wedge of $\hat{\mathcal{V}}_1$.

5.4   Vacuum AdS$_{2+1}$

In this section we give constant tension brane solutions in global AdS$_{2+1}$, then verify the connected wedge theorem by explicit calculations in that setting. In this case the converse of Theorem 1 holds, and a bulk scattering region is present if and only if the entanglement wedge is connected. This is similar to the situation for the $2 \to 2$ theorem, where the converse holds for vacuum AdS$_{2+1}$ [77].

5.4.1   Constant tension branes in global AdS$_{2+1}$

We will consider a simple model where the bulk matter action is set to zero, and the brane has constant tension. This corresponds to a Lagrangian

$$L^B_{\text{matter}} = -\frac{1}{8\pi G_N} T. \tag{5.52}$$

Extremizing the action (5.4), we obtain the vacuum Einstein's equations in the bulk and a boundary condition for the brane:

$$(K_{ab} - K h_{ab}) = -T h_{ab} \ . \tag{5.53}$$

---

[11]A more rigorous argument for this would follow the strategy of §5.2.

209
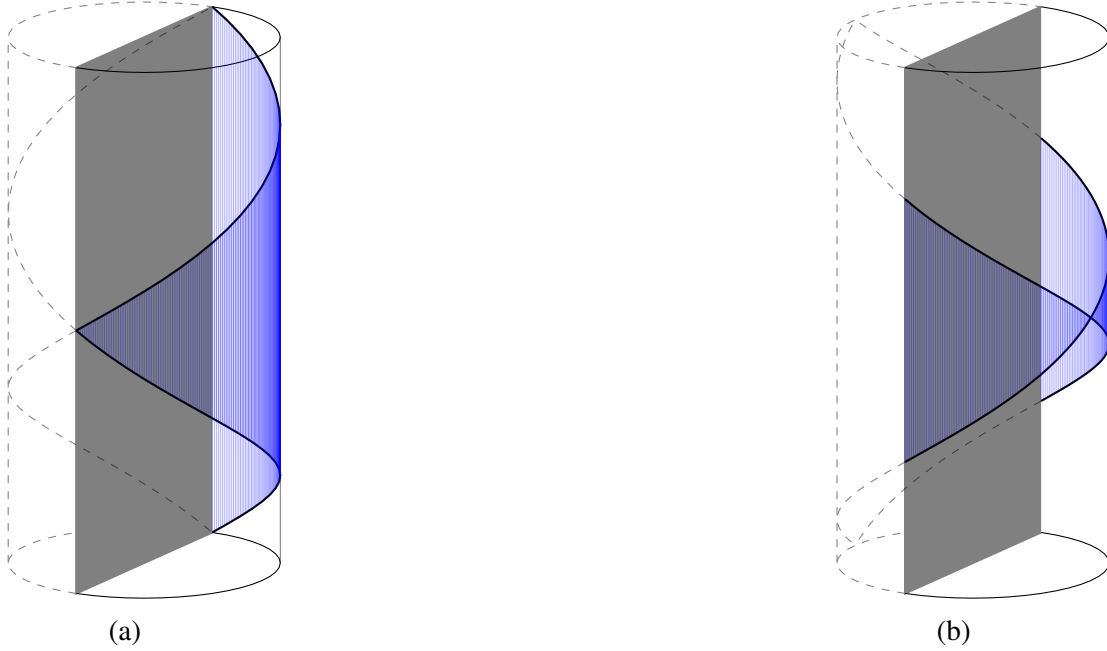
Figure 5.7: Global AdS$_{2+1}$ with a ETW brane. We've shown the $T = 0$ case for simplicity. Poincaré patches are shaded in blue. (a) An edge centered choice of Poinaré patch. In the associated Poincaré solution the ETW brane is flat, described by (5.57). (b) A Poincaré patch centered at $\sigma = 0$. In Poincaré coordinates the brane trajectory is a hyperbola, described by (5.60).

(a)   (b)
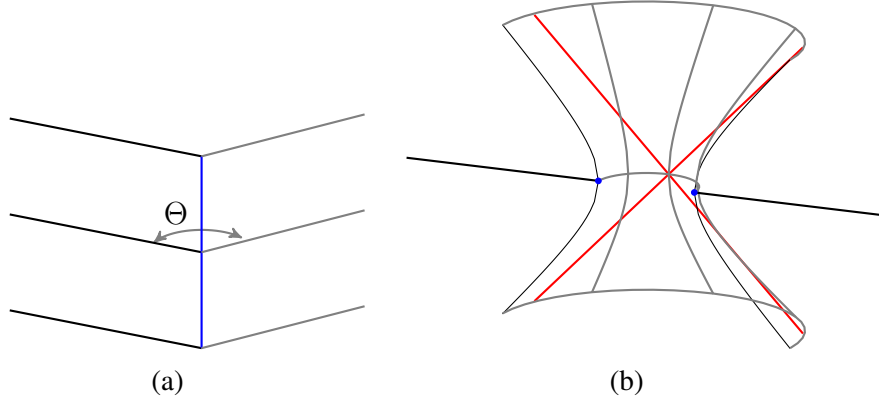
Figure 5.8: (a) Poincaré-AdS$_{2+1}$ with a constant tension ETW brane, as obtained by taking an edge-centered patch of the global spacetime, as shown in Fig. 5.7b. (b) Poincaré-AdS$_{2+1}$ with a constant tension ETW brane, as obtained by taking a patch as shown in Fig. 5.7a. The brane forms a hyperbola, and the two edge trajectories are $x = \pm\sqrt{1 + t^2}$. The horizons $\sigma = \pm\nu$ chosen in the global geometry map to $x = \pm t$, $z = (1 - \sin\Theta)/\cos\Theta$ in Poincaré coordinates, which we've shown in red.

We can solve this along with Einstein's equations. The solutions of interest are described by the metric

$$\mathrm{d}s_{2+1}^2 = \cosh^2\rho\,\mathrm{d}s_{1+1}^2 + \mathrm{d}\rho^2 = \cosh^2\rho\left(\ell^2\frac{-\mathrm{d}\nu^2 + \mathrm{d}\sigma}{\cos^2\sigma}\right) + \mathrm{d}\rho^2, \qquad (5.54)$$

with $\mathrm{d}s_{1+1}^2$ the line element for a global $1 + 1$ dimensional AdS space. Allowing $-\infty < \rho < \infty$, this is global AdS$_{2+1}$. To add an ETW brane we restrict to $\rho_0 < \rho < \infty$, where the brane is located at $\rho = \rho_0$ and

$$T = \frac{1}{\ell}\tanh(\rho_0/\ell). \qquad (5.55)$$

We will call the (ν, σ, ρ) coordinates *slicing coordinates*, since ρ foliates AdS$_{1+1}$ slices to form an $_{2+1}$ spacetime.

There are two ways of taking Poincaré patches of this spacetime that will be of interest to us. First, as shown in Fig. 5.7a, we can center our Poincaré patch on one of the edges,

211

$\sigma = \pm\pi/2$. The associated Poincaré coordinates are related to slicing coordinates by

$$t = \frac{\sin\nu}{\cos\nu - \sin\sigma}, \quad x = \frac{\cos\sigma\tanh\rho}{\cos\nu - \sin\sigma}, \quad z = \frac{\cos\sigma\,\mathrm{sech}\rho}{\cos\nu - \sin\sigma}. \tag{5.56}$$

Under this transformation the boundary becomes the half line $x > 0$, with one edge located at $x = 0$. The other edge is at $x = \infty$. The ETW branes trajectory is

$$\frac{x}{z} = \tan\Theta, \tag{5.57}$$

where Θ is related to the tension T by $\ell T = \sin\Theta$. Solutions of this form are shown in Fig. 5.8a.

Using this planar solution we can relate the bulk parameter T to CFT data. In the CFT, one can calculate the entropy of an interval of size L ending on the CFT-boundary,

$$S(L) = \frac{c_{\mathrm{bulk}}}{6}\log\frac{L}{\epsilon} + g_{\mathcal{B}}. \tag{5.58}$$

The second term is known as the *boundary entropy* [60], and counts the degrees of freedom located at the edge. The Ryu-Takayanagi prescription reproduces this entropy expression in the simple constant tension model if we relate the tension and boundary entropy according to

$$g_{\mathcal{B}} = \frac{\ell}{4G_N}\mathrm{arctanh}(\ell T). \tag{5.59}$$

The second Poincaré patch we will be interested in is centered at $\sigma = 0$, as shown in Fig. 5.7b. This coordinate change is most easily performed using the embedding space formalism, see §5.4.2. The ETW brane in this Poincaré patch is described by

$$x^2 - t^2 + (z + \tan\Theta)^2 = \sec^2\Theta \tag{5.60}$$

The edge trajectories are described by $t = \pm\sqrt{x^2 - 1}$. This solution was studied in Chapter 4 in the context of brane models of black holes and island formation, which we will also take up in §5.5. A solution of this type is shown in Fig. 5.8b.

5.4.2 *Coordinate systems and embedding space

Here, we briefly discuss the different coordinate systems used for AdS. Rather than explicitly map between coordinates, we use the embedding space formalism, following [157] closely. Recall that we can view AdS_{d+1} as (the universal cover of) the hyperboloid in $\mathbb{R}^{2,d-1}$, given by

$$X_0^2 + X_{d+1}^2 - \sum_{i=1}^d X_i^2 = \ell_{\mathrm{AdS}}^2 \ .$$

We set $\ell_{\mathrm{AdS}} = 1$ for convenience. Different choices of coordinates map to different parametrizations of this hyperboloid. For instance, consider standard global coordinates on AdS_{d+1}:

$$\mathrm{d}s_{d+1}^2 = -\cosh^2 \hat{\rho} \, \mathrm{d}\hat{t} + \mathrm{d}\hat{\rho}^2 + \sinh^2 \hat{\rho} \, \mathrm{d}\Omega_{d-1}^2 \ ,$$

where $\hat{t}$ is global (Lorentzian) time, and the Ω_i are spherical coordinates on $\mathbb{S}^{d-1}$. This corresponds to the parametrization

$$X_0 = \cosh \hat{\rho} \cos \hat{t}$$
$$X_i = \Omega_i \sinh \hat{\rho}$$
$$X_{d+1} = \cosh \hat{\rho} \sin \hat{t} \ .$$

We employ the slicing coordinates

$$\mathrm{d}s_{d+1}^2 = \cosh^2 \rho \, \mathrm{d}s_d^2 + \mathrm{d}\rho^2 \ ,$$

with global coordinates $\mathrm{d}s_d^2$ on the slices. This arises from the parametrization

$$X_0 = \cosh \rho \, \cosh r \cos \nu$$
$$X_a = \Omega_a \cosh \rho \sinh r$$
$$X_d = \sinh \rho$$
$$X_{d+1} = \cosh \rho \, \cosh r \sin \nu \ ,$$

where $a = 1, \ldots, d - 1$ correspond to spherical coordinates for $\mathbb{S}^{d-2}$ on the AdS_d slices. In the global coordinates on AdS_{d+1} or AdS_d, we can always compactify to the "Einstein static universe" coordinates $\hat{\sigma}, \sigma$ defined by

$$\tan \hat{\sigma} = \sinh \hat{\rho}, \quad \tan \sigma = \sinh \rho,$$

with (for instance)

$$\mathrm{d}s_d^2 = \frac{-\mathrm{d}\nu^2 + \mathrm{d}\sigma^2 + \sin^2 \theta \, \mathrm{d}\Omega_{d-2}^2}{\cos^2 \sigma}. \tag{5.61}$$

Note that for $d > 2$, $\rho > 0$, and hence $\sigma \in [0, \pi/2)$. However, for $d = 2$, we can trade in the 0-sphere $\Omega^0 = \{\pm 1\}$ and take $\rho \in \mathbb{R}$, hence $\sigma \in [-\pi/2, \pi/2)$. This is the coordinate system used in (5.54). Finally, there is the Poincaré slicing,

$$\mathrm{d}s_{d+1}^2 = \frac{1}{z^2}(-\mathrm{d}t^2 + \mathrm{d}x^2 + x^2 \mathrm{d}\Omega_{d-2}^2) \,,$$

with parametrization

$$X_0 = \frac{1}{2z}(z^2 + x^2 - t^2 + 1)$$
$$X_a = \frac{x\Omega_a}{z}$$
$$X_d = \frac{1}{2z}(z^2 + x^2 - t^2 - 1)$$
$$X_{d+1} = \frac{t}{z} \,.$$

For a brane at fixed $\rho = \rho_0$, setting X_d equal in these three parametrizations leads to

$$\sinh \rho_0 = \Omega_d \sinh \hat{\rho} = \frac{1}{2z}(z^2 + x^2 - t^2 - 1) \,. \tag{5.62}$$

5.4.3 Null rays and entanglement

In the solutions (5.54), we will check the theorem in the case that the input and output regions are points, $\hat{\mathcal{C}}_1 = \{c_1\}$ and $\hat{\mathcal{R}}_i = \{r_i\}$. We will calculate the travel time of null rays in the geometry (5.54), used to perform the bulk local strategy, and compare to a calculation of entanglement entropy on the field theory side.

We can transform slicing coordinates (5.54) into the following form:

$$ds_{2+1}^3 = \frac{\cosh^2 \rho}{\sin^2 \theta}(-d\nu^2 + d\theta^2 + \sin^2 \theta \, d\varphi^2) , \tag{5.63}$$

where $\ell_{\mathrm{AdS}} = 1$, $\theta = \sigma + \pi/2 \in [0, \pi]$, and $\varphi \in [\varphi_{\mathcal{B}}, \pi]$ is a warping coordinate for the copies of AdS_{1+1}, with $\varphi = 0$ the position of the asymptotic region and $\varphi = \varphi_{\mathcal{B}}$ the location of the brane. While the brane has the geometry of a copy of global AdS_{1+1}, the bulk is conformally equivalent to a patch of $\mathbb{R} \times \mathbb{S}^2$ enclosed by two lines of longitude. In these coordinates, it is easy to trace out light cones. As discussed in more detail below, if Alice sends a signal from $c_1 = (0, \theta_0)$ light rays will arrive at the brane at angle θ at a time

$$\cos[\nu(\theta)] = \cos \theta_0 \cos \theta + \sin \theta_0 \sin \theta \cos \varphi_{\mathcal{B}} . \tag{5.64}$$

Next we study the von Neumann entropy of subregions of the CFT. This can obtained using the replica trick in the BCFT. We start by analytically continuing the Lorentzian metric (5.63) to Euclidean time $\tau = i\nu$, and choose a defining factor to obtain the BCFT on $M_E = \mathbb{R} \times [0, \pi]$. Following the calculation of [2], we can calculate the entanglement entropy of the (Euclidean) interval $A := [w_1, w_2]$, for $w_j = \tau_j + i\theta_j$. The phase transition occurs at

$$e^{12g_{\mathcal{B}}/c} = \left| \frac{\cosh(\Delta\tau) - \cos(\Delta\theta)}{2 \sin(\theta_1) \sin(\theta_2)} \right| , \tag{5.65}$$

where $\Delta w = w_2 - w_1 = \Delta\tau + i\Delta\theta$, $\Delta\theta = \theta_2 - \theta_1$ and $\Delta\tau = \tau_2 - \tau_1$, c is the central charge of the CFT, and $g_{\mathcal{B}} := \log\langle 0|B\rangle$ is the boundary entropy.

Let us see how this comes about.

Light rays

Let's consider the reflection of bulk light rays in the simplest case, vacuum AdS_{2+1} with a brane of tension T. We can write the global metric (for $\ell_{AdS} = 1$) in the slicing coordinates AdS_{1+1}:

$$ds_{2+1}^2 = \cosh^2 \rho\, ds_{1+1}^2 + d\rho^2 = \cosh^2 \rho \left(\frac{-d\nu^2 + d\theta^2}{\sin^2 \theta} \right) + d\rho^2, \qquad (5.66)$$

where ρ_0 is the position of the brane and $\rho = \infty$ the boundary, global Lorentzian time is $\nu \in \mathbb{R}$, and $\theta = \sigma + \pi/2 \in [0, \pi]$. Null rays are simple in conformally flat coordinates, which we find by defining a new warping coordinate

$$\varphi = \frac{\pi}{2} + 2\tan^{-1}\left[\tanh\left(\frac{\rho}{2}\right)\right] = 2\tan^{-1} e^{\rho}, \quad d\varphi^2 = \frac{d\rho^2}{\cosh^2 \rho}, \qquad (5.67)$$

with $\varphi \in [\varphi_{\mathcal{B}}, \pi]$ for a brane at $\varphi_{\mathcal{B}} = \varphi(\rho_0)$. Then our global metric becomes

$$ds_3^2 = \frac{\cosh^2 \rho}{\sin^2 \theta}(-d\nu^2 + d\theta^2 + \sin^2 \theta\, d\varphi^2), \qquad (5.68)$$

which is conformally equivalent to patch of $\mathbb{S}^2 \times \mathbb{R}$ enclosed by two lines of longitude. Since null rays do not see the conformal factor, our problem reduces to propagating light rays on the sphere. With respect to some affine parameter λ, we have null geodesic equation

$$-\dot{\nu}^2 + \dot{\theta}^2 + \sin^2 \theta\, \dot{\varphi}^2 = 0.$$

If we set $\dot{\nu} = 1$, our problem reduces to finding geodesic lengths on the sphere, with affine time measuring these lengths.

A null ray will start at some initial point θ_0 and with some initial direction θ_0' at the boundary $\varphi = \pi$. It travels into the bulk, reflects off the brane at $\varphi_{\mathcal{B}}$, and finally returns to the boundary at some final position θ_1. From the cosine rule for spherical trigonometry, the geodesic distance to the brane obeys

$$d = \cos^{-1}[\cos \theta_0 \cos \theta_1 + \sin \theta_0 \sin \theta_1 \cos(\varphi_{\mathcal{B}})]. \qquad (5.69)$$

Thus, the global time it takes a null ray to reach the brane with respect to the parameterization $\dot{\nu} = 1$ is

$$\nu(\theta) = \cos^{-1}\left[\cos\theta_0\cos\theta + \sin\theta_0\sin\theta\cos(\varphi_{\mathcal{B}})\right]. \tag{5.70}$$

Entanglement entropy

We now calculate entanglement entropy from the field theory side.

First, we analytically continue $\tau = i\nu$, so that

$$ds_3^2 = \frac{\cosh^2\rho}{\sin^2\theta}(d\tau^2 + d\theta^2 + \sin^2\theta\,d\varphi^2). \tag{5.71}$$

Choosing a defining function to remove the prefactor as we approach the boundary, the dual BCFT is defined on $[0, \pi] \times \mathbb{R}$. The first step is to map the strip to the upper half-plane (UHP), $z = x + iy$ for $y \geq 0$. Let $w = \tau + i\theta = \log z$. Then correlation functions for primary operators $\mathcal{O}_i$ on the strip and UHP are related by

$$\langle\mathcal{O}_1(w_1)\cdots\mathcal{O}_k(w_k)\rangle_{\text{strip}} = \prod_i |z_i|^{\Delta_i}\langle\mathcal{O}_1(z_1)\cdots\mathcal{O}_k(z_k)\rangle_{\text{UHP}}. \tag{5.72}$$

We define the distances $z_{ij} = |z_i - z_j|$ and $z_{i\bar{j}} = |z_j - \bar{z}_j|$ for future convenience.

A twist operator creates an n-fold branched cover of the geometry via boundary conditions. The one-point function for a twist in the presence of a boundary is

$$\langle\Phi_n(w_1)\rangle_{\text{strip}} = \left|\frac{z_1}{z_{1\bar{1}}}\right|^{d_n} e^{(1-n)g_{\mathcal{B}}}, \tag{5.73}$$

where the twist scaling dimension for central charge c and replica number n is given by [63]

$$d_n = \frac{c}{12}\left(n - \frac{1}{n}\right). \tag{5.74}$$

A gap and small OPE coefficients [2] imply the simple form for a correlator of twists:

$$\langle \Phi_n(w_1)\Phi_{-n}(w_2)\rangle_{\text{strip}} = \min\left\{ \left|\frac{z_1 z_2}{z_{12}^2}\right|^{d_n}, \left|\frac{z_1 z_2}{z_{1\bar{1}} z_{2\bar{2}}}\right|^{d_n} e^{2g_{\mathcal{B}}(1-n)} \right\}.$$

(5.75)

The entanglement entropy is given by the limit

$$
\begin{aligned}
S_{w_1 w_2} &= \lim_{n\to 1^+} \frac{1}{1-n} \log\langle \Phi_n(w_1)\Phi_{-n}(w_2)\rangle_{\text{strip}} \\
&= \min\left\{ \frac{c}{6}\log\left|\frac{z_{12}^2}{z_1 z_2}\right|, \frac{c}{6}\log\left|\frac{z_{1\bar{1}} z_{2\bar{2}}}{z_1 z_2}\right| + 2g_{\mathcal{B}} \right\}.
\end{aligned}
$$

(5.76)

We have neglected the UV regulator, since it cancels when we calculate the transition between expressions. This occurs at

$$e^{12g_{\mathcal{B}}/c} = \left|\frac{z_{12}^2}{z_{1\bar{1}} z_{1\bar{2}}}\right| = \left|\frac{\cosh(\Delta\tau) - \cos(\Delta\theta)}{2\sin(\theta_1)\sin(\theta_2)}\right|$$

(5.77)

where $w_j = \tau_j + i\theta_j$, $\Delta\tau = \tau_2 - \tau_1$, and $\Delta\theta = \theta_2 - \theta_1$. Reverting to $\nu = -i\tau$, this becomes

$$e^{12g_{\mathcal{B}}/c} = \left|\frac{\sin[(\Delta\theta + \Delta\nu)/2]\sin[(\Delta\theta - \Delta\nu)/2]}{\sin(\theta_1)\sin(\theta_2)}\right|.$$

(5.78)

A connected wedge

To relate the location of the brane in different coordinates, first note that

$$\rho_0 = \frac{6}{c}g_{\mathcal{B}}\ .$$

Hence, by (5.67),

$$e^{12g_{\mathcal{B}}/c} = \tan^2\left(\frac{\varphi_{\mathcal{B}}}{2}\right)\ .$$

(5.79)

Consider an input point $c_1 = (\theta_0, 0)$, and two edge output points $r_1 = (0, t_1)$, $r_2 = (\pi, t_2)$. The backward light cones intersect at coordinates

$$x = \frac{1}{2}(\nu_1 - \nu_2 + \pi, \nu_1 + \nu_2 - \pi) = (\theta_1, \nu_g).$$

(5.80)

218

Similarly, the forward light cone of c_1 and the backward cone of x intersect at two points,

$$L = (\theta_L, \nu_L) = \frac{1}{2}(\theta_1 + \theta_0 - \nu_g, \theta_0 - \theta_1 + \nu_g) \tag{5.81}$$

$$R = (\theta_R, \nu_R) = \frac{1}{2}(\theta_1 + \theta_0 + \nu_g, \theta_1 - \theta_0 + \nu_g) . \tag{5.82}$$

In order to successfully use a bulk strategy, Alice must send a bulk light ray so that it hits the brane in the past of the point on the brane with boundary coordinates x. The extreme case is when her null ray hits x itself. From (5.69), this occurs at a boundary time $\nu_\mathcal{B}$ given by

$$\cos(\nu_\mathcal{B}) = \cos\theta_0 \cos\theta_1 + \sin\theta_0 \sin\theta_1 \cos(\varphi_\mathcal{B}). \tag{5.83}$$

We expect that this is precisely the time at which (L, R) experiences a phase transition in entanglement entropy. From (5.78), the transition occurs at

$$e^{12g_\mathcal{B}/c} = \tan^2\left(\frac{\varphi_\mathcal{B}}{2}\right) = \left|\frac{\sin[(\nu_g + \theta_1 - \theta_0)/2]\sin[(\nu_g + \theta_0 - \theta_1)/2]}{\sin[(\theta_0 + \theta_1 - \nu_g)/2]\sin[(\theta_0 + \theta_1 - \nu_g)/2]}\right|$$
$$= \left|\frac{\cos\nu_g + \cos(\theta_1 - \theta_0)}{\cos\nu_g - \cos(\theta_1 - \theta_0)}\right| , \tag{5.84}$$

where we have simplified with trigonometric identities. To verify the connected wedge theorem, we will show from (5.83) and (5.84) that $\nu_g = \nu_\mathcal{B}$. We first use the trigonometric identity

$$\tan^2\left(\frac{\varphi_\mathcal{B}}{2}\right) = \frac{1 - \cos(\varphi_\mathcal{B})}{1 + \cos(\varphi_\mathcal{B})} . \tag{5.85}$$

We can isolate $\cos(\varphi_\mathcal{B})$ in (5.83). Substituting this expression into (5.85) yields

$$\tan^2\left(\frac{\varphi_\mathcal{B}}{2}\right) = \frac{\sin\theta_0 \sin\theta_1 + \cos\theta_0 \cos\theta_1 - \cos\nu_\mathcal{B}}{\sin\theta_0 \sin\theta_1 - \cos\theta_0 \cos\theta_1 + \cos\nu_\mathcal{B}} = \left|\frac{\cos\nu_\mathcal{B} + \cos(\theta_1 - \theta_0)}{\cos\nu_\mathcal{B} - \cos(\theta_1 - \theta_0)}\right| . \tag{5.86}$$

Comparing to (5.84), we find $\nu_\mathcal{B} = \nu_g$ as claimed.

Returning to Lorentzian time, $\nu = -i\tau$, (5.65) gives

$$e^{12g_\mathcal{B}/c} = \left|\frac{\sin[(\Delta\theta + \Delta\nu)2]\sin[(\Delta\theta - \Delta\nu)2]}{\sin(\theta_1)\sin(\theta_2)}\right| . \tag{5.87}$$

We note that the brane angle $\varphi_{\mathcal{B}}$ is related to the boundary entropy by

$$e^{6g_{\mathcal{B}}/c} = \tan\left(\frac{\varphi_{\mathcal{B}}}{2}\right) . \tag{5.88}$$

This follows from (5.59) and the relation $c = 3\ell_{\mathrm{AdS}}/2G_N$. In the next section, we combine these facts about light rays and entanglement to confirm the connected wedge theorem for pure AdS_{2+1} ended by constant tension branes.

5.4.4   A check of the connected wedge theorem

Let $c_1 = (0, \theta_0)$ be the input point. Without loss of generality, consider output points r_0, r_π on opposite edges.[12] The backward light cones for these points intersect at some point $x = (\nu_1, \theta_1)$, and hence the decision region is $\hat{\mathcal{V}}_1 = \hat{J}^+(c_1) \cap \hat{J}^-(x)$. If $\hat{\mathcal{V}}_1$ intersects the edges of the BCFT, then the boundary local strategy can be trivially performed: Alice travels to the edge, decodes her qubit, and sends the results to r_0 and r_π.

We will be interested in the case where this strategy cannot be performed, and hence $\hat{\mathcal{V}}_1 = \hat{D}[A]$ for a boundary interval A with endpoints

$$L = (\theta_L, \nu_L) = \frac{1}{2}(\theta_1 + \theta_0 - \nu_g, \theta_0 - \theta_1 + \nu_g), \tag{5.89}$$

$$R = (\theta_R, \nu_R) = \frac{1}{2}(\theta_1 + \theta_0 + \nu_g, \theta_1 - \theta_0 + \nu_g) . \tag{5.90}$$

To perform a bulk local strategy, Alice must shoot null rays in the bulk so they intersect the brane in the past of the point on the brane with boundary coordinates x. This strategy marginally succeeds when the light ray hits x itself.[13] If she sends it from c_1, (5.64) tells us it arrives at the brane at a time $\nu_{\mathcal{B}}$ obeying

$$\cos \nu_{\mathcal{B}} = \cos \theta_0 \cos \theta_1 + \sin \theta_0 \sin \theta_1 \cos \varphi_{\mathcal{B}} . \tag{5.91}$$

---

[12]If they are on the same edge, $\hat{V}_1$ intersect the edge and the theorem is trivially true.

[13]From (5.63), we note that each AdS_{1+1} slice is conformally equivalent to the flat boundary. Since this conformal factor is invisible to light rays, the point of intersection on the brane has the same boundary coordinates as the intersection on the boundary.

Our connected wedge theorem states that when this ray can arrive at x, or $\nu_{\mathcal{B}} \leq \nu_1$, A has a brane-connected entanglement wedge.

Using equations (5.87)–(5.90), the transition to a brane-connected entanglement wedge occurs at a time t_g obeying

$$\tan^2\left(\frac{\varphi_{\mathcal{B}}}{2}\right) = \left|\frac{\cos\nu_g + \cos(\theta_1 - \theta_0)}{\cos\nu_g - \cos(\theta_1 - \theta_0)}\right|. \tag{5.92}$$

Fixing θ_0, θ_1 and solving for ν_1, some algebra shows it obeys (5.91). In other words, the transition to a connected entanglement wedge occurs precisely when the bulk local strategy becomes possible. This explicitly verifies the connected wedge theorem for vacuum AdS_{2+1}.

As a simple illustration take $\theta_0 = \theta_1 = \pi/2$, corresponding to edge output points at equal times. From (5.88), the phase transition occurs at a time ν_g given by

$$\tan^2\left(\frac{\varphi_{\mathcal{B}}}{2}\right) = \left|\frac{\sin^2(\nu_g/2)}{\sin[(\pi + \nu_g)/2]\sin[(\pi - \nu_g)/2]}\right| = \tan^2\left(\frac{\nu_g}{2}\right),$$

in other words, when $\nu_P = \varphi_{\mathcal{B}}$. But from (5.64), a light ray from c_1 arrives at the brane at time $\nu_{\mathcal{B}} = \varphi_{\mathcal{B}}$. So the phase transition occurs precisely when Alice is able to perform the quantum task using the bulk local strategy.

5.5 The connected wedge theorem and islands

In this section, we point out that, in brane models, the $1 \to 2$ connected wedge theorem reveals the formation of islands in the Ryu-Takayanagi formula. Indeed from the perspective of physics on the brane, the RT surface attaching to the brane corresponds to the formation of an island [6, 76, 149, 150, 151, 152, 153]. The connected wedge theorem then relates the formation of this island to causal features of the higher dimensional AdS geometry. In this section we make more precise how we can view the brane as a black hole and a portion of the CFT as the radiation system, and finally apply the connected wedge theorem in this context.
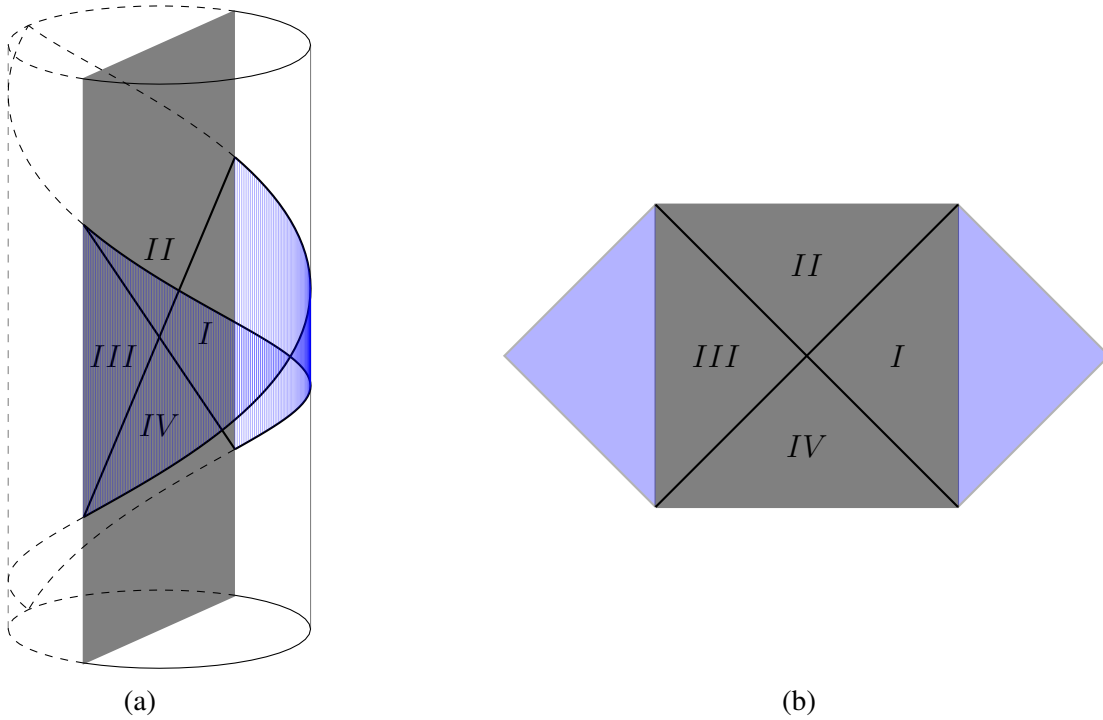
Figure 5.9: Choosing an appropriate Poincaré patch of the global spacetime, we find a two-sided black hole geometry (on the brane) coupled to two flat regions (wedges of the CFT). The end points of the two flat regions are coupled in the global picture. Note that we are most interested in the case where $T \approx 1$ and gravity localizes to the brane. We have drawn the $T = 0$ case however to simplify the diagram.

5.5.1 The black hole and the radiation system

We will focus on the solutions described in §5.4, which have a constant tension brane ending a pure, global, AdS_{2+1} spacetime. We are most interested in the case where $T \approx 1$, where gravity localizes to the brane [138]. As noted in the introduction, choosing $\hat{C}_1, \hat{R}_1, \hat{R}_2$ to be extended regions gives no additional power to the connected wedge theorem in these solutions, and consequently for simplicity we will take $\hat{C}_1 = c_1$, $\hat{R}_1 = r_1$, $\hat{R}_2 = r_2$ where c_1, r_1, r_2 are points on the boundary of AdS, and in particular r_1, r_2 sit in the edge.

For constant tension solutions we have two simplifications that will prove useful in understanding the connected wedge theorems relationship to islands. The first simplification is that for constant tension branes light rays run tangent to the brane. This allows us to define horizons in the brane by choosing points r_1 and r_2 on the edge, and considering their forward light cones,

$$
\begin{aligned}
H_1 &= [\partial J^+(r_1)]_{\mathcal{B}}, \\
H_2 &= [\partial J^+(r_2)]_{\mathcal{B}}.
\end{aligned}
\tag{5.93}
$$

These horizons intersect at $p_{\mathcal{B}} = (\sigma = 0, \nu = 0)$. From these horizons, define regions $I - IV$ as in Fig. 5.9. Region II is the black hole interior, while I and IV are the right and left exteriors.

The second simplification is that the $1 \rightarrow 2$ theorem is if and only if for constant tension solutions. This will let us conclude that an island forms if and only if a certain scattering configuration occurs. This is not essential, as we may still be interested in a sufficient condition for the formation of an island.

To make the black hole features of these constant tension brane solutions more explicit, consider going to the Poincaré patch shown in Fig. 5.9a. This patch includes the entire black hole, along with two wedge shaped portions of the CFT and a portion of the AdS bulk. Forgetting the bulk picture and focusing on the brane coupled to CFT picture, we have the spacetime shown in Fig. 5.9b.

Explicitly the Poincaré patch is described by a metric

$$ds^2 = \frac{\ell^2}{z^2}(-dt^2 + dx^2 + dz^2) \tag{5.94}$$

with brane located at

$$x^2 - t^2 + (z + \tan\Theta)^2 = \sec^2\Theta, \tag{5.95}$$

where Θ is related to the tension T according to $T = \sin\Theta$. The Poincaré patch includes only the $-\pi/2 < \nu < \pi/2$ portion of the brane. The points r_1 and r_2 are mapped to $x = t = -\infty$ and $-x = t = -\infty$. The details of this coordinate change are given in §5.4.2.

In Poincaré coordinates the edge trajectory is $x = \pm\sqrt{1+t^2}$. These trajectories asymptote to the light rays $x = \pm t$. Mapping the horizons $v = \pm\sigma$ to Poincaré we find horizons

$$z = \frac{1 - \sin\Theta}{\cos\Theta} \quad , \quad x = \pm t. \tag{5.96}$$

One can also verify directly in the Poincaré geometry that these are the horizons by studying null geodesics in the brane geometry, as in the previous chapter.

Next we should identify the radiation system. The entire CFT is coupled to the black hole at the two edges, and information can escape from the black hole into anywhere in the CFT. It seems sensible however to not consider the portion of the CFT which reconstructs the black hole exterior regions as being part of the radiation system. It is straightforward to identify the CFT dual to the left and right exterior black hole regions. The interval $Y_1 = \{\sigma \in (-\pi/2, 0), \nu = 0\}$ has region I inside its entanglement wedge. Similarly the interval $Y_2 = \{\sigma \in (0, \pi/2), \nu = 0\}$ has region II inside its entanglement wedge. This excludes $D(Y_1)$ and $D(Y_2)$ from the radiation system.

The remaining portion of the CFT is the future and past of the point

$$x = (\nu = 0, \sigma = 0, \rho = \infty). \tag{5.97}$$

224

The future of x reconstructs region II of the brane, so we should identify this with the radiation system. To specify that radiation has been collected only up until a certain time, we can choose a second point c_1 and define

$$\hat{R} = J^+(x) \cap J^-(c_1). \tag{5.98}$$

For c_1 at an early time so that R is small, the entanglement wedge of R will be disconnected from the brane, and R does not see inside of the black hole. At late enough times though, $\mathcal{E}_W(R)$ connects to the brane. Where this transition occurs will be controlled by the connected wedge theorem. Note also that since the minimal surfaces are at constant σ, they will in fact lie exactly on the horizons. This is illustrated in Fig. 5.10.

5.5.2   The connected wedge theorem and behind the horizon

Finally, we can apply the connected wedge theorem to this black hole on the brane. In fact, we need a time reversed variant of the theorem, which follows immediately from Theorem 1 (we also specialize to the case where the input and output regions are points),

Theorem 5. *($2 \rightarrow 1$ **connected wedge theorem**) Consider three points r_1, r_2, c_1 in an asymptotically AdS$_{2+1}$ spacetime with an end-of-the-world brane, with c_1 in the boundary and r_1, r_2 on the edge. Then if*

$$J_{12 \to 1} = J^+(r_1) \cap J^+(r_2) \cap J^-(c_1) \tag{5.99}$$

is non-empty, the entanglement wedge of

$$\hat{\mathcal{V}}_1 = \hat{J}^+(r_1) \cap \hat{J}^+(r_2) \cap \hat{J}^-(c_1) \tag{5.100}$$

is attached to the brane.

The two input points of the theorem we identify with the points r_1 and r_2 we used above to define the black hole horizons H_1 and H_2. The region $\hat{\mathcal{V}}_1$ becomes the subsystem of the radiation which has been collected since $J^+(r_1) \cap J^+(r_2) = J^+(x)$, so $\hat{\mathcal{V}}_1 = \hat{R}$.
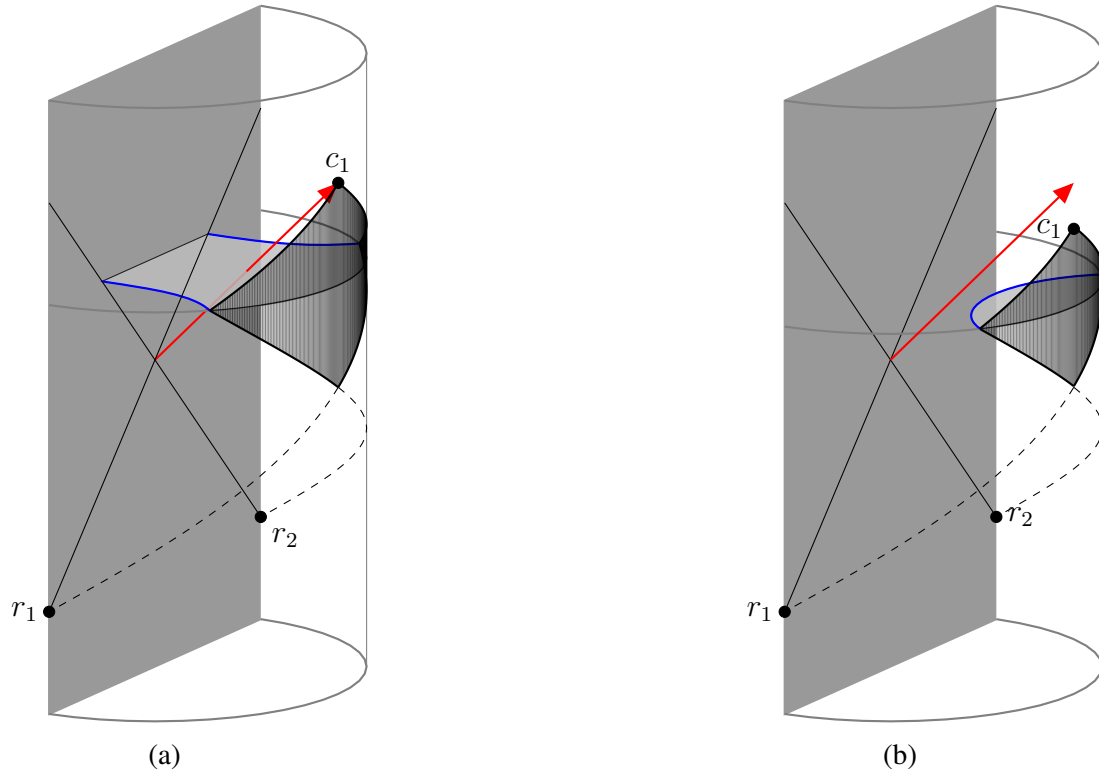
Figure 5.10: Theorem 1 along with time reversal implies a $2 \to 1$ connected wedge theorem. We can view the light rays beginning at r_1 and r_2 as defining the horizons of a black hole. The region $\hat{\mathcal{V}}_1$ is then the radiation system. (a) When a light ray reaches $\hat{\mathcal{V}}_1$ from the black hole interior, the entanglement wedge of $\hat{\mathcal{V}}_1$ must connect to the brane, so that $\hat{\mathcal{V}}_1$ reconstructs a portion of the interior. (b) When the black hole is causally disconnected from the black hole interior, the entanglement wedge of $\hat{\mathcal{V}}_1$ may be disconnected from the brane.
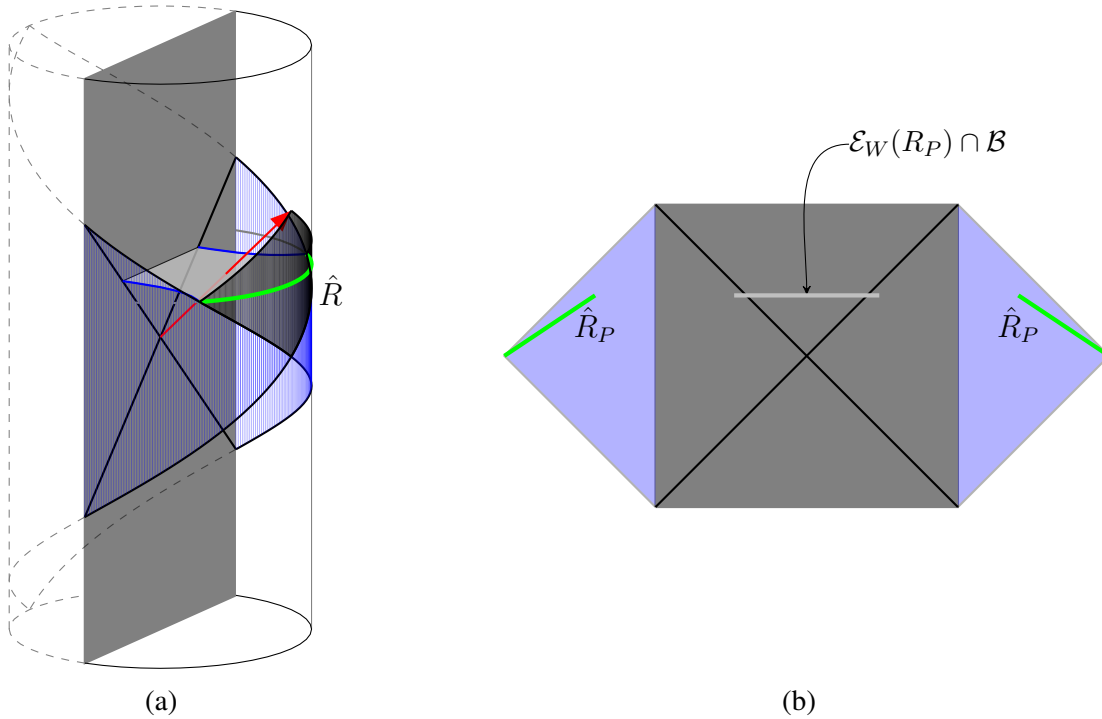
Figure 5.11: (a) The radiation system R (time-slice in green) picked out by the connected wedge theorem sits outside the Poincaré patch. (b) A nearby region $\hat{R}_P$ inside the patch has $\hat{R}_1$ inside of its domain of dependence, so that $\hat{R}_P$ has an island whenever $\hat{R}_1$ does. The entanglement wedge of $\hat{R}_P$ (shown in light gray) will include a small portion of the black hole exterior in its entanglement wedge.

Applying Theorem 5 along with its converse (which holds because we are in the constant tension solutions) gives a simple condition for when the radiation system reconstructs a portion of the black hole interior: an island forms if and only if there is a causal curve from the black hole interior into the radiation system.

This causal picture for island formation immediately reveals a set of simple operators that probe behind the black hole horizon. In particular consider an operator $\mathcal{O}_y$, which is localized near a point y, with y in $\hat{R}$ and in the future of the black hole interior (such points exist by our theorem). These operators directly probe the black hole interior by virtue of being in its future.

Notice that the radiation system $\hat{R}$ sits outside of the Poincaré patch we identified

above. Thus it sits outside of the black hole spacetime. Ideally, we would understand which subregions of the Poincaré patch reconstruct the black hole interior. To do this, we need only note that a nearby subregion $\hat{R}_P$ of the Poincaré patch includes $\hat{R}$ in its domain of dependence. See Fig. 5.11. Evolving the state on this subregion forward using the global Hamiltonian, we can construct the state of the radiation system $\hat{R}_1$. Notice that $\hat{R}_P$ is slightly larger than $\hat{R}$ and will include a small portion of the black hole exterior in its entanglement wedge.

To write operators which probe behind the black hole horizon in the Hilbert space of V_P, we can start with the operators $\mathcal{O}_y$ which live in $\hat{\mathcal{V}}_1$ and time evolve backward using the global Hamiltonian. We continue this time evolution until $\mathcal{O}_y$ is some non-local operator $\mathcal{O}_{y,P}$ living on V_P.

It is interesting that time evolution with the global Hamiltonian, along with local operators, can be used to probe the black hole interior. We should perhaps be unsurprised however, as the situation is analogous to the traversable wormhole [158]: in both cases we have a left and right CFT (or in our setting, BCFT), which we couple and then time evolve to find that information from behind the black hole horizon has emerged at the boundary. In the traversable wormhole the coupling is a double trace term which can be understood perturbatively, while in our setting the coupling is due to time evolution with the global Hamiltonian.[14]

5.6 Discussion

The relationship between entanglement and geometry in AdS/CFT has lead to a number of insights into how gravitational physics can be recorded into quantum mechanical degrees of freedom. The $2 \rightarrow 2$ connected wedge theorem brings a new element to this connection in that it directly ties boundary entanglement to bulk light cones, rather than the minimal surfaces appearing in the Ryu-Takayanagi formula. The $1 \rightarrow 2$ theorem extends this to the context of spacetimes with ETW branes.

In this chapter we have proven the $1 \rightarrow 2$ connected wedge theorem. The theorem

---

[14]We thank Henry Lin for pointing out this analogy to us.

is motivated by a quantum tasks argument, and proven using the focusing theorem. The tasks argument gives an operational reason why the theorem should be true: if the bulk scattering region is non-empty, the boundary CFT requires the decision region $\hat{\mathcal{V}}_1$ to know information stored on the brane. Otherwise, the CFT is unable to reproduce bulk physics. The focusing theorem based proof relies on the null membrane, a structure that allows comparison of the areas of brane-detached extremal surfaces and brane-attached surfaces. When the scattering region is non-empty, we showed there exists a null membrane that connects a brane-detached extremal surface to a brane-attached one with less area.

We discussed in detail one application of the $1 \to 2$ theorem to brane models of information escape from black holes and the formation of islands. In that context, the $1 \to 2$ theorem gives an alternative prescription for determining when an island forms based on light rays in the auxiliary geometry. Given the generality of the theorem however and the assortment of other applications such geometries have found recently, we may expect additional applications in the future.

Below we make a number of comments.

Better bounds on mutual information

The key technical tool used here to complete the quantum tasks argument for the $1 \to 2$ connected wedge theorem was Lemma 4, which gave a bound

$$\frac{1}{2}I(\hat{\mathcal{V}}_1 : \bar{Q}) \geq n(-\log 2^{h(2\epsilon)}\beta) - 1 + O((\epsilon/\beta)^n).$$

This bound was first shown in [154]. It is interesting to ask if this bound can be improved further. Supposing a fraction $1 - \delta$ of the **M** tasks need to be completed successfully for the $\mathbf{M}^{\times n}$ task to be declared successful, it is straightforward to achieve

$$\frac{1}{2}I(\hat{\mathcal{V}}_1 : \bar{Q}) = (1 - \delta)n. \tag{5.101}$$

Thus, $(1 - \delta)n$ is the best lower bound on the mutual information we can hope for. Given such a bound, and assuming we can take $\delta = O(1/n)$, we could directly find that the boundary region $\hat{\mathcal{V}}_1$ approximately reconstructs Q [159, 160]. With the existing bound, we

can instead only conclude $I(\hat{\mathcal{V}}_1 : \bar{Q}) = O(1/G_N)$, then use the Ryu-Takayanagi formula to conclude this means the entangling surface are brane-anchored, then use the understanding of entanglement wedge reconstruction to conclude this means $\hat{\mathcal{V}}_1$ reconstructs Q. Post-hoc, we can interpret this as being due to $\hat{\mathcal{V}}_1$ needing Q to undo H^q and complete the task. The better bound presented above would more directly connect the task argument to bulk reconstruction.

Relation to correlation functions

An un-explored question is the relationship between the quantum tasks considered here and features of CFT correlation functions. Recall from [82, 17, 161, 83] that when there is a bulk point p with $c_1, c_2 \prec p \prec r_1, r_2$ and p is null separated from each of the four points, there is a perturbative singularity in four point functions $\langle \mathcal{O}(c_1)\mathcal{O}(c_2)\mathcal{O}(r_1)\mathcal{O}(r_2) \rangle$. The appearance of this point p also signals the appearance of a scattering region, and so the $2 \to 2$ connected wedge theorem implies large mutual information between the decision regions.

The connected wedge theorem and the appearance of perturbative singularities are related by the bulk geometry — indeed the singularity in the four point function, via the bulk point, implies a large mutual information. In [78], the authors suggested that this should have a CFT explanation, but so far no explanation has been offered.

This question also has a natural analogue in the $1 \to 2$ connected wedge theorem. In particular it is plausible that the three point function $\langle \mathcal{O}(c_1)\psi(r_1)\psi(r_2) \rangle$, where ψ is an edge operator, has a perturbative singularity when the three operator insertion points are null separated from a single point on the brane.[15] Comparing to the $1 \to 2$ theorem, these singularities would then imply the entanglement wedge of the decision region is connected to the brane. We will discuss this problem in great detail in the next chapter.
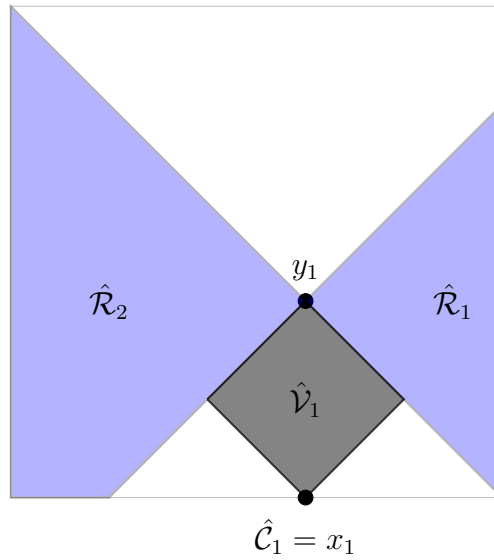
Figure 5.12: View of the boundary of Poincaré-AdS$_{2+1}$. The edge is located at $x = 0$. A region $\hat{\mathcal{V}}_1$ is specified, and we are interested in using the connected wedge theorem to determine if the entanglement wedge of $\hat{\mathcal{V}}_1$ is attached to the brane. The Fig. shows a choice of regions $\hat{\mathcal{R}}_1, \hat{\mathcal{R}}_2$ and $\hat{\mathcal{C}}_1$ which can be used in the theorem. Notice that the input region $\hat{\mathcal{C}}_1$ is taken to be a point x_1.

$1 \to 2$ **theorem in planar brane solutions**

By using extended input and output regions, [154] applied the $2 \to 2$ connected wedge theorem non-trivially in Poincaré-AdS$_{2+1}$. Here, we have mostly focused on a point based formulation, and on a class of global solutions with constant tension branes ending pure AdS. However we can also use extended input and output regions and apply the $1 \to 2$ theorem non-trivially in Poincaré-AdS$_{2+1}$ with a brane.

Consider in particular the pure AdS solutions with planar branes discussed in §5.4. The boundary is the half plane defined by $x < 0$, and the brane sits at

$$x/z = \sin \Theta. \tag{5.102}$$

Suppose we are given a region on the boundary $\hat{\mathcal{V}}_1$, and we would like to apply the $1 \to 2$ theorem to determine if its entanglement wedge is brane attached or detached. Call x_1 the earliest point on $\hat{\mathcal{V}}_1$, and y_1 the latest point on $\hat{\mathcal{V}}_1$ so that $\hat{\mathcal{V}}_1 = \hat{J}^+(x_1) \cap \hat{J}^-(y_1)$. To apply the theorem non-trivially, choose

$$
\begin{aligned}
\hat{\mathcal{C}}_1 &= x_1 \\
\hat{\mathcal{R}}_1 &= D((y_1, 0]) \\
\hat{\mathcal{R}}_2 &= D((-\infty, y_1))
\end{aligned}
\tag{5.103}
$$

where by $D(\cdot)$ we mean the domain of dependence. This is shown in Fig. 5.12. Then the $1 \to 2$ connected wedge theorem applies non-trivially, and in fact in these solutions the entanglement scattering region will be non-empty exactly when the entanglement wedge of $\hat{\mathcal{V}}_1$ is connected.

---

[15]This is the case for the two point function $\langle \mathcal{O}(c_1)\mathcal{O}(r_1)\rangle$ in a BCFT. For further discussion, and a complementary perspective on causality and spectral properties arising from two-point functions in a BCFT, see the upcoming work [**?**].

Higher dimensions

The $1 \rightarrow 2$ connected wedge theorem is true for any asymptotically AdS spacetime where the bulk and brane matter satisfy the NEC. However, it is possible that in some spacetimes there will only be trivial configurations of the theorem, meaning that when the bulk scattering region is non-empty the decision region $\hat{\mathcal{V}}_1$ touches the brane, and so immediately has a connected entanglement wedge.

We have focused on the example of asymptotically global AdS$_{2+1}$, and discussed Poincaré-AdS$_{2+1}$ in the last section, where there are many non-trivial configurations. It would be interesting to better understand however when the theorem applies non-trivially in higher dimensions.

Evaporating black holes

In §5.5 we applied the connected wedge theorem to the static, two sided black hole model introduced in Chapter 4. While information does escape from this black hole, it is in thermal equilibrium with the radiation system and does not evaporate. The connected wedge theorem applies much more generally however, including to models of evaporating black holes, since the theorem is proven in the context of dynamical spacetimes. It would be interesting to do this explicitly, for example in the dynamical models we considered in the previous chapter.

5.7   Conclusion

In this chapter, we considered a scenario in which BCFT observers perform a distributed quantum computation using data about the boundary conditions. They can perform this in the BCFT with sufficient entanglement. Alternatively, if the BCFT is holographic, they can travel into the bulk. The feasibility of the bulk strategy requires that the appropriate entanglement wedge includes part of the ETW brane, consistent with entanglement wedge reconstruction. We proved this using both geometric techniques and arguments from quantum information theory. In the context of black holes and the models considered

in the previous chapter, we can run the theorem in reverse and arrive at a simple criterion for the recoverability of information from the black hole interior.

We briefly discussed the relation between the connected wedge theorem (in $2 \to 2$ and $1 \to 2$ forms) to CFT correlators. In field theory terms, the quantum task is really a correlator which encodes a "scattering problem", and the existence of bulk strategies should correspond to a singularity in the correlator. We will explore this problem in much greater detail in the next chapter, and use it to dramatically constrain the operator content of holographic BCFTs, along similar lines to Chapter 3.

Chapter 6

Looking for a Bulk Brane

6.1 Introduction

Is every consistent theory of quantum gravity a string theory? There are many ways to attempt to ask this question or even just to define the terms. Since string theory involves non-perturbative higher-dimensional objects or branes, in the context of AdS/CFT one way of asking this question is to study whether, given a holographic conformal field theory (CFT), defect operators in the CFT are described by gravitational branes in the dual bulk. That is, does every holographic CFT have a well-behaved spectrum of branes? As a step in this general direction, in this chapter we ask if, given a holographic CFT, every conformal boundary condition is properly described by the bulk gravitational effective field theory, allowing for the addition of a semiclassical end-of-the-world (ETW) brane.

A closely related—but more concrete—ambition is to sharpen the holographic dictionary for boundary conformal field theories (BCFT). That is, given a holographic CFT, what additional assumptions—if any—must be made for an associated BCFT to be described by the bulk gravitational effective field theory (again allowing for the addition of semiclassical branes)? And can we explicitly write the mapping between solutions of the boundary bootstrap and semiclassical bulk+brane actions?

Sharpening the holographic dictionary for BCFTs is timely. Recent works [6, 140, 141, 3, 151, 150, 162, 152, 153, 163, 164] have employed a BCFT as a model of a lower-

dimensional gravitational system coupled to an auxiliary CFT. A BCFT is then a concrete and calculable model for studying Euclidean wormholes and islands. In these works, it has been assumed that the BCFT has a good holographic dual with an ETW brane. Furthermore, it has been suggested that one might be able to minimally UV-complete coarse-grained gravitational theories by adding ETW branes to the theory [165, 166]. But just how realistic or typical are well-behaved ETW branes in a theory of gravity?

A similar program for sharpening the duality between CFTs and bulk gravitational effective field theory was initiated in [17]. There, the conformal bootstrap was used to argue that any CFT such that

1. simple correlators factorize in a $1/c$ expansion; and

2. the spectrum is gapped such that below some large Δ_{gap} the only operators are simple light operators and their multi-trace composites

is dual to a bulk theory of semiclassical Einstein gravity. A great deal of subsequent work on the holographic bootstrap has strengthened and refined this claim, for example [161, 167, 168, 169, 170, 171, 172, 173, 174, 175, 176, 177]. In this chapter, we will initiate this program for BCFTs. The chapter is structured as follows:

- In the remainder of this introductory section, we preview our results, and give detailed background on the boundary bootstrap.

- To understand what a holographic BCFT looks like in terms of its spectrum of boundary operators, in §6.2 we examine the simplest possible model, namely empty AdS cut off by an ETW brane.

- We take the operator spectrum found in our simple model and explain its meaning in §6.3 by studying the bulk causal structure and the Lorentzian continuation of BCFT two-point functions.

- We establish a general correspondence between the boundary operator spectrum and the bulk causal structure in §6.4. This suggests that microscopic fine-tuning is required for a geometric brane, and leads to a conjecture of necessary and sufficient conditions for a holographic BCFT.

- Finally, we conclude with a discussion in §6.5.

6.1.1 Preview of results

To begin the parallel program for BCFTs, we first note that the holographic CFT bootstrap typically begins with the assumption that the bootstrap can be studied in a $1/c$ expansion about a universal mean field theory solution (MFT) determined by the CFT two-point function. For example, a scalar four-point function would have the schematic form

$$\langle \phi\phi\phi\phi \rangle = \sum \langle \phi\phi \rangle^2_{\text{univ}} + O\left(\frac{1}{c}\right) , \tag{6.1}$$

where $\langle \phi\phi \rangle_{\text{univ}}$ is the universal CFT two-point function.

In contrast to a CFT, the BCFT two-point function is not universal and kinematically behaves similarly to a CFT four-point function [57, 88, 84]. Moreover, unlike for the holographic CFT, there is no restriction from the BCFT or its gravitational dual that this two-point function should be perturbatively close to a known universal solution like the MFT. Thus, before attempting to understand an analogous correspondence between bulk+brane interactions and perturbative solutions to the BCFT bootstrap, we must first understand the leading order, non-perturbative backreaction of the boundary on the bulk gravitational solution.

To understand what is special about the leading order solution for a BCFT with a simple bulk dual, we will argue that it is useful to rotate to Lorentzian signature, since the Lorentzian BCFT two-point function can probe the *bulk causal structure*. When the BCFT has a semiclassical gravitational dual, the bulk causal structure often implies the existence of new approximate singularities in the BCFT[1] (see Fig. 6.1). Similar singularities for scattering at bulk points in a CFT have been noted before, and their CFT origins were discussed in detail in [83].[2]

---

[1] We don't expect these to be true singularities of the BCFT. Rather, much like the semiclassical singularities predicted by scattering at a bulk point, these will be flattened out at the scale of the gap when the gravitational theory becomes non-local [83].

[2] Lorentzian CFT correlation functions and the singularities from bulk points have been used as a powerful diagnostic of bulk geometry [178, 179, 180].
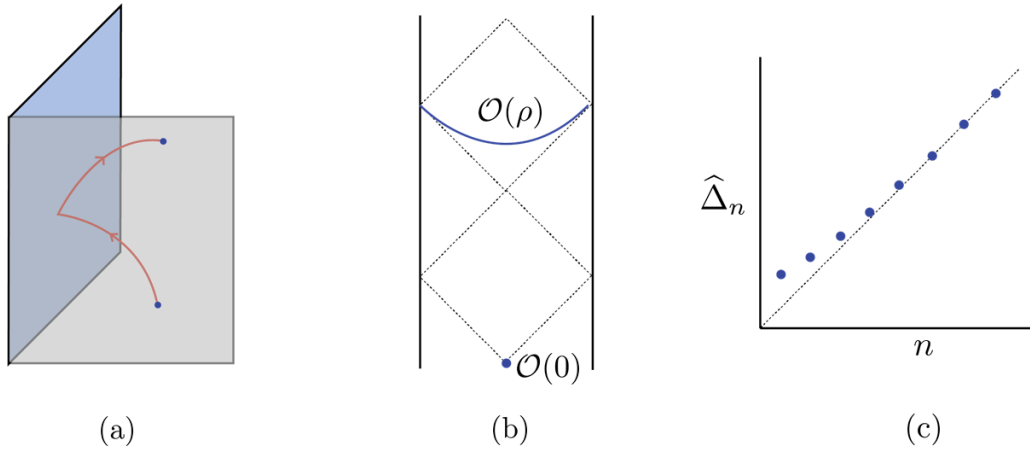
Figure 6.1: (a) A light ray leaving the boundary and returning to the boundary at a later time (in this example reflecting off an ETW brane). (b) The bulk causal structure then implies new 'bulk brane' singularities in the BCFT to the future of a BCFT operator. (c) The bulk brane singularities require a careful alignment of operator dimensions appearing on the boundary of the BCFT.

On the BCFT side, these new bulk singularities can only be obtained through the careful alignment of boundary operator dimensions over some large range of dimensions up to a "boundary gap" $\widehat{\Delta}_{\mathrm{gap}}$. The careful alignment of these operators makes such a bulk causal structure fragile. We find no constraints from the CFT being holographic that fix these specific dimensions.

From the fragility of the bulk causal structure, we suggest that holographic boundary conditions are sparse in the space of all boundary conditions for a holographic CFT. On top of the assumptions already necessary for our CFT to be holographic, we must further make a new set of assumptions about the boundary condition itself. Namely, we would like to conjecture that a holographic CFT with a boundary condition whose

1. correlators factorize in an expansion about a (non-universal) free bulk solution; and

2. boundary operator spectrum is gapped such that below some large $\widehat{\Delta}_{\mathrm{gap}}$ the only operators are simple light operators and their multi-trace composites;

is dual to a bulk theory of semiclassical gravity with the possible addition of an ETW brane with a local action. It is the first of these conditions that this chapter suggests is not generic

238

and must be assumed, although there are subtleties related to this point that appear when we study more complicated top-down constructions of holographic BCFTs. The second condition, and the necessity and sufficiency of these two conditions together, will *not* be addressed here.

6.1.2   Review of BCFT

Critical phenomena involving a boundary are described by boundary conformal field theories, which involve generalizations of the many familiar concepts and tools of conformal field theories. To arrive at a BCFT, one typically introduces a boundary to a known CFT (i.e. we have a finite slab of material). One may also introduce additional degrees of freedom living on the boundary, which can be coupled to the CFT degrees of freedom. A complete specification of the theory then involves imposing boundary conditions for the the bulk degrees of freedom, as well as dynamics for the boundary excitations. If this can be done in a manner that maximally preserves conformal invariance, or by flowing to a conformal fixed point, the resulting theory is a BCFT. For a given CFT, there may be many different possible choices of conformally-invariant boundary conditions (or conformal fixed points), each of which is described by a different BCFT.

Symmetries

The most basic tool in studying a BCFT is conformal representation theory: the excitations of the theory organize themselves into representations of a reduced conformal symmetry group that is left unbroken by the new boundary. When the BCFT lives on the half-plane $\mathbb{R}^{d-1} \times \mathbb{R}_+$ with a planar boundary, the unbroken symmetry is $\mathrm{SO}(d,1) \subset \mathrm{SO}(d+1,1)$, which is the set of transformations that maps the half-plane back to itself. We will use coordinates on this space given by $x = (x_0, \vec{x}, x_\perp)$, where $x_0, \vec{x}$ are Euclidean coordinates parallel to the boundary and $x_\perp$ is our coordinate orthogonal to the planar boundary. We depict these coordinates in Fig. 6.2.
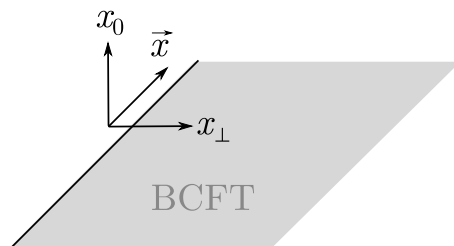
Figure 6.2: A BCFT on a half-plane $\mathbb{R}^{d-1} \times \mathbb{R}^+$. Here, x_0 and $\vec{x}$ are coordinates parallel to the boundary; $x_\perp$ is a coordinates perpendicular to the planar boundary, which sits at $x_\perp = 0$.

CFT Operators and Boundary Operators

Because a BCFT only modifies the CFT along the boundary, the spectrum of CFT operators and their algebra remains unchanged. Localized on the boundary, however, we have new *boundary operators*, $\hat{\mathcal{O}}_I$. These operators are organized into representations of $\mathrm{SO}(d, 1)$, which are partially labeled by a boundary conformal dimension $\hat{\Delta}_I$. The boundary conformal dimension is just the usual eigenvalue of the unbroken d-dimensional dilation operator (which dilates both along and away from a point on the boundary). As is familiar, any such representation has a primary and descendants and we use this structure to organize our description of the BCFT in much the same way as we do for CFTs.

State-Boundary Operator Map

By the usual logic of the state-operator mapping, there is a one-to-one map between boundary operators of the BCFT and states of the theory quantized on a half-sphere $H\mathbb{S}^{d-1}$. This follows from the half-plane picture by using an infinite dilation to map back to a point on the boundary. Alongside the state-boundary operator map, we still also have the regular CFT state-operator map when we quantize the theory on a sphere $\mathbb{S}^{d-1}$ which does not intersect the boundary.

The state-boundary operator map allows us to write a *boundary operator expansion*

(BOE), whereby any CFT operator can be written as a sum over boundary operators

$$\mathcal{O}_i(x) = \frac{\mathcal{A}_{\mathcal{O}_i}}{(2x_\perp)^\Delta} + \sum_J \frac{\mathcal{B}_{iJ}}{(2x_\perp)^{\Delta_i - \Delta_J}} \widehat{C}[x_\perp, \partial_{\vec{x}}] \widehat{\mathcal{O}}_J(x_0, \vec{x}), \qquad (6.2)$$

where the sum over J is over boundary primary operators and the differential operator $\widehat{C}$ which contributes the contributions of descendants is fixed by conformal invariance. Likewise, the BCFT inherits the regular OPE from the CFT without a boundary:

$$\mathcal{O}_i(x)\mathcal{O}_j(y) = \sum_k \frac{\mathcal{C}_{ij}^k}{|x - y|^{\Delta_i + \Delta_j - \Delta_k}} C[x - y, \partial_y] \mathcal{O}_k(y). \qquad (6.3)$$

Correlation Functions

Because of the reduced symmetry, BCFT correlation functions involving CFT operators away from the boundary are less constrained than those of a CFT without a boundary. A useful 'trick' for characterizing the kinematic constraints on a BCFT correlator is to view the correlator as doubled with operator insertions mirrored across the boundary (each copy carrying half the conformal weight of the original operator).

Following the logic of doubling, one can easily see that a scalar CFT operator has a one-point function that behaves kinematically like a CFT two-point function

$$\langle \mathcal{O}(x) \rangle = \frac{\mathcal{A}_{\mathcal{O}}}{(2x_\perp)^\Delta}, \qquad (6.4)$$

where the coefficient $\mathcal{A}_{\mathcal{O}}$ which determines the size of the vacuum expectation value is a free parameter of the theory, unlike in a CFT, because we choose not to change the normalization of our CFT operators.

Likewise, the two-point function of scalar operators in a BCFT behaves much like a CFT four-point function and thus no longer fixed by conformal invariance. It can be written in terms of an undetermined function of a single conformally-invariant cross-ratio,

$$\langle \mathcal{O}(x)\mathcal{O}(y) \rangle = \frac{1}{|4x_\perp y_\perp|^\Delta} \mathcal{G}(\xi), \qquad (6.5)$$

241

where the cross-ratio can be defined as

$$\xi = \frac{(x-y)^2}{4x_\perp y_\perp} = \frac{(x_0 - y_0)^2 + (\vec{x} - \vec{y})^2 + (x_\perp - y_\perp)^2}{4x_\perp y_\perp} \, . \tag{6.6}$$

Boundary Bootstrap

The function $\mathcal{G}(\xi)$ that appears in (6.5) must decompose into irreducible representations of the conformal symmetry. There are two ways to perform this decomposition. We can take the operators near to each other, $\xi \to 0$, and use the CFT OPE to fuse the two operators into a sum of bulk operators. We can then evaluate the sum over local operators in the BCFT. The result is an expansion in terms of bulk conformal blocks g^B [181, 84, 88]:

$$\text{Bulk Channel}: \qquad \mathcal{G}(\xi) = \sum_i a_i \, g^B_{\Delta_i}(\xi) \, , \tag{6.7}$$

where i labels CFT bulk primaries and the coefficients a_i are the product of the bulk OPE coefficient and one-point function coefficient of $\mathcal{O}_i$,

$$a_i = \mathcal{C}^i \mathcal{A}_i. \tag{6.8}$$

Alternatively, we can take the operators to the boundary, $\xi \to \infty$, and use the BOE to expand each operator as a sum of boundary operators. We then evaluate the two-point functions of the resulting summed boundary operators, which are fixed by conformal invariance. The result is an expansion in terms of boundary blocks g^b [181, 84, 88]:

$$\text{Boundary Channel}: \qquad \mathcal{G}(\xi) = \sum_I b_I \, g^b_{\widehat{\Delta}_I}(\xi) \, , \tag{6.9}$$

where I labels boundary primary operators and b_I is the square of their BOE coefficients

$$b_I = \mathcal{B}_I^{\,2} \, . \tag{6.10}$$

The equivalence of the expansions in terms of either the boundary conformal blocks or
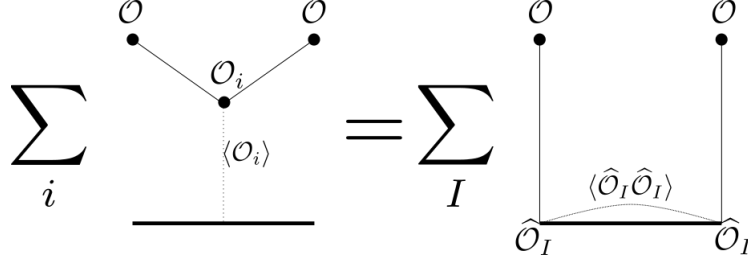
Figure 6.3: Pictorial representation of 6.11. The thick line represents the boundary; thin lines represent fusion of external operators into bulk or boundary operators; dotted lines represent correlators.

bulk conformal blocks,

$$\sum_{\mathcal{O}'} a_i g^B_{\Delta_i}(\xi) = \sum_I b_I g^b_{\widehat{\Delta}_I}(\xi) \, , \tag{6.11}$$

is a BCFT version of *crossing symmetry* and gives bootstrap equations that can be studied with analogous tools as in the CFT case [84, 181]. We depict the crossing symmetry visually in Fig. 6.3.

Scalar Blocks

As shown in [88], the scalar conformal blocks, obtained by solving the Casimir equation for the full and reduced conformal symmetry, are

$$g^B_\Delta(\xi) = \xi^{\Delta/2 - \Delta_{\text{ext}}} {}_2F_1\left(\frac{\Delta}{2}, \frac{\Delta}{2}; \Delta - \frac{d}{2} + 1; -\xi\right) \, , \tag{6.12}$$

$$g^b_{\widehat{\Delta}}(\xi) = \xi^{-\widehat{\Delta}} {}_2F_1\left(\widehat{\Delta}, \widehat{\Delta} - \frac{d}{2}; 2\widehat{\Delta} + 2 - d; -\xi^{-1}\right) \, , \tag{6.13}$$

where Δ_{ext} is the dimension of the external operators.

There are branch point singularities in $\mathcal{G}(\xi)$ at $\xi \to 0, \infty$. As in [181], we take the branch cut to run from $(-\infty, 0)$, so that the Lorentzian continuation ξ lives on the cut plane $\mathbb{C} \backslash (-\infty, 0)$.

Radial Coordinates

We can also introduce radial coordinates [120, 182], which will simplify some of our expressions:

$$\xi = \frac{(1-\rho)^2}{4\rho} \ .$$

(6.14)

This takes the cut ξ-plane to the unit disk $|\rho| < 1$, with $\xi \in (0, \infty)$ mapped to $\rho \in (0, 1)$. The boundary block is then

$$g_{\widehat{\Delta}}^b(\rho) = \left[\frac{4\rho}{(1-\rho)^2}\right]^{\widehat{\Delta}} {}_2F_1\left(\widehat{\Delta}, \widehat{\Delta} - \frac{d}{2} + 1; 2\widehat{\Delta} + 2 - d; \frac{-4\rho}{(1-\rho)^2}\right)$$

(6.15)

$$= (4\rho)^{\widehat{\Delta}} {}_2F_1\left(\widehat{\Delta}, \frac{d-1}{2}; \widehat{\Delta} - \frac{d}{2} + \frac{3}{2}; \rho^2\right) \ ,$$

(6.16)

where on the second line, we used a quadratic transformation.

Holographic BCFT

In [91, 59] (following [183, 90]) it was proposed that the holographic dual of a BCFT should be a bulk geometry, $\mathcal{M}$, terminated by an ETW brane, $\mathcal{B}$, that acts as an additional infrared boundary for the gravitational theory. The new boundary $\mathcal{B}$ meets the standard asymptotically AdS boundary at the location of the BCFT boundary (see Fig. 6.4). The gravitational sector of the bulk+brane theory is proposed to have an action that now includes a standard Gibbons-Hawking boundary term on the brane

$$S_G = \frac{1}{16\pi G_N} \int_{\mathcal{M}} \mathrm{d}^{d+1}x \, \sqrt{|g|}(R - 2\Lambda) + \frac{1}{8\pi G_N} \int_{\mathcal{B}} \mathrm{d}^d y \, \sqrt{|h|}(K - T) \,,$$

(6.17)

where h is the induced metric on the brane, K is the trace of the extrinsic curvature, and T is the tension of the ETW brane. One also expects the same bulk AdS matter action as the original CFT without a boundary as well a new matter action living on the ETW brane:

$$S = S_G + \int_M \mathcal{S}_{\mathrm{AdS}}^m + \int_B \mathcal{S}_{\mathrm{ETW}}^m \,.$$

(6.18)

The residual $\mathrm{SO}(d,1)$ symmetry of the BCFT fixes the bulk geometry to take the highly-constrained form

$$\mathrm{d}s^2 = \mathrm{d}r^2 + e^{2A(r)}\mathrm{d}s^2_{\mathrm{AdS}_d}, \tag{6.19}$$

where a lower-dimensional AdS_d is warped over a radial direction with some warp factor $A(r)$. The warp factor is determined by whatever vacuum expectation values are sourced by the ETW matter action $\mathcal{S}^m_{\mathrm{ETW}}$, but must asymptotically approach that of empty AdS_{d+1} where $A(r) = \ln\cosh(r)$ as $r \to -\infty$. (We will work in coordinates where the AdS radius $L = 1$.) The ETW brane will sit on some constant radial slice $r = r_0$, fixed by the combination of the tension T and the particular warp factor $A(r)$.

Holographic BCFT Dictionary

Here we review the holographic dictionary for a scalar bulk field in a BCFT. We explain how to construct bulk operators in bottom-up models and how to extract their corresponding boundary operator expansion data. We follow closely the treatment in [184], although we will use slightly different conventions.

Consider a bulk scalar field operator $\phi(\vec{y}, u, r)$ of mass M. By the standard AdS/CFT dictionary, this field is dual to a CFT operator $\mathcal{O}_\Delta$ of dimension

$$\Delta = \frac{1}{2}\left(d + \sqrt{d^2 + 4M^2}\right). \tag{6.20}$$

At leading order, the bulk field satisfies the free wave equation on the warped background

$$\left(\Box_{\mathcal{M}} - M^2\right)\phi = 0. \tag{6.21}$$

We can write a solution of this wave equation in the form

$$\sum_n \bar{\psi}_n(r)\hat{\phi}_n(\vec{y}, w), \tag{6.22}$$

where the $\hat{\phi}_n$ are fields of mass m_n satisfying the Klein-Gordon equation $\Box_d\hat{\phi}_n = m_n^2\hat{\phi}_n$ in AdS_d. Substituting the mode expansion into (6.21) we find that the radial modes $\bar{\psi}_n(r)$

must solve

$$\bar{\psi}_n''(r) + dA'(r)\bar{\psi}_n'(r) + e^{-2A(r)}m_n^2\bar{\psi}_n(r) - M^2\bar{\psi}_n(r) = 0. \tag{6.23}$$

To completely determine the mode expansion, we must also specify a complete set of boundary conditions. As we are looking for the bulk operator, we require that our solution be normalizable as we approach the AdS boundary, in other words

$$\bar{\psi}_n(r) \underset{r\to\infty}{=} e^{-r\Delta}\left(1 + \ldots\right), \tag{6.24}$$

and furthermore choose that the leading term is unit normalized.

A second boundary condition is specified on the bulk brane, where the specific condition is determined by the terms appearing in the brane action. Together, these two boundary conditions determine the correct modes ψ_n and eigenvalues m_n, giving the bulk scalar operator

$$\phi(\vec{y}, u, r) = \sum_n \psi_n(r)\hat{\phi}_n(\vec{y}, w). \tag{6.25}$$

The last step in writing down (6.25) is to fix the correct rescaling of the mode functions $\psi_n = c_n\bar{\psi}_n$. The rescaling is determined by enforcing the canonical commutation relations for the bulk field. Note that with this proper normalization in place, the mode functions have the asymptotic form $\psi_n(r) = c_n e^{-r\Delta} + \ldots$.

To determine the c_n we require that the operators ϕ and $\hat{\phi}_n$ satisfy the equal time canonical commutation relations

$$[\phi(t, \vec{v}_1, u_1, r_1), \pi(t, \vec{v}_2, u_2, r_2)] = i\delta^{d+1}(\vec{v}_1 - \vec{v}_2, u_1 - u_2, r_1 - r_2), \tag{6.26}$$

$$[\phi_n(t, \vec{v}_1, u_1), \pi_m(t, \vec{v}_2, u_2)] = i\delta^d(\vec{v}_1 - \vec{v}_2, u_1 - u_2)\delta_{m,n}, \tag{6.27}$$

where $\vec{y} = (t, \vec{v})$ and where $\pi \equiv -\sqrt{-g}g^{tt}\partial_t\phi$ and $\pi_n \equiv -\sqrt{-\tilde{g}}\tilde{g}^{tt}\partial_t\phi_n$ are the canonically conjugate fields to ϕ and π_n, with $\tilde{g}$ the induced metric on the AdS$_d$ slices of fixed r. This gives

$$\int_{r_0}^{\infty} dr \cosh^{d-2}(r)\psi_n(r)\psi_m(r) = \frac{1}{c_n^2}\delta_{nm}, \tag{6.28}$$

246

which we can evaluate to obtain c_n.

Having derived the bulk scalar operator, we can now take the boundary limit to obtain the dual CFT operator. The mode expansion in terms of the AdS_d operators directly gives the dual boundary operator expansion [184]. However, it is even cleaner to relate the bulk modes to boundary operators by considering the bulk and boundary two-point functions, which we will do in the following.

Consider the bulk two-point function in our mode expansion:

$$\langle \phi(\mathbf{x}_1)\phi(\mathbf{x}_2)\rangle = \sum_{n,m} \psi_n(r_1)\psi_m(r_2) \left\langle \hat{\phi}_n(x_1, u_1)\hat{\phi}_n(x_2, u_2) \right\rangle \tag{6.29}$$

$$= \sum_{n,m} \psi_n(r_1)\psi_m(r_2) G^{(\mathrm{AdS}_d)}_{\Delta_n}(x_1, u_1; x_2, u_2). \tag{6.30}$$

Using the known form of the AdS_d two-point function (see e.g. [185]),

$$G^{(\mathrm{AdS}_d)}_\Delta(\xi) = \mathcal{C}_{\Delta,d-1} 2^{-2\Delta} \xi^{-\Delta} \, {}_2F_1\left(\Delta, \Delta - \frac{d}{2} + 1, 2\Delta - d + 2, -\frac{1}{\xi}\right) \tag{6.31}$$

where

$$\mathcal{C}_{\Delta,d-1} = \frac{\Gamma(\Delta)}{2\pi^{\frac{d-1}{2}}\Gamma(\Delta - d/2 + 3/2)}, \tag{6.32}$$

one can compute the CFT two-point function in the standard way:

$$\langle \mathcal{O}_1 \mathcal{O}_2 \rangle = \lim_{r_1, r_2 \to \infty} \cosh^{2\Delta}(r) \frac{1}{\mathcal{C}_{\Delta,d}} \langle \phi(X_1)\phi(X_2)\rangle. \tag{6.33}$$

Because the AdS_d bulk-to-bulk propagator (6.31) and boundary conformal block (6.13) are identical (up to a constant), we immediately find

$$\langle \mathcal{O}_1 \mathcal{O}_2 \rangle = \frac{1}{\mathcal{C}_{\Delta,d}} \sum_n \left(\lim_{r_1, r_2 \to \infty} \cosh^{2\Delta}(r)\psi_n(r_1)\psi_n(r_2) \right) \mathcal{C}_{\Delta_n,d-1} 2^{-2\Delta} g^b_{\Delta_n}(\xi), \tag{6.34}$$

which we can rewrite as

$$\langle \mathcal{O}_1 \mathcal{O}_2 \rangle = \frac{1}{\mathcal{C}_{\Delta,d}} \sum_n c_n^2 \mathcal{C}_{\Delta_n,d-1} 2^{-2\Delta_n} g^b_{\Delta_n}(\xi). \tag{6.35}$$

From comparing this expression to (6.9), we conclude two things:

1. The spectrum of boundary operators appearing in the BOE of $\mathcal{O}_\Delta$ is given by

$$\left\{ \Delta_n = \frac{1}{2} \left(d - 1 - \sqrt{(d-1)^2 + 4m_n^2} \right) \right\} . \tag{6.36}$$

2. The BOE coefficients are given by

$$\mathcal{B}_n = \frac{1}{2^{\Delta_n}} \sqrt{\frac{\mathcal{C}_{\Delta_n, d-1}}{\mathcal{C}_{\Delta, d}}} c_n . \tag{6.37}$$

6.2   Simplest bulk model

To understand the leading-order free two-point function in a holographic theory, we begin by studying the simplest possible bottom-up model: empty AdS terminated by an ETW brane. In our radial coordinates (6.19), the AdS_d foliation of AdS_{d+1} takes the form

$$\mathrm{d}s^2 = \mathrm{d}r^2 + \cosh^2(r) \left(\frac{\mathrm{d}\vec{y}^2 + \mathrm{d}u^2}{u^2} \right) . \tag{6.38}$$

The location of the brane is given by some $r = r_0$, determined by the tension. See Fig. 6.4. It will also sometimes be useful to change to an 'angular' coordinate using $\tanh(-r) = \cos(\varphi)$ so that

$$\mathrm{d}s^2 = \csc^2 \varphi \left[\mathrm{d}\varphi^2 + \left(\frac{\mathrm{d}\vec{y}^2 + \mathrm{d}u^2}{u^2} \right) \right] , \tag{6.39}$$

simplifying the conformal structure of the metric.

We consider a free scalar field, ϕ, whose dual CFT operator has dimension Δ. We will need to impose boundary conditions at the location of the brane. As a simple choice, we choose Neumann boundary conditions on the field, $\partial_r \phi(r_0) = 0$, although the qualitative features of our results will not depend on this specific choice. Using the mode expansion explained in §6.1.2,

$$\phi(\vec{y}, u, r) = \sum_n c_n \bar{\psi}_n(r) \hat{\phi}_n(\vec{y}, u) , \tag{6.40}$$
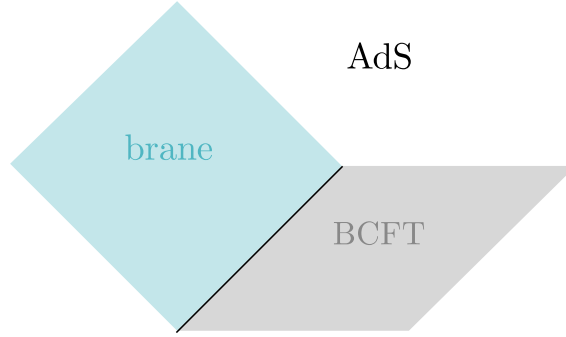
Figure 6.4: Our simple model in which the bulk is locally AdS_{d+1}, but is terminated by an ETW brane. We depict here the AdS_d foliation of AdS_{d+1}.

we find the two independent radial solutions of the EOM to be

$$\psi_{n(1)}(r) = \sin^{d/2}(\varphi) P_\nu^\mu(\cos\varphi), \tag{6.41}$$

$$\psi_{n(2)}(r) = \sin^{d/2}(\varphi) \left(\frac{1 - \cos\varphi}{1 + \cos\varphi}\right)^{\frac{\mu}{2}} {}_2F_1\left(\nu + 1, -\nu, \mu + 1, \frac{1 - \cos\varphi}{2}\right), \tag{6.42}$$

where we have chosen to use our angular coordinate φ, while ν and μ are

$$\nu = \Delta_n - \frac{d}{2}, \tag{6.43}$$

$$\mu = \Delta - \frac{d}{2}. \tag{6.44}$$

The asymptotic behaviour of these solutions as $r \to \infty$ is

$$\psi_{n(1)} \sim e^{-r(d-\Delta)}, \quad \psi_{n(2)} \sim e^{-r\Delta}, \tag{6.45}$$

which is what we expect from the non-normalizable and normalizable solutions of the wave equation, respectively.

Taking into account our boundary condition on the brane, only the modes $\psi_{n(1)}$ which satisfy $\psi'_{n(1)}(r_0) = 0$ are admissible. Since each radial function $\psi_{n(1)}(r)$ is related to a corresponding co-dimension 1 field $\phi_n(\vec{y}, w)$, with a dimension Δ_n given by (6.36), we expect that the condition $\psi'_{n(1)}(r_0) = 0$ will restrict the spectrum of Δ_n to take on only a

discrete set of values.

In the limit of large Δ_n, we can explicitly solve the equation $\psi'_{n(1)}(r_0) = 0$ for Δ_n to obtain

$$\Delta_n = \frac{d-1}{2} + \frac{\left(n + \frac{1}{2}\left(\Delta - \frac{d}{2}\right) + \frac{1}{4}\right)\pi}{\arccos(\tanh(r_0))}, \quad n \in \mathbb{Z} \quad (\text{large } \Delta_n). \tag{6.46}$$

In our angular coordinates, where the brane sits at φ_0, this simplifies to

$$\Delta_n = \frac{d-1}{2} + \frac{\left(n + \frac{1}{2}\left(\Delta - \frac{d}{2}\right) + \frac{1}{4}\right)\pi}{\varphi_0}, \quad n \in \mathbb{Z}. \tag{6.47}$$

Note that, in $d = 2$, the position r_0 of the brane is understood to be related to the defect entropy g of the CFT by [59]

$$g = \frac{r_0}{4G}, \tag{6.48}$$

which gives

$$\Delta_n^{d=2} = \frac{1}{2} + \frac{\left(n + \frac{\Delta}{2} - \frac{1}{4}\right)\pi}{\arccos(\tanh(2Gg))}, \quad n \in \mathbb{Z}. \tag{6.49}$$

Using (6.50) and the explicit expressions for $\psi_n(r)$ in Eq. (6.42), we can solve for c_n in the asymptotic limit of large n, which is the same limit in which we evaluated the scaling dimensions Δ_n of the operators ϕ_n. This gives the expression

$$c_n \approx \frac{\pi^{1/4}\sqrt{(1+\mu)}}{2}\sqrt{\frac{\Gamma(\mu+1/2)}{\Gamma(\mu+2)\Gamma(2\mu+1)}}\left(\frac{2}{\arccos(\tanh r_0)}\right)^{\mu+1}\left(\frac{\pi}{4}(4n+2\mu+1)\right)^{\mu+1/2}, \tag{6.50}$$

with $\mu = \Delta - d/2$, as before.

From Eq. (6.37), we can then compute the the BOE coefficients by plugging in the above c_n into the expression

$$\mathcal{B}_n = \frac{1}{2^{\Delta_n}}\sqrt{\frac{\mathcal{C}_{\Delta_n, d-1}}{\mathcal{C}_{\Delta, d}}}c_n. \tag{6.51}$$

250

In the large n limit, we can write this as

$$\mathcal{B}_n = 2^{-\frac{n}{\varphi_0}} n^{\Delta - \frac{d+1}{4}} B + \dots \tag{6.52}$$

with B a constant independent of n:

$$B = e^{\frac{3}{4} - \frac{d}{4}} \pi^{-\frac{d}{4} + \Delta + \frac{1}{2}} 2^{\frac{\pi(d-2\Delta-1)}{4\varphi} - \frac{d-1}{2}} \varphi^{\frac{d-1}{4} - \Delta} \left[\Gamma(\Delta) \Gamma(-d/2 + \Delta + 1) \right]^{-1/2} . \tag{6.53}$$

We conclude from this simple model that the information about the bulk geometry, namely—given our restricted assumptions—the location of ETW brane at φ_0, appears in two places:

1. The asymptotic spacing $\gamma = \lim_{n \to \infty} \Delta_{n+1} - \Delta_n = \frac{\pi}{\varphi_0}$ of boundary operator dimensions.

2. The asymptotic growth of the BOE coefficients $\mathcal{B}_n \sim \exp\left(\frac{n}{\varphi_0} \ln 2 \right)$.

What is not yet clear is why the information about the brane is encoded in this particular way and how it generalizes to a lesson about all BCFTs with good bulk duals. To make this next step, we must turn to the Lorentzian structure of two-point functions in a (holographic) BCFT.

6.3 Lorentzian BCFT singularities

In this section, we will consider the singularities associated with a scalar two-point function in a Lorentzian BCFT. We start by discussing the field theory setup and the expected structure of kinematic singularities. For BCFTs with a simple holographic dual, we consider the apparent singularities that arise from the bulk causal structure. In particular, we consider the bulk null rays that are reflected off the brane, and compute the cross-ratio of the return locus for these rays.

6.3.1 BCFT singularities in general dimension

In Euclidean signature, a CFT correlator has singularities whenever two operators become coincident (and is analytic otherwise). Similarly, a Euclidean BCFT correlation function will have singularities only when operators approach each other, or when they approach the boundary. (We can think of this as an operator approaching their mirrored double across the boundary.)

In terms of a scalar BCFT two-point function, and our cross ratio ξ defined in (6.6), the singularity when the two operators approach each other corresponds to the limit $\xi \to 0$. In this limit, the correlator will diverge like

$$\langle \mathcal{O}(x)\mathcal{O}(y) \rangle = \frac{1}{|x-y|^{2\Delta}} + \dots \tag{6.54}$$

or, correspondingly, $\mathcal{G}(\xi) \sim \xi^{-\Delta}$. When the operators approach the boundary, in the limit $\xi \to \infty$, the correlator diverges like

$$\langle \mathcal{O}(x)\mathcal{O}(y) \rangle = \frac{\mathcal{A}^2}{|4x_\perp y_\perp|^{\Delta}} + \dots \tag{6.55}$$

or, correspondingly, $\mathcal{G}(\xi) \sim \mathcal{A}^2$. Unlike the CFT case, there is no third Euclidean singularity, which could be thought to correspond to the operator $\mathcal{O}(y)$ approaching the mirror of $\mathcal{O}(x)$.

In Lorentzian signature, we similarly expect a singularity when $\mathcal{O}(y)$ approaches the lightcone of $\mathcal{O}(x)$ at the cross-ratio $\xi = 0$. We can also continue the Lorentzian two-point function around the branch point at $\xi = 0$ to the timelike region $\xi < 0$. Here there is another possible singularity where the $\mathcal{O}(y)$ approaches the reflection of the lightcone of $\mathcal{O}(x)$ off the boundary at $\xi = -1$. This is known as the *Regge Limit* of the BCFT [181] and it has been shown that the BCFT diverges here at worst as $\mathcal{G}(\xi) \sim (\xi + 1)^{-\Delta}$. This is exactly the singularity one would expect from approaching the lightcone of the 'mirror' of $\mathcal{O}(x)$. We depict the Lorentzian causal structure and the corresponding cross-ratios in Fig. 6.5.

When we change to radial coordinates, placing $\mathcal{O}(y)$ in the timelike region to the future
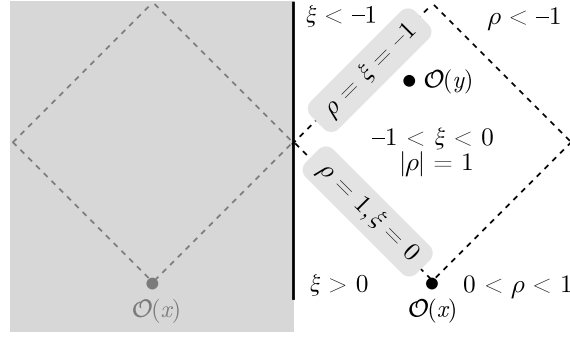
Figure 6.5: We depict various regions of the Lorentzian interval for a BCFT in terms of various cross-ratios. Importantly we note that the causal diamond bounded by the lightcone of the operator $\mathcal{O}(x)$ and its reflection off the boundary is described by the radial cross-ratio ρ living on the unit circle. It interpolates between the initial lightcone at $\rho = e^{i0}$ and the reflected ligthcone at $\rho = e^{i\pi}$.

of $\mathcal{O}(x)$, but before the reflected lightcone, corresponds to $\rho = e^{i\varphi}$ for $\varphi \in [0, \pi]$. At one end $\rho = 1$ ($\varphi = 0$) is the lightcone of $\mathcal{O}(x)$ at $\xi = 0$ and at the other end $\rho = -1$ ($\varphi = \pi$) is the reflected lightcone of $\mathcal{O}(x)$ at $\xi = -1$. We also indicate the ρ-regions in Fig. 6.5.

It has been argued that a CFT correlation function should only have singularities at points corresponding to Landau diagrams [83] where null particles interact at local vertices. By the same logic, we expect the only singularities of a BCFT two-point function to be that on the lightcone and its reflection. We do not not attempt to prove this statement in general, but we can follow [83], and show that it holds in a 2D BCFT.

6.3.2 BCFT singularities in 2D

Consider insertions z_i on the (Euclidean) upper-half plane, with distances z_{ij} and $z_{i\bar{j}}$ defined as usual. We will be interested in the correlator $\langle \mathcal{O}(z_1) \mathcal{O}(z_2) \rangle$ and its Lorentzian continuation.

OPE expansion

The OPE expansion of our BCFT two-point correlator is just a sum over holomorphic Virasoro conformal blocks. In the bulk CFT channel $\xi \to 0$, we have

$$\mathcal{F}(\eta) := \langle \mathcal{O}(z_1)\mathcal{O}(z_2) \rangle = \sum_h C_{\mathcal{O}\mathcal{O}h} A_h \mathcal{V}_h(1 - \eta), \tag{6.56}$$

where $C_{\mathcal{O}\mathcal{O}h}$ are bulk CFT OPE coefficients, B_h is the one-point function associated with the primary h, and $\xi = (1 - \eta)/\eta$. In the boundary channel $\eta \to 0$ ($\xi \to \infty$), we have

$$\mathcal{F}(\eta) = \sum_{\hat{h}} |B_{\mathcal{O}\hat{h}}|^2 \mathcal{V}_{\hat{h}}(\eta), \tag{6.57}$$

where $B_{\mathcal{O}h}$ is a boundary OPE coefficient. It is possible to expand Virasoro blocks as [119]

$$\mathcal{V}_h(\eta) = (16q)^{h-(c-1)/24} [\eta(1 - \eta)]^{(c-1)/24 - 2h} \theta_3(q)^{(c-1)/2 - 16h} H(h, q), \tag{6.58}$$

where $H(h, q)$ is a power series in q which can be determined recursively, θ_3 is a Jacobi theta function, and q is the elliptic nome defined by

$$q = e^{i\pi\tau(\eta)}, \quad \tau = i\frac{K(1 - \eta)}{K(\eta)}, \quad K(\eta) = \frac{1}{2}\int_0^1 \frac{dt}{\sqrt{t(1 - t)(1 - \eta t)}}. \tag{6.59}$$

This can be inverted to give $\eta = [\theta_2(q)/\theta_3(q)]^4$.

The pillow geometry

The parameter τ appearing in q is the modulus of a torus which covers the Riemann sphere twice. We will proceed with this construction, using Cardy's doubling trick to suppose we have a whole plane to play around with. We will pick a torus T^2 which branches at $0, \eta, 1, \infty$, a Riemann surface described by the following equation:

$$y^2 = x(x - \eta)(x - 1), \tag{6.60}$$

254
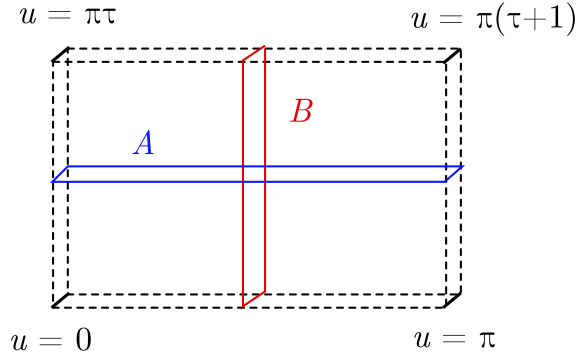
Figure 6.6: The $\mathbb{Z}_2$ quotient of the torus leads to a double-cover of the sphere which is flat except for conical defects at the corners, with uniformizing coordinates u as indicated. The A and B cycles of the torus can be associated with bulk and boundary OPE channels in the (B)CFT, with insertions at the corners.

where $x, y \in \hat{\mathbb{C}}$ are points on the Riemann sphere. This is the Weierstrass cubic associated with the lattice $\Lambda = \langle 1, \tau \rangle$ which quotients the complex plane to give the torus. This provides a double cover of the sphere since the defining equation is invariant under $y \mapsto -y$, and the fixed points of this map are precisely the branch points. The pillow has the topology of a sphere, and is flat, except for conical defects at these branch points, as depicted in Fig. 6.6.

The fundamental domain of the torus is oblique for general τ, but we can transform it into a rectangle using a *uniformizing* coordinate u defined by

$$\mathrm{d}u = \frac{L}{\theta_3(q)^2} \frac{\mathrm{d}x}{y}. \tag{6.61}$$

This has width $2\pi L$, as one can check by performing the x integral. The $\mathbb{Z}_2$ action $y \mapsto -y$ becomes $u \mapsto -u$. In the u coordinates, the defects have coordinates

$$u(x = 0) = 0, \quad u(x = \eta) = \pi, \quad u(x = 1) = \pi(\tau + 1), \quad u(x = \infty) = \pi\tau. \tag{6.62}$$

We can cut the pillow in half in two ways: the horizontal A cycle and the vertical B cycle, which separate the corners into pairs, also shown in 6.6.

255

Evaluating the correlator

We now consider how to implement this in the BCFT. In the BCFT, $\eta = z_{12}z_{34}/z_{13}z_{24}$. Thus, our insertions and their mirror images have the following identification on the pillow in u coordinates:

$$z_1 \mapsto 0, \quad z_{\bar{1}} \mapsto u = \pi, \quad z_2 = \pi\tau, \quad z_{\bar{2}} = \pi(\tau + 1). \tag{6.63}$$

Thus, the boundary lies on the B cycle, and we should quantize on the A cycle. If we normalize this cycle to have length 2π (or π in the halved geometry), then the relevant Hamiltonian is just the dilatation operator in radial quantization (now on a half-cylinder), $H = L_0 - c/24$.

We evolve upwards by $\pi\tau$, i.e., with Euclidean time evolution operator

$$e^{i\pi\tau(L_0 - c/24)} = q^{L_0 - c/24}. \tag{6.64}$$

The change to u coordinates is a Weyl rescaling, leading to an anomalous contribution to the correlator. Performing this change and regularizing as in [83], we obtain

$$\mathcal{F}(\eta) = \Lambda(\eta)g(q) \tag{6.65}$$

$$g(q) = \langle \mathcal{O}(u = 0)\mathcal{O}(u = \pi\tau)\rangle_{\text{pillow}} \tag{6.66}$$

$$\Lambda(\eta) = \theta_3(q)^{c/2 - 16h}[\eta(1 - \eta)]^{c/24 - 2h}. \tag{6.67}$$

We can think of the pillow two-point function $g(q)$ as an expectation value

$$g(q) = \langle \psi | q^{L_0 - c/24} | \psi \rangle, \quad |\psi\rangle = \mathcal{O}(0)|0\rangle, \tag{6.68}$$

where due to our choice of quantization, $\langle \psi | = \langle 0 | \mathcal{O}(\pi\tau)$. To be clear, here $|0\rangle$ is the vacuum state on the half-cylinder. In the boundary channel, factoring out the Λ prefactor also gives

$$g(q) = \sum_{\hat{h}} |B_{\mathcal{O}\hat{h}}|^2 \tilde{\mathcal{V}}_{\hat{h}}(q), \quad \tilde{\mathcal{V}}_{\hat{h}}(q) = \Lambda(\eta)^{-1}\mathcal{V}_{\hat{h}}(\eta). \tag{6.69}$$

We can split the block into descendants:

$$\tilde{\mathcal{V}}_{\hat{h}}(q) = \sum_{n \geq 0} a_n q^{n+\hat{h}-c/24}. \tag{6.70}$$

In a unitary BCFT, the $a_n \geq 0$, since otherwise we can construct a linear combination of descendants with negative norm.

The bulk channel is naturally interpreted as quantizing on the B cycle:

$$g(q) = \langle \psi' | \bar{q}^{L_0 - c/24} | B \rangle, \tag{6.71}$$

where $|\psi'\rangle = \mathcal{O}(\pi\tau)\mathcal{O}(0)|0\rangle$, $|0\rangle$ now the vacuum state for the full cylinder, and $\bar{q} = e^{-\pi i/\tau}$ is the S-transformed modular parameter. Performing the bulk OPE expansion of our two operators, we end up with precisely the sum of bulk Virasoro primaries weighted by OPE coefficients and one-point functions given above.

Seeking Lorentzian singularities

Mapping the unit disk $|\rho| \leq 1$ to the q variable leads a region sitting inside the unit disk of q, and hitting the boundary at $q = \pm 1$, which corresponds to $\rho = \pm 1$, and hence $\eta = 1, -\infty$, or $\xi = 0, -\infty$ in our preferred cross-ratio. Note that $g(q)$ is finite inside the unit disk, since it is given by an expansion in powers of q with positive, bounded coefficients. We depict this in Fig. 6.7 (left) below.

We would like to use the behaviour of $g(q)$ to deduce that the only Lorentzian singularities are the light-cone singularities. Let us define

$$\log q \left[\xi = -\cos^2\left(\frac{\phi}{2}\right) \right] = -\sigma(\phi) + i\theta(\phi), \tag{6.72}$$

where ϕ is the argument of ρ. We plot the values of $\sigma(\theta) = -\log|q|$ in Fig. 6.7 (right). It is positive except when $\phi \in \pi\mathbb{Z}$. Recall that $\rho = re^{i\phi} = e^{\tau + i\phi}$ in radial quantization, so that when we continue to the Lorentzian cylinder, $\tau = it$, the analytically continued nome

257
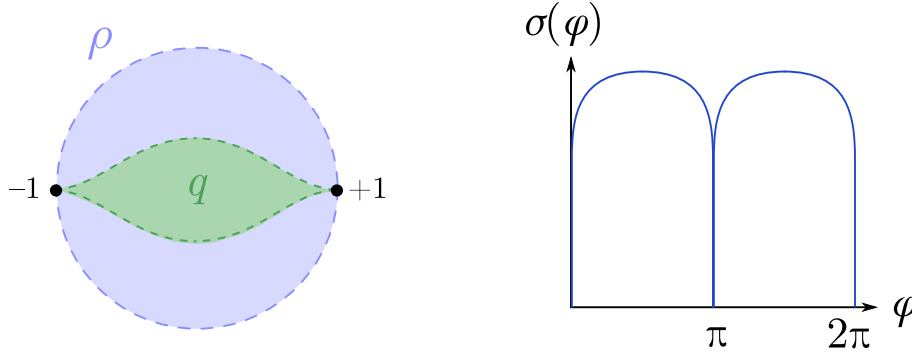
Figure 6.7: *Left.* Relation between the radial ρ variable and the nome q. *Right.* The real part of $-\log q$ as a function of Lorentzian cross-ratio.

becomes $q = e^{-\sigma(\phi+t)+i\theta(\phi+t)}$. The Cauchy-Schwarz inequality then gives

$$|g(q)| \leq \langle\psi||q|^{L_0-c/24}|\psi\rangle = g(e^{-\sigma(\phi-t)}). \tag{6.73}$$

This is the Euclidean pillow correlator again, which is finite except when $q = 1$, i.e., $\sigma = 0$, or $\phi + t \in \pi\mathbb{Z}$. These are precisely the light-cone singularities. We have thus proved that the only singularities in a 2D BCFT are the expected Euclidean and lightcone singularities, as advertised.

6.3.3 Bulk singularities

The location of the BCFT singularities we have just listed are universal and kinematic, in the sense they can be read off the behaviour of individual conformal blocks without consulting the spectrum. But for a BCFT with a simple holographic dual, a new type of singularity can emerge: an insertion now generates a lightcone in the *gravitational bulk* as well as the boundary. Bulk light-rays can head into the infrared gravitational geometry and return some time later to the boundary, indicating new singularities in the BCFT. When the bulk geometry is "shallow" (for example, when the geometry ends on a brane with a large negative tension), these singularities may even occur before the boundary light ray has returned.

To illustrate this behaviour, we begin by examining our simple toy model where empty

AdS is terminated by an ETW brane. We can re-write our angular metric (6.39) in the form

$$ds^2_{\text{Euc}} = \frac{1}{\sin^2 \theta \sin^2 \varphi} \left(d\tau^2 + \cos^2 \theta d\Omega^2_{d-2} + d\theta^2 + \sin^2 \theta \, d\varphi^2 \right) , \qquad (6.74)$$

by turning the AdS$_d$-radial coordinate on the slices into a second angular coordinate θ.[3] The angular radial coordinate θ on the slices takes values $\theta \in [0, \pi/2]$ with 0 being the boundary of AdS. Recall that the other coordinate ϕ takes values in the range $\varphi \in [0, \varphi_b]$ and is found from the coordinate change $\cos \varphi = \tanh(-r)$, while $d\Omega^2_{d-2}$ is the line element on the $\mathbb{S}^{d-2}$ that parametrizes the rest of the AdS$_d$ slice. Ignoring the conformal factor, we can see that the angular coordinates (θ, φ) together form part of an $\mathbb{S}^2$. By continuing to Lorentzian time, we arrive at the metric

$$ds^2_{\text{Lor}} = \frac{1}{\sin^2 \theta \sin^2 \varphi} \left(-dt^2 + \cos^2 \theta d\Omega^2_{d-2} + d\theta^2 + \sin^2 \theta \, d\varphi^2 \right) . \qquad (6.75)$$

We will perform our bulk causal calculations in these coordinates.

To begin, we restrict ourselves to consider null rays travelling on the 2-sphere at a fixed position on the $\mathbb{S}^{d-2}$ in (6.75). This is a straightforward affair. Consider a null ray $x^\mu(\lambda) = (t(\lambda), \theta(\lambda), \varphi(\lambda)))$, with affine parameter λ. The conformal factor drops out, leaving a simple null geodesic equation

$$- \dot{t}^2 + \dot{\theta}^2 + \sin^2 \theta \, \dot{\varphi}^2 = 0 . \qquad (6.76)$$

We are free to take $\dot{t} = 1$, so that affine time elapsed simply measures distance along the sphere, and the calculation of the return locus reduces to a problem of spherical trigonometry. Without loss of generality, we take the initial insertion to lie at $x^\mu = (0, \theta_0, 0)$. The null ray will head off into the bulk with some initial direction $\dot{\theta}_0 = \dot{\theta}(0)$, bounce off the brane at $\varphi = \varphi_b$, and return to the boundary $\varphi = 0$ at some angle θ_1 and time $\Delta t = d$ measured by the distance travelled.

To simplify the kinematics further, we can *double* the width of the wedge to $2\varphi_b$.

---

[3]By radial coordinate, we mean the global AdS$_d$-radial coordinate on the slices. These global AdS coordinates can be obtained simply by switching to polar coordinates on the slice, with an origin on the boundary.

Figure 6.8: (a) A 2D spatial-slice of AdS$_3$ cutoff by an ETW brane. (b) The same spatial slice conformally mapped to part of the two-sphere. The path of a null geodesic is marked in red.

There is now no need to consider the reflection off the brane, since the light ray sails smoothly through the mirror and arrives at the reflected boundary. It follows immediately from spherical trigonometry[4] that the initial position θ_0, direction $\dot{\theta}_0$, return angle θ_1 and elapsed time $\Delta t = d$ are related by

$$\cos d = \cos \theta_0 \cos \theta_1 + \sin \theta_0 \sin \theta_1 \cos \varphi_b . \tag{6.77}$$

We show the spatial path of one of these null geodesics in Fig. 6.8.

To compute the cross-ratio, ξ, for this locus, note that the flat BCFT coordinates are related to our polar coordinates $x_1 = e^{it} \cos \theta$ and $x_\perp = e^{it} \sin \theta$. Plugging in (6.77), the analytically continued cross-ratio is

$$\xi = \frac{(e^{i\Delta t} \cos \theta_1 - \cos \theta_0)^2 + (e^{i\Delta t} \sin \theta_1 - \sin \theta_0)^2}{4 e^{i\Delta t} \sin \theta_1 \sin \theta_0} = - \sin^2 \varphi_b . \tag{6.78}$$

This is pleasingly simple. In terms of our radial cross-ratio (6.14), it is even simpler:

$$\rho = e^{i2\varphi_b} . \tag{6.79}$$

We show the return locus for varying φ_b in Fig. 6.9. We conclude that the bulk causal structure of our simple ETW brane model predicts a singularity in the BCFT at the cross-ratio (6.79). This occurs away from the expected BCFT singularities at $\rho = 1, 0, -1$.

---

[4]Specifically, the spherical law of cosines.
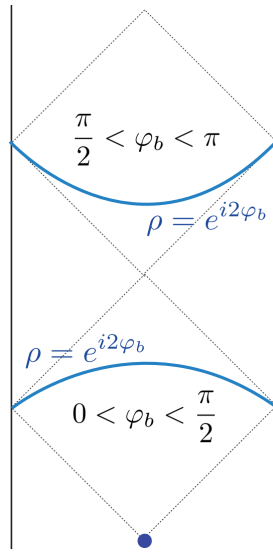
Figure 6.9: An illustration of two example return loci for branes of different tension. When the brane tension is positive, φ_b is greater than $\pi/2$ and null geodesics return to the boundary along a curve in the upper causal diamond. When the brane tension is negative, φ_b is less than $\pi/2$ and null geodesics return to the boundary along a curve in the lower causal diamond.

General warp factor

We can repeat the same argument with minor modifications for a more general warped background plus ETW brane as in (6.19). In this case, one only needs to find the appropriate angular coordinate to put the metric in the form

$$\mathrm{d}s^2_{\mathrm{Lor}} = \frac{1}{\sin^2\theta f(\varphi)}\left(-\mathrm{d}t^2 + \cos^2\theta\,\mathrm{d}\Omega^2_{d-2} + \mathrm{d}\theta^2 + \sin^2\theta\,\mathrm{d}\varphi^2\right)\,, \tag{6.80}$$

for some function $f(\varphi)$ determined by the warp factor $A(r)$. Because the causal structure does not depend on this unknown conformal factor, we again find the return locus to be

$$\rho = e^{i2\varphi_b}\,, \tag{6.81}$$

where $\varphi_b = \int_{-\infty}^{r_b} e^{-A(r)}\mathrm{d}r$. We note, in particular, that the causal structure of the bulk and of the return locus to the boundary is independent of the Euclidean distance to the brane. In contrast to this work, the Euclidean distance is what appears in holographic calculation of boundary entropy in 2d CFTs, for example, and many calculations of entanglement entropy.

General geodesics

While calculating null geodesics which are not at a fixed position on the $\mathbb{S}^{d-2}$ would be slightly more challenging, there is no need to go to the trouble. The BCFT two-point function is a function only of a single cross-ratio, up to a conformally-covariant pre-factor. Thus, having mapped part of the null cone to the locus $\rho = e^{i2\varphi_b}$, we can conclude that null geodesics with non-zero momentum on the sphere must also return at another point on the sphere with the same cross-ratio. Or, in other words, we can map any two unit vectors on the AdS_d slices into each other by a conformal transformation and so all of the null rays are equivalent.

6.4 Illuminating the brane

In §6.2 we showed how the bulk geometry of a simple ETW brane model is encoded in the spectrum and BOE coefficients of the dual BCFT. And in §6.3 we showed that the bulk causal structure also predicts new Lorentzian singularities in the BCFT from null rays that reflect off the bulk ETW brane. We now put these two sides of the coin together and explain how one entails the other.[5]

The boundary conformal block, written in terms of our radial cross-ratio (6.16), has a simple large dimension limit

$$\lim_{\widehat{\Delta}\to\infty} g^b_{\widehat{\Delta}}(\rho) = (4\rho)^{\widehat{\Delta}} \frac{1}{(1-\rho^2)^{(d-1)/2}} \ . \tag{6.82}$$

We consider this large-dimension limit at the return time of the bulk null cone, (6.79), to see that

$$\lim_{\widehat{\Delta}\to\infty} g^b_{\widehat{\Delta}}(e^{i2\varphi_b}) = 4^{\widehat{\Delta}} e^{i2\widehat{\Delta}\varphi_b} \frac{1}{(1-e^{i4\varphi_b})^{(d-1)/2}} \ . \tag{6.83}$$

When we plug in the asymptotic spacing of boundary operator dimensions in our simple model, (6.47),

$$\widehat{\Delta} = \widehat{\Delta}_0 + n\frac{\pi}{\varphi_b} \ , \tag{6.84}$$

we see that the block takes the form

$$\lim_{n\to\infty} g^b_{\widehat{\Delta}_n}(\rho) = e^{i2\widehat{\Delta}_0\varphi_b} 4^{\widehat{\Delta}_n} \frac{1}{(1-e^{i4\varphi_b})^{(d-1)/2}} \ . \tag{6.85}$$

The spacing of the boundary operator dimensions has exactly cancelled the n-dependence of the phase precisely at the return time of bulk null cone.

These conformal blocks will then all add coherently at this point so that the sum over conformal blocks is

$$e^{i2\widehat{\Delta}_0\varphi_b} 4^{\widehat{\Delta}_0} \frac{1}{(1-e^{i4\varphi_b})^{(d-1)/2}} \sum_n 2^{2n\frac{\pi}{\varphi_b}} b_n \ . \tag{6.86}$$

---

[5]Or heads from one to the other. Pun obviously intended.

Consequently, this sum can potentially diverge. To see that this is in fact the case, we plug in the large-n BOE coefficients from (6.52). Dropping the prefactor, near the return time at $\rho = \exp\left[i2\varphi_b(1 + \epsilon)\right]$ the sum over n gives

$$\sum_n e^{2\pi in\epsilon} n^{2\Delta - \frac{d+1}{2}} . \tag{6.87}$$

This is just a Fourier transform of the BOE coefficients. Doing the Fourier transform and extracting the singular contributions, we find Lorentzian singularities in the two-point function proportional to

$$\mathcal{G}(\rho) \sim \frac{1}{(\rho_b - \rho)^{2\Delta - \frac{d-1}{2}}} \frac{1}{(-1 - \rho)^{\frac{d-1}{2}}} . \tag{6.88}$$

We conclude that the bulk causal structure has been mapped into a particular regular asymptotic spacing of the boundary operators that appear in the BOE.

Our story is a very close analogue, both in spirit and technically, to the story in [83]. There the authors explained how the causal structure of the dual AdS vacuum leads to new singularities in CFT four-point functions. These result from local interactions that happen at a point in the AdS bulk geometry. The bulk point isn't expected to be a true singularity of the four-point function—these are believed to occur only where predicted by Landau diagrams in the boundary theory. Rather it is a resonance in the correlator that is smoothed out at the scale of the cut-off where bulk locality breaks down.

Similarly, we don't expect to find true new singularities in the BCFT two-point function. On the bulk side, we don't expect the brane to be exactly local. It will have some intrinsic width at which it will smear out bulk signals that reflect off the brane. On the boundary side, we only expect singularities where allowed by BCFT Landau diagrams. Thus, above some cutoff scale $\widehat{\Delta}_{\mathrm{gap}}$ that determines the width of the brane we expect the careful alignment of boundary operator dimensions to break down. Above this dimension, operators contribute with incoherent phases, truncating the divergent sum in (6.87)

No bulk branes (at least generically)

We have argued that we don't expect the bulk brane singularity to be a true singularity of the BCFT. Nevertheless, the validity of our semiclassical description, a bulk geometry terminated by an ETW brane, over a large range of scales requires the careful alignment of boundary operator dimensions up to some large $\widehat{\Delta}_{\mathrm{gap}}$.

We conjecture that this careful alignment is not a generic feature of BCFTs, even when the underlying CFT has a good gravitational description. Thus, an operator spectrum and BOE coefficients consistent with a bulk ETW brane geometry must be another input or assumption about the particular boundary condition of the CFT, much in the way we have to assume features of the spectrum of a large c CFT such that it has a good semiclassical gravitational description.

We do know that the correlation functions of a BCFT become those of the underlying CFT when all insertions are far from the boundary. Thus, we do not claim that the geometry will break down everywhere in the bulk. Rather, our claim is that generically there cannot be the type of simple causal structure consistent with an ETW brane geometry. The lack of fine-tuned dimensions prohibits null-rays from leaving the boundary and returning in reasonably short times.[6]

In the spirit of [17], we can formalize our conjecture as the following:

Conjecture 1. *A holographic CFT with boundary condition B will have a good bulk dual provided*

1. *correlation functions factorize about a (non-universal) free bulk solution; and*

2. *the boundary operator spectrum is gapped such that below some large $\widehat{\Delta}_{\mathrm{gap}}$ the only operators are simple boundary operators and their multi-trace composites.*

It is the first of these conditions—the existence of a consistent leading-order free bulk two-point function—that we have argued shouldn't generically look like an ETW brane. We leave the examination of the second of these conditions to future work, but we note

---

[6]Of course, if we are willing to wait sufficiently long times, we can produce a resonance in an arbitrary theory by waiting for the phases of any finite number of blocks to align in the future. It's not clear that these types of resonances should have a *simple* gravitational interpretation.

that aspects of this are challenging without a characterization of the space of solutions to the first assumption.

Note that the causal structure of the four-point function in a holographic CFT also requires a similar alignment of operator dimensions. Specifically, in a holographic CFT one obtains "double-twist operators" due to the crossing equations and the presence of the identity operator; the stress tensor then fixes their anomalous dimensions, which asymptotically go to zero at both large spin and large central charge. These two facts explain the emergence of the "bulk point" [83], where scattering between CFT operators occurs in the bulk but not the boundary.

In a defect CFT, a similar story generically emerges [186]: for a defect of codimension q, there are boundary operators associated to derivatives of bulk primaries in the q directions transverse to the defect. Their anomalous dimension goes to zero at large "transverse spin" (i.e. the charge of the residual $SO(q - 1, 1)$ symmetry). This control of the anomalous dimensions clearly vanishes in an interface or boundary CFT. We no longer have any transverse spin to work with when $q = 1$, even though we still have operators given by derivatives of bulk primaries in the remaining transverse direction. To have a good bulk dual, these operators must possess non-trivial anomalous dimensions that aren't fixed by symmetry and universal properties alone. A BCFT is then a simple setting where we have insufficient symmetry to fix the form of the vacuum two-point function and it must be an input.

A useful analogy in holographic CFTs for when the free correlators are not fixed by symmetry is an excited state. Excited states in a holographic CFT will not generically have a good bulk geometry and hence will not have a good causal structure. Thus, we do not expect to see the approximate singularities of a local bulk geometry except in carefully chosen states. We suggest good ETW brane geometries are far from generic in the space of BCFTs in much the same way good bulk geometries are far from generic in the Hilbert space.

266

6.5 Discussion

We have argued that a powerful probe of the putative bulk geometry of a BCFT is the Lorentzian two-point function. The two-point function is sensitive to the (approximate) causal structure of the bulk and is a probe of how null rays can reflect off the IR geometry and return to the boundary.

In the case that the bulk geometry is terminated by an ETW brane, we argued in §6.2 that this is indicated in the two-point function of simple CFT operators by a fixed, careful alignment of the boundary operator dimensions appearing in the BOE. We suggest that there is no reason to expect such spacing generically in the possible boundary conditions for a given holographic CFT. Thus, we have argued that an ETW brane is not generically the correct bulk description of a conformal boundary condition for a holographic CFT.

Boundary vs. bulk causality

In the ETW brane scenario, when the brane is close to the boundary, bulk null rays can reflect off the bulk brane and return to their point of origin more quickly than a null ray confined to the boundary. This is the region (in Fig. 6.5) where $-1 < \xi < 0$. In a 2D CFT with the simplest AdS+ETW brane bulk, for example, this happens when the boundary entropy is negative.

There is some apparent (if perhaps naive) tension here with causality: a bulk observer can learn information about the boundary condition more quickly than they can causally probe the boundary of the CFT itself. On the other hand, these signals return in the causal future of the boundary point, so there is no sharp conflict with boundary causality. More-over, it's important to note that information about the boundary condition isn't localized at the boundary itself. As just one obvious example, information about the boundary condition is encoded in one-point functions measurable arbitrarily far from the boundary.

There are other cases where a bulk singularity in the region $-1 < \xi < 0$ would actually be in conflict with boundary causality. In an ICFT (folded to be seen as a BCFT) a bulk singularity in this region between a RHS and LHS operator would correspond to a signal travelling acausally across the defect to the other side. It would be interesting to have top-

down constructions where information about the boundary can be causally accessed more quickly via the bulk than via the CFT.

Bootstrap constraints

We have argued that the constraints on the boundary spectrum necessary for agreement with a simple bulk geometry appear fragile and are not expected to be generic. Moreover, the existence of more complicated top-down constructions also seems to imply that a fixed regular spacing cannot be the only allowed possibility. Nevertheless, we have not ruled out the possibility that the alignment of boundary operator dimensions follows from some simpler assumptions, perhaps by using an appropriate bootstrap argument. It would be interesting to explore this further.

2D CFTs

In Chapter 3, it was shown that the entanglement entropy of an interval in a 2D BCFT is consistent with the AdS+ETW brane proposal, provided the assumption of vacuum block dominance in the BCFT. It is somewhat surprising that the bulk would reproduce the correct entanglement entropy, even if it fails to satisfy the constraints laid out in this chapter. One possible resolution is that the entanglement entropy is a rather weak probe of the bulk geometry in this setting. When in this disconnected phase, the entropy depends only on the boundary entropy and measures only the integrated distance to the brane. It would be interesting if the assumption of vacuum block dominance also placed constraints in the Lorentzian bulk brane regime we considered here.

6.6   Conclusion

In this chapter, we have explored the connection between the existence of a geometric dual with an ETW brane, and the structure of singularities in correlators in the dual BCFT. We discovered that, if the brane exists, then for each primary operator in the BCFT we have an apparently independent tuning of the operator spectrum. This suggests that ETW branes

are highly non-generic, even when the underlying CFT is holographic. Small changes to the spectrum will result in a misalignment of operator dimensions, and a corresponding loss of the apparent bulk brane, as probed by the two-point function.

This is unsurprising, since CFTs are non-generic, and states with good geometric duals in a holographic CFT are non-generic. It does mean, however, that we should not expect constructions with geometric ETW branes to work generically. For instance, in the context of boundary state black holes, they are likely to be atypical, and understanding the origin of the Page curve will require more general constructions. Nevertheless, they are consistent with bulk causality and can therefore provide insight into the nature of the mechanism in a specialized setting.

Chapter 7

Conclusion

Motivated by the smooth interior of the maximally extended Ads-Schwarzschild geometry dual to the thermofield double, we constructed one-sided microstates of a black hole in Chapter 2. The basic strategy was to cut the Euclidean path integral preparing the thermofield double in half, introducing a symmetric, high-energy boundary state at the cut. From the AdS/BCFT correspondence, we argued that this incision was dual to a co-dimension one surface in the bulk called an end-of-the-world brane, smoothly terminating the spacetime. Using this geometry and a modified version of the Ryu-Takayanagi formula, we found that for large regions of the BCFT and suitable boundary states, the minimal surface falls through the horizon and attaches to the brane. By virtue of entanglement wedge reconstruction, this gives us access to behind-the-horizon physics in the BCFT.

In Chapter 3, we considered boundary microstates in $d = 2$, and computed entanglement entropy in the 2d BCFT as a correlator of twist operators. By introducing constraints on the operator spectrum and OPE coefficients, we ensured dominance of the vacuum block, verifying the gravitational predictions of the Ryu-Takayanagi formula in a class of holographic BCFTs. This provided an important self-consistency check of the proposed dual and the modified RT formula.

Having computed a twist correlator in one background, we can immediately compute the correlator in any conformally related background. We used this freedom in Chapter 4 to

map the calculation of entanglement entropy for a Euclidean BCFT on the upper half-plane to a thermal state on a half-line. The Lorentzian continuation is a dynamically evolving spacetime with a black hole on the brane itself. The entanglement entropy exhibits a transition at late times, dual in the bulk to a transition in minimal surfaces, after which the entanglement wedge includes part of the black hole interior. This region is called an island, and provides an in-principle mechanism for information to escape the black hole, relating our construction to progress on the information paradox. We analyzed a related example in which there is genuine energy loss and not merely an "information radiation" transition in minimal surface.

To sharpen the relation between information propagation and islands, in Chapter 5 we proved a theorem relating the performability of certain distributed quantum computations in the BCFT to a transition in minimal surface in the bulk. By reinterpreting this theorem, we showed that information is able to causally escape a black hole and into a reservoir, through an emergent higher dimension, only if an island has formed.

Finally, in Chapter 6 we recast these quantum tasks as correlators in the BCFT. By seeking appropriate CFT singularities, dual to the existence of a bulk scattering vertex on the brane, we were led to a set of finely-tuned constraints on the boundary operator spectrum. This suggests that in the presence of a brane, bulk causal structure is fragile and the microscopic conditions which preserve it are non-generic. For a 2d BCFT, we also showed that there are no true singularities corresponding to bulk scattering vertices, so they must be smeared into resonances even when the spectrum is finely tuned to ensure approximate bulk causal structure.

This does not imply that we should abandon holographic models which feature ETW branes. Rather, it teaches us that, similar to the AdS/CFT correspondence itself, symmetry is not enough to guarantee the emergence of geometry. We also need some microscopic conditions on correlators to guarantee that geometry is not "fuzzed out" by quantum effects. With these conditions in place, we get toy models where features simplify and puzzles resolve. And like AdS/CFT, we expect these toy models will yield qualitative and quantitative hints about how to approach the problems of black hole physics in a more general setting.

271

Bibliography

[1] S. Cooper, M. Rozali, B. Swingle, M. Van Raamsdonk, C. Waddell and D. Wakeham, *Black hole microstate cosmology*, *JHEP* **07** (2019) 065 [`1810.10601`].

[2] J. Sully, M.V. Raamsdonk and D. Wakeham, *BCFT entanglement entropy at large central charge and the black hole interior*, *JHEP* **03** (2021) 167 [`2004.13088`].

[3] M. Rozali, J. Sully, M. Van Raamsdonk, C. Waddell and D. Wakeham, *Information radiation in BCFT models of black holes*, *JHEP* **05** (2020) 004 [`1910.12836`].

[4] A. May and D. Wakeham, *Quantum tasks require islands on the brane*, *Class. Quant. Grav.* **38** (2021) [`2102.01810`].

[5] W. Reeves, M. Rozali, P. Simidzija, J. Sully, C. Waddell and D. Wakeham, *Looking for (and not finding) a bulk brane*, *JHEP* **12** (2021) 002 [`2108.10345`].

[6] A. Almheiri, R. Mahajan, J. Maldacena and Y. Zhao, *The Page curve of Hawking radiation from semiclassical geometry*, *JHEP* **03** (2020) 149 [`1908.10996`].

[7] L. Fidkowski, V. Hubeny, M. Kleban and S. Shenker, *The Black hole singularity in AdS / CFT*, *JHEP* **02** (2004) 014 [`hep-th/0306170`].

[8] J.M. Maldacena, *The Large N limit of superconformal field theories and supergravity*, *Adv. Theor. Math. Phys.* **2** (1998) 231 [`hep-th/9711200`].

[9] S.S. Gubser, I.R. Klebanov and A.M. Polyakov, *Gauge theory correlators from noncritical string theory*, *Phys. Lett. B* **428** (1998) 105 [`hep-th/9802109`].

[10] E. Witten, *Anti-de Sitter space and holography*, *Adv. Theor. Math. Phys.* **2** (1998) 253 [`hep-th/9802150`].

[11] O. Aharony, S.S. Gubser, J.M. Maldacena, H. Ooguri and Y. Oz, *Large N field theories, string theory and gravity*, *Phys. Rept.* **323** (2000) 183 [`hep-th/9905111`].

[12] P. Di Francesco, P. Mathieu and D. Senechal, *Conformal Field Theory*, Graduate Texts in Contemporary Physics, Springer-Verlag, New York (1997), 10.1007/978-1-4612-2256-9.

[13] M. Ammon and J. Erdmenger, *Gauge/gravity duality: Foundations and applications*, Cambridge University Press (2015), 10.1017/CBO9780511846373.

[14] D. Harlow, *TASI Lectures on the Emergence of Bulk Physics in AdS/CFT*, vol. TASI2017, p. 002, 2018, DOI [`1802.01040`].

[15] D. Harlow, *Jerusalem Lectures on Black Holes and Quantum Information*, *Rev. Mod. Phys.* **88** (2016) 015002 [`1409.1231`].

[16] T. Hartman, *Lectures on Quantum Gravity and Black Holes*, Cornell University lecture notes (2015).

[17] I. Heemskerk, J. Penedones, J. Polchinski and J. Sully, *Holography from Conformal Field Theory*, *JHEP* **10** (2009) 079 [`0907.0151`].

[18] J.D. Brown and M. Henneaux, *Central Charges in the Canonical Realization of Asymptotic Symmetries: An Example from Three-Dimensional Gravity*, *Commun. Math. Phys.* **104** (1986) 207.

[19] D. Marolf, *States and boundary terms: Subtleties of Lorentzian AdS / CFT*, *JHEP* **05** (2005) 042 [`hep-th/0412032`].

[20] K. Skenderis and B.C. van Rees, *Real-time gauge/gravity duality: Prescription, Renormalization and Examples*, *JHEP* **05** (2009) 085 [`0812.2909`].

[21] J.M. Bardeen, B. Carter and S.W. Hawking, *The Four laws of black hole mechanics*, *Commun. Math. Phys.* **31** (1973) 161.

[22] J.B. Hartle and S.W. Hawking, *Path Integral Derivation of Black Hole Radiance*, *Phys. Rev. D* **13** (1976) 2188.

[23] S.W. Hawking, *Particle Creation by Black Holes*, *Commun. Math. Phys.* **43** (1975) 199.

[24] E. Witten, *Anti-de Sitter space, thermal phase transition, and confinement in gauge theories*, *Adv. Theor. Math. Phys.* **2** (1998) 505 [`hep-th/9803131`].

[25] S.W. Hawking and D.N. Page, *Thermodynamics of Black Holes in anti-De Sitter Space*, *Commun. Math. Phys.* **87** (1983) 577.

[26] J.D. Bekenstein, *Black holes and entropy*, *Phys. Rev. D* **7** (1973) 2333.

[27] J.D. Bekenstein, *Generalized second law of thermodynamics in black hole physics*, *Phys. Rev. D* **9** (1974) 3292.

[28] S.W. Hawking, *Gravitational radiation from colliding black holes*, *Phys. Rev. Lett.* **26** (1971) 1344.

[29] S.D. Mathur, *Fuzzballs and the information paradox: A Summary and conjectures*, `0810.4525`.

[30] J.M. Maldacena, *Eternal black holes in anti-de Sitter*, *JHEP* **04** (2003) 021 [`hep-th/0106112`].

[31] W. Israel, *Thermo field dynamics of black holes*, *Phys. Lett. A* **57** (1976) 107.

[32] A. Einstein, B. Podolsky and N. Rosen, *Can quantum mechanical description of physical reality be considered complete?*, *Phys. Rev.* **47** (1935) 777.

[33] M. Van Raamsdonk, *Comments on quantum gravity and entanglement*, `0907.2939`.

[34] M. Van Raamsdonk, *Building up spacetime with quantum entanglement*, *Gen. Rel. Grav.* **42** (2010) 2323 [`1005.3035`].

[35] J. Maldacena and L. Susskind, *Cool horizons for entangled black holes*, *Fortsch. Phys.* **61** (2013) 781 [`1306.0533`].

[36] A. Einstein and N. Rosen, *The Particle Problem in the General Theory of Relativity*, *Phys. Rev.* **48** (1935) 73.

[37] S. Ryu and T. Takayanagi, *Aspects of Holographic Entanglement Entropy*, *JHEP* **08** (2006) 045 [`hep-th/0605073`].

[38] S. Ryu and T. Takayanagi, *Holographic derivation of entanglement entropy from AdS/CFT*, *Phys. Rev. Lett.* **96** (2006) 181602 [`hep-th/0603001`].

[39] H. Casini, M. Huerta and R.C. Myers, *Towards a derivation of holographic entanglement entropy*, *JHEP* **05** (2011) 036 [`1102.0440`].

[40] A. Lewkowycz and J. Maldacena, *Generalized gravitational entropy*, *JHEP* **08** (2013) 090 [`1304.4926`].

[41] V.E. Hubeny, M. Rangamani and T. Takayanagi, *A Covariant holographic entanglement entropy proposal*, *JHEP* **07** (2007) 062 [`0705.0016`].

[42] X. Dong, A. Lewkowycz and M. Rangamani, *Deriving covariant holographic entanglement*, *JHEP* **11** (2016) 028 [`1607.07506`].

[43] A.C. Wall, *Maximin Surfaces, and the Strong Subadditivity of the Covariant Holographic Entanglement Entropy*, *Class. Quant. Grav.* **31** (2014) 225007 [`1211.3494`].

[44] T. Faulkner, A. Lewkowycz and J. Maldacena, *Quantum corrections to holographic entanglement entropy*, *JHEP* **11** (2013) 074 [`1307.2892`].

[45] N. Engelhardt and A.C. Wall, *Quantum Extremal Surfaces: Holographic Entanglement Entropy beyond the Classical Regime*, *JHEP* **01** (2015) 073 [`1408.3203`].

[46] C. Akers, N. Engelhardt, G. Penington and M. Usatyuk, *Quantum Maximin Surfaces*, *JHEP* **08** (2020) 140 [`1912.02799`].

[47] A.C. Wall, *Ten Proofs of the Generalized Second Law*, *JHEP* **06** (2009) 021 [`0901.3865`].

[48] B. Czech, J.L. Karczmarek, F. Nogueira and M. Van Raamsdonk, *The Gravity Dual of a Density Matrix*, *Class. Quant. Grav.* **29** (2012) 155009 [`1204.1330`].

[49] D.L. Jafferis, A. Lewkowycz, J. Maldacena and S.J. Suh, *Relative entropy equals bulk relative entropy*, *JHEP* **06** (2016) 004 [`1512.06431`].

[50] X. Dong, D. Harlow and A.C. Wall, *Reconstruction of Bulk Operators within the Entanglement Wedge in Gauge-Gravity Duality*, *Phys. Rev. Lett.* **117** (2016) 021601 [`1601.05416`].

[51] T. Faulkner and A. Lewkowycz, *Bulk locality from modular flow*, *JHEP* **07** (2017) 151 [`1704.05464`].

[52] J. Cotler, P. Hayden, G. Penington, G. Salton, B. Swingle and M. Walter, *Entanglement Wedge Reconstruction via Universal Recovery Channels*, *Phys. Rev. X* **9** (2019) 031011 [`1704.05839`].

[53] M. Headrick, V.E. Hubeny, A. Lawrence and M. Rangamani, *Causality & holographic entanglement entropy*, *JHEP* **12** (2014) 162 [`1408.6300`].

[54] V.E. Hubeny and M. Rangamani, *Causal Holographic Information*, *JHEP* **06** (2012) 114 [`1204.1698`].

[55] N. Engelhardt and A.C. Wall, *Extremal Surface Barriers*, *JHEP* **03** (2014) 068 [`1312.3699`].

[56] T. Hartman and J. Maldacena, *Time Evolution of Entanglement Entropy from Black Hole Interiors*, *JHEP* **05** (2013) 014 [`1303.1080`].

[57] J.L. Cardy, *Conformal Invariance and Surface Critical Behavior*, *Nucl. Phys. B* **240** (1984) 514.

[58] M. Fujita, T. Takayanagi and E. Tonni, *Aspects of AdS/BCFT*, *JHEP* **11** (2011) 043 [1108.5152].

[59] T. Takayanagi, *Holographic Dual of BCFT*, *Phys. Rev. Lett.* **107** (2011) 101602 [1105.5165].

[60] I. Affleck and A.W.W. Ludwig, *Universal noninteger 'ground state degeneracy' in critical quantum systems*, *Phys. Rev. Lett.* **67** (1991) 161.

[61] P. Calabrese and J.L. Cardy, *Entanglement entropy and quantum field theory*, *J. Stat. Mech.* **0406** (2004) P06002 [hep-th/0405152].

[62] P. Calabrese and J. Cardy, *Entanglement entropy and conformal field theory*, *J. Phys. A* **42** (2009) 504005 [0905.4013].

[63] P. Calabrese and J. Cardy, *Quantum quenches in 1 + 1 dimensional conformal field theories*, *J. Stat. Mech.* **1606** (2016) 064003 [1603.02889].

[64] K. Jensen and A. O'Bannon, *Holography, Entanglement Entropy, and Conformal Field Theories with Boundaries or Defects*, *Phys. Rev. D* **88** (2013) 106006 [1309.4523].

[65] T. Hartman, *Entanglement Entropy at Large Central Charge*, 1303.6955.

[66] E. Shaghoulian, *Emergent gravity from Eguchi-Kawai reduction*, *JHEP* **03** (2017) 011 [1611.04189].

[67] J. Cardy and E. Tonni, *Entanglement Hamiltonians in two-dimensional conformal field theory*, *J. Stat. Mech.* **1612** (2016) 123103 [1608.01283].

[68] N.N. Bogolyubov, *On a New method in the theory of superconductivity*, *Nuovo Cim.* **7** (1958) 794.

[69] J.G. Valatin, *Comments on the theory of superconductivity*, *Nuovo Cim.* **7** (1958) 843.

[70] D. Harlow, J. Maltz and E. Witten, *Analytic Continuation of Liouville Theory*, *JHEP* **12** (2011) 071 [`1108.4417`].

[71] V. Mukhanov and S. Winitzki, *Introduction to Quantum Effects in Gravity*, Cambridge University Press (2007), 10.1017/CBO9780511809149.

[72] S.W. Hawking, *Black Holes and Thermodynamics*, *Phys. Rev. D* **13** (1976) 191.

[73] J.D. Bekenstein, *Statistical Black Hole Thermodynamics*, *Phys. Rev. D* **12** (1975) 3077.

[74] D.N. Page, *Average entropy of a subsystem*, *Phys. Rev. Lett.* **71** (1993) 1291 [`gr-qc/9305007`].

[75] G. Penington, *Entanglement Wedge Reconstruction and the Information Paradox*, *JHEP* **09** (2020) 002 [`1905.08255`].

[76] A. Almheiri, N. Engelhardt, D. Marolf and H. Maxfield, *The entropy of bulk quantum fields and the entanglement wedge of an evaporating black hole*, *JHEP* **12** (2019) 063 [`1905.08762`].

[77] A. May, *Quantum tasks in holography*, *JHEP* **10** (2019) 233 [`1902.06845`].

[78] A. May, G. Penington and J. Sorce, *Holographic scattering requires a connected entanglement wedge*, *JHEP* **08** (2020) 132 [`1912.05649`].

[79] M. Tomamichel, S. Fehr, J. Kaniewski and S. Wehner, *A monogamy-of-entanglement game with applications to device-independent quantum cryptography*, *New Journal of Physics* **15** (2013) 103002 [`1210.4359`].

[80] H. Buhrman, N. Chandran, S. Fehr, R. Gelles, V. Goyal, R. Ostrovsky et al., *Position-based quantum cryptography: Impossibility and constructions*, *SIAM Journal on Computing* **43** (2014) 150 [`1009.2490`].

[81] S. Gao and R.M. Wald, *Theorems on gravitational time delay and related issues*, *Class. Quant. Grav.* **17** (2000) 4999 [`gr-qc/0007021`].

[82] M. Gary, S.B. Giddings and J. Penedones, *Local bulk S-matrix elements and CFT singularities*, *Phys. Rev. D* **80** (2009) 085005 [`0903.4437`].

[83] J. Maldacena, D. Simmons-Duffin and A. Zhiboedov, *Looking for a bulk point*, *JHEP* **01** (2017) 013 [`1509.03612`].

[84] P. Liendo, L. Rastelli and B.C. van Rees, *The Bootstrap Program for Boundary CFT$_d$*, *JHEP* **07** (2013) 113 [`1210.4258`].

[85] I. Kourkoulou and J. Maldacena, *Pure states in the SYK model and nearly-AdS_2 gravity*, `1707.02325`.

[86] A. Almheiri, A. Mousatov and M. Shyani, *Escaping the Interiors of Pure Boundary-State Black Holes*, `1803.04434`.

[87] E. Witten, *Instability of the Kaluza-Klein Vacuum*, *Nucl. Phys. B* **195** (1982) 481.

[88] D.M. McAvity and H. Osborn, *Conformal field theories near a boundary in general dimensions*, *Nucl. Phys. B* **455** (1995) 522 [`cond-mat/9505127`].

[89] J.L. Cardy, *Boundary conformal field theory*, `hep-th/0411189`.

[90] A. Karch and L. Randall, *Open and closed string interpretation of SUSY CFT's on branes with boundaries*, *JHEP* **06** (2001) 063 [`hep-th/0105132`].

[91] M. Fujita, T. Takayanagi and E. Tonni, *Aspects of AdS/BCFT*, *JHEP* **11** (2011) 043 [`1108.5152`].

[92] J. Louko and D. Marolf, *Single exterior black holes and the AdS / CFT conjecture*, *Phys. Rev. D* **59** (1999) 066002 [`hep-th/9808081`].

[93] J. de Boer, R. Van Breukelen, S.F. Lokhande, K. Papadodimas and E. Verlinde, *On the interior geometry of a typical black hole microstate*, *JHEP* **05** (2019) 010 [`1804.10580`].

[94] T. Banks, M.R. Douglas, G.T. Horowitz and E.J. Martinec, *AdS dynamics from conformal field theory*, `hep-th/9808016`.

[95] C. Fefferman and C.R. Graham, *The ambient metric*, *Ann. Math. Stud.* **178** (2011) 1 [`0710.0919`].

[96] P. Kraus, *Dynamics of anti-de Sitter domain walls*, *JHEP* **12** (1999) 011 [`hep-th/9910149`].

[97] B. Freivogel, V.E. Hubeny, A. Maloney, R.C. Myers, M. Rangamani and S. Shenker, *Inflation in AdS/CFT*, *JHEP* **03** (2006) 007 [`hep-th/0510046`].

[98] I. Bah, A. Faraggi, L.A. Pando Zayas and C.A. Terrero-Escalante, *Holographic entanglement entropy and phase transitions at finite temperature*, *Int. J. Mod. Phys. A* **24** (2009) 2703 [`0710.5483`].

[99] N. Bao and H. Ooguri, *Distinguishability of black hole microstates*, *Phys. Rev. D* **96** (2017) 066017 [`1705.07943`].

[100] B. Czech, J.L. Karczmarek, F. Nogueira and M. Van Raamsdonk, *Rindler Quantum Gravity*, *Class. Quant. Grav.* **29** (2012) 235025 [`1206.1323`].

[101] M. Van Raamsdonk, *Building up spacetime with quantum entanglement II: It from BC-bit*, `1809.01197`.

[102] R. Emparan, *AdS / CFT duals of topological black holes and the entropy of zero energy states*, *JHEP* **06** (1999) 036 [`hep-th/9906040`].

[103] M. Chiodaroli, E. D'Hoker and M. Gutperle, *Simple Holographic Duals to Boundary CFTs*, *JHEP* **02** (2012) 005 [`1111.6912`].

[104] M. Chiodaroli, E. D'Hoker and M. Gutperle, *Holographic duals of Boundary CFTs*, *JHEP* **07** (2012) 177 [`1205.5303`].

[105] M. Gutperle and J. Samani, *Holographic RG-flows and Boundary CFTs*, *Phys. Rev.* **D86** (2012) 106007 [`1207.7325`].

[106] A. Recknagel and V. Schomerus, *Boundary Conformal Field Theory and the Worldsheet Approach to D-Branes*, Cambridge Monographs on Mathematical Physics, Cambridge University Press (2013), 10.1017/CBO9780511806476.

[107] A. Karch and L. Randall, *Open and closed string interpretation of SUSY CFT's on branes with boundaries*, JHEP **06** (2001) 063 [hep-th/0105132].

[108] A. Faraji Astaneh and S.N. Solodukhin, *Holographic calculation of boundary terms in conformal anomaly*, Phys. Lett. B **769** (2017) 25 [1702.00566].

[109] E. D'Hoker, J. Estes and M. Gutperle, *Exact half-BPS Type IIB interface solutions. I. Local solution and supersymmetric Janus*, JHEP **06** (2007) 021 [0705.0022].

[110] E. D'Hoker, J. Estes and M. Gutperle, *Exact half-BPS Type IIB interface solutions. II. Flux solutions and multi-Janus*, JHEP **06** (2007) 022 [0705.0024].

[111] O. Aharony, L. Berdichevsky, M. Berkooz and I. Shamir, *Near-horizon solutions for D3-branes ending on 5-branes*, Phys. Rev. D **84** (2011) 126003 [1106.1870].

[112] B. Assel, C. Bachas, J. Estes and J. Gomis, *Holographic Duals of D=3 N=4 Superconformal Field Theories*, JHEP **08** (2011) 087 [1106.4253].

[113] T. Anous, T. Hartman, A. Rovai and J. Sonner, *Black Hole Collapse in the 1/c Expansion*, JHEP **07** (2016) 123 [1603.04856].

[114] J.L. Cardy, O.A. Castro-Alvaredo and B. Doyon, *Form factors of branch-point twist fields in quantum integrable models and entanglement entropy*, J. Statist. Phys. **130** (2008) 129 [0706.3384].

[115] E. Perlmutter, *Comments on Renyi entropy in AdS$_3$/CFT$_2$*, JHEP **05** (2014) 052 [1312.5740].

[116] A.A. Belavin, A.M. Polyakov and A.B. Zamolodchikov, *Infinite Conformal Symmetry in Two-Dimensional Quantum Field Theory*, Nucl. Phys. B **241** (1984) 333.

[117] H. Dorn and H.J. Otto, *Two and three point functions in Liouville theory*, *Nucl. Phys. B* **429** (1994) 375 [`hep-th/9403141`].

[118] A.B. Zamolodchikov and A.B. Zamolodchikov, *Structure constants and conformal bootstrap in Liouville field theory*, *Nucl. Phys. B* **477** (1996) 577 [`hep-th/9506136`].

[119] A.B. Zamolodchikov, *Conformal symmetry in two-dimensional space: Recursion representation of conformal block*, *Theoretical and Mathematical Physics* **73** (1987) 1088.

[120] D. Pappadopulo, S. Rychkov, J. Espin and R. Rattazzi, *OPE Convergence in Conformal Field Theory*, *Phys. Rev.* **D86** (2012) 105043 [`1208.6449`].

[121] B. Chen and J.-J. Zhang, *On short interval expansion of Rényi entropy*, *JHEP* **11** (2013) 164 [`1309.5453`].

[122] P. Calabrese, J. Cardy and E. Tonni, *Entanglement entropy of two disjoint intervals in conformal field theory II*, *J. Stat. Mech.* **1101** (2011) P01021 [`1011.5482`].

[123] G.H. Hardy and S. Ramanujan, *Asymptotic formulæ in combinatory analysis*, *Proceedings of the London Mathematical Society* **s2-17** (1918) 75.

[124] T. Hartman, C.A. Keller and B. Stoica, *Universal Spectrum of 2d Conformal Field Theory in the Large c Limit*, *JHEP* **09** (2014) 118 [`1405.5137`].

[125] S.W. Hawking, *Breakdown of Predictability in Gravitational Collapse*, *Phys. Rev. D* **14** (1976) 2460.

[126] D.N. Page, *Information in black hole radiation*, *Phys. Rev. Lett.* **71** (1993) 3743 [`hep-th/9306083`].

[127] A. Almheiri, D. Marolf, J. Polchinski and J. Sully, *Black Holes: Complementarity or Firewalls?*, *JHEP* **02** (2013) 062 [`1207.3123`].

[128] A. Almheiri, D. Marolf, J. Polchinski, D. Stanford and J. Sully, *An Apologia for Firewalls*, *JHEP* **09** (2013) 018 [`1304.6483`].

[129] D. Marolf and J. Polchinski, *Gauge/Gravity Duality and the Black Hole Interior*, *Phys. Rev. Lett.* **111** (2013) 171301 [`1307.4706`].

[130] S.L. Braunstein, S. Pirandola and K. Życzkowski, *Better Late than Never: Information Retrieval from Black Holes*, *Phys. Rev. Lett.* **110** (2013) 101301 [`0907.1190`].

[131] S.D. Mathur, *The Information paradox: A Pedagogical introduction*, *Class. Quant. Grav.* **26** (2009) 224001 [`0909.1038`].

[132] M. Van Raamsdonk, *Evaporating Firewalls*, *JHEP* **11** (2014) 038 [`1307.1796`].

[133] C. Akers, N. Engelhardt and D. Harlow, *Simple holographic models of black hole evaporation*, *JHEP* **08** (2020) 032 [`1910.00972`].

[134] J.V. Rocha, *Evaporation of large black holes in AdS: Coupling to the evaporon*, *JHEP* **08** (2008) 075 [`0804.0055`].

[135] A. Almheiri, X. Dong and D. Harlow, *Bulk Locality and Quantum Error Correction in AdS/CFT*, *JHEP* **04** (2015) 163 [`1411.7041`].

[136] D.N. Page, *Finite upper bound for the Hawking decay time of an arbitrarily large black hole in anti–de Sitter spacetime*, *Phys. Rev. D* **97** (2018) 024004 [`1507.02682`].

[137] Y.C. Ong, *Hawking Evaporation Time Scale of Topological Black Holes in Anti-de Sitter Spacetime*, *Nucl. Phys. B* **903** (2016) 387 [`1507.07845`].

[138] L. Randall and R. Sundrum, *An Alternative to compactification*, *Phys. Rev. Lett.* **83** (1999) 4690 [`hep-th/9906064`].

[139] S. Antonini and B. Swingle, *Cosmology at the end of the world*, *Nature Phys.* **16** (2020) 881 [`1907.06667`].

[140] A. Almheiri, T. Hartman, J. Maldacena, E. Shaghoulian and A. Tajdini, *Replica Wormholes and the Entropy of Hawking Radiation*, *JHEP* **05** (2020) 013 [1911.12333].

[141] G. Penington, S.H. Shenker, D. Stanford and Z. Yang, *Replica wormholes and the black hole interior*, *JHEP* **03** (2022) 205 [1911.11977].

[142] T. Faulkner, *The Entanglement Renyi Entropies of Disjoint Intervals in AdS/CFT*, 1303.7221.

[143] T. Shimaji, T. Takayanagi and Z. Wei, *Holographic Quantum Circuits from Splitting/Joining Local Quenches*, *JHEP* **03** (2019) 165 [1812.01176].

[144] P. Caputa, T. Numasawa, T. Shimaji, T. Takayanagi and Z. Wei, *Double Local Quenches in 2D CFTs and Gravitational Force*, *JHEP* **09** (2019) 018 [1905.08265].

[145] M. Miyaji, S. Ryu, T. Takayanagi and X. Wen, *Boundary States as Holographic Duals of Trivial Spacetimes*, *JHEP* **05** (2015) 152 [1412.6226].

[146] P. Simidzija and M. Van Raamsdonk, *Holo-ween*, *JHEP* **12** (2020) 028 [2006.13943].

[147] A. May and M. Van Raamsdonk, *Interpolating between multi-boundary wormholes and single-boundary geometries in holography*, *JHEP* **04** (2021) 185 [2011.14258].

[148] T. Hartman, Y. Jiang and E. Shaghoulian, *Islands in cosmology*, *JHEP* **11** (2020) 111 [2008.01022].

[149] A. Almheiri, R. Mahajan and J.E. Santos, *Entanglement islands in higher dimensions*, *SciPost Phys.* **9** (2020) 001 [1911.09666].

[150] H. Geng, A. Karch, C. Perez-Pardavila, S. Raju, L. Randall, M. Riojas et al., *Information Transfer with a Gravitating Bath*, *SciPost Phys.* **10** (2021) 103 [2012.04671].

[151] H. Geng and A. Karch, *Massive islands*, *JHEP* **09** (2020) 121 [`2006.02438`].

[152] H.Z. Chen, R.C. Myers, D. Neuenfeld, I.A. Reyes and J. Sandor, *Quantum Extremal Islands Made Easy, Part I: Entanglement on the Brane*, *JHEP* **10** (2020) 166 [`2006.04851`].

[153] H.Z. Chen, R.C. Myers, D. Neuenfeld, I.A. Reyes and J. Sandor, *Quantum Extremal Islands Made Easy, Part II: Black Holes on the Brane*, *JHEP* **12** (2020) 025 [`2010.00018`].

[154] A. May, *Holographic quantum tasks with input and output regions*, *JHEP* **08** (2021) 055 [`2101.08855`].

[155] S. Nezami and M. Walter, *Multipartite Entanglement in Stabilizer Tensor Networks*, *Phys. Rev. Lett.* **125** (2020) 241602 [`1608.02595`].

[156] D. Marolf, A.C. Wall and Z. Wang, *Restricted Maximin surfaces and HRT in generic black hole spacetimes*, *JHEP* **05** (2019) 127 [`1901.03879`].

[157] A. Karch and L. Randall, *Geometries with mismatched branes*, *JHEP* **09** (2020) 166 [`2006.10061`].

[158] P. Gao, D.L. Jafferis and A.C. Wall, *Traversable Wormholes via a Double Trace Deformation*, *JHEP* **12** (2017) 151 [`1608.05687`].

[159] B. Schumacher and M.D. Westmoreland, *Entanglement and perfect quantum error correction*, *Journal of Mathematical Physics* **43** (2002) 4279 [`quant-ph/0201061`].

[160] B. Schumacher and M.D. Westmoreland, *Approximate quantum error correction*, *Quantum Information Processing* **1** (2002) 5 [`quant-ph/0112106`].

[161] J. Penedones, *Writing CFT correlation functions as AdS scattering amplitudes*, *JHEP* **03** (2011) 025 [`1011.1485`].

[162] H. Geng, A. Karch, C. Perez-Pardavila, S. Raju, L. Randall, M. Riojas et al., *Inconsistency of islands in theories with long-range gravity*, *JHEP* **01** (2022) 182 [`2107.03390`].

[163] D. Neuenfeld, *The Dictionary for Double Holography and Graviton Masses in d Dimensions*, `2104.02801`.

[164] D. Neuenfeld, *Homology conditions for RT surfaces in double holography*, *Class. Quant. Grav.* **39** (2022) 075009 [`2105.01130`].

[165] D. Harlow and D. Jafferis, *The Factorization Problem in Jackiw-Teitelboim Gravity*, *JHEP* **02** (2020) 177 [`1804.01081`].

[166] P. Gao, D.L. Jafferis and D.K. Kolchmeyer, *An effective matrix model for dynamical end of the world branes in Jackiw-Teitelboim gravity*, *JHEP* **01** (2022) 038 [`2104.01184`].

[167] Z. Komargodski and A. Zhiboedov, *Convexity and Liberation at Large Spin*, *JHEP* **11** (2013) 140 [`1212.4103`].

[168] S. El-Showk and K. Papadodimas, *Emergent Spacetime and Holographic CFTs*, *JHEP* **10** (2012) 106 [`1101.4163`].

[169] A.L. Fitzpatrick, J. Kaplan, D. Poland and D. Simmons-Duffin, *The Analytic Bootstrap and AdS Superhorizon Locality*, *JHEP* **12** (2013) 004 [`1212.3616`].

[170] N. Afkhami-Jeddi, T. Hartman, S. Kundu and A. Tajdini, *Einstein gravity 3-point functions from conformal field theory*, *JHEP* **12** (2017) 049 [`1610.09378`].

[171] M. Kulaxizi, A. Parnachev and A. Zhiboedov, *Bulk Phase Shift, CFT Regge Limit and Einstein Gravity*, *JHEP* **06** (2018) 121 [`1705.02934`].

[172] D. Meltzer and E. Perlmutter, *Beyond $a = c$: gravitational couplings to matter and the stress tensor OPE*, *JHEP* **07** (2018) 157 [`1712.04861`].

[173] M.S. Costa, T. Hansen and J.a. Penedones, *Bounds for OPE coefficients on the Regge trajectory*, *JHEP* **10** (2017) 197 [`1707.07689`].

[174] X.O. Camanho, J.D. Edelstein, J. Maldacena and A. Zhiboedov, *Causality Constraints on Corrections to the Graviton Three-Point Coupling*, *JHEP* **02** (2016) 020 [`1407.5597`].

[175] A. Belin, D.M. Hofman and G. Mathys, *Einstein gravity from ANEC correlators*, *JHEP* **08** (2019) 032 [`1904.05892`].

[176] M. Kologlu, P. Kravchuk, D. Simmons-Duffin and A. Zhiboedov, *Shocks, Superconvergence, and a Stringy Equivalence Principle*, *JHEP* **11** (2020) 096 [`1904.05905`].

[177] S. Caron-Huot, D. Mazac, L. Rastelli and D. Simmons-Duffin, *AdS bulk locality from sharp CFT bounds*, *JHEP* **11** (2021) 164 [`2106.10274`].

[178] N. Engelhardt and G.T. Horowitz, *Towards a Reconstruction of General Bulk Metrics*, *Class. Quant. Grav.* **34** (2017) 015004 [`1605.01070`].

[179] N. Engelhardt, *Into the Bulk: A Covariant Approach*, *Phys. Rev. D* **95** (2017) 066005 [`1610.08516`].

[180] S. Hernández-Cuenca and G.T. Horowitz, *Bulk reconstruction of metrics with a compact space asymptotically*, *JHEP* **08** (2020) 108 [`2003.08409`].

[181] D. Mazáč, L. Rastelli and X. Zhou, *An analytic approach to $BCFT_d$*, *JHEP* **12** (2019) 004 [`1812.09314`].

[182] M. Hogervorst and S. Rychkov, *Radial Coordinates for Conformal Blocks*, *Phys. Rev. D* **87** (2013) 106004 [`1303.1111`].

[183] A. Karch and L. Randall, *Locally localized gravity*, *JHEP* **05** (2001) 008 [`hep-th/0011156`].

[184] O. Aharony, O. DeWolfe, D.Z. Freedman and A. Karch, *Defect conformal field theory and locally localized gravity*, *JHEP* **07** (2003) 030 [`hep-th/0303249`].

[185] J. Penedones, *TASI lectures on AdS/CFT*, in *Theoretical Advanced Study Institute in Elementary Particle Physics: New Frontiers in Fields and Strings*, pp. 75–136, 2017, DOI [`1608.04948`].

[186] M. Lemos, P. Liendo, M. Meineri and S. Sarkar, *Universality at large transverse spin in defect CFT*, *JHEP* **09** (2018) 091 [`1712.08185`].